The Cryogenic Parallel Heat Pipe System for Application to Conduction Cooled Superconducting Magnet

伝導冷却超伝導磁石への応用を目指した
極低温パラレルヒートパイプシステムの研究

Ramnarong WANISON

DOCTOR OF PHILOSOPHY

Department of Accelerator Science

School of High Energy Accelerator Science

The Graduate University for Advanced Studies, SOKENDAI

2021

Supervisor:	Prof. NAKAI, Hirotaka Assc. Prof. KIMURA, Nobuhiro
Examiners:	Prof. MAKIDA, Yasuhiro Assc. Prof. OKAMURA, Takahiro Prof. SASAKI, Ken-ichi Asst. Prof. SHIMIZU, Hirotaka Prof. NAKAI, Hirotaka Assc. Prof. KIMURA, Nobuhiro Honorary Prof. MURAKAMI, Masahide Asst. Prof. TAKADA, Suguru
Day of Final Evaluation:	19 August 2021
Day of Submission:	10 June 2021

ABSTRACT

The High Energy Accelerator Research Organization, known as KEK, whose purpose is to operate the largest particle physics laboratory in Japan. Numerous experiments have been conducted at KEK, especially in cryogenic science and engineering that involve the study to support accelerator science research mostly for superconducting magnets. Since a superconducting magnet must be cooled to cryogenic temperatures during operation therefore, a cooling system is necessary. A cryogenic heat pipe has been proposed for the application to conduction-cooled superconducting magnets to improve the efficacy of cooling systems. However, a cryogenic heat pipe has operation limits such as low maximum heat transport capability, Q_{max}. The parallel heat pipe system, which is composed of a combination of individual heat pipes, can enhance the performance of a single heat pipe with respect to Q_{max}, and expand the operating temperature range. This is the experimental study to survey thermal behavior of cryogenic heat pipes under condition of a wide range of heat load and of heat pipe operating states; from the normal heat pipe operation to the local dry-out state. The heat pipes tested in this research were commercially available, but working fluid was replaced by nitrogen (N_2) or argon (Ar) or neon (Ne) to work at cryogenic temperatures. The size of the tubular copper heat pipe is; 6 mm in outer diameter and 200 mm in length. The thermal performance of the heat pipes was examined together with the effects of the working fluid filling ratios, the inclination angle, the condenser temperatures as well as the wick structures such as axial groove (G), sintered metal powder (S), and combination of them (GS). The parallel heat pipe system, which consists of an N_2-heat pipe and an Ar-heat pipe, or of an N_2-heat pipe and an Ne-heat pipe arranged in parallel, was tested in order to investigate the thermal performance for extending the operating temperature ranges. The effective thermal resistance, the axial temperature distribution and the pressure inside the heat pipes were measured for a wide range

of heat load. The thermal behavior even in the local dry-out state for large heat input was also examined for the potential application to a conduction-cooled superconducting magnet. It was experimentally confirmed that the commercially available conventional heat pipes being replaced the working fluid with nitrogen, argon or neon could operate normally at temperatures of 63–87, 83–110 and 27–35 K, respectively.

The followings are the major experimental results obtained in the present study. The prediction of the heat pipe operation at near the critical temperature of the working fluid shows that the maximum heat transport capability, Q_{max}, becomes very small, since the latent heat of vaporization becomes zero at the point. The filling ratio of working fluid should be higher than 50% to activate the cryogenic heat pipe, and the working fluid filling ratio considerably affects Q_{max} of the heat pipe. The gravity force acting on the excess liquid puddle accumulated in the end portion of the condenser section causes increasing of Q_{max} in cases of the filling ratio larger than 100%. The inclination angle of larger than 10° in the case when the evaporator section is below the condenser section can much enhance the value of Q_{max}. The minimum value of the overall thermal resistance, R_{th}, which appeared during the normal heat pipe operation, was 0.20, 0.25 and 0.12 K/W for the N_2-heat pipe, the Ar-heat pipe and the Ne-heat pipe, respectively. It was found that the effective thermal conductance was approximately 150 times superior to that of the heat pipe without working fluid filled where heat transferred by conduction through a copper tube wall, and 75 times superior to that of a simple copper rod having the same diameter and length as the heat pipe. The performance rank by the wick structures on the basis of Q_{max} is as follows in descending order: GS, S and G. It was the results of the experiments that the N_2-heat pipe, the Ar-heat pipe and the Ne-heat pipe with the GS wick structure and 100% filling ratio had the values of Q_{max}, 12, 14 and 7 W, respectively. The parallel heat pipe system can enhance the performance of the single heat pipe with respect to Q_{max}, which was 29 W in the case of the operating temperature of 87 K. It is seen that even in the local dry-out state the heat pipe still has high heat transfer rate compared to solid copper. This seems to indicate it can be utilized for cooling of superconducting magnets from room temperature.

It is experimentally confirmed that the commercially available conventional heat pipe can be utilized as a cryogenic heat pipe for the application to conduction-cooled superconducting magnets. It was demonstrated that the wide range of cryogenic heat pipe operation consisting not only of the normal heat pipe operation but also the local dry-out state is effective for thermal management owing to very small temperature gradient and cooling from room temperature.

THESIS OUTLINE

The outline and the structure of this thesis are introduced in this section. The thesis consists of seven chapters, as follows.

Chapter 1: **INTRODUCTION:**

The background, motivation and objectives of this study. Introduction of the cryogenic heat pipe by using a commercially available conventional heat pipe to superconducting magnet cooling application, and of the experiments that were performed in this study.

Chapter 2: **FUNDAMENTALS OF HEAT PIPES:**

Description of the fundamentals of heat pipes including the historical development of heat pipes, working principle, types of heat pipes, working fluids and operating temperature ranges, wick design and structure, and heat transfer limits.

Chapter 3: **LITERATURE REVIEW:**

Summarizing and finding the knowledge gap from previous studies in order to define the scope of the present research and think more deeply about the experimental results obtained so far as well as the recent cryogenic heat pipes.

Chapter 4: **EXPERIMENTAL APPARATUS:**

Experimental apparatus and measurement technique used in this experiment including the two different kinds of cooling methods, cooling with a liquid nitrogen bath and a cryocooler.

Chapter 5: **EXPERIMENTAL PROCEDURE:**

Experimental procedure including the preparation and method of the experiment, technique, and safety for operating the experiment at cryogenic temperatures.

Chapter 6: **RESULTS AND DISCUSSION:**

Experimental results of the single heat pipes and the parallel heat pipe system on thermal behavior in the normal heat pipe operation and the dry-out state characterized by the overall thermal resistance.

Chapter 7: **CONCLUSION.**

ACKNOWLEDGMENT

First of all, I would like to express my special appreciation and thanks to my supervisor Associate Professor KIMURA Nobuhiro, the Cryogenics Science Center, KEK, for all his invaluable support and guidance. I really appreciate his encouragement, genuine and constant supervision, brilliant ideas, support and motivation throughout the entire study.

My deepest gratitude goes to Professor Emeritus MURAKAMI Masahide at the University of Tsukuba, who is Professor Emeritus at University of Tsukuba, for all the support and encouragement he gave me. Without his guidance and constant feedback, this study would not have been achievable.

I would like to express my sincere gratitude to Professor NAKAI Hirotaka, the Accelerator Laboratory, KEK, for all of his supports during I was studying in SOKENDAI.

I would also like to thank Assistant Professor TAKADA Suguru, the National Institute for Fusion Science (NIFS), for good suggestion and discussion to the experiment on my study.

Sincerely thank the members in the Cryogenics Science Center, KEK, for their very kind assistance in the experiment. Miss A. Ueda for helping us to design the experimental set up and Mr. G. Namai for supporting to construct the experimental set up.

Special thanks to Professor Pradit TERDTOON and his Heat Pipe and Heat System Laboratory, Chiang Mai University, Thailand, for supplying commercially available heat pipes to this study.

Finally, I would like to gratefully acknowledge financial support from the Japanese government scholarship (Ministry of Education, Culture, Sports, Science and Technology, MEXT) for supporting on my whole study.

TABLE OF CONTENTS

LIST OF FIGURES

LIST OF TABLES

NOMENCLATURE

Symbol	Description	Units
A_v	vapor core cross-sectional area	m^2
A_w	wick cross-sectional area	m^2
d_v	vapor core diameter	m
f_v	drag coefficient for vapor flow	
F_l	frictional coefficient for liquid flow	s/m^4
F_v	frictional coefficient for vapor flow	s/m^4
g	gravitational acceleration	m/s^2
k_e	effective thermal conductivity of liquid-saturated wick	W/(m·K)
k_l	thermal conductivity of liquid	W/(m·K)
k_w	thermal conductivity of wick material	W/(m·K)
K	wick permeability	m^2
L	total length of heat pipe	m
L_a	length of heat pipe adiabatic section	m
L_c	length of heat pipe condenser section	m
L_e	length of heat pipe evaporator section	m
L_{eff}	effective length of heat pipe	m
m	working fluid mass	kg
P_i	the pressure of working gas in gas reservoir before heat pipe was cooled by liquid nitrogen or by a cryocooler	Pa
P_f	the pressure of working gas in gas reservoir after gas flew into heat pipe and then was cooled by liquid nitrogen or by a cryocooler and was finally saturated in wick structure	Pa
P_v	vapor pressure	Pa

$\Delta P_{\perp}$	hydrostatic pressure difference in direction perpendicular to pipe axis	Pa
Q	heat load	W
$Q_{b,\ max}$	boiling limit for heat transfer	W
$Q_{c,\ max}$	capillary limit for heat transfer	W
$Q_{e,\ max}$	entrainment limit for heat transfer	W
$Q_{s,\ max}$	sonic limit for n heat transfer	W
$Q_{v,\ max}$	viscous limit for heat transfer	W
r_c	effective capillary radius	m
r_s	the average sphere radius of the sintered metal particles	m
$r_{h,\ l}$	hydraulic radius for liquid flow	m
$r_{h,\ s}$	hydraulic radius of wick at vapor-wick interface	m
$r_{h,\ v}$	hydraulic radius for vapor flow	m
r_i	inner radius of heat pipe	m
r_v	vapor core radius	m
R_v	gas constant for vapor	J/(kg·K)
Re_v	vapor flow Reynolds number	
T	working fluid temperature	K
T_e	wall temperature in the evaporator section	K
T_a	wall temperatures in the adiabatic section	K
T_c	wall temperature in the condenser section	K
T_v	vapor temperature	K
V_r	volume of gas reservoir	m^3
γ_v	vapor specific heat ratio	
μ_l	liquid dynamic viscosity	Pa·s
μ_v	vapor dynamic viscosity	Pa·s

ρ_l	liquid density	kg/m^3
ρ_v	vapor density	kg/m^3
ε	wick porosity	
λ	latent heat of vaporization	J/kg
σ	surface tension coefficient	N/m
ψ	heat pipe inclination measured from horizontal position, positive for evaporator-down position	rad

Chapter 1
INTRODUCTION

High temperature superconductivity (HTS) has the potential to revolutionize the field of superconducting magnets for particle accelerators, energy storage systems as well as medical applications. HTS magnets can be operated at not extremely low temperatures (20–77 K). Since the critical temperature of HTS is rather high, the material has a very large operating margin to temperature, which is beneficial to avoid quenching and, in general, to increase the reliability of the magnet, HTS is the main factor of interest for the accelerator magnets of the future. This is, indeed, a significant improvement over low temperature superconducting (LTS) magnets that are generally operated at a temperature of ~4 K and to generate the magnetic field that usually limited. Moreover, the fact that the operating temperature of HTS magnets do not need to be as precise as that of LTS magnets brings some simplification to the cryogenic system. Therefore, HTS magnets can even bear some temperature rise without significant loss in performance.

Since superconductivity is, in general, a phenomenon occurring at extremely low temperature, and therefore, cryogenic systems must be used to cool down superconductivity-related equipment. In recent conduction-cooled superconducting magnet systems, a cryocooler is employed to cool the magnets down to a certain operating temperature without using any cryogen. The cold head of a cryocooler has a so strict place restriction that it needs to be located in a low magnetic field area to avoid degradation of the cooling performance due to magnetic field effect. Therefore, the conductive cooling scheme is crucial in developing superconducting magnet systems, in which some conduction heat transfer paths must be provided between cryocoolers and magnets.

A quench, which is characterized by the irreversible transition of a zone of the conductor from the superconducting state to the normal (resistive) state, may originate from the loss of cooling due to a cryogenic system failure or a vacuum system failure. In the event of a quench, if no appropriate technical measures were taken, a magnet could be in danger of overheating owing to the high level of electric current density in the superconductor. When it is no longer in a superconductive state as electrical wire will have finite amount of electrical resistance, the high current flowing through the resistance will generate enormous heat in the cryogenic system.

HTS magnets can, in general, produce higher magnetic fields with higher stability against a quench compared to LTS magnets. Nevertheless, it is difficult to remove the local heat generated in a HTS magnet, because the thermal diffusivity decreases in the operating temperature range above 30 K. Therefore, large temperature gradient may easily occur in a magnet, which could cause degradation of superconducting property. In order to operate a conduction-cooled superconducting magnet system efficiently, heat pipes, which use cryogenic fluid (nitrogen, argon, or neon) as a working fluid, are proposed to use as a conductive link of a conduction-cooled superconducting magnet system.

The conventional heat pipe is a closed tube with a porous capillary wick inside it. The wick is saturated with condensed liquid phase of a working fluid and the remaining volume of the tube is occupied by vapor phase of the working fluid. The heat pipe can transfer heat from one end to another with a very small temperature gradient by evaporation and condensation of a working fluid. It has the capability of transporting a large amount of heat with small unit size, and the thermal characteristics are orders of magnitude better than simple solid such as copper.

Currently, conventional heat pipes are commercially available, of which use has the following advantages: high heat response, high maximum heat transport capability, low thermal resistance, high design flexibility, and maintenance-free. The commercially available heat pipes that were used in the present experiments were originally designed to use water as a working fluid for such room temperature applications as the cooling of electronic devices that generate very large amount of heat due to higher performance, in which fans or heat sinks may not be suitable to remove such a large amount of heat within a limited space. They were miniature heat pipes designed and fabricated by Fujikura Thailand Ltd., which has a diameter of 3–6 mm and length of 100–300 mm. They are made of copper with several kinds of wick structures such as an axial groove wick, a sintered metal powder wick, and a combination of axial groove and sintered metal powder wicks.

In order to operate the commercially available heat pipes in a conduction-cooled superconducting magnet system at a cryogenic temperature, the working fluid must be replaced with cryogenic fluid such as argon, nitrogen, neon or even helium in case of cooling of LTS magnets. In general, such fluid properties are much different between these cryogenic fluids and water as the surface tension to produce the capillary pressure to pump liquid phase back to the evaporator section and the latent heat of vaporization to transport heat to the condenser section. These fluid properties of the cryogenic fluids are, in general, smaller than those of water, and the viscosity of cryogen is higher. As a result, it is natural that the maximum amount of heat that can be transported, Q_{max}, by cryogenic heat pipes is rather lower than that of water heat pipes. Some special design may be necessary for the cryogenic heat pipes in order to enhance Q_{max} of cryogenic heat pipes, for example, by selected material of heat pipes that must be compatible with cryogenic working fluid and carefully designed wick structure that can cope with small surface tension and high viscosity of cryogenic fluids that can improve the capillary pressure in wick structure and reduce the friction force caused by working fluid flow.

On the other hand, it would be very valuable if the commercially available conventional heat pipes can well operate at cryogenic temperatures, and it will be possible to avoid new special design and fabrication exclusively for cryogenic heat pipes that must cost high. Additionally, the quality and the performance of commercially available heat pipes are uniform and thus would be high in reliability due to mass production, and they are readily available at a low price.

The above points were emphasized in this study because what was particularly pursued in this study was not high-performance heat pipes, but rather to pursue the details of the thermal behavior of cryogenic heat pipes for potential applications to superconducting magnet cooling. The combination wick structure of axial grooves and sintered metal powder wick was selected for the present cryogenic heat pipe experiment. Axial groove wick is formed by the extrusion of a groove-shaped plug with the same inner radius. Since the width of grooves are generally larger than the capillary radius of other wicks, the capillary pumping pressure is rather small. On the other hand, the permeability and the effective thermal conductivity are rather high, which would be suitable for dealing with high viscosity of cryogenic fluids. Sintered metal powder wick is manufactured by packing tiny metal particles in powder form between an inner heat pipe wall and a mandrel. The capillary pressure developed by the sintered metal wick that can be more readily predicted is generally large, but the permeability is rather low. Sintered metal-groove composite wick employs the benefits of having small pores for generating high capillary pumping pressure owing to a sintered metal wick and having large pores for increasing the permeability of the liquid return path owing to groove wick.

It is the detailed thermal performance of the commercially available conventional heat pipes from Fujikura Ltd. that was investigated by using nitrogen, argon, or neon as a working fluid (N_2-heat pipe, Ar-heat pipe, or Ne-heat pipe) in order to operate at cryogenic temperatures. They have an outer diameter of 6 mm and a length of 200 mm with the combination wick structure consisting of axial grooves and sintered metal powder. Actually, liquid nitrogen (LN_2) temperature (77 K) is a kind of the normal temperature for superconducting magnets (cooling temperature for HTS magnets or temperature of thermal shield for LTS magnets that are cooled down to temperature about 4 K). However, for the operation or storage at room temperature or higher temperatures, there is a concern that the inside gas pressure of N_2-heat pipe will become extremely high. An Ar-heat pipe can operate at the temperatures higher than 77 K or even higher than the critical temperature of nitrogen 126 K. It is, moreover, a merit of Ar-heat pipes that they have higher maximum heat transport capability Q_{max} because of having higher surface tension than N_2. For applications below LN_2 temperature, an Ne-heat pipe can be used for cooling a superconducting magnet which has operating temperature lower than 77 K, for example, at 39 K for the critical temperature of MgB_2 wire.

It must be a good technical idea for expanding the operating temperature range that two or three of N_2-heat pipe, Ar-heat pipe, or Ne-heat pipe are arranged in parallel simultaneously so as to operate as a parallel heat pipe system. In fact, the temperature ranges between the triple point temperature and the critical temperature are 24.5–44.5, 61.3–126.2, and 83.8–150.8 K, respectively for neon, nitrogen, and argon. Therefore, the parallel heat pipe would be able to operate at a temperature range between 24.5 and 150.8 K. Furthermore, within the overlapping working temperature range of the N_2-heat pipe and the Ar-heat pipe, 83.8–126.2 K, the performance of the parallel heat pipe system certainly is improved compared to individual heat pipes. The investigation of the parallel heat pipe system in this research must certainly be the first attempt.

Additionally, this experiment was further extended towards the study of the thermal performance of the dry-out state that occurs locally in the evaporator section or expanding to a part of the adiabatic section for very large heat input. In case of the normal heat pipes, when the dry-out occurs, almost endless rise in the temperature occurs in the evaporator section and it enters a dangerous situation. However, in case of the cryogenic heat pipes of which condenser section is thermally tightly connected to a cryocooler, even if the local dry-out occurs, the heat pipe operation still continues in other sections than the evaporator section and the pressure inside the heat pipe is not extremely high, and thus higher heat transfer performance is still achieved compared with thermal conduction through solid copper with the same dimensions.

In conclusion, the application of the parallel heat pipe system and even the utilization of the local dry-out state will lead to the improvement of the cooling of superconducting magnets after occurring of a quench as well as thermal management of superconducting magnets.

1.1 Objectives of Study

The objectives of this study as well as the background and the motivation are summarized as follows;

- Investigation of the performance of commercially available heat pipes at LN_2, LAr, or LNe temperature as a cryogenic heat pipe, which were originally designed for room temperature applications. Verification of the validity of the theoretical performance prediction of cryogenic heat pipes. Verification whether they can be applied to cool high temperature superconducting magnets. The parameters and chart to be acquired: effective thermal resistance, maximum heat transport capability, mode map showing the heat pipe operating state.

- Test of the performance of the parallel heat pipe system that consists of the two of the N_2-, Ar-, and Ne-heat pipes for wide range of the operating temperature. Examination of the heat transfer performance prediction method for the parallel heat pipe system.

- The examination of the thermal behavior of cryogenic heat pipes in the local dry-out state, where the evaporator section is in a partially or completely dried-out state and the temperature starts to significantly rise, and the verification of practicality of the state.

- Search for the application method of cryogenic heat pipes for cooling superconducting magnets in some space applications and accelerators for the high energy physics research.

1.2 Experiments in This Study

The experiments in this study were performed to test the commercially available conventional heat pipes using neon, nitrogen, or argon as a working fluid in both a single and a parallel heat pipe arrangement. The lists of experiments are shown below;

For single heat pipe arrangement

- Effect of the filling ratio; normal fill (100%), low fill (< 100%), and high fill (>100%)
- Effect of the inclination angle; the evaporator section above/below the condenser section
- Effect of the condenser temperature as a heat sink temperature
- Impact of wick structure

For Parallel heat pipe arrangement

- Effect of the condenser temperature, 27, 35, 77, 82, 84, and 87 K, and of the combination of axial groove and sintered metal powder wick structure
- Performance (the composite thermal resistance) prediction method

Chapter 2
FUNDAMENTALS OF HEAT PIPE

In this chapter, the fundamentals of heat pipes are described, which include the historical development of heat pipes, the working principle, working fluids and operating temperature ranges, the wick design and structure, the heat transfer limits, and the types of heat pipes.

2.1 Heat Pipe Development History

Of many different types of heat transport systems, the het pipe may be one of the most efficient systems known today [1]. Heat pipes are heat transfer devices that can transport large amount of heat through a small cross-sectional area compared with other conventional methods over a considerable distance with no additional power input to the system. The heat pipe operation is characteristic in the operation involving very small end-to-end temperature drop, requiring no mechanical or electrical power input, no maintenance, a very long-time usage, and the ability to control and transport high heat rates in various temperature levels, which are all unique features of heat pipes.

The Perkins tube was introduced by the Perkins family from the mid-nineteenth to the twentieth century through a series of patents in the United Kingdom. Most of the Perkins tubes were wickless gravity-assisted heat pipes or thermosyphons, in which heat transfer was achieved by a change of phase (evaporation and condensation) and operated vertically with a condenser section above an evaporator section. The Perkins tube design closest to the present heat pipe was patented by Jacob Perkins in 1836 [2]. This design was a closed tube containing a small quantity of water operating as a two-phase liquid–vapor cycle.

The heat pipe was first introduced by Gaugler [3] of the General Motors Corporation in the U.S. (Patent No. 2350348). Gaugler had suffered from refrigeration problems at that time. His requirement was to develop a device that could evaporate liquid at a point (high-temperature zone) above the place where condensation (cold-temperature zone) could occur without requiring any additional work to move the liquid back to the higher level (from a cold-temperature zone to a high-temperature zone). The design of Gaugler was a device consisted of a closed tube in which liquid would absorb heat at one location causing the liquid to evaporate. The vapor would then travel down the length of the tube, where it would recondense and release its latent heat. Liquid would then travel back up the tube via capillary pressure to start the process over. In order to move the liquid back up to a higher point, Gaugler suggested “the use of a capillary structure consisting of a sintered iron wick”. A refrigeration unit designed by Gaugler used a heat pipe to transfer the heat from the interior of a compartment to a pan of crushed ice below. However, this idea was not used by General Motors for the refrigeration problem.

The concept of a heat pipe in conjunction with the space program was revived by Trefethen in 1962 [4]. In 1964, significant progress began when the heat pipe was independently reinvented, and a patent application was filed by Grover at the Los Alamos National Laboratory. Several prototype heat pipes were designed by Grover et al. [5] and Grover [6]. The first heat pipe used water as a working fluid and was soon followed by a sodium heat pipe at 1100 K of operating temperature. The use of heat pipes by Grover and his co-workers have shown as a high efficiency heat transmission system. Grover [6] invented the term "Heat Pipe" in a U.S. patent application submitted by Grover on behalf of the U.S. Atomic Energy Commission and stated that “with certain limitations on the manner of use, a heat pipe may be regarded as a synergistic engineering structure which is equivalent to a material having a thermal conductivity greatly exceeding that of any known metal." Theoretical study of heat pipes in the patent application by Grover [6] was limited but they provided experimental result of stainless-steel heat pipes with a screen wick by using silver and lithium as working fluids.

The preliminary theoretical results and design tools were reported in the first publication on the heat pipe analysis by Cotter in 1965 [7]. After this report was published, research of heat pipes has been started worldwide. The United Kingdom Atomic Energy Laboratory at Harwell started the experiment of sodium heat pipes to be used as thermionic diode converters. Furthermore, scientists started conducting heat pipes research outside the U.S. including Germany, France, and other countries.

The early development of applications of heat pipes progressed at a slow pace. It is a notable advantage that heat pipes utilize capillary action that can work without any external forces or pump even in micro gravitational fields. In order to reduce the cost of energy, the role of heat pipes and thermosyphons in energy saving applications has begun to be recognized by the manufacturing community. Nowadays, all developed countries are actively engaged in heat pipe research, production, and commercialization.

The historical development of heat pipes is summarized in Figure 2.1. After preliminary theory of heat pipes was published by Cotter in 1965 [7], many research of heat pipes have been started worldwide including publications of many textbooks on heat pipe theory [8–12].

2.2 Working Principle of Heat Pipes

A heat pipe of which schematic illustration is shown in Figure 2.2 is a tubular device of different shapes whose inner surface is lined with a porous capillary wick and can transfer heat rapidly away from the source. The wick is saturated with liquid phase of a working fluid and the remaining volume of the tube is occupied by vapor phase. The heat pipe is divided into three sections along its axial direction: the evaporator section, adiabatic section and condenser section. Heat applied externally to the evaporator section is conducted across the pipe wall and the wick structure, where the working fluid vaporizes. The resulting difference in the pressure drives vapor from the evaporator section to the condenser section where it condenses and releases the latent heat of vaporization to a heat sink in that section of heat pipe. The capillary pressure is developed, where the depletion of liquid by evaporation causes the liquid-vapor interface in the evaporator section to recess into the wick surface [8]. This capillary pressure pumps the condensed fluid back to the evaporator section for re-evaporation. The heat pipe can continuously transport the latent heat of vaporization from the evaporator section to the condenser section without drying out the wick. This process will continue as long as the flow passage for the working fluid is not blocked, and sufficient capillary pressure is maintained.

The amount of heat that can be transported as latent heat of vaporization is usually several orders of magnitude larger than that can be transported as sensible heat in conventional convective systems [8]. The heat pipe can transport a large amount of heat with a small unit size. Because of their thin wick structure and the small temperature drop for their vapor flow, heat pipes having the thermal characteristics orders of magnitude larger than those of solid conductors have been developed.

In the evaporator section, the menisci of the liquid–vapor interface are strongly curved, and therefore the fluid retracts into the pores of the wick. In contrast, the menisci in the condenser section are almost flat throughout the condensation process. Owing to the surface tension of the working fluid having a curved structure of the interface, a capillary pressure occurs at the liquid–vapor interface. The variation in the curvature of the meniscus between liquid and vapor along the interface results in the capillary pressure changing along the heat pipe. The difference in the capillary pressure pumps the working fluid against the pressure losses generated in liquid and vapor and the gravity and acceleration forces. The vapor pressure variation along the heat pipe is due to friction, inertia and blowing (evaporation) and suction (condensation) effects, while the liquid pressure changes mainly as a result of friction [1]. Figure 2.3(a) illustrates the axial variations of the shape of the liquid–vapor interface in the heat pipe. At low vapor flow, the liquid–vapor interface is almost flat near the end cap of the condenser section due to zero local pressure gradient. Figure 2.3(b) illustrates the liquid pressure and vapor pressure in the case of low vapor flow rates. For cryogenic heat pipes, the vapor velocity is quite low due to low value of the maximum heat transport capability. At the end cap of the evaporator section, the maximum local pressure difference occurs, which is equal to the sum of the pressure drops in the vapor and the liquid across the heat pipe when the body forces are neglected. However, when body forces are considered such as a gravitational force, as the liquid pressure drop becomes higher, the capillary pressure must be even higher by that amount in order to return the liquid back to the evaporator section for re-evaporate.

2.3 Working Fluids and Operating Temperature Range

For the applications of heat pipes, the operating temperature range should be considered. Therefore, in the design of heat pipes, working fluid that is appropriate to the temperature range should be selected. Every working fluid has particular fluid properties which vary depending on the operating temperature. A good working fluid for heat pipes should have high latent heat of vaporization, surface tension, and thermal conductivity. Table 2.1 shows the melting points and boiling points at 1 atm and their critical temperature of various working fluids. The effective temperature range typically extends from the temperature where the saturation vapor pressure is greater than 0.1 atm to that less than 20 atm. Temperature ranges are divided into four categories: cryogenic, low, intermediate, and high ranges.

Cryogenic heat pipes operate between 4 and 200 K. The maximum of the heat transport capability for these kinds of heat pipes is low compare with heat pipes operating at higher temperatures, due to small heat of vaporization, high viscosity, and small surface tension. Therefore, some special design consideration may be needed for cryogenic heat pipes. Additionally, some types of heat pipes are not appropriate to operate in cryogenic temperature range.

The low temperature range is from 200 to 500 K. Most heat pipes operate within this range in applications. Water is the most common working fluid in this temperature range, as it has good thermophysical properties such as large heat of vaporization and surface tension. The practical range for copper-water heat pipes is 283–560 K. Other working fluids often used within this range include ammonia and acetone

In the intermediate temperature range, heat pipes operate between 450 and 750 K. Mercury inherently has extremely attractive properties such as its high thermal conductivity. However, problems with wetting the wick and pipe wall present some difficulties in using mercury in capillary-driven heat pipes. The toxicity of mercury is also a serious problem. A review of intermediate temperature fluids based on life test experiments was reported by Anderson et al. in 2007 [13]. Other common working fluids in this range are Dowtherm-A and NaK.

The high temperature range for heat pipes is over 750 K. Liquid-metal working fluid such as silver, potassium, or sodium are often used for heat pipes. The heat transfer performance of liquid–metal heat pipes is generally much higher than those of heat pipes operating in other temperature ranges, due to very high values of the latent heat of vaporization, thermal conductivity, and surface tension.

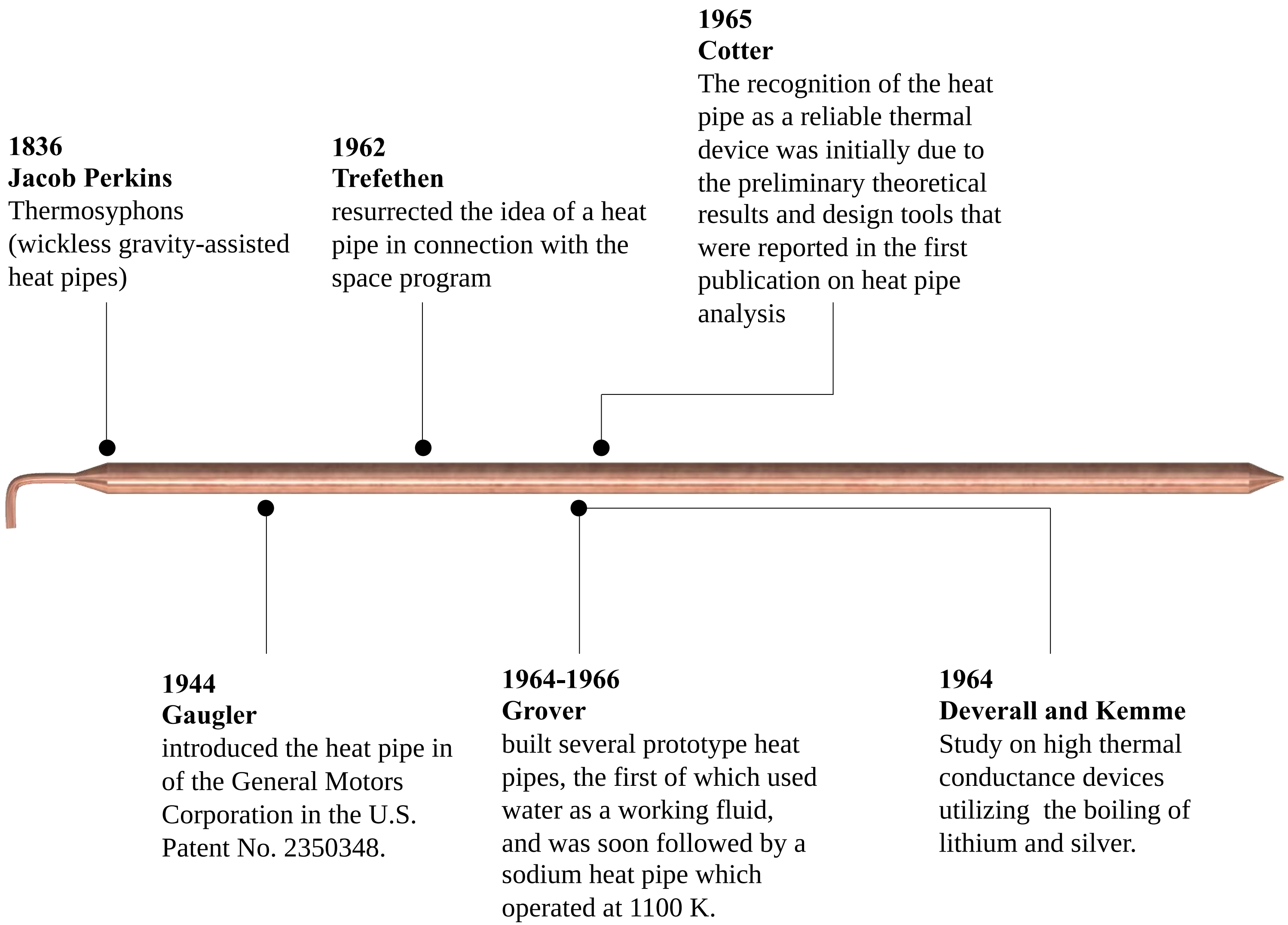

Figure 2.1 *Timeline of historical development of heat pipes*

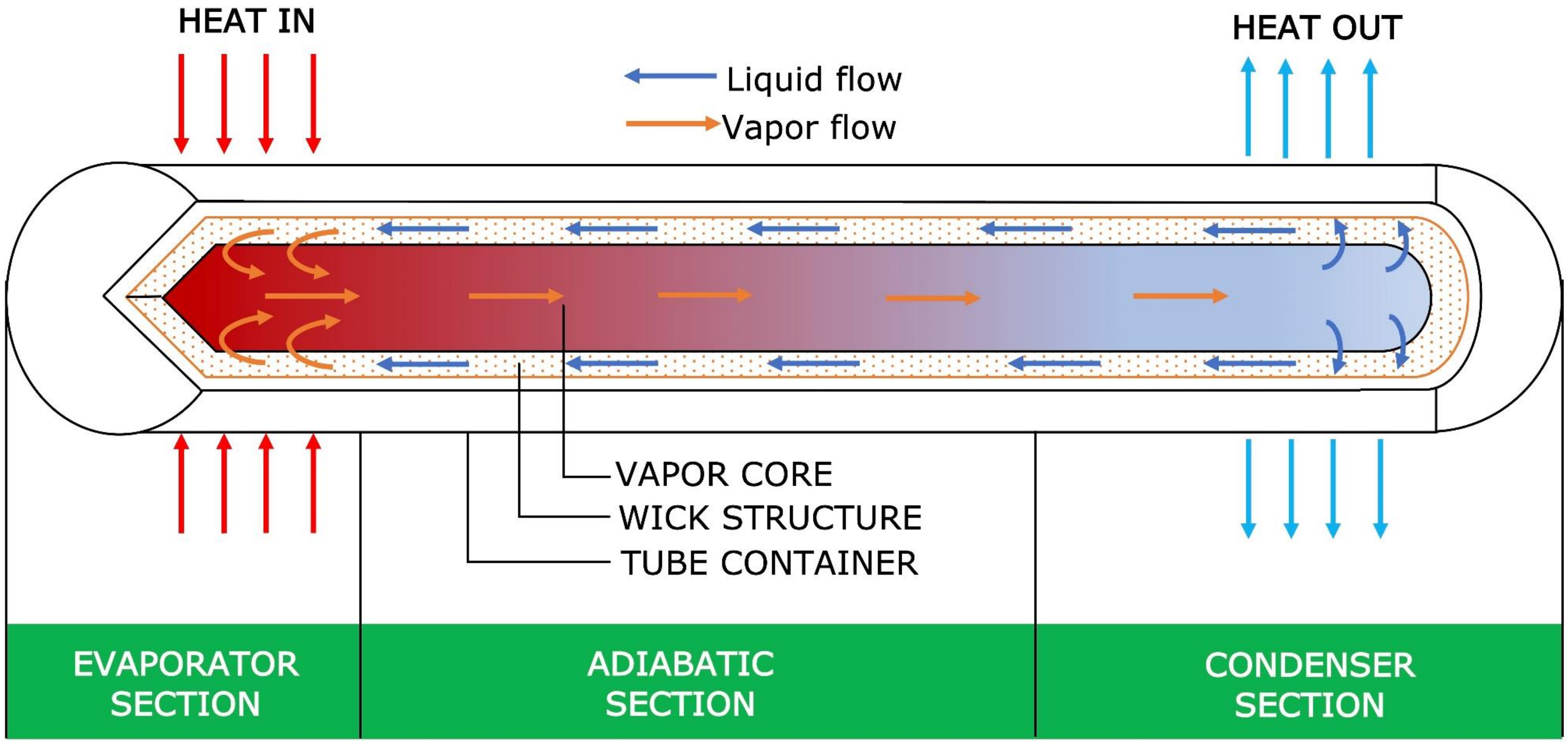

Figure 2.2 *Heat pipe.*

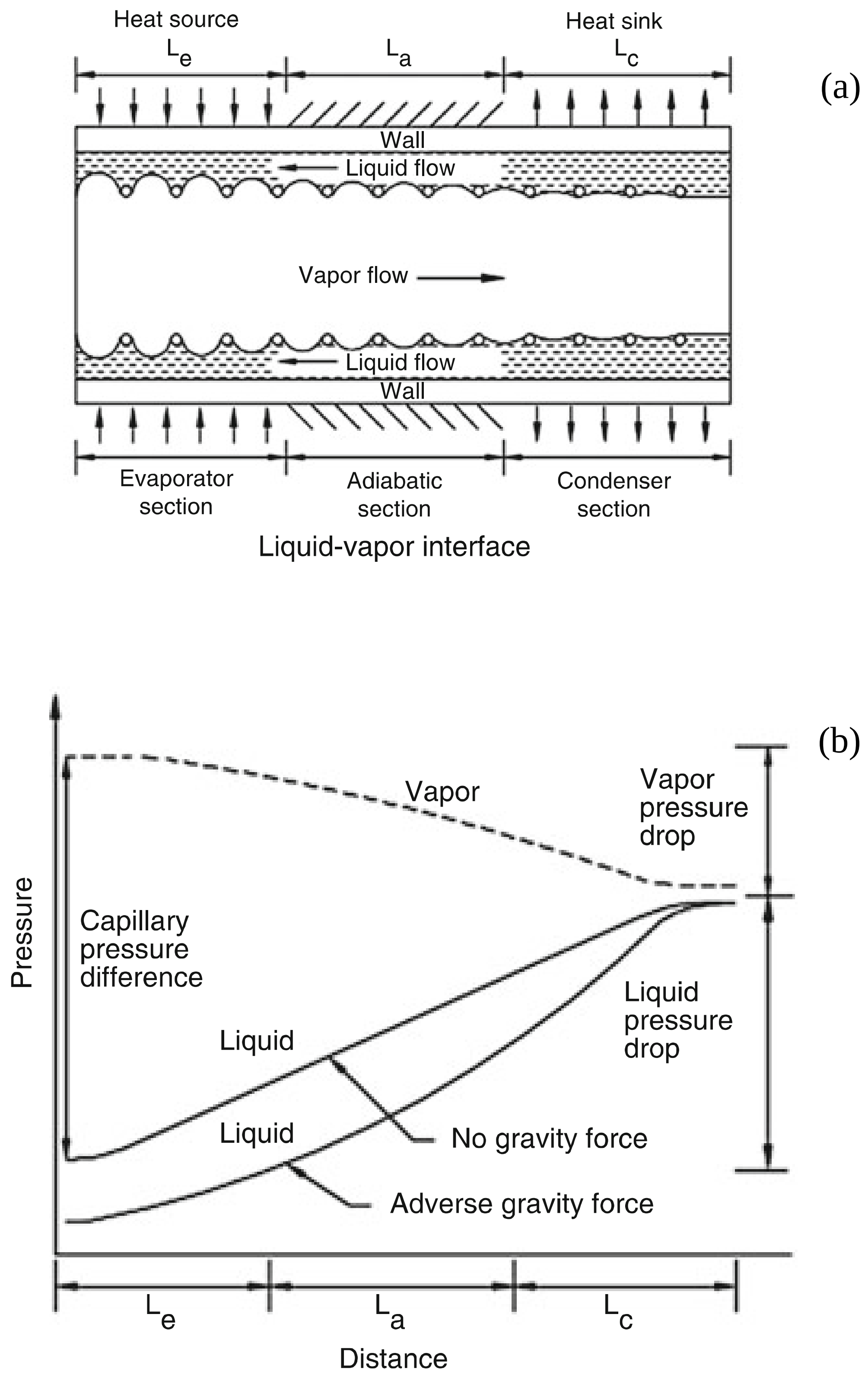

Figure 2.3 *(a) Side view of the liquid–vapor interface, and (b) vapor and liquid pressure variation along a heat pipe [14]. Please note that the vapor pressure variation is exaggerated here for the sake of clarity, and the actual vapor pressure variation is much smaller than this.*

Table 2.1 *Working fluids and temperature ranges of heat pipes [12].*

Working Fluid	Melting Point, K at 1 atm	Boiling Point, K at 1 atm	Critical Point, K	
Helium	1.0	4.21	5.2	Cryogenic Temperature Range
Hydrogen	13.8	20.38	33.2	
Neon	24.4	27.09	44.4	
Nitrogen	63.1	77.35	126.2	
Argon	83.9	87.29	150.8	
Oxygen	54.7	90.18	154.6	
Methane	90.6	111.4	190.55	
Krypton	115.8	119.7	209.48	
Ethane	89.9	184.6	305.33	
R134a	172.0	246.6	374.21	
Ammonia	195.5	239.9	405.5	Low Temperature Range
Pentane	143.1	309.2	469.6	
Acetone	180.0	329.4	508	
Methanol	175.1	337.8	512.6	
Ethanol	158.7	351.5	516.25	
Heptane	182.5	371.5	540.61	
Toluene	178.1	383.7	591.79	
Water	273.1	373.1	647	
Naphthalene	353.4	490	748	
Dowtherm A	285.1	527.0	770	Intermediate Temperature Range
NaK	260.9	1058		
Cesium	301.6	943.0	2057	
Rubidium	312.7	959.2	2093	High Temperature Range
Potassium	336.4	1032	2223	
Sodium	371.0	1151	2573	
Lithium	453.7	1615	3220	
Calcium	1112	1762		
Silver	1234	2485		

Poplaski et al. [15] reviewed the past experimental and theoretical studies on the applications of nanofluids in various types of heat pipes. Furthermore, Poplaski et al. [15] developed a full numerical simulation code to account for the effect of nanofluids in a conventional heat pipe.

Table 2.2 *Generalized results of compatibility tests for heat pipes [12].*

Working fluid	Compatible material	Incompatible material
Acetone	Aluminum, stainless steel	
Ammonia	Aluminum, cold rolled steel, nickel, stainless steel	Copper, titanium
Cesium	Haynes®, Inconel®, niobium, stainless steel, titanium	Copper, copper-nickel, Monel®
Dowtherm A	Aluminum, stainless steel, titanium	Copper, copper-nickel
Helium	Stainless steel, titanium	
Heptane	Aluminum	
Hydrogen	Stainless steel	
Lithium	Molybdenum, niobium, tungsten	Inconel®, nickel, stainless steel, titanium
Methanol	Copper, stainless steel	Aluminum, titanium
Nitrogen	Aluminum, stainless steel	
Potassium	Haynes®, Inconel®, stainless steel	Copper, Monel®
R134a	Stainless steel	
Silver	Molybdenum, tungsten	Rhenium
Sodium	Haynes®, Inconel®, stainless steel	Titanium
Water	Copper, Monel®, nickel, titanium	Aluminum, Inconel®, stainless steel

The compatibility among materials and working fluids used in heat pipes must be carefully considered, and thus is of crucial to reliable long-term use, as incompatible materials can chemically react with one another, leading to failure. Materials selection should be attempted depending on the wick design and temperature range to find wick and container materials with high thermal conductivity for the evaporator and condenser sections while working fluids should have high latent heat of evaporation and beneficial thermal-fluid properties. Selected common materials include copper, stainless steel, nickel, and aluminum for container and wick. Water, methanol, ammonia, and sodium are some common working fluids. Wick options can vary greatly depending on the needs of applications. Common wicks include metal screens, grooves, sintered metal powders and felts, and foams [14, 16]. Longevity of a heat pipe is highly dependent on the material selection of wick and container that are compatible with working fluid. Compatible combination between container materials and working fluids are presented in Table 2.2.

2.4 Structural Design of Wick

The wick is necessary inside a heat pipe to return condensed fluid to the evaporator section. Small pores in a wick structure are needed to develop high capillary pressure at a liquid–vapor interface, while large pores function for minimal liquid flow resistance and for an uninterrupted highly conductive heat flow path across the wick thickness for small temperature drop. Various types of wick structures have been developed in order to optimize the performance of heat pipes.

There are three important wick properties as keys for the heat pipe design [16]:

Effective Pore Radius: The minimum pore radius should be as small as possible to raise the capillary pressure. This enhances the ability to pump condensate back to the evaporator.

Permeability: This determines the ease with which liquid can flow through the wick. The permeability should be large to reduce the liquid pressure drop. The larger this value, the greater the heat transport capacity.

Effective Thermal Conductivity: The effective thermal conductivity of a wick should be as high as possible in order to provide small temperature drops across the wick in the evaporator and condenser sections.

Wick structures can be classified into two general classes, namely homogeneous wicks and composite wicks. The homogeneous wicks are made of single material, while the composite wicks consist of two or more materials. Typical examples of homogeneous wicks and composite wicks are illustrated in Figures 2.4 and 2.5, respectively.

Sintered porous metal wick as shown in Figure 2.4(a) is manufactured by packing tiny metal particles in powder form between the inner heat pipe wall and a mandrel, and then it is sintered. This wick allows generating large capillary pumping pressure to be developed at the liquid–vapor interface, but so small internal pores often cause a larger pressure drop in the liquid flow passage.

Axially grooved wick is shown in Figure 2.4(b). This wick is formed by extrusion or by broaching grooves into the inner surface of a heat pipe. Several types, such as rectangular, triangular, and trapezoidal grooved wicks have been proposed and used. They can be used for the cryogenic and moderate temperature applications and also for liquid metal heat pipes. Highly conductive metal fins of grooves can provide low resistance for heat flow across a wick, but the capillary pressure developed is quite small, and it is difficult to machine grooves in long heat pipes.

For both high capillary pressure and high thermal conductivity, sintered porous metal and axially grooved structure may be combined as a composite wick, as shown in Figure 2.5, in order to take advantage of having small pressure drop for liquid flow in the axially grooved wick and large capillary pressure of sintered porous metal. Sintered-metal and axial-groove combined wicks are manufactured by inserting a mandrel into the center of an axially grooved pipe, and then copper powder is poured into the pipe around the mandrel. After the powder is sufficiently packed, the semifinished parts are placed into a sintering oven. The copper powders stick each other and to the pipe inner surface after a while.

(a) Sintered porous metal *(b) Axial Grooves*

Figure 2.4 *Cross sections of homogeneous wick structures.*

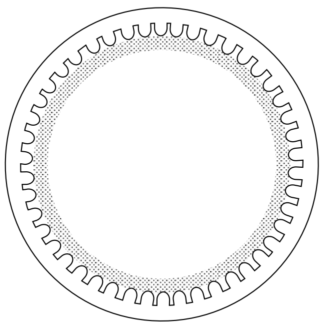

Groove covered with sintered metal

Figure 2.5 *Cross sections of composite wick structures.*

The heat transfer performance of the cryogenic heat pipe with nitrogen, or argon, or neon as a working fluid tested in this research is probably different from those of moderate-temperature or liquid metal heat pipes, even if they all have similar geometry. Because of differences in thermophysical properties of working fluid, such as the surface tension, viscosity, thermal conductivity, latent heat and density, this research was proposed to investigate experimentally the operating characteristics of cryogenic heat pipes with nitrogen, argon, or neon as a working fluid including the examination of the detailed thermal behavior of cryogenic heat pipes even in the dry-out state, where the evaporator section of a heat pipe is in partially or completely dry-out state. Also, the experimental results will be compared with existing theoretical predictions.

2.5 Limitations of Heat Transport Capabilities

Heat pipes operate under a number of physical constraints including the capillary, entrainment, boiling, sonic and viscous limits that fundamentally affect their performance. If the heat added to a heat pipe exceeds one of the limitations of the inside a vapor–liquid cycle, the heat pipe becomes disturbed, and at the end dry-out may occur in the evaporator section. The maximum heat transport capability decided by each limitation is expressed by Equations (2.1), (2.10), (2.11), (2.13) [8] and (2.14) [9].

The type of limitation restricting the heat transport capability is in reality determined by the limitation that has the lowest value of the heat addition under consideration. The magnitude of the heat transfer restricted by these different limitations is in turn dependent upon various properties of the working fluid, wick structure, and the heat pipe dimensions.

2.5.1 Capillary limit

The vapor and liquid flows in a heat pipe are driven by the pressure difference due to evaporation and condensation and by the capillary pumping pressure, respectively. There are some pressure losses occurring throughout the vapor and liquid flows. For a heat pipe to function properly, the net capillary pumping pressure between the evaporator and the condenser sections must be higher than the total pressure loss. Otherwise, insufficient liquid flow to the evaporator section causes dry-out in the evaporator section. The losses in the liquid and vapor flows are summarized as follows [17];

- Inertial and viscous pressure drops occurring in vapor phase flow
- Inertial and viscous pressure drops occurring in liquid phase flow

- Pressure loss occurring in phase transition in the evaporator section
- Pressure loss occurring in phase transition in the condenser section
- Hydrostatic pressure difference in the normal direction to the heat pipe axis
- Axial hydrostatic pressure difference

The expression of the capillary limit can be formulated under the following assumptions;

a) For vapor phase flow, only the viscous pressure loss is considered, and the inertial effect is neglected.
b) The phase transition loss of vapor is neglected.
c) The vapor flow is assumed to be one dimensional in the axial direction.

Under these assumptions, the expression for the maximum heat transport capability governed by the capillary limit can be obtained as shown in Equation (2.1)

$$Q_{c,\,max} = \frac{P_c - \Delta P_{\perp} + P_e}{(F_l + F_v)L_{eff}} \quad . \tag{2.1}$$

Here the effective length of heat pipe, L_{eff}, is defined by

$$L_{eff} = 0.5L_e + L_a + 0.5L_c \quad . \tag{2.2}$$

Equation (2.1) is derived from the equations of momentum conservation. The control volume used in the derivation and the detailed mathematical steps of the derivation can be found in Reference 8. Capillary pumping pressure and other pressure losses are represented by;

Maximum capillary pressure:

$$P_c = {}^{2\sigma \cos\alpha}\!/_{r_c} \, . \tag{2.3}$$

It can be seen in this equation that the maximum capillary pressure is obtained when the cosine of the wetting angle is unity (α = 0).

Gravitational force in the direction perpendicular to the heat pipe axis is written as:

$$\Delta P_{\perp} = \rho_l \, g \, d_v \sin\psi \quad . \tag{2.4}$$

The inclination angle of the heat pipe, ψ (between +90°: evaporator bottom and -90°: evaporator top) is measured from a horizontal line.

In case of filling ratio higher than 100%, gravitational force (P_e) exerted excess liquid column with a height of h is included in Equation (2.1).

$$P_e = \rho_l \, g \, h \, . \tag{2.5}$$

The frictional coefficient for liquid flow is:

$$F_l = \frac{\mu_l}{K A_w \rho_l \lambda} \, . \tag{2.6}$$

And the frictional coefficient for vapor flow is:

$$F_v = \frac{(f_v \, Re_v) \, \mu_v}{2 \, r_{h,\,v}^2 \, A_v \, \rho_v \, \lambda} \quad . \tag{2.7}$$

For evaluating F_v, the value of ($f_v \, Re_v$) that depends upon flow conditions needs to be given. It is customary to specify the flow conditions by some non-dimensional quantities, namely, the vapor Reynolds number, Re_v, and the Mach number, M_v. These quantities, in the present notation, are defined as follows, respectively [8]:

$$Re_v = \frac{2 r_{h,\,v} \, Q}{A_v \, \mu_v \, \lambda} \, , \tag{2.8}$$

$$M_v = \frac{Q}{A_v \rho_v \lambda \sqrt{\gamma_v R_v T_v}} \ , \tag{2.9}$$

where γ_v is the specific heat ratio of vapor, which is equal to 1.67, 1.4, or 1.33 for monoatomic, diatomic, or polyatomic vapor, respectively [8], $r_{h,\,v}$ is hydraulic radius for vapor flow (m), Q is heat load (W), A_v is vapor core cross-sectional area (m^2), μ_v is vapor dynamic viscosity (Pa· s), λ is latent heat of vaporization (J/kg), ρ_v is vapor density (kg/m^3), R_v is gas constant for vapor (J/(kg·K)), and T_v is vapor temperature (K).

Under the circumstances of this experiment, as the values of Re_v and M_v are less than 2300 and 0.2, respectively, the vapor flow can be considered laminar and incompressible. For laminar flow the values of ($f_v Re_v$) needed for Equation (2.7) is a constant which can be equal to 16 for a circular vapor flow passage from the well know Hagen-Poiseuille's solution [8].

A key for proper operation of a heat pipe is the wick structure. A wick structure works as a flow path in which liquid flows from the condenser to the evaporator sections. Low flow resistance is desirable for the liquid flow. Therefore, the permeability of a wicking structure must be enough high. On the other hand, the capillary pumping pressure is generated by the wick. In order to have high capillary pumping pressure, wick structures with small pore sizes are desirable. The maximum capillary pumping pressure increases with decreasing the pore size. As the wick permeability decreases with decreasing the pore size, wick design will involve rather complicated trade-off processes.

2.5.2 Entrainment limit

Two phases of working fluid, liquid and vapor, coexist everywhere in a heat pipe. In the adiabatic section of a heat pipe, vapor flows to the condenser section through the vapor core region, and at the same time, liquid flows to the evaporator section through the wick structure.

These two flows in opposite directions to each other with a boundary on the free surface form a counter flow structure.

In this counterflow of liquid and vapor, viscous shear force interaction arises on the liquid–vapor interface. In the operation of a heat pipe, if the viscous shear force becomes larger than the liquid surface tension, droplets of liquid may be entrained into the vapor flow and flow towards the condenser section. At this point the entrainment limit has been reached. This back flow of liquid towards the condenser section causes liquid shortage in the evaporator section, and finally “dry-out” appears in the evaporator section. The dry-out described here means both partial (local) and total liquid depletion in the evaporator section, and results in a rapid temperature rise and finally in the failure of heat pipe operation. The mathematical expression for the entrainment heat transport limit is;

$$Q_{e,\,max} \quad = \quad A_v\,\lambda \left(\frac{\sigma\,\rho_v}{2\,r_{h,\,s}} \right)^{1/2} \quad . \tag{2.10}$$

As the surface tension of the liquid increases, it becomes more difficult to force the liquid to be entrained into the vapor flow. It is obvious that as the surface tension of fluid increases, so does the entrainment limit. The entrainment limit is usually effective in the adiabatic section of a heat pipe, where the relative flow velocity between the liquid and vapor become maximum.

2.5.3 Boiling Limit

The boiling limit is reached upon the onset of bubble formation in the wick structure of the evaporator section. In the evaporator section, it is assumed that nucleate boiling may occur during the evaporation process caused by strong heating. However, as the heat input further increases, the boiling state transfers from the nucleate boiling to the film boiling. The film boiling makes liquid difficult to return to the evaporator section, resulting in insufficient liquid flow to the evaporator section, and then dry-out spots appear in the wick structure. The mathematical expression for the boiling heat transport limit is;

$$Q_{b,\,max} \;=\; \frac{2\pi L_e\, k_e\, T_v}{\lambda\rho_v\, ln(r_i/r_v)}\left(\frac{2\sigma}{r_n}\right)\;. \tag{2.11}$$

To evaluate $Q_{b,\,max}$ defined by Equation (2.11), the value of r_n is necessary to be specified. For conventional heat pipes, which have been carefully processed so as to eliminate all non-condensable gases, a conservative approach would take the values of r_n equal to 2.54×10^{-7} m [8]. For the effective thermal conductivity of liquid-saturated wick, k_e, Maxwell [18] has derived an expression to give the thermal conductivity of such a heterogeneous material;

$$k_e \;=\; k_w\left[\frac{2+k_l/k_w-2\varepsilon(1-k_l/k_w)}{2+k_l/k_w+\varepsilon(1-k_l/k_w)}\right]\;. \tag{2.12}$$

Here, it is often pointed out that it strongly depends on the fluid properties.

2.5.4 Sonic limit

The sonic limit occurs when the vapor flow velocity approaches to the sonic velocity (equal to the speed of sound) resulting in a choked flow at the exit of the evaporator section. Under this choked flow condition, the mass flow rate no more increases. Therefore, the heat transfer becomes limited, and further increase of the heat flux becomes impossible. Unlike other limitations, the sonic limit does not cause an operation failure like the dry-out. It only limits the heat transfer capability of a heat pipe. In normal cases of the sonic limit further increase in the heat input results in the rise of the temperature of the heat pipe to increase the sonic velocity, which in turn increases the vapor mass flow rate. As the operating temperature decreases, the vapor pressure of the working fluid decreases. As a result, it is expected that the heat transport capability of the heat pipe under the sonic limit condition decreases with the decrease of the temperature. Therefore, the sonic limit is apt to occur at lower operating temperatures. The sonic limit appears in the entire heat pipe. The mathematical expression for the sonic heat transport limit is;

$$Q_{s,\,max} = A_v\,\rho_v\,\lambda \left[\frac{\gamma_v\,R_v\,T_v}{2(\gamma_v+1)}\right]^{1/2} . \tag{2.13}$$

For Equation (2.13) to be valid, there are some assumptions made:

- One dimensional flow is assumed.
- Frictional effects are neglected.
- It is assumed that the inertial effects dominate.
- Vapor flow is assumed to be an ideal gas flow.

Under the above assumptions, Equation (2.13) is derived on the basis of the equations of the conservation of energy and momentum. The details of the derivation of the expression can be found in Reference 8.

2.5.5 Viscous limit

The final limitation for the operation of heat pipes is the viscous limit. This limit is caused by the viscous pressure loss in vapor phase flow and the vapor pressure of the working fluid. The vapor pressure difference is the force that drives the vapor from the evaporator section to the condenser section. When the viscous loss in vapor phase becomes larger than the vapor pressure, then the vapor cannot be driven to the condenser section and the heat pipe cannot operate. This limit becomes effective at lower temperatures when the vapor pressure of the working fluid is very low. The mathematical expression for the viscous heat transport limit is;

$$Q_{v,\,max} = \frac{A_v\, r_v^2\, \lambda\, \rho_v\, P_v}{16\mu_v\, L_{eff}} \,. \tag{2.14}$$

The effect of the viscous limit appears in the whole sections of a heat pipe, as it depends on the vapor pressure difference between the evaporator and the condenser sections.

One of the five operating limits described above governs the heat pipe performance according to the working conditions and to the fluid properties, such as the operating temperature, and the wick structure properties. The transition points among these limits depend on the working fluid and wick structure. Table 2.3 shows the comparison of limitations of heat transport capabilities. It was found from this table that the capillary limit is overwhelmingly the lowest limitation of heat transport capabilities for nitrogen heat pipe at 77 K of operating temperature. For other working fluids, Ar and Ne, it has been confirmed that the magnitude of Q_{max}, and thus the order of the magnitude, does not change over their operating temperature range. Therefore, the capillary limit was used for the theoretical prediction of the maximum heat transport capability. Furthermore, the capillary limit is also the lowest limitation for all operating temperature ranges in case of neon (24–44 K), nitrogen (63–126 K), and argon (83–150 K). Thus, in this study, only the capillary limit was considered.

Table 2.3 *Variation of the maximum heat transport capability of nitrogen heat pipe with sintered powder copper as a wick structure and 77 K of operating temperature.*

Limitation	Equation	Max. Heat transport capability
Capillary	$Q_{c,\,max} = \dfrac{2\sigma/r_c - \Delta P_{\perp}}{\left(\dfrac{\mu_l}{KA_w\,\rho_l\,\lambda} + \dfrac{(f_v\ Re_v)\mu_v}{2\,r_{h,\,v}^2\,A_v\,\rho_v\,\lambda}\right)L_{eff}}$	12 W
Boiling	$Q_{b,\,max} = \dfrac{2\pi L_e\ k_e\ T_v}{\lambda\rho_v\ ln(r_i/r_v)}\left(\dfrac{2\sigma}{r_n}\right)$	292 W
Entrainment	$Q_{e,\,max} = A_v\,\lambda\left(\dfrac{\sigma\,\rho_v}{2\,r_{h,\,s}}\right)^{1/2}$	60 W
Sonic	$Q_{s,\,max} = A_v\,\rho_v\,\lambda\left[\dfrac{\gamma_v\,R_v\,T_v}{2(\gamma_v+1)}\right]^{1/2}$	994 W
Viscous	$Q_{v,\,max} = \dfrac{A_v\,r_v^2\,\lambda\,\rho_v\,P_v}{16\mu_v\,L_{eff}}$	350949 W

2.6 Other Types of Heat Pipes

There are many types of heat pipes, which offer great flexibility in their design and capabilities. There are various sizes of heat pipes from as small as the range of micrometer (micro heat pipe) to a size as large as the range of meter. Every heat pipe has an evaporator section and a condenser section, where working fluid evaporates and condenses. Many heat pipes also have an adiabatic section, where there is no heat in or out, located between an evaporator section and a condenser section. Multiple evaporators, condensers and adiabatic sections can be designed in some heat pipes. The capillary force developed in a wick function to circulate the working fluid. However, it is also possible to use gravitational, centrifugal, electrostatic, or osmotic forces to return fluid from a condenser section to an evaporator section.

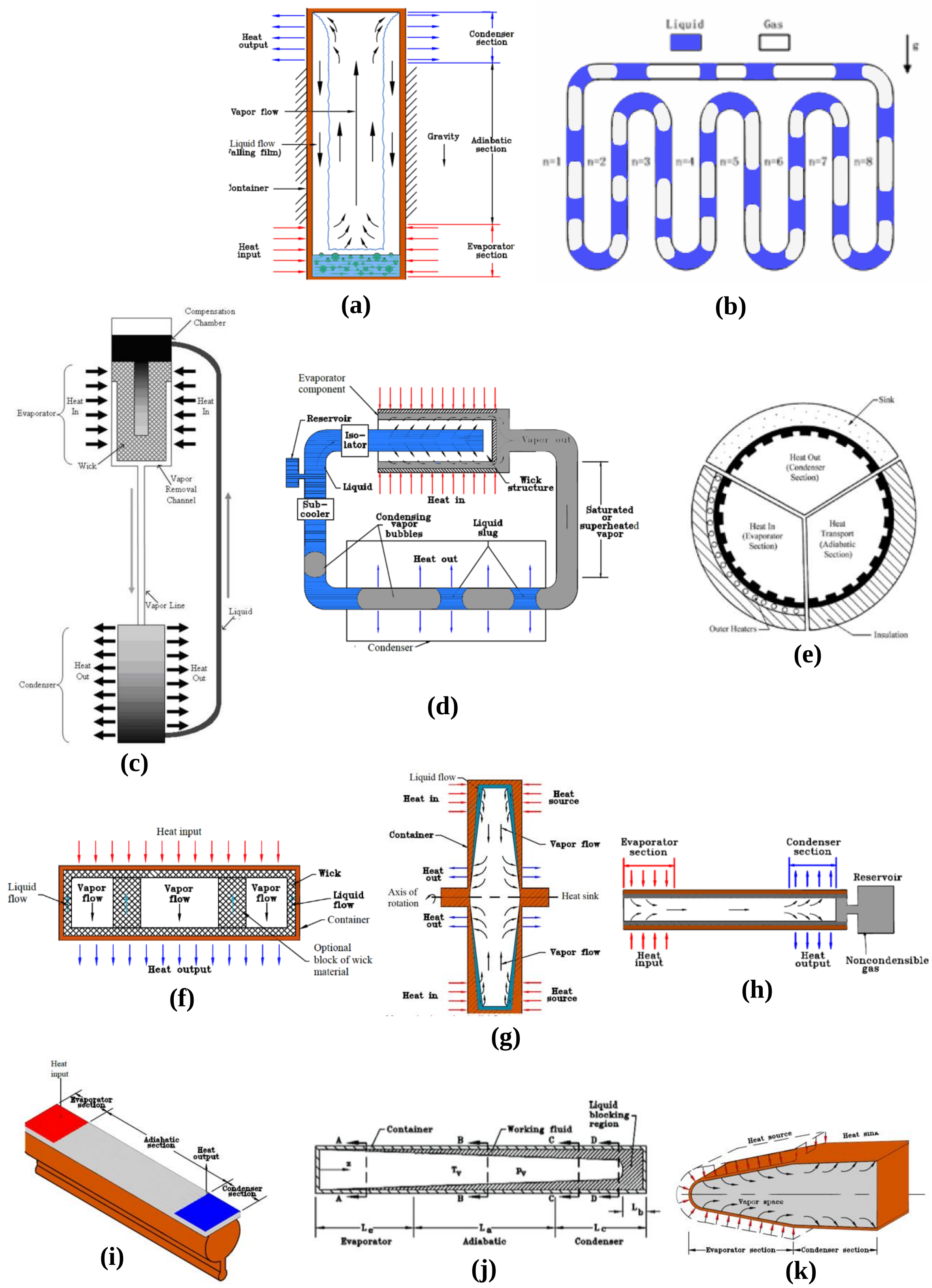

Figure 2.6 *Several different types of heat pipes [14]; (a) Thermosyphon, (b) Pulsating heat pipe, (c) Loop heat pipe, (d) Capillary pumped loop heat pipe, (e) Annular heat pipe, (f) Vapor chamber, (g) Rotating heat pipe, (h) Gas-loaded heat pipe, (i) Monogroove heat pipe, (j) Micro and miniature heat pipes, (k) Leading-edge heat pipe.*

A heat pipe container is usually circular in shape for convenience of design and fabrication. Other shapes have nevertheless been investigated, such as flat heat pipes, conical heat pipes (rotating heat-pipes), and flexible corrugated heat pipes. Possible or existing types of heat pipes are listed below;

- Two-phase closed thermosyphon
- Pulsating heat pipe
- Loop heat pipe
- Capillary pumped loop heat pipe
- Annular heat pipe
- Vapor chamber
- Rotating heat pipe
- Gas-loaded heat pipe
- Mono-groove heat pipe
- Micro and miniature heat pipes
- Leading-edge heat pipe

Various types of heat pipes with their performance characteristics are described below.

2.6.1 Two-phase closed thermosyphon

A two-phase closed thermosyphon, shown in Figure 2.6(a), is a gravity-assisted wickless heat pipe [19]. A condenser section is located above an evaporator section so that the condensate liquid of working fluid can return by gravity. The sonic, vapor pressure or entrainment limits are the constraints on the operation of a thermosyphon as with capillary driven heat pipes. The entrainment limit is more profound in the thermosyphon than in conventional heat pipes due to the phenomenon related to liquid free surface. The counterpart of the entrainment limit in thermosyphons is sometimes called flooding [19], which is the most severe limitation in the operation. Sudden oscillation in the wall temperature and vapor pressure rise will occur due to the flooding limit. The boiling limit in thermosyphons is attributable to the occurrence of film boiling instead of nucleate boiling. Once vapor film is formed between the pipe wall of a thermosyphon and the liquid in the evaporator section, the boiling limit of the thermosyphon may occur. For a small filling ratio of working fluid, the dry-out limit will be apt to occur, where all the working fluid is kept in the form of liquid film and thus there is no liquid pool that should be formed in the evaporator section. In this case, any further increase in the heat input will cause rapid increase in the temperature at the bottom part of the evaporator section. The operation of the thermosyphon highly depends on the filling ratio of the working fluid. It has been demonstrated experimentally for thermosyphons without wick structure that the maximum heat transport capability increased when the filling ratio of the working fluid increased up to a certain value. In some designs of thermosyphons, a wick structure is lined to delay flooding and to enhance the affinity between the wall and the liquid. In general, for the thermosyphon the capillary limit need not be considered as gravity is the main driving force for condensate liquid return.

2.6.2 Pulsating heat pipe

The pulsating heat pipe (PHP), Figure 2.6(b), is made from a long capillary tube bent into many turns, with the evaporator and condenser sections located in these turns [3]. The successful operation of the PHP has been demonstrated experimentally when working fluid is partially charged with the filling ratio between 40% and 60% of the total interior volume of the tube [14]. Since the diameter of a PHP is very small (usually less than 5mm) [20], vapor plugs and liquid slugs are formed as a result of capillary action. Heat added to the evaporator section causes evaporation or boiling of working fluid, which increases the vapor pressure in the heating section. At the same time, the pressure in the cooling section decreases due to condensation. The liquid slugs and vapor plugs are driven to the cooling section by the pressure difference. The liquid slugs and vapor plugs remained in the cooling section are then driven to the next heating section, which will drive the liquid slugs and vapor plugs to return to the cooling section again. This process causes the oscillating motion of liquid slugs and vapor plugs, and accordingly heat is transported from the heating section to the cooling section by the pulsative motion of the working fluid in the axial direction of the tube. In contrast to conventional heat pipes (the type of heat pipe in this research), the characteristics of PHPs are that there is no wick structure to return the condensate liquid to the heating section. Therefore, there is no countercurrent flows between the liquid and vapor. There is no need to consider the entrainment limit in case of the PHP. Additionally, the PHP weight is less than that of a conventional heat pipe, making it an excellent candidate for a heat transfer device in space applications. Since the diameter of the PHP is very small, the surface tension plays a greater role than the gravitational force, allowing operating in a microgravity environment.

2.6.3 Loop heat pipe

The loop heat pipe (LHP) [1, 21], Figure 2.6(c), was invented in Russia in 1971 by Gerasimov and Maydanik [22]. Operation of the LHP is based on the same physical processes of evaporation and condensation as conventional heat pipes. The LHP consists of a capillary pump (or evaporator), a compensation chamber (or reservoir), a condenser, and liquid and vapor lines. The wicks are only present in the evaporator and the compensation chamber. The high capillary force is created in the evaporator due to fine-pored wicks (primary wicks) such as sintered nickel, titanium, and copper powder with an effective pore radius of 0.7–15μm and a porosity of 55–75% [14]. The compensation chamber (CC) that is an important component in the LHP, is connected to the evaporator. In normal operation, the CC is designed to handle excess liquid in the LHP. A secondary wick (usually with larger pores) is in the position to physically connect the evaporator and the CC in order to supply liquid from the CC to the primary wick when operated under microgravity condition or when CC is located below the evaporator section. Heat input to wall of the evaporator section causes the working fluid to vaporize into the vapor line. The vapor is collected by a system of grooves and headers, and flows down to the condenser section, and condenses in the condenser section. The condensate collects at the bottom of the small annulus in the condenser section by gravity and/or capillary action. The vapor pressure of the working fluid forces this condensate up the central pipe where condensate refills the CC. Both the liquid and vapor lines are made of small diameter wickless tube, and thus LHPs can be made flexible and bendable. LHPs provide only very small temperature difference over long distance without sensitivity to gravity. Several factors make the LHP to be desirable for spacecraft applications. Since the wick structure is present only in the evaporator section, the tube walls of vapor and liquid lines can be smooth, which reduces the pressure loss in the vapor and liquid flows. The pressure drops throughout the system are also reduced because the vapor and liquid flow are co-current.

2.6.4 Capillary pumped loop heat pipe

The capillary pumped loop heat pipe (CPL) [1], Figure 2.6(d), was first proposed by Stenger in 1966 at the NASA Lewis Research Center. The evaporator section consists of a hollow rod of wick material capped at one end that is force fitted into an internally axially grooved pipe. Heat applied to the outer surface of the evaporator vaporizes the liquid working fluid, which then travels down the length of the axially grooved vapor channels and then into the vapor header. The vapor flows to the condenser section, where it condenses first in a form of film on the inner wall of the pipe and flows back to the evaporator section forming a liquid slug. Before reaching the evaporator section, the liquid passes through a sub-cooler in order to collapse any remaining vapor bubbles. The capillary pressure generated in the wick structure continuously pumps the working fluid through the loop. For the fundamentals of both CPL and LHP, some confusion still exists regarding their similarities and distinctions in operation, as well as the limitations of these two devices.

2.6.5 Annular heat pipe

The annular heat pipe, Figure 2.6(e), is almost similar to the conventional heat pipe. The main difference is that the cross-section of the vapor space in an annular heat pipe is annular instead of circular, [19, 23]. This allows the design of wick structure both on the inside of the outer pipe and on the outside of the inner pipe. In fact, the surface area for heat input and output can be significantly increased without increasing the outer diameter of the pipe. Therefore, annular heat pipes offer greater efficiency, in terms of heat transfer rate per cross-sectional area, but can be more difficult to manufacture compared with conventional heat pipes.

2.6.6 Vapor chamber

The vapor chamber, Figure 2.6(f), is a kind of a capillary-driven planar heat pipe (flat-plate heat pipe in a rectangular or disk shape) with a small aspect ratio [1, 24–26]. When the condenser section is below the evaporator section in a gravity field, additional wick block is required between the evaporator section and the condenser section to assist condensate return. However, if the condenser is above the evaporator, there is no need to provide a wick in the condenser section. In order to uniformly distribute the liquid over the entire surface to avoid dry-out, a wick is necessary over the evaporator section. Since heat flow is two- or three-dimensional, the vapor chamber is an excellent candidate for use in electronic device cooling applications, especially with high heat flux applications. Vapor chambers can be placed in direct contact with CPUs using heat transfer enhancement agents between them, thus can reduce the overall thermal resistance of heat sinks.

2.6.7 Rotating heat pipe

Rotating heat pipes [27], Figure 2.6(g), operate by using centrifugal force to return liquid to the evaporator section rather than by gravitational forces or capillary forces. There are two designs of rotating heat pipes: a cylinder and a disk shape. Cylindrical rotating heat pipes have been used to cool the rotating parts of electric motors and metal-cutting tools such as drill bits, and end mills [14]. Disk-shaped heat pipes have been proposed to effectively cool turbine components and automobile brakes [14].

2.6.8 Gas-loaded heat pipe

The gas-loaded heat pipe, Figure 2.6(h) is a type of variable conductance heat pipe [28]. Some amount of noncondensing gas is introduced into the vapor space, and it will expand and contract depending on the pressure and temperature. This action limits the surface area in which the working fluid vapor can contact the condenser, preventing it from transferring heat through some part of the condenser where non-condensing gas occupies. This phenomenon can allow these heat pipes to maintain a nearly constant evaporator temperature regardless of the heat input. Gas-loaded heat pipes are also used in applications that require precise amounts of heat to be transferred either in or out [12].

2.6.9 Monogroove heat pipe

The monogroove heat pipe developed by Grumman, Figure 2.6(i), utilizes a pipe with extruded cross section which can separate the vapor space from the liquid return path [29, 30]. Heat input and output are through the flat face on top of the vapor space. Since heat is not conducted across the wall with wick structure for the liquid return path, the chance of arterial blockage due to vapor bubbles is significantly reduced. Wick structure is placed along the interior surface to deliver condensate from the artery to the evaporator. Monogroove heat pipes are proposed to be used for multi-kilowatt space radiator heat rejection systems [14].

2.6.10 Micro and miniature heat pipes

The micro heat pipe, Figure 2.6(j), is defined as heat pipes in which the mean curvature of the liquid–vapor interface is comparable in magnitude to the reciprocal radius of the vapor flow channel [31–34]. In micro heat pipes the hydraulic diameter is 10–500 μm, while miniature heat pipes have hydraulic diameters ranging from 0.5 to 5 mm [35]. These heat pipes are used in nano- and micro-scale applications [12].

2.6.11 Leading-edge heat pipe

The leading-edge heat pipe, Figure 2.6(k), is proposed for applications such as hypersonic aircraft and reentry spacecraft leading edge cooling [36]. Leading-edge heat pipes must be designed geometrically for their specific application. For aircraft applications, the heat pipe must be shaped into the geometry of a leading edge of a wing, while for a spacecraft it takes the form of a heatshield between the capsule and the atmosphere [12].

2.7 References

[1] A. Faghri, Heat Pipe Science and Technology, Washington, D.C.: Taylor & Francis, 1995.

[2] J. Perkins, "Steam-engines; generating steam; evaporating and boiling fluids for certain purposes". UK Patent 7059, 12 April 1836.

[3] R. S. Gaugler, "Heat transfer device". US Patent 2350348A, 6 June 1944.

[4] L. Trefethen, "On the Surface Tension Pumping of Liquids or a Possible Role of the Candlewick in Space Exploration," *G.E. Tech. Info., Serial No. 615 D114.,* 1962.

[5] G. M. Grover, T. P. Cotter and G. F. Erickson, "Structures of Very High Thermal Conductance," *Journal of Applied Physics,* vol. 35, no. 6, 1964.

[6] G. M. Grover, "Evaporation-Condensation Heat Transfer Device". US Patent 3229759A, 18 January 1966.

[7] T. P. Cotter, Theory of Heat Pipes, Los Alamos Scientific Laboratory Report No. LA-3246-MS, 1965.

[8] S. W. Chi, Heat pipe theory and practice, United States: Hemisphere, 1976.

[9] P. Dunn and D. A. REAY, Heat pipes, Oxford: Pergamon Press Ltd., 1982.

[10] B. Zohuri, Heat Pipe Design and Technology, AG Switzerland: Springer Nature, 2016.

[11] D. A. Reay, P. A. Kew and R. J. McGlen, Heat Pipes Theory, Design and Applications, Oxford: Elsevier Ltd., 2014.

[12] F. A. Kulacki, "Heat Pipes and Thermosyphons," in *Handbook of Thermal Science and Engineering,* Switzerland, Springer International Publishing AG , 2018, pp. 2166-2204.

[13] W. G. Anderson, R. W. Bonner, P. M. Dussinger, J. R. Hartenstine, D. B. Sarraf and I. E. Locci, "Intermediate temperature fluids life tests - Experiments," in *5th International Energy Conversion Engineering Conference,* St. Louis, Missouri, 2007.

[14] A. Fahgiri, "Heat Pipes, Review, Opportunities and Challenges," *Frontiers in Heat Pipes (FHP),* vol. 5, no. 1, pp. 1-48, 2014.

[15] L. Poplaski, S. Benn and A. Faghri, "Thermal performance of heat pipes using nanofluids," *International Journal of Heat and Mass Transfer,* vol. 107, pp. 358-371, 2017.

[16] A. Faghri, Heat pipe science and technology, Columbia, Missourie: Global Digital Press, 2016.

[17] G. P. Peterson, An Introduction to Heat Pipes, Testing and Applications, New York: John Wiley & Sons, 1994.

[18] G. A. Asselman and D. B. Green, "The heat pipe - an applied technology," *Philips Technical Review,* p. 169–186, 1972.

[19] A. Faghri, M. M. Chen and M. Morgan, "Heat Transfer Characteristics in Two-Phase Closed Conventional and Concentric Annular Thermosyphons," *Journal of Heat Transfer,* vol. 111, no. 3, pp. 611-618, 1989.

[20] A. Faghri and Y. Zhang, "Advances and Unsolved Issues in Pulsating Heat Pipes," *Heat Transfer Engineering,* vol. 29, no. 1, pp. 20-44, 2008.

[21] Y. F. Maydanik, "Loop heat pipes," *Applied Thermal Engineering,* vol. 25, no. 5-6, pp. 635-657, 2005.

[22] Y. F. Maydanik, Y. G. Ferchtater and K. A. Goncharov, "Capillary Pump Loop for the systems of Thermal Regulation of Spacecraft," in *4th European Symposium on Space Environmental Control Systems,* Florence, Italy, 1991.

[23] A. Faghri and S. Thomas , "Performance Characteristics of a Concentric Annular Heat Pipe: Part I—Experimental Prediction and Analysis of the Capillary Limit," *Journal of Heat Transfer,* vol. 111, no. 4, pp. 844-850, 1989.

[24] M. Mochizuki, Y. Saito, F. Kiyooka and T. Nguyen, "High Power Cooling Chips by Heat Pipes and Advanced Heat Spreader," in *8th International Heat Pipe Symposium,* Kumamoto, Japan, 2006.

[25] M. Mochizuki, T. Nguyen, Y. Saito, F. Kiyooka and Wuttijumnong, V, "Advanced micro-channel vapor chamber for cooling high power processors," in *Proceedings of the ASME InterPack Conference, IPACK 2007,* Vancouver, Canada, 2007.

[26] B. Xiao and A. Faghri, "A three-dimensional thermal-fluid analysis of flat heat pipes," *International Journal of Heat and Mass Transfer,* vol. 51, no. 11-12, pp. 3113-3126, 2008.

[27] V. H. Gray, "The Rotating Heat Pipe—A Wickless, Hollow Shaft for Transferring High Heat Fluxes," in *Proceedings of ASME/AIChE Heat Transfer Conference,* Minneapolis, MN, 1969.

[28] C. Harley and A. Faghri, "Transient Two-Dimensional Gas-Loaded Heat Pipe Analysis," *Journal of Heat Transfer,* vol. 116, no. 3, pp. 716-723, 1994.

[29] J. Alario, R. Haslett and R. Kosson, "The Monogroove High Performance Heat Pipe," in *AIAA 16th Thermophysics Conference,* Palo Alto, CA, 1981.

[30] J. P. Alario, "Monogrove Heat Pipe Radiator Shuttle Flight Experiment: Design, Analysis, and Testing," in *Proceedings of the 14th Intersociety Conference on Environmental systems*, San Diego, CA, 1984.

[31] T. P. Cotter, "Principles and prospects for micro heat pipes," in *Proceedings of 5th international heat pipe conference*, Tsukuba, Japan, 1984.

[32] G. P. Peterson, "Overview of micro heat pipe research and development," *Applied Mechanics Reviews*, vol. 45, no. 5, p. 175–189, 1992.

[33] Y. Cao and A. Faghri, "Micro/Miniature Heat Pipes and Operating Limitations," *Journal of Enhanced Heat Transfer,* vol. 1, no. 3, pp. 265-274, 1994.

[34] D. Khrustalev and A. Faghri, "Thermal Analysis of a Micro Heat Pipe," *Journal of Heat and Mass Transfer,* vol. 116, no. 1, pp. 189-198, 1994.

[35] R. Hopkins, A. Faghri and D. Khrustalev, "Flat Miniature Heat Pipes with Micro Capillary Grooves," *Journal of Heat Transfer,* vol. 121, no. 1, pp. 102-109, 1999.

[36] Y. Cao and A. Faghri, "Conjugate Modeling of High-Temperature Nosecap and Wing Leading-Edge Heat Pipes," *Journal of Heat Transfer,* vol. 115, no. 3, pp. 819-822, 1993.

Chapter 3
LITERATURE REVIES

Literature review is important to understand the state of the art of heat pipes and to find the knowledge gap so that the author can define the scope of the research and think more deeply about the experimental results. In this chapter, literature review on the recent cryogenic heat pipes will be presented.

3.1 Commercially Available Heat Pipes

Cooling fans and/or fin heat sink had been used for the cooling of CPUs in desktop or laptop computers. However, for the demand of higher performance CPUs, which generate larger heat, fans or heat sinks may not become adequate. Additionally, space for heat sink and dissipation is limited in many laptops. Even though large space is unavailable, it is required to use a larger fin heat sink and a fan and also higher air-cooling device. Satisfying these requirements would result in noise generation, reducing reliability and demand for higher power consumption for fan. To solve these problems, the use of heat pipes was considered, as heat pipes can transport larger amount of heat with a very small temperature drop.

Thang Nguyen, Masataka Mochizuki et al. [1–3] introduced miniature heat pipes (conventional type of heat pipes) for the thermal management of high-performance CPUs. The miniature heat pipe was designed and fabricated by Fujikura Ltd. It has a diameter of 3–6 mm and a length of 100–300 mm. They developed three heat pipe-based cooling systems as follows;

Heat pipe with heat spreader plate: Commonly a heat pipe is used to reject heat from a CPU to an aluminum plate placed under a keyboard or on a chassis of a laptop.

Hybrid system: A combination of a heat pipe, a channel plate aluminum heat sink and a fan.

Hinged heat pipe system: It consists of two heat pipes and a hinge connector. The primary heat pipe is fixed in contact with a heat source (CPU), transferring heat to the secondary heat pipe via a hinge connector that thermally joins the two heat pipes together. The secondary heat pipe is used to transfer heat to an aluminum heat spreader plate. The connector conducts heat from the primary to secondary heat pipes, and also allows the secondary heat pipe to rotate when opening and closing the laptop cover.

The test result shows that it is capable to dissipate 10–12 W of heat generated from the CPU while maintaining its surface temperature at lower than 95 °C.

Recently, heat pipes which were designed to operate at room temperature by using water as a working fluid are commercially available, which were used in this study. In this study, the operation of the commercially available heat pipes was examined at cryogenic temperatures by using nitrogen, argon or neon as a working fluid. If they can well operate at cryogenic temperatures, it will be possible to avoid new special design and fabrication exclusively for cryogenic heat pipes that cost high. Additionally, the quality and the performance of commercially available heat pipes are uniform due to mass production, and they are readily available at cheap price.

3.2 Design of Evaporator and Condenser Lengths

Xiao Ping Wu [4] analyzed the optimized L ratio (L_e / L_c), that is the ratio of the lengths of evaporator section to condenser section for miniature heat pipes. The analysis result on miniature heat pipes with 4 mm to 6 mm of diameter, which are quite frequently used in heat piped heat sink applications, showed that the optimal L ratio was between 0.3 and 0.6. Larger diameter heat pipes result in smaller optimal L ratio. Larger diameter of a pipe can provide larger evaporation area, which results in that the vaporization thermal resistance decreases thus the condenser length should be increased for balancing.

In the present study, the evaporator and condenser lengths were set to 30 mm and 65 mm, respectively. Therefore, the resulting L ratio is 0.46 that was just in the optimum range between 0.3 and 0.6 suggested in the above study. In the preliminary study phase of the present cryogenic heat pipes, 15 mm of the evaporator length was adopted, and later it was changed to 30 mm in order to investigate the performance change with the variation of the evaporator length. It was considered that the maximum heat transport capability of the heat pipe tested in this study was governed by the capillary limit that does, in principle, not depend on the evaporator length. Therefore, the variation in the evaporator length, 15 mm, or 30 mm, may cause little variation in the performance of the cryogenic heat pipe.

3.3 Effects of Wick Structures, Inclination Angle and Filling Ratio

Loh et al. [5] compared the thermal performances of heat pipes caused by the change in the wick structure at various inclination angles. The mesh, groove, and sintered powder wick structures were investigated in their experiment. The physical dimensions of the heat pipe were 200 mm in length and 6 mm in diameter, and water was used as a working fluid. In each test, the inclination angle was varied from +90˚ (the evaporator is right below the condenser section) to -90˚ (the evaporator is right above the condenser section) and the heat load was varied between 5–35 W. It was found that the heat source position and gravity (the inclination angle) have less effect on the sintered powder metal wicked heat pipes due to the fact that this wick produces the strongest capillary action. It was also suggested that grooved or mesh heat pipes were not desirable to use in the orientation of the evaporator above the condenser section. However, the grooved heat pipe had better thermal performance than mesh and sintered powder metal heat pipes in the inclination angle range of +90˚ to 0˚ (horizontal).

Mozumder et al. [6] fabricated and tested a miniature heat pipe using a copper tube of 5 mm in diameter and 150 mm in length with a heat transfer capability of 10 W. Experiments were conducted with and without working fluid for different thermal loads to assess the thermal performance of the heat pipe. The heat pipe was filled with working fluid of 35, 55, 85 and 100% of the evaporator volume and tested for different heat inputs and working fluids. It should be noted that this definition of the filling ratio is different from that in the present study, as described later. The working fluids chosen for the study were those commonly used ones, namely, water, methanol, and acetone. In cases of water and methanol as a working fluid, it was observed that the maximum value of the heat transfer coefficient, or the minimum value of the thermal resistance, appeared at 85% filling ratio. Tests at lower or higher filling ratio than 85% resulted in lower values of the heat transfer coefficient, or higher values of the thermal resistance than those at 85%. So, it can be simply stated that the thermal performance of water miniature heat pipes is best at 85% filling ratio. In case of acetone as a working fluid, it was clear that at higher filling ratios an acetone miniature heat pipe performed well showing higher values of the heat transfer coefficient, or lower values of the thermal resistances. For lower filling ratios the performance degraded if acetone was used as a working fluid.

Since the thermophysical properties of cryogenic fluids are quantitatively different from those of water, the fundamental experiments were conducted in this study also to test the effects of different wick structures and the inclination angle in the cryogenic temperature range by using neon, nitrogen, and argon as a working fluid.

3.4 Cryogenic Heat Pipes

Dudheker [7] studied a cryogenic heat pipe made of stainless steel with 845 mm in length and 19 mm in diameter equipped with modacrylic fiber wick and using nitrogen as a working fluid. The experiment was conducted to study the operating characteristics of a cryogenic heat pipe such as the effective thermal conductivity and the axial temperature distribution for various levels of power input, which were compared with those of a copper rod. The effect of the inclination angle on the performance was also examined. It was found from the experiment in case of horizontal heat pipe installation that the effective thermal conductivity was approximately 8 times larger than that of copper and increased to 20 times larger than that of copper (≈ 400 W/(m·K)) for the case of 5.25˚ inclination angle with the evaporator below the condenser. However, as the angle of inclination increased with the orientation of the evaporator above the condenser the effective thermal conductivity decreased and so did the maximum heat transport capability.

M.S. Muniappan and A.S. Muniappan [8, 9] studied the thermal performance of cryogenic grooved heat pipes of 180 and 300 mm in length and 12.72 and 15.5 mm in diameter using nitrogen or oxygen as a working fluid. The wick structures were the combination of stainless-steel wire mesh (4 layers) and trapezoidal grooves (17 grooves). It was found the performance of the heat pipe that was evaluated in terms of the effective thermal conductivity was 3 times improvement over simple conduction cooling such as by using a solid copper rod at 100 K.

It was decided on the basis of these previous research results that in the present study the sintered copper powder and groove combination wick structure was adopted due to its high capillary force and low flow resistance, which would lead to the improvement of the thermal performance.

3.5 For Expanding Operating Temperature Range

For expanding the operating temperature range, there are two possible approaches to cope with some difficulties. One way is to fill a mixture of different working fluids into a single heat pipe. It was once considered that a mixture working fluid could expand the heat pipe operation temperature range, wider than that of a single-fluid heat pipe. However, many works have proved that the heat pipes with mixed working fluid could not work if there were no overlapping operational temperature ranges of the components [10] or they could not work better if the difference in the critical temperatures of the components was too large [11]. The other approach is to use separate heat pipes with different working fluids so as to form a parallel heat pipe system, though this approach still has some limitations on the method of applications, especially in the cases of ultra-low temperature, in which the systems need to be compact, and the space is limited for complex structures. The latter approach will be pursued in this study.

3.5.1 Mixed working fluids

Z.Q. Long and P. Zhang [12] investigated the heat transfer performance of a cryogenic thermosyphon with N_2-Ar binary-mixture as a working fluid. They found that this cryogenic thermosyphon could work in the range of 64–150 K. The dry-out limit was apt to occur in cases of small Ar molar fractions (smaller than 0.503), and the heat transfer limit of this cryogenic thermosyphon increased with the increase of Ar molar fraction. It may be concluded that the presence of Ar in the working fluid can enhance the heat transfer limit of the cryogenic thermosyphon. The further increase of the heat transfer limit is suppressed at a nearly constant value about 156 W by the onset of film boiling of LN_2 in the evaporator section in the case of the Ar molar fraction of 0.503 or higher.

Brice Felder et al. [13] developed a cryogenic thermosyphon by using helium-neon as a mixture of working fluid for the cooling system of a Gd-Bulk HTS synchronous motor. Jisung

Lee et al. [11] investigated the transient heat transfer behavior and examined the cool-down time from 300 K to 50 K of a cryogenic thermosyphon by using N_2-CF_4 as a mixture working fluid. Kenneth M. Armijo and Van P. Carey [14] investigated the performance characteristics of a gravity/capillary driven heat pipe using a water-alcohol mixture as a working fluid. T. Kiatsiriroat et al. [15] tested the thermosyphons using a mixture working fluid, ethanol-water and TEG-water, to work at the temperatures between 50–225 °C.

3.5.2 Parallel thermosyphon

Prenger F.C. et al. [16] investigated various cryogenic heat pipe combinations acting as cryocooler thermal shunts used to shorten the cool-down time. Their copper cryogenic heat pipe was the thermosyphon with 300 mm in length 13 mm in outer diameter. The working fluids were ethane, nitrogen, and oxygen (one working fluid for one heat pipe). During cool-down the heat pipes act as thermal shunts connecting the cooling load and the first stage of the cryocooler. The heat removed from the load which was mechanically attached to the second stage was thermally shared by the first and second stages of the cryocooler. As the load temperature continued to decrease and then fell below the triple point of the one of heat pipe working fluids, the heat pipe became inoperable as the working fluid froze, and thermally disconnecting the load from the first stage of the cryocoolers. From this investigation, they concluded that oxygen heat pipe had a wider operating temperature range (60–155 K) and greater transport capability compared with nitrogen one. Thus, an oxygen heat pipe was selected to operate with an ethane heat pipe (in parallel) as a thermal shunt between the first and second stages of the cryocooler system.

Prenger F.C. et al. [17] also presented some results of prototype heat pipe shunts using oxygen and ethane for cooling down in a temperature range from 300 to 60 K. The test results were in good agreement with the predictions by the Los Alamos National Laboratory (LANL) heat pipe model. The analysis of the system performance predicted that the cool-down time could be reduced by nearly a factor of two. In the present study, the parallel heat pipe system, which consisted of single Ne-, N_2-, and Ar-heat pipes, were examined, which was to be used for a conduction-cooled superconducting magnet in the temperature range from 300 to 24 K.

3.6 Heat Pipes for Superconducting Magnet Cooling Application

Kyohei Natsume et al. [18–21] successfully developed and demonstrated a cryogenic oscillating, OHP, (or pulsating, PHP) heat pipe for the conduction cooling of high-T_c superconducting (HTS) magnets. The cryogenic oscillating heat pipe was made of stainless-steel tube with 1.59 mm (1/16 in.) in outer diameter and 0.78 mm in inner diameter. The working fluids tested in the research were hydrogen (H_2), neon (Ne) and nitrogen (N_2), of which operating temperature ranges were 17–27, 26–34, and 67–91 K, respectively. The heat pipes were set at the inclination angles of -90˚ to +90˚. They got the results from the experiments that the effective thermal conductivities were 500–3500 W/(m K) (H_2), 1000–8000 W/(m K) (Ne) and 5000–18000 W/(m K) (N_2), respectively. They concluded that it was possible to dramatically improve the cooling performance of HTS magnets by using cryogenic OHPs.

Luis Diego Fonseca et al. [22] investigated a cooling system using a pulsating heat pipe (PHP) for the cooling of low temperature superconducting magnets. The PHP using helium as a working fluid was operated at 4.2 K. It was made of stainless steel having inner and outer diameters of 0.5 mm and 0.8 mm, respectively. The length of the PHP was 332 mm with 32 U-shaped bends at each end and it has 64 straight sections (total 21.25 m). The results showed that the He-PHP had the thermal conductivity of 2457 W/(m K) with the optimum filling ratio of 25.35%.

Seokho Kim et al. [23] fabricated and tested a contractible heat pipe to be used to connect the first and the second stages of a cryocooler to reduce the cool-down time of a conduction-cooled superconducting magnet. The function of the contractible heat pipe was the ON/OFF operation of the thermal connection between the first and the second stages of the cryocooler.

Philip E. Blumenfeld et al. [24] developed a cryogenic heat pipe to be used as thermal intercepts between the conventional and HTS sections, which was a unique feature of the Superconductivity Technology Center (STC) at LANL on the Current Lead Test Facility (CLTF). The development of this facility was planned in two phases: Phase one supported the tests at the electric current up to 200 A, and in the phase two the current capacity was increased to 1000 A. In both test phases, low voltage (less than 10 V) were supported. The working fluid was nitrogen, which was charged in the heat pipe at a pressurized state up to 2000 psig at room temperature. The warm end temperature of the HTS lead was variable from 65 K to over 90 K by controlling the heat pipe evaporator temperature. The cold end temperature was variable up to 30 K.

Daniel W. Kwon et al. [25] investigated an operation of high temperature superconducting (HTS) coil in space. In their research, the heat pipe, 86 cm long and 4 cm pipe diameter, using nitrogen as a working fluid and a stainless-steel mesh as the wick structure was used in a cryogenic thermal control system to maintain the wire temperature below the critical temperature, of which condition must be maintained over the entire Electromagnetic Formation Flight (EMFF) coil, for cooling the HTS wire to carry a large current at low power. For commercially available HTS wire, the critical temperature is 110 K.

A. Yamamoto et al. [26] have successfully developed the MgB_2 superconducting solenoid for the klystron beam focusing and demonstrated the performance of the central field of 0.8 T, operated at a temperature range of 20 ~ 25 K at the AC-plug power of < 3 kW. It may extend to a large-scale application, enabling an overall power saving of ~100 MW for 5000 klystron operation. In this operating temperature range, a neon heat pipe may be suitable applying to the cooling system to achieve the purpose above.

The recent studies of cryogenic heat pipes, which are cited from the journal of Cryogenics, are summarized in Table 3.1. Cryogenic pulsating heat pipes were mostly investigated for low temperature engineering applications. They are easy to fabricate due to wickless structure, and present extremely good heat spreading performance due to large heat transfer areas in the evaporator and condenser sections. However, for successful start-up of a cryogenic pulsating heat pipe, it should be ensured that enough amount of liquid remains in the evaporator section during the start-up phase, otherwise it is possible that liquid cannot be supplied from the condenser to the evaporator sections due to high vapor pressure. Additionally, since there is no wick structure inside, cryogenic pulsating heat pipes may not be able to operate under microgravity condition in case when all liquid occupies the condenser section only.

The heat pipes tested in this study are very small in size so that they can be used in any limited space and are easy for assembly. Also, because of the wick structure inside, they can operate even in microgravity condition.

Table 3.1 *Summary of studies in cryogenic heat pipe*

Author	**Year**	**Type**	**Wick**	**Wall Material**	**Dimension (mm)**	**Working fluid**	**Operating Temp. (K)**	**Q_{max} (W)**	**Note**
X. Sun, et al. [27]	2020	Pulsating heat pipe	-	Copper (Evap. & Cond.) Stainless Steel (Adia.)	L_e = 55 L_a = 500 L_c = 55 D_o = 3.3 D_i = 2.3	H_2	19	5.5	Effect of number of turns
H. Cho, et al. [28]	2020	Loop heat pipe	Sintered nickel wick	Stainless Steel	L_e = 75 L_c = 70 D_o = 18.6 D_i = 16.57, L_a = 680 D_o = 3.175 D_i = 1.755	N_2	90-100	12.17	
M. Li, et al. [29]	2019	Pulsating heat pipe	-	Stainless Steel	L_e = 50 L_a = 100 L_c = 50 D_o = 0.8 D_i = 0.5	He	4.2	1.2	Effect of filling ratio and orientation
X. Sun, et al. [30]	2019	Pulsating heat pipe	-	Copper (Evap. & Cond.) Stainless Steel (Adia.)	L_e = 55 L_a = 500 L_c = 55 D_o = 3.3 D_i = 2.3	H_2	19, 21, 23	5.5	Pulsating heat pipe with two turns

Author	**Year**	**Type**	**Wick**	**Wall Material**	**Dimension (mm)**	**Working fluid**	**Operating Temp. (K)**	**Q_{max} (W)**	**Note**
M. Li, et al. [31]	2018	Pulsating heat pipe	-	Stainless Steel	L_e = 50 L_a = 100 L_c = 50 D_o = 0.8 D_i = 0.5	He	4.2	1.1	Effect of number of turns
R. Bruce, et al. [32]	2018	Pulsating heat pipe	-	Stainless Steel	L_e = 330 L_a = 330 L_c = 330 D_o = 2.0 D_i = 1.5	N_2	75	25.0	
Q. Liang, et al. [33]	2018	Pulsating heat pipe	-	Copper	L_e = 100 L_a = 280 L_c = 100 D_o = 2.0 D_i = 1.0	Ne	28 30 32	25.0 28.0 33.0	
Q. Liang, et al. [34]	2017	Pulsating heat pipe		Stainless Steel	L_e = 35 L_a = 95 L_c = 35 D_o = 1.5 D_i = 0.9	Ne	30	4.93	
Philippe Gully [35]	2014	Conventional heat pipe	Copper braid	Stainless Steel	L = 250 D_o = 5 D_i = 4 and L = 1200 D_o = 5.5 D_i = 5	He	1.4 – 2.0	0.012	

Author	Year	Type	Wick	Wall Material	Dimension (mm)	Working fluid	Operating Temp. (K)	Q_{max} (W)	Note
Z.Q. Long and P. Zhang [36]	2013	Thermosyphon	-	Copper (Evap. And Cond.) Stainless Steel (Adia.)	L_e = 70 L_c = 150 D_o = 44 D_i = 10, L_a = 50 D_o = 14 D_i = 10	He	5.2	0.7	
L. Bai, et al. [37]	2012	Loop heat pipe	Sintered nickel powder.	Stainless Steel	L_e = 35 D_o = 44 D_i = 10, L_a = 640 L_c = 450 D_o = 2 D_i = 1	N_2	80 – 120	12	
Z.Q. Long and P. Zhang [38]	2012	Thermosyphon	-	Copper (Evap. And Cond.) Stainless Steel (Adia.)	L_e = 70 L_c = 150 D_o = 44 D_i = 10, L_a = 50 D_o = 14 D_i = 10	N_2	77	180	

Author	Year	Type	Wick	Wall Material	Dimension (mm)	Working fluid	Operating Temp. (K)	Q_{max} (W)	Note
P. Gully, et al. [39]	2011	Loop heat pipe	Sintered Stainless Steel 316L powder.	Stainless Steel & Copper	L_e = 64 D_o = 22, L_a = 50 D_o = 14, L_c = 150 D_o = 14	N_2	80	19	
K. Natsume, et al. [20]	2011	Pulsating heat pipe	-	Stainless Steel	L_e = 30 L_a = 100 L_c = 30 D_o = 1.59 D_i = 0.78	N_2 Ne H_2	67–91, 26–34, 17–27	7 1.5 1.2	
J. Lee, et al. [11]	2010	Thermosyphon	-	Copper (Evap. And Cond.) Stainless Steel (Adia.)	L_e = 30 L_c = 30 D_o = 30, L_a = 100 D_o = 12.7	N_2-CF_4 (mix)	50	-	Study on transient thermodynamic behavior and its cool-down time
Daniel W. Kwon, et al. [25]	2009	Conventional heat pipe	Stainless steel mesh	Copper	L_{tot} = 855 L_c = 60 D_o = 40	N_2	77	50	

Author	Year	Type	Wick	Wall Material	Dimension (mm)	Working fluid	Operating Temp. (K)	Q_{max} (W)	Note
Junghyun Lee, et al. [40]	2009	Thermosyphon	-	Copper (Evap. And Cond.) Stainless Steel (Adia.)	$L_{e,1}$ = 39 $L_{e,2}$ = 37 L_c = 36 D_o = 50 D_i = 42 L_a = 50 x 2 D_o = 46 D_i = 42	N_2	77	5.3	(Q_{max} of testing for each eveporator)
M. Abdel-Bary, et al. [41]	2009	Conventional heat pipe	Internal plastic tube for the liquid flow	Stainless Steel coated with 0.1 µm thickness shiny gold layer	Le = 50 La = 200 D_o = 5 D_i = 4.8 L_c = 70 D_o = 16 D_i = 15.8	H_2	14.9 – 15.5	1.1	

3.7 References

[1] M. Mochizuki, Y. Saito, K. Goto, T. Nguyen, P. Ho, M. Malcolm and M. P. Morando, "Hinged heat pipes for cooling notebook PCs," in *Thirteenth Annual IEEE. Semiconductor Thermal Measurement and Management Symposium,* Austin, TX, USA, 1997.

[2] T. Nguyen, M. Mochizuki, K. Mashiko, Y. Saito, L. Sauciuc and R. Boggs, "Advanced cooling system using miniature heat pipes in mobile PC," in *ITherm'98. Sixth Intersociety Conference on Thermal and Thermomechanical Phenomena in Electronic Systems (Cat. No.98CH36208)*, Seattle, WA, USA, 1998.

[3] T. Nguyen, M. Mochizuki, K. Mashiko, Y. Saito and I. Sauciuc, "Use of heat pipe/heat sink for thermal management of high performance CPUs," in *Sixteenth Annual IEEE Semiconductor Thermal Measurement and Management Symposium (Cat. No.00CH37068),* San Jose, CA, USA, 2000.

[4] Xiao Ping Wu, M. Mochizuki, Y. Saito, T. Nguyen, V. Wuttijumnong and D. Wu, "Analyzing and modeling on optimized L-ratio of evaporator section to condenser section for micro heat pipe heat sinks," in *Ninteenth Annual IEEE Semiconductor Thermal Measurement and Management Symposium*, San Jose, CA, USA, 2003.

[5] C. K. Loh, E. Harris and D. J. Chou, "Comparative study of heat pipes performances in different orientations," in *Semiconductor Thermal Measurement and Management IEEE Twenty First Annual IEEE Symposium,* San Jose, CA, USA, 2005.

[6] A. K. Mozumder, A. F. Akon, M. S. H. Chowdhury and S. C. Banik, "PERFORMANCE OF HEAT PIPE FOR DIFFERENT WORKING FLUIDS AND FILL RATIOS," *Journal of Mechanical Engineering,* vol. ME 41, no. 2, pp. 96-102, 2010.

[7] J. Dudheker, "A study of a nitrogen heat pipe," Masters Theses. 5460., Missouri, 1971.

[8] M. S. Kumar and A. S. Kumar, "INVESTIGATION ON START-UP CHARACTERISTICS OF CRYOGENIC HEAT PIPES," *Journal of Engineering and Applied Sciences,* vol. 6, no. 6, pp. 58-61, 2011.

[9] M. S. Kumar and A. S. Kumar, "EXPERIMENTAL INVESTIGATIONS ON AN AXIAL GROOVED CRYOGENIC HEAT PIPE," *THERMAL SCIENCE,,* vol. 16, no. 1, pp. 133-138, 2012.

[10] K. Hijikata, S. J. Chen and C. L. Tien, "Non-condensable gas effect on condensation in a two-phase closed thermosyphon," *International Journal of Heat and Mass Transfer,* vol. 27, no. 8, pp. 1319-1325, 1984.

[11] J. Lee, Y. Kim and S. Jeong, "Transient thermodynamic behavior of cryogenic mixed fluid thermosiphon and its cool-down time estimation," *Cryogenics,* vol. 50, no. 5, pp. 352-358, 2010.

[12] Z. Q. Long and P. Zhang, "Heat transfer characteristics of thermosyphon with N2–Ar binary mixture working fluid," *International Journal of Heat and Mass Transfer,* vol. 63, pp. 204-215, 2013.

[13] B. Felder, M. Miki, Z. Deng, K. Tsuzuki, N. Shinohara, M. Izumi and H. Hayakawa, "Development of a Cryogenic Helium-Neon Gas Mixture Cooling System for Use in a Gd-Bulk HTS Synchronous Motor," *IEEE Transactions on Applied Superconductivity,* vol. 21, no. 3, pp. 2213 - 2216, 2011.

[14] K. M. Armijo and V. P. Carey, "An Experimental Study of Heat Pipe Performance Using Binary Mixture Fluids That Exhibit Strong Concentration Marangoni Effects," *Journal of Thermal Science and Engineering Applications,* vol. 3, no. 3, pp. 031003-1-7, 2011.

[15] T. Kiatsiriroat, A. Nuntaphan and J. Tiansuwan, "Thermal Performance Enhancement of Thermosyphon Heat Pipe with Binary Working Fluids," *Experimental Heat Transfer: A Journal of Thermal Energy Generation, Transport, Storage, and Conversion,* vol. 13, no. 2, pp. 137-152, 2000.

[16] F. C. Prenger, D. D. Hill, D. E. Daney, M. A. Daugherty, G. F. Green, J. Chafe, M. Heiberger and A. Langhorn, "Heat Pipes for Enhanced Cooldown of Cryogenic Systems," in *Ross R.G. (eds) Cryocoolers 9*, Boston, MA, Springer, 1997, pp. 831-839.

[17] F. C. Prenger, D. D. Hill, D. E. Daney, M. A. Daugherty, G. F. Green, J. Chafe, M. Heiberger and A. Langhorn, "Performance of Crycooler Shunt Heat Pipes," *Advances in Cryogenic Engineering,* vol. 43, pp. 1521-1528, 1998.

[18] T. Mito, K. Natsume, N. Yanagi, H. Tamura, T. Tamada, K. Shikimachi, N. Hirano and S. Nagaya, "Development of Highly Effective Cooling Technology for a Superconducting Magnet Using Cryogenic OHP," *IEEE Transactions on Applied Superconductivity,* vol. 20, no. 3, pp. 2023-2026, 2010.

[19] T. Mito, K. Natsume, N. Yanagi, H. Tamura, T. Tamada, K. Shikimachi, N. Hirano and S. Nagaya, "Achievement of High Heat Removal Characteristics of Superconducting Magnets With Imbedded Oscillating Heat Pipes," *IEEE Transactions on Applied Superconductivity,* vol. 21, no. 3, pp. 2470-2473, 2011.

[20] K. Natsume, T. Mito, N. Yanagi, H. Tamura, T. Tamada, K. Shikimachi, N. Hirano and S. Nagaya, "Heat transfer performance of cryogenic oscillating heat pipes for effective cooling of superconducting magnets," *Cryogenics,* vol. 51, no. 6, pp. 309-314, 2011.

[21] K. Natsume, T. Mito, N. Yanagi, H. Tamura, T. Tamada, K. Shikimachi, N. Hirano and S. Nagaya, "Development of Cryogenic Oscillating Heat Pipe as a New Device for

Indirect/Conduction Cooled Superconducting Magnets," *IEEE Transactions on Applied Superconductivity,* vol. 22, no. 3, pp. 4703904-4703904, 2012.

[22] Luis Diego Fonseca, Franklin Miller and John Pfotenhauer, "A helium based pulsating heat pipe for superconducting magnets," in *ADVANCES IN CRYOGENIC ENGINEERING: Transactions of the Cryogenic Engineering Conference - CEC,* Anchorage, Alaska, USA, 2014.

[23] S. Kim, S. Jeong, H. B. Jin and K. Sim, "Contractible Heat Pipe for Conduction Cooled Superconducting Magnets," *Journal of the Korea Institute of Applied Superconductivity and Cryogenics,* vol. 5, no. 1, pp. 76-80, 2003.

[24] P. E. Blumenfeld, C. Prenger, E. W. Roth and J. A. Stewart, "High temperature superconducting current lead test facility with heat pipe intercepts," *IEEE Transactions on Applied Superconductivity,* vol. 9, no. 2, pp. 527-530, 1999.

[25] D. W. Kwon and J. R. Sedwick, "Cryogenic heat pipe for cooling high temperature superconductors," *Cryogenics,* vol. 49, no. 9, pp. 514-523, 2009.

[26] A. Yamamoto, S. Michizono, W. Wuench, I. Syratchev, G. Mcmonagle, N. C. Lasheras, S. Calatroni, S. Stepnes, H. Watanabe, H. Tanaka, S. Kido, T. Koga, Y. Koga and K. Takeuchi, "Applying Superconducting Magnet Technology for High-efficiency Klystrons in Particle Accelerator RF Systems," *IEEE Transactions on Applied Superconductivity,* vol. 30, no. 4, pp. 1-4, 2020.

[27] X. Sun, S. Li, B. Jiao, Z. Gan, J. Pfotenhauer, B. Wang, Q. Zhao and D. Liu, "Experimental study on hydrogen pulsating heat pipes under different number of turns," *Cryogenics,* vol. 111, 2020.

[28] H. Cho, L. Jin and S. Jeong, "Experimental investigation on performances and characteristics of nitrogen-charged cryogenic loop heat pipe with wick-mounted condenser," *Cryogenics,* vol. 105, 2020.

[29] M. Li, L. Li and D. Xu, "Effect of filling ratio and orientation on the performance of a multiple turns helium pulsating heat pipe," *Cryogenics,* vol. 100, pp. 62-68 , 2019.

[30] X. Sun, S. Li, B. Jiao, Z. Gan and J. Pfotenhauer, "Experimental study on a hydrogen closed-loop pulsating heat pipe with two turns," *Cryogenics,* vol. 97, pp. 63-69 , 2019.

[31] M. Li, L. Li and D. Xu, "Effect of number of turns and configurations on the heat transfer performance of helium cryogenic pulsating heat pipe," *Cryogenics,* vol. 96, pp. 159-165 , 2018.

[32] R. Bruce, M. Barba, A. Bonelli and B. Baudouy, "Thermal performance of a meter-scale horizontal nitrogen Pulsating Heat Pipe," *Cryogenics,* vol. 93, pp. 66-74 , 2018.

[33] Q. Liang, Y. Li and Q. Wang, "Effects of filling ratio and condenser temperature on the thermal performance of a neon cryogenic oscillating heat pipe," *Cryogenics*, vol. 89, pp. 102-106, 2018.

[34] Q. Liang, Y. Li and Q. Wang, "Experimental investigation on the performance of a neon cryogenic oscillating heat pipe," *Cryogenics,* vol. 84, pp. 7-12, 2017.

[35] P. Gully, "Long and high conductance helium heat pipe," *Cryogenics*, vol. 64, p. 255–259, 2014.

[36] Z. Q. Long and P. Zhang, "Experimental investigation of the heat transfer characteristics of a helium cryogenic thermosyphon," *Cryogenics,* vol. 57, pp. 95-103, 2013.

[37] L. Bai, G. Lin, H. Zhang, J. Miao and D. Wen, "Experimental study of a nitrogen-charged cryogenic loop heat pipe," *Cryogenics*, vol. 52, no. 10, p. 557–563, 2012.

[38] Z. Q. Long and P. Zhang, "Impact of cooling condition and filling ratio on heat transfer limit of cryogenic thermosyphon," *Cryogenics,* vol. 52, no. 1, p. 66–76, 2012.

[39] P. Gully, Q. Mo, T. Yan, P. Seyfert, L. Guillemet, P. Thibault and J. Liang, "Thermal behavior of a cryogenic loop heat pipe for space application," *Cryogenics*, vol. 51, no. 8, p. 420–428, 2011.

[40] J. Lee, J. Ko, Y. Kim, S. Jeong, T. Sung, Y. Han, J.-P. Lee and S. Jung, "Experimental study on the double-evaporator thermosiphon for cooling HTS (high temperature superconductor) system," *Cryogenics*, vol. 49, no. 8, pp. 390-397 , 2009.

[41] M. Abdel-Bary, S. Abdel-Samad, G. A. Elawadi, K. Kilian and J. Ritman, "A thin gold coated hydrogen heat pipe-cryogenic target for external experiments at COSY," *Cryogenics,* vol. 49, no. 5, pp. 192-197, 2009.

Chapter 4
EXPERIMENTAL APPARATUS

In this chapter, the description of the apparatus and measurement techniques used in this experimental research is presented. The cryogenic heat pipe experimental apparatus is shown in Figure 4.1. The main part of the experimental apparatus consists of a pressure unit, a data acquisition unit, and a test section. The two different kinds of cooling methods were used: cooling with a LN_2 bath and a cryocooler, which are called the first and the second test section, respectively. Since the first that uses an LN_2 bath has a limitation with respect to the control of the condenser temperature (a difficulty arises at the temperatures lower than 77 K), the test section was modified to use a cryocooler instead of LN_2 bath so that the experiments can be performed in a wider condenser temperature range. In this research, the experimental data were mostly taken by using the experimental setup that used the second test section with a cryocooler. The functions of each unit are described as follows.

4.1 Pressure Unit

The pressure unit functions the supply of the working gas into the heat pipe and maintaining the pressure in the heat pipe. This unit consists of a high-pressure gas cylinder (for nitrogen, argon and neon gases), gas reservoirs for supplying the working fluid in gas phase into a heat pipe, several valves, and pressure sensors. The gas reservoir having a constant volume (0.3 L) was used reducing the gas pressure in filling process of the working fluid to the

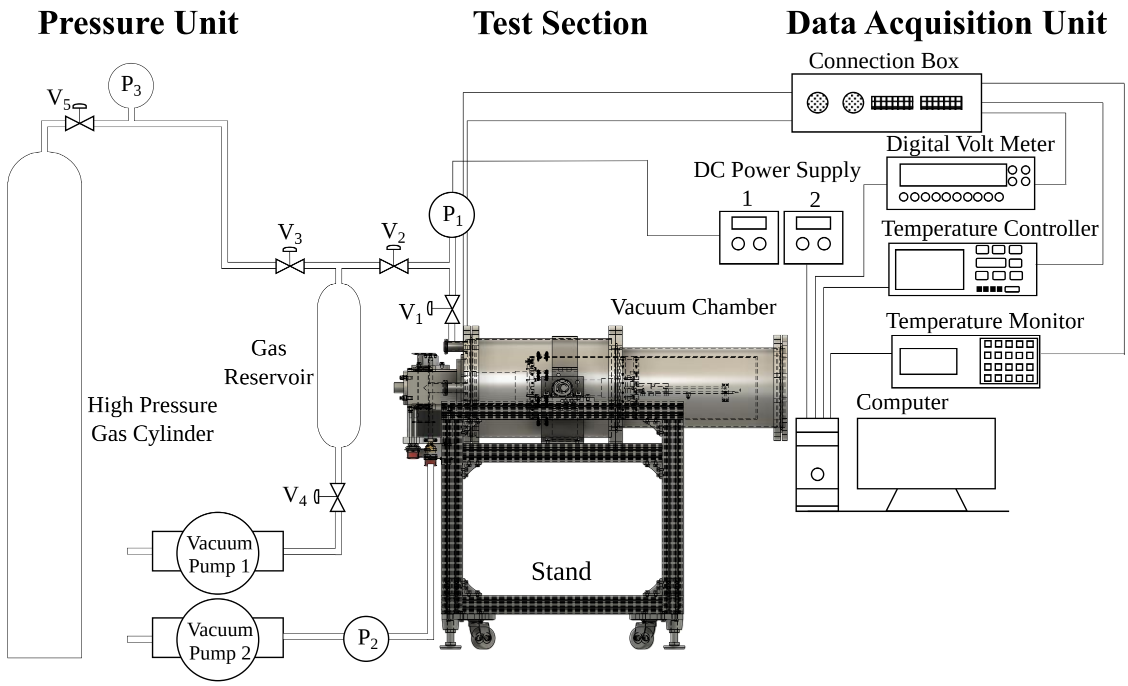

Figure 4.1 *Experimental apparatus of cryogenic heat pipe.*

heat pipe in gas phase at room temperature. Two vacuum pumps were used, one for evacuating the heat pipe before filling working fluid, and another for evacuating the vacuum chamber to high vacuum throughout the experiment. A pressure sensor, Senzes model CAV-001MP-02-V, was used to measure the absolute pressure of the working fluid inside the reservoir tank during the filling process and to monitor the vapor pressure inside the heat pipe during the experiment. In order to convert the pressure inside the heat pipe readily to the saturated vapor temperature ($T_{sat}(p)$) of nitrogen, argon, and neon, and to avoid the effect of variation of atmospheric pressure, an absolute pressure sensor with an operating range limit of 0.0–1.0 MPa was used. The vacuum level inside the vacuum chamber was measured by another pressure sensor. The Oerlikon Leybold PHOENIX L300 Helium Leak Detector was used for leak testing of the vacuum chamber, the heat pipes, the filling tubes, and the connecting tubes.

4.2 Data Acquisition Unit

The data acquisition unit consists of a connection box, two DC power supplies, a digital voltmeter, a temperature monitor, two temperature controllers and a personal computer. The connection box located in the room temperature environment allowed connecting the electric cables between the inside of the vacuum chamber (24–110 K) and the outside of the vacuum chamber by feedthroughs at the top flange of vacuum chamber. A DC power supply (the maximum output voltage and current were 70 V and 1.0 A, respectively) was used to supply electric power as the heat input to the heater at the evaporator section. Another constant voltage DC power supply (the maximum output voltage and output current are 18 V and 2 A, respectively) was used for the activation of the pressure sensors. A digital voltmeter (Keithley 2000 multimeter with scanning function) measured the output from the pressure sensors and the heat input to the heaters. In order to measure the electric current, the voltage drop across a 0.1 Ω of external shunt resistor connected with a D.C. power supply was measured with the digital voltmeter. The data from the 8 temperature sensors were acquired with the Lake Shore model 218 temperature monitor. Heaters and calibrated temperature sensors were used for controlling the temperatures of the condenser section and the filling tube, respectively with the Lake Shore model 336 and model 331 temperature controllers. In cases of the temperature higher than LN_2 temperature for the experiment of the Ar-heat pipe, the condenser section temperature was kept at a predetermined constant temperature. The filling tube connected to the heat pipe must be heated during the experiments because there was a concern that it would freeze due to excessive cooling by the cryocooler. The personal computer was used with LabVIEW software to control and record the data from the measuring instruments.

4.3 Test Section with Liquid Nitrogen Bath

The cooling unit with liquid nitrogen bath can cool down and maintain the temperature of the condenser section at LN_2 temperature (normal boiling temperature 77 K) or liquid argon (LAr) temperature (87 K) [1, 2]. However, in cases of liquid argon temperature experiments where the heat pipe was operated at a temperature higher than 77 K, an auxiliary heater, a temperature sensor, and stainless-steel thin plate of 0.5 mm in thickness was needed as a thermal barrier between the condenser section and the bottom plate of the liquid nitrogen bath. The liquid nitrogen bath locates inside the vacuum chamber as shown in Figure 4.2. The vacuum chamber has an inner diameter of 300 mm and a height of 600 mm, made of stainless steel. The cylindrical liquid nitrogen bath of 165 mm diameter and 400 mm height made of stainless steel was located inside the vacuum chamber, which was welded to the top flange of the vacuum chamber via a neck tube of 50 mm in diameter and 80 mm in length, also made of stainless steel for reducing the thermal conductive heat leak from the room temperature region to the liquid nitrogen bath due to its low thermal conductivity. The bottom of the cylindrical liquid nitrogen bath was made of copper in order to take advantage of the high thermal conductivity of copper to keep the condenser section at the LN_2 temperature and joined with stainless-steel thin plate by brazing process. The heat pipe was thermally contacted to the bottom plate of the cylindrical liquid nitrogen bath through a copper block which forms a condenser section. The stainless-steel capillary tube, 500 mm in length and having an inside diameter of 0.18 mm, was used as an evacuating and filling tube for a heat pipe. The whole outer surface of the liquid nitrogen bath together with the stainless-steel capillary filling tube and the heat pipe were wrapped with 30 layers of multilayer insulation (MLI) for thermal isolation. The top flange of the vacuum chamber has two 22-pin electric feedthroughs linking the lead wires for the heater and the temperature sensors.

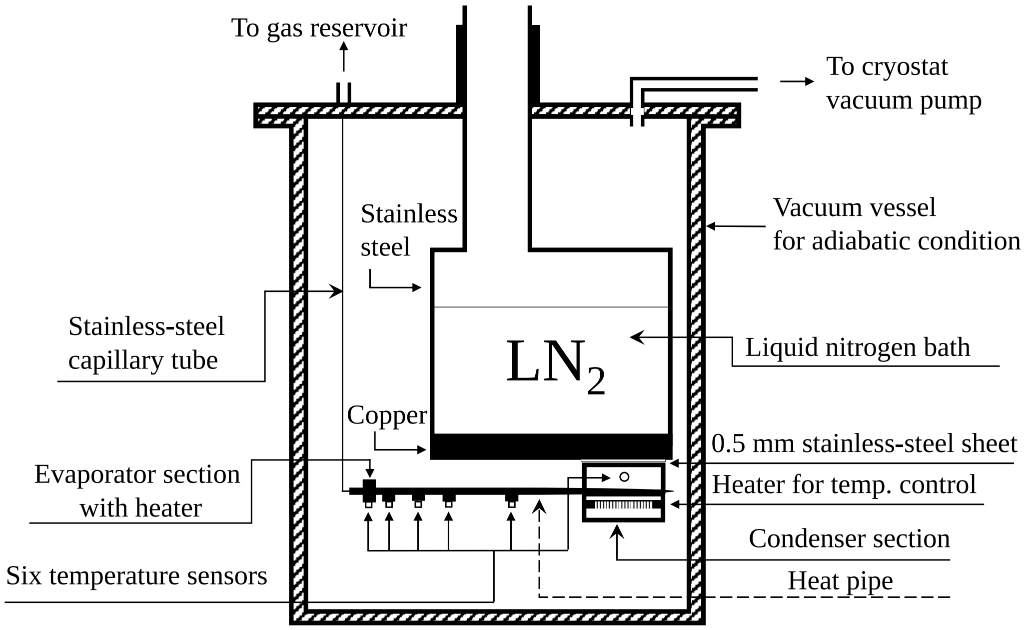

Figure 4.2 *Cross section of vacuum chamber for cooling unit with liquid nitrogen bath.*

4.4 Test Section with Cryocooler

The test section by using a cryocooler performs cooling down and maintaining the temperature at a cryogenic temperature range (in this experiment, 27–110 K). The test section includes a vacuum chamber, a cryocooler, a thermal shield, an evaporator, an adiabatic and a condenser section, thermal links, heat pipes, temperature sensors, filling tubes, and heaters.

4.4.1 Vacuum chamber and support stand

The vacuum chamber is shown in Figure 4.3 to maintain the inside pressure at low level and was divided into two parts, both made of stainless steel. Both parts were connected to form the vacuum chamber. The first part has an inner diameter of 267.4 mm, a thickness of 3.5 mm and a height of 318 mm (the length from the cold head to 2nd stage of the cryocooler). It was connected to the top flange having an outer diameter of 335 mm and a thickness of 16.0 mm as shown in Figure 4.4. The cryocooler was attached to the top flange, which has a vacuum port and an electrical feedthrough. The second part of the vacuum chamber having an inner

(a) First part

(b) Second part

Figure 4.3 *Vacuum chamber*

Figure 4.4 *Top flange of vacuum chamber*

diameter of 216.3 mm, a thickness of 3 mm and a height of 353 mm was connected to the first part of the vacuum chamber. The second part could be removed while changing the heat pipe for next experiment.

The support stand which firmly supports the vacuum chamber and allows the vacuum chamber to rotate in a vertical plane to adjust the angle of the vacuum chamber for the test of the inclination angle effect of a heat pipe. In most experiments unless specified otherwise, the heat pipe was set horizontally (the inclination angel of 0˚). The stand which was constructed from 50 x 50 mm aluminum frame elements has a dimension of 570 x 570 x 575 mm. It includes rundles, leveling mounts and pillow block bearings.

4.4.2 Cryocooler

The appearance of the cryocooler used in the present heat pipe experiment, RDK-415D model by Sumitomo Heavy Industries, Ltd. (SHI) [3], is shown in Figure 4.5, which is a 4K Gifford-McMahon (GM) cryocooler featuring a two-stage cooling. The specifications of the cryocooler are shown in Table 4.1.

The GM cryocoolers was first developed in 1960 [4]. It began to be used in the 1980s for the cooling of charcoal adsorber down to about 15 K in cryopumps. In the late 1980s the GM cryocooler further began to be used for the cooling of radiation shields in MRI equipment for reducing the boil-off rate of liquid helium that was required to maintain the superconducting magnet at 4.2 K. The utilization of regenerator made with rare-earth material that has high heat capacity in the range of 4–20 K allowed the GM cryocooler to achieve temperatures of 4 K [5] in 1990. The function of the cryocooler is to cool the condenser section of the heat pipe to the desired cryogenic temperatures.

4.4.3 Thermal shield

In order to minimize the thermal radiation heat load to the cryocooler system, the thermal shield shown in Figure 4.6. was provided together with multilayer insulation (MLI) that was wrapped around the outer surface of the thermal shield. It was divided to two parts, which were connected via two connectors made of copper shown in Figure 4.7. The first part shown in Figure 4.6(a) was connected to the 1st stage of the cryocooler via the connector I, and the other end was connected to the connector II. It has an outer diameter of 164 mm, a height of 225 mm and thickness of 2 mm. The second part of the thermal shield, having an outer diameter of 164 mm, a height of 290 mm and thickness of 2 mm shown in Figure 4.6(b), was connected to the connector II of the thermal shield.

Figure 4.5 *RDK-415D 4K cryocooler [3].*

Table 4.1 *Specifications of cryocooler [3].*

Power Supply	50 Hz	60 Hz
2nd Stage Capacity	1.5 W @ 4.2 K	
1st Stage Capacity	35 W @ 50 K	45 W @ 50 K
Minimum Temperature	< 3.5 K	
Cooldown Time to 4.2 K	< 60 Minutes	
Weight	18.5 kg (40.8 lbs.)	
Dimensions (H×W×D)	557 × 180 × 294 mm	
Maintenance	10000 hours	
Regulatory Compliance	UL/CE, RoHS	

The connector I of the thermal shield, having an outer diameter of 164 mm and thickness of 12 mm shown in Figure 4.7(a), was connected to the 1st stage of the cryocooler. It has a large opening with a diameter of 90 mm in which the 1st stage of the cryocooler can be mounted,

(a) *First part.* (b) *Second part.*

Figure 4.6 *Thermal shield.*

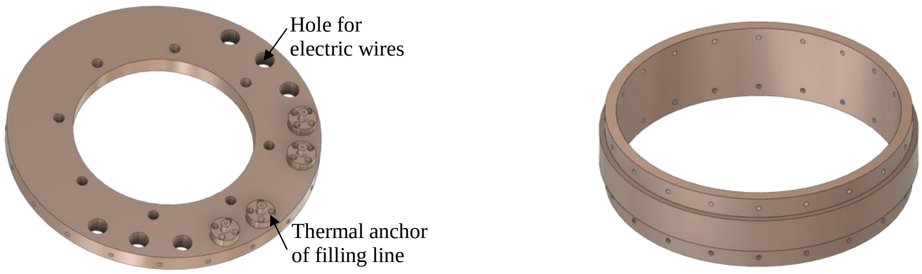

(a) *Connector I.* (b) *Connector II.*

Figure 4.7 *Connectors of thermal shield.*

and six holes of 10 mm diameter through which the electric wires pass. It also has 4 thermal anchors attached to the filling tube for cutting heat leak from the room temperature parts. The connector II of the thermal shield, Figure 4.7(b), combines both parts of the thermal shields. The second part of the thermal shield can be removed while changing the heat pipe or modifying the experimental setup. Other function of the connector II was to connect the thermal links to the condenser section. (The detail will be described in Section 4.4.7). The assembled thermal shield with the connectors I and II and the cryocooler combined is shown in Figure 4.8. All of these were integrated and wrapped in 30 layers of MLI for thermal isolation. The thermal shield was used not only for minimization of the thermal radiation heat

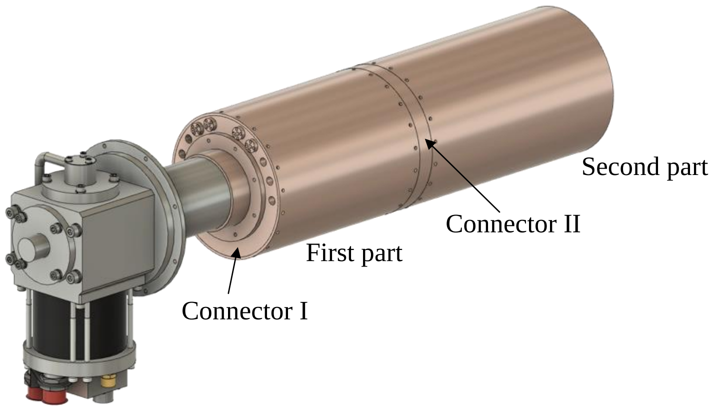

Figure 4.8 *Assembled thermal shields and cryocooler.*

load but also to be as a thermal link between the 1st stage of the cryocooler and the condenser section (Section 4.4.7.)

4.4.4 Evaporator section

The evaporator section block shown in Figure 4.9 is composed of a top element and two bottom elements, all of which were made of aluminum to reduce the weight for preventing bending of the heat pipe with the evaporator section block. Two temperature sensors attached to each bottom element measure the temperatures in the evaporator section of two heat pipes. The common top element having a dimension of 30 mm in length and 57 mm in width has a through hole of 6.35 mm for embedding a cartridge-type heater (50 W and 50 V). Both the top and bottom elements have semi-circular grooves of 6.1 mm in diameter and 30 mm in length for installing two heat pipes. The heat pipes were fixed so as to be sandwiched between the grooves of both elements via indium foil of 0.1 mm in thickness (Figure 4.10) to enhance heat transfer. Hear transfer grease, Apiezon N [6] (Figure 4.11), was applied to the heater hole before installation of the heater.

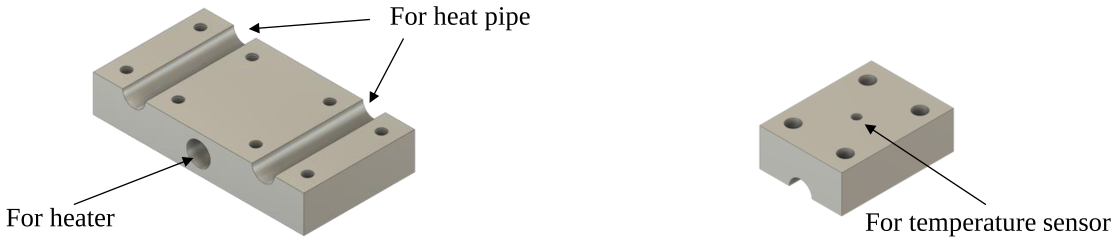

(a) Top part.　*(b) Bottom part.*

Figure 4.9 *Aluminum blocks for evaporator section.*

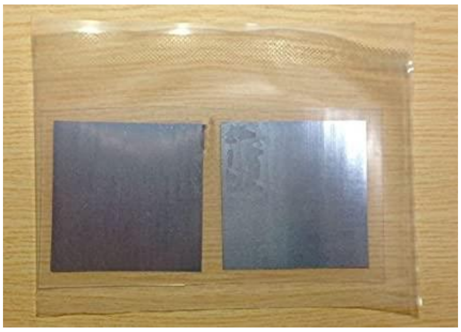

Figure 4.10 *Indium sheet*

Figure 4.11 *Apiezon N grease*

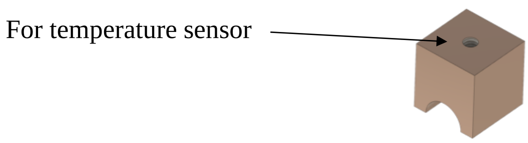

Figure 4.12 *Copper mount for thermometer at adiabatic section.*

4.4.5 Thermometer mount for the adiabatic section

Thermometer mount shown in Figure 4.12, having a dimension of 10 x 10 x 10 mm made of copper, were attached directly to the outer surface of the adiabatic section of the heat pipe by soldering. The temperature of the adiabatic section of each heat pipe was measured at two locations.

4.4.6 Condenser section block and connector plates I and II to cryocooler

The copper blocks, both the top and the bottom elements made of copper composing the condenser section are shown in Figure 4.13. Two top elements having a tapped hole of M4 size have a dimension of 30 mm (W), 65 mm (L), 18 (H) as shown in Figure 4.13(a). The bottom element, shown in Figure 4.13(b), has a dimension of 65 mm (W), 70 mm (L), 24 (H). There are two holes with a diameter of 6.35 mm for inserting the cartridge-type heaters and two small holes for air release (bottom side). Both the top and the bottom elements have semi-circular grooves of 6.1 mm in diameter and 65 mm in length for installing the heat pipe. A temperature sensor was attached to the top element to measure the temperature of the condenser section. One calibrated temperature sensor, attached to the bottom element of the condenser section, functions to control the temperature of the condenser section at a predetermined temperature together with the two controlling heaters. The connector plates I and II, shown in Figure 4.14, were designed to connect or disconnect the bottom part of the condenser section and the 2nd stage of the cryocooler. If the heat pipe operating temperature (the condenser temperature) is much lower than liquid nitrogen temperature, the connector plate I thermally makes connect with the plate II to directly connect the bottom element of the condenser section to the 2nd stage of the cryocooler. However, in cases when the operating temperature is liquid nitrogen temperature or higher, for example in case of parallel heat pipe system (two heat pipes) experiments, three copper blocks, Figure 4.15, with a through hole would be attached between the connector plates I and II. On the other hand, when the operating temperature is high or the heat pipe is operated around the lower limit of the heater power for the condenser section, the connector plates I and II would be thermally separated completely and plastic bolts would be used to ensure thermal isolation between the condenser section and the 2nd stage of cryocooler. In this case, the condenser section is cooled only by the 1st stage of cryocooler.

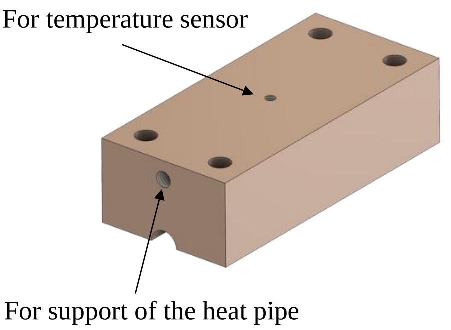

(a) Top element.

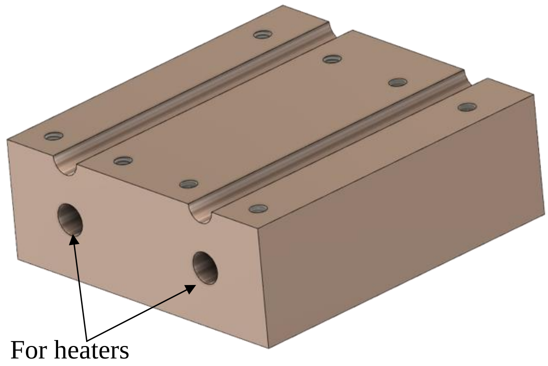

(b) Bottom element.

Figure 4.13 *Copper blocks for condenser section.*

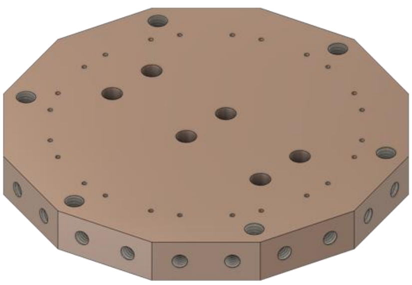

(a) Connector plate I

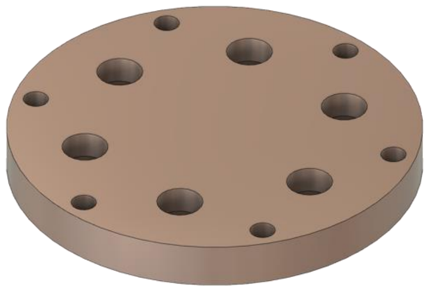

(b) Connector plate II

Figure 4.14 *Connector plates between condenser section and cryocooler.*

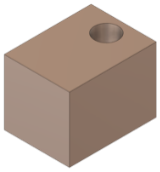

Figure 4.15 *Copper block to separate the connector plates I and II*

The connector plate I, Figure 4.14(a), dodecagonal in shape or twelve-sided polygon, has two tapped holes of M4 size on each side (total 24 tapped holes). The reason for making it twelve-sided polygon, which have an outer diameter of 90 mm and thickness of 10 mm and made of copper, is to increase the contact areas for attaching thermal links. The bottom element of the condenser section was attached to the connector plate I. The connector plate II, Figure 4.14(b), was attached to the 2nd stage of the cryocooler. It also has an outer diameter of 90 mm and a thickness of 10 mm, made of copper.

4.4.7 Thermal links

Thermal links, shown in Figure 4.16, were used to conduct heat between the condenser section and the 1st stage of the cryocooler. Twenty-four thermal link elements were attached between the connector plate I of the condenser section (Figure 4.14a) and the connector II of thermal shield (Figure 4.7b). In this experiment, the lowest operating temperature was 27 K, while the cryocooler has a capability of cooling even down to lower than 4 K at the 2nd stage. Therefore, to maintain the temperature of the condenser section at 27 K or higher, three copper blocks (Figure 4.15) for separating the connector plates I and II were used to weaken the thermal contact between the 2nd stage of the cryocooler and the condenser section, and furthermore, two heaters were installed at the bottom part of the condenser section. Additionally, due to the temperature difference between the 1st and 2nd stages of the cryocooler, heat can be taken from the 1st stage of the cryocooler via the first part of thermal shield (Figure 4.6a), thermal links (Figure 4.16), and the connector plate I of the condenser section (Figure 4.14a) to the condenser section. The actual installation situation of the thermal links is shown in Figure 4.17.

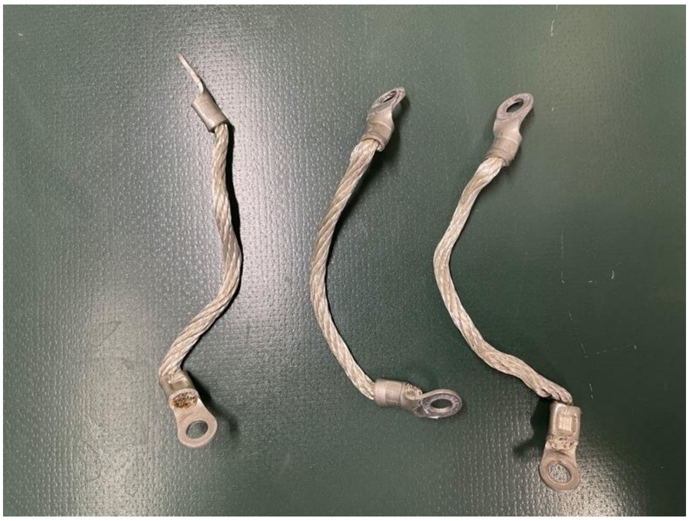

Figure 4.16 *Thermal links.*

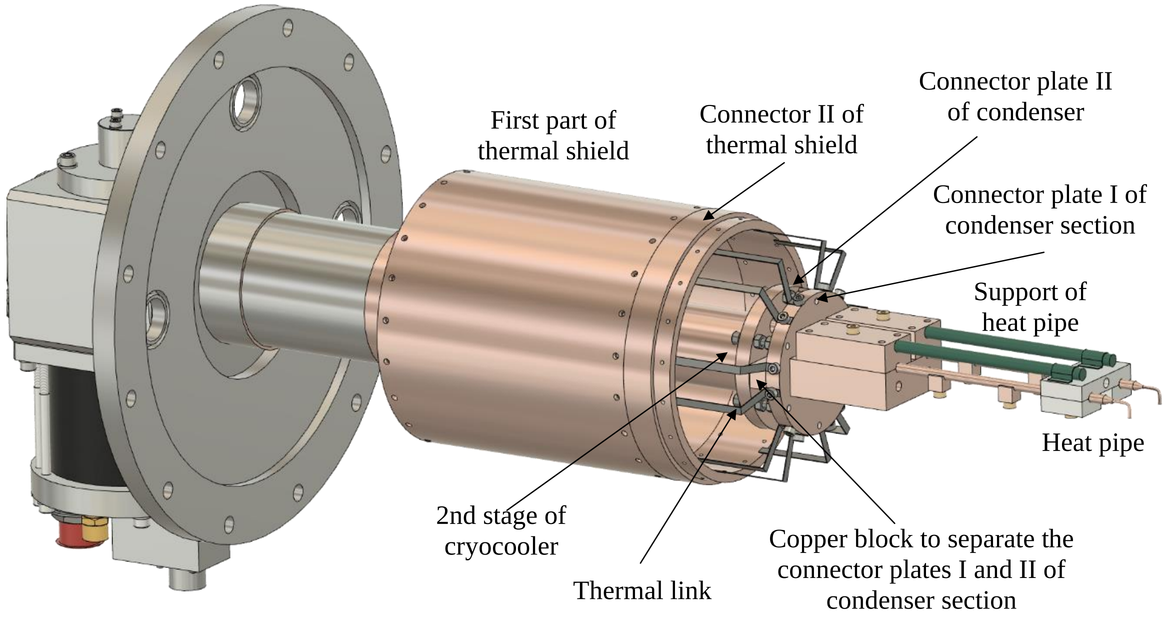

Figure 4.17 *Installation of thermal links.*

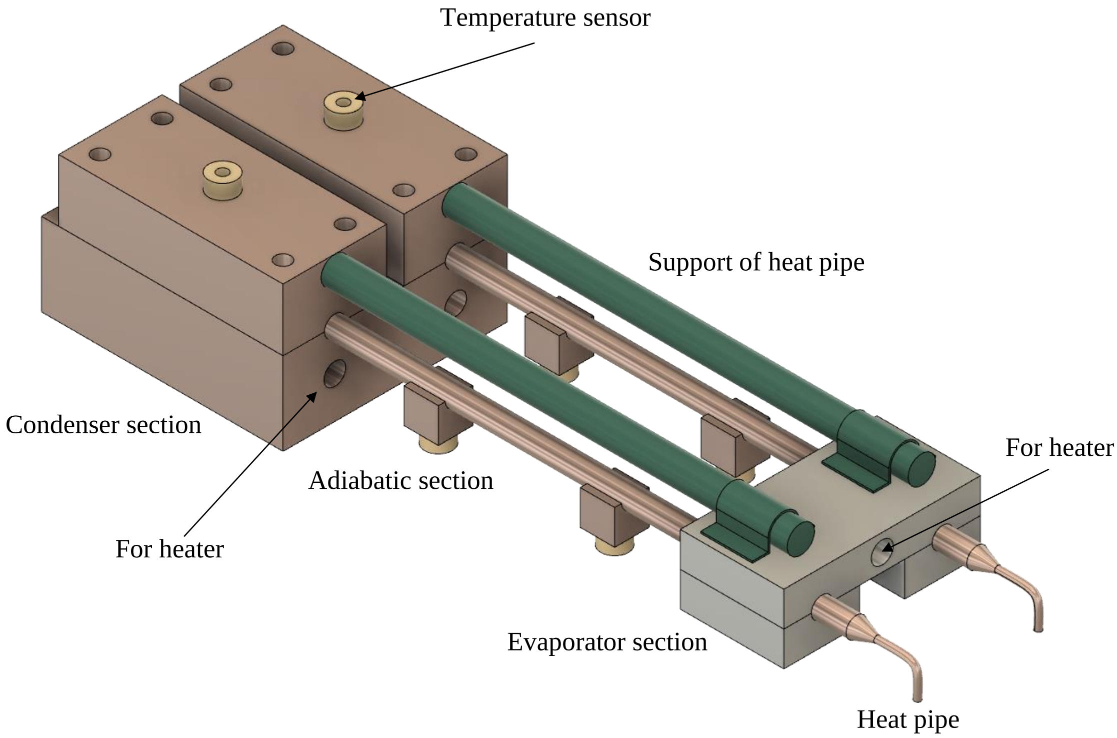

Figure 4.18 *Setup of parallel heat pipe system.*

4.4.8 Installation of heat pipe and support

Heat pipes tested in this study are commercially available ones manufactured by Fujikura Thailand Ltd. [7]. They were originally designed for use at room temperature with water as a working fluid. In this research, they were tested at cryogenic temperatures (27–110 K) by using argon, nitrogen or neon as a working fluid. The assembly consisting of the evaporator section, the adiabatic section, the condenser section, and the support for mounting the heat pipes is shown in Figure 4.18. Each heat pipe made of copper has an outer diameter of 6 mm and a total length of 200 mm. The lengths of the evaporator section, the adiabatic section and the condenser section of the heat pipe are 30, 95 and 65 mm, respectively. Three kinds of wick structures, axial grooves wick, homogeneous sintered copper powder wick, and grooves and homogeneous sintered copper powder composite wick, were tested. The details of the wick structures are shown in Figure 4.19 and Table 4.2, respectively.

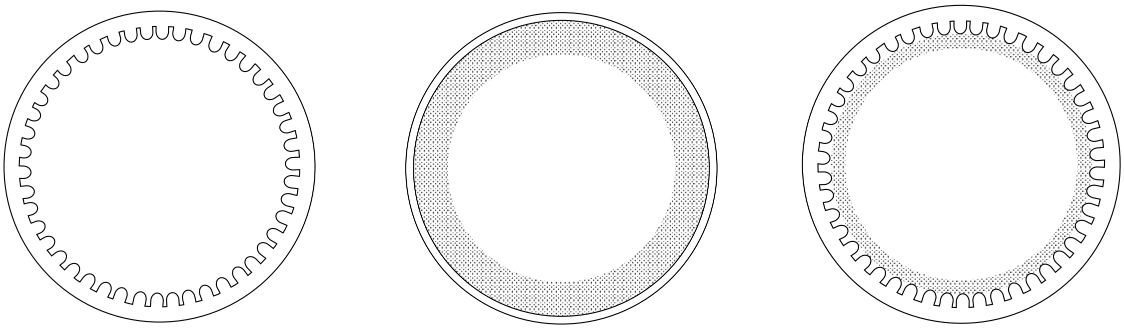

(a) Groove (b) Sintered (c) Sintered-Groove

Figure 4.19 *Wick structures of heat pipes.*

Table 4.2 *Specifications of heat pipe*

Parameter	**Value**
Tube wall material	Copper (C1020)
Working fluid	Nitrogen, Argon, Neon
Outer diameter (OD)	6 mm
Heat pipe length	200 mm
Evap., Adiabat., Cond. lengths	30, 95, 65 mm
Axial groove	
Thickness of wall	0.26 mm
Groove depth	0.20 mm
Groove width	0.27 mm
Number of grooves	50
Sintered metal wick	
Thickness of wall	0.20 mm
Thickness of sintered wick	0.80 mm
Average sphere radius of copper powder	85 µm
Permeability (Grooved, Sintered)	3.04×10^{-9}, 6.67×10^{-11}
Porosity of wick, ϵ (Grooved, Sintered)	0.82, 0.57

The manufacturing process for the homogeneous sintered copper powder wick is as follows: A mandrel was inserted into the center of a heat pipe and copper powder was poured into the pipe around the mandrel. After the powder was tightly packed and compressed, the pipes were put into a sintering oven. After this high temperature process, the copper powder would stick to the pipe inside wall and to itself, forming many internal pockets like a sponge. The support of the heat pipe was made of G10 fiberglass which has very low thermal conductivity (0.3W/(m·K) at 100 K) [8]. It was laid between the top part of the condenser section and evaporator section in order to prevent bending down of the heat pipe around evaporator section.

4.4.9 Temperature sensors

There are two types of temperature sensors used in this experiment. One type is Lake Shore DT-670 silicon diode sensors for the measurement of the temperature of the heat pipe, and another is PT-100 platinum resistance thermometers (PRTs) for the measurement of the temperature of the filling tube. Two types of temperature sensors were selected depending on the mounting method of the temperature sensors. As it is difficult to make a threaded hole for mounting a DT-670 sensors to the filling tube, the PT-100 thermometer which is a wire-wound thermometer was selected.

DT-670 sensor, shown in Figure 4.20, has, in general, better accuracy over a wider temperature range. The standard voltage versus temperature response curve for the DT-670 sensors is provided (±0.25 K accuracy from 2.0 K to 100.0 K) from the manufacturer, and within this temperature range DT-670 sensors are interchangeable. For this reason, individual calibration for DT-670 sensors is not required in many applications. DT-670 sensors are commercially available for general cryogenic use in the 1.4 K to 500 K temperature range. For applications requiring higher accuracy, DT-670-SD sensors (calibrated temperature sensor) are available with calibration in the full 1.4 K to 500 K temperature range (±40 mK at 77 K and ±25 mK at 305 K in accuracy) [9].

PT-100 platinum resistance thermometer (PRT), shown in Figure 4.21, is an excellent choice for use as a cryogenic temperature sensing and control element in the temperature range from 30 K to 873 K (±0.25 K at 73 K to 305 K). Inside this temperature range, PRTs offer high

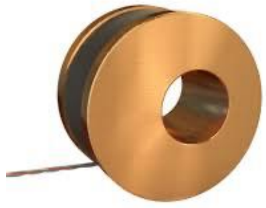

Figure 4.20 *DT-670 silicon diode sensor*

Figure 4.21 *PT-100 platinum resistance thermometer*

repeatability and nearly constant sensitivity (dR/dT). PRTs are also useful as control elements in high magnetic field environments where errors approaching 1 K are inevitable. PRTs are interchangeable above 70 K. The use of controlled-purity platinum assures uniformity from one device to another [10].

The axial temperature distribution along a heat pipe was measured by four temperature sensors on the external surface of the heat pipe. These four temperature sensors designated as T_e (in the evaporator section), T_{a1}, T_{a2} (in the adiabatic section), and T_c (in the condenser section) are all Lake Shore DT-670 silicon diode sensors. The location and the mounting method of the temperature sensors are shown in Figure 4.22. The evaporator temperature sensor (T_e, calibrated temperature sensor) was located at x = 25 mm measured from the evaporator end of the heat pipe, just at the middle of the evaporator section. The temperature sensors (T_{a1} and T_{a2}) for the adiabatic section were located at x = 70 and 120 mm from the evaporator end, respectively. The condenser temperature sensor (T_c) was located at x = 167.5 mm from the evaporator end, just at the middle of the condenser section.

An additional calibrated temperature sensor of DT-670 was attached at the bottom side of the condenser section, of which location was opposite side of the condenser temperature sensor T_c. This temperature sensor and the two heaters were connected to the temperature controller to control the temperature of the condenser section at a constant value.

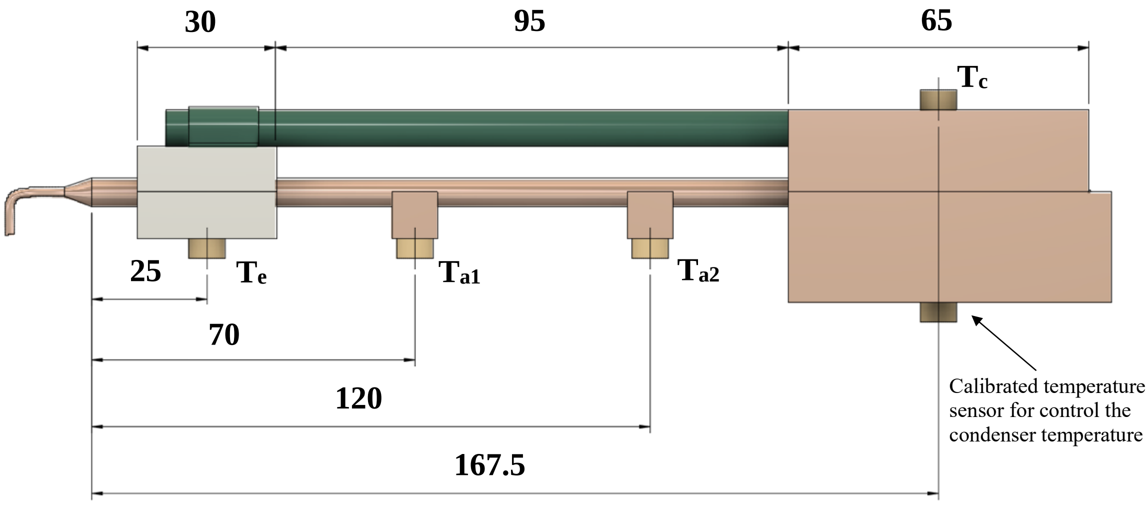

Figure 4.22 *The schematic diagram of the heat pipe with temperature measurement sensor locations. All dimensions are in mm.*

The temperature of the filling tube was measured with the PT-100 PRT at the mid-length point the of the filling tube. This temperature may be a representative of the filling tube because it is only one measuring point over 1000 mm in length.

4.4.10 Filling tube

The stainless-steel capillary tube, shown in Figure 4.23, having a 500 mm in length (total 1000 mm) and an inside diameter of 0.18 mm was used as an evacuating and filling tube of the heat pipe. It was divided for two parts, the first part starts from the outside of the vacuum chamber at room temperature, and the second part was connected to the heat pipe. Both were joined near the 2nd stage of the cryocooler. The installation of the filling tube starts from the room temperature side outside the vacuum chamber, and through the vacuum chamber and the hole of the connector I of thermal shield (Figure 4.7a) and was finally connected to the end of the heat pipe near the evaporator section as shown in Figure 4.24.

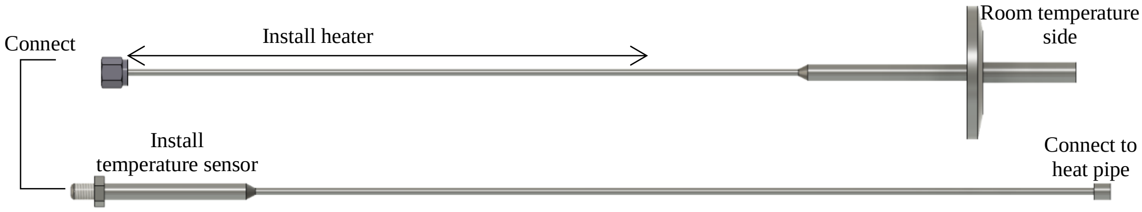

Figure 4.23 *Filling tube.*
(Please note that length in this figure is not scale)

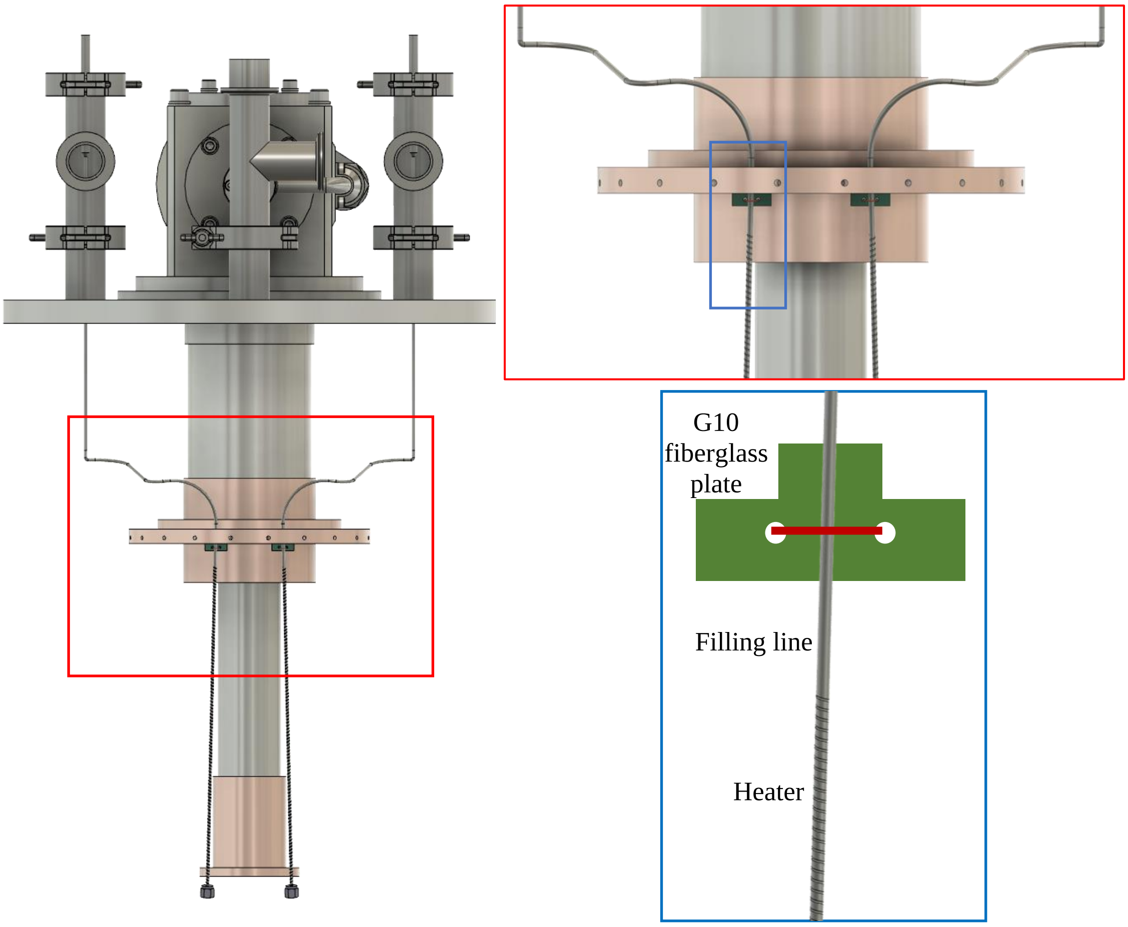

Figure 4.24 *Installation of filling tube with G10 plate and heater*

When the heat pipe was cooled by using the cryocooler during the preliminary experiment, the result was that the pressure inside the heat pipe measured through the filling tube did not change to working liquid pressure (1 bar approximately) even the temperature of the condenser section reached below boiling point. The pressure was as the same value as the initial filling pressure in gas phase (> 4 bar). This turned out to be the result of the working fluid freezing inside the pipe and clogging the filling tube and therefore the whole working fluid was not allowed moving into the heat pipe and condensing in the condenser section. The 1st stage of the cryocooler, in general, has a capability to keep lower temperature than the triple point of nitrogen, 63.14 K approximately.

The G10 fiberglass plate was used to fix and support the filling tube, as shown in Figure 4.24, and also can prevent the filling tube from touching the connector I of the thermal shield (Figure 4.7a, thermal anchors of the filling tube were omitted in the figure). Manganese wire heater was used, which was wrapped around the filling tube to warm it up, as shown in Figure 4.24, to ensure that there is no bulk solid or liquid phase remaining inside the filling tubes. Solid or liquid phase of the working fluid may block the filling tube, and causes that the pressure inside the heat pipe cannot be measured correctly and the amount of the working fluid filled to the heat pipe is not correct. It, for example in reality, happened that for expected 100% filling ratio, only 90% was filled in the heat pipe and 10% remained in the filling tube as solid or liquid phase. The filling tubes were wrapped with metal tape in the heated section for uniformly heating, and the whole was wrapped with 10 layers of multilayer insulation for thermal isolation from the lower temperature area.

4.4.11 Heaters

A cartridge heater-type used for cryogenic heat pipe heating is shown in Figure 4.25, having 6.35 mm in outer diameter and 30 mm in length. The standard heat rating and the maximum input voltage are 50 W and 50 V, respectively. One heater was installed at the evaporator section for heating the heat pipe, and the other two heaters were installed in the condenser block for controlling the temperature of the condenser section at a predetermined

Figure 4.25 *Cartridge type heaters of 6.35 mm in outer diameter and 30.0 mm in length*

constant value. The two heaters together with the calibrated temperature sensor (DT-670 silicon diode sensor) were connected to the Lake Shore model 336 temperature controller.

Manganese wire with a diameter of 0.1 mm was used as a heater for the filling tube. It has a resistance of 14 Ω/m. The first part of the filling tube was wrapped with manganese wire of 1.5 m with resistance of 21 Ω. The manganese wire and the PT-100 PRTs were connected to the model 331 temperature controller.

4.5 References

[1] R. Wanison. et al., "A study of thermal performance change of cryogenic heat pipes by wick structures for wide range of working fluid filling ratio," in *The Cryogenic Engineering Conference (CEC) 2019, 21-25 July 2019, Hartford, Connecticut, USA*, 2020.

[2] R. Wanison. et al., "A study of the thermal behavior of a nitrogen heat pipe for a wide range of heat loads at several filling ratios," in *27th International Cryogenics Engineering Conference and International Cryogenic Materials Conference 2018 (ICEC-ICMC 2018) 3–7 September 2018, Oxford, United Kingdom*, 2019.

[3] "RDK-415D 4K Cryocooler Series," SHI Cryogenics Group, [Online]. Available: http://www.shicryogenics.com/products/4k-cryocoolers/rdk-415d-4k-cryocooler-series/.

[4] H. O. McMahon and W. E. Gifford, "A New Low-Temperature Gas Expansion Cycle," *Advances in Cryogenic Engineering*, vol. 5, p. 354, 1960.

[5] T. Kuriyama. et al., "High Efficient two-Stage gm Refrigerator with Magnetic Material in the Liquid Helium Temperature Region," *Advances in Cryogenic Engineering. Advances in Cryogenic Engineering*, vol. 35, p. 1261, 1990.

[6] "Apiezon," M&I Materials Ltd, 2020. [Online]. Available: https://apiezon.com/products/vacuum-greases/apiezon-n-grease/.

[7] "Thermal," Fujikura Ltd., [Online]. Available: https://www.fujikura.com/solutions/thermal/.

[8] "Material Properties: G-10 CR (Fiberglass Epoxy)," NIST: National Institute of Standards and Technology, [Online]. Available: https://trc.nist.gov/cryogenics/materials/G-10%20CR%20Fiberglass%20Epoxy/G10CRFiberglassEpoxy_rev.htm.

[9] "DT-670 Silicon Diodes," Lake Shore Cryotronics, Inc., [Online]. Available: https://www.lakeshore.com/products/categories/overview/temperature-products/cryogenic-temperature-sensors/dt-670-silicon-diodes.

[10] "Platinum," Lake Shore Cryotronics, Inc., [Online]. Available: https://www.lakeshore.com/products/categories/overview/temperature-products/cryogenic-temperature-sensors/platinum.

Chapter 5
EXPERIMENTAL PROCEDURE

This chapter describes the experimental procedure, including the preparation and method of the experiment. Technique and safety for operating the experiment at cryogenic temperature are also described.

5.1 Preparation of Experiment

First, the electric wiring for the experimental apparatus was inspected. Next, the experimental apparatus was assembled, and the leak test of the heat pipe, the vacuum chamber, and the connecting tubes was performed by using the Oerlikon Leybold PHOENIX L300 helium leak detector to ensure airtightness and thermal isolation of the heat pipe system from the external room temperature environment by exhausting conductive residual gas.

However, it was found that there were still possible heat transfer phenomena to the thermal shield chamber by thermal conduction through many electric wires. Residual gas conduction can, in addition, introduce a non-negligible contribution in case of a non-perfect vacuum. As thermal radiation is normally the dominating heat input source, the use of MLI and thermal shielding is normally employed as the protection measures. In order to experimentally estimate the total amount of heat leak to the heat pipe, some heat was intentionally added to the evaporator section from the heater while the heat pipe was completely evacuated. It was observed that there was some temperature difference between the

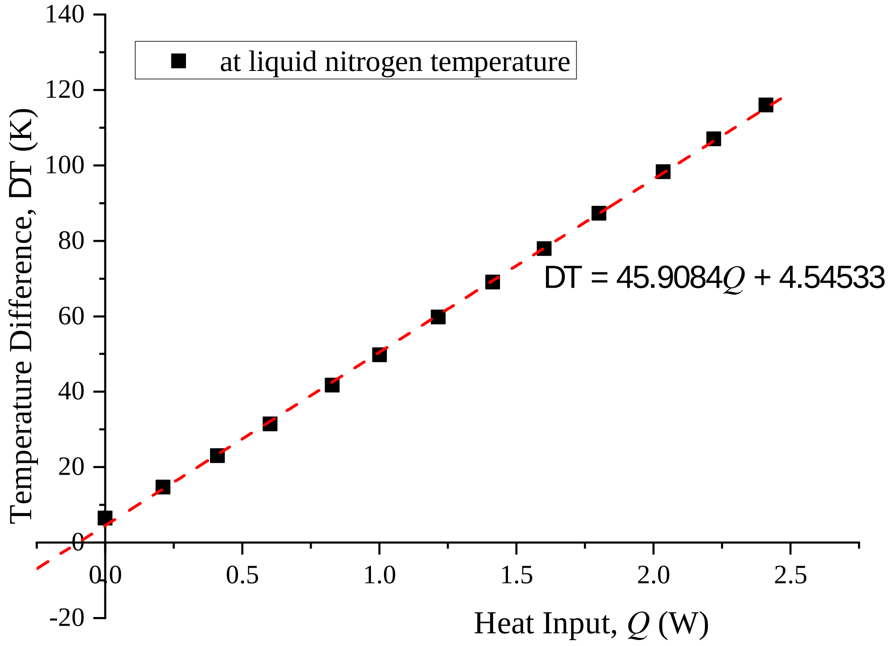

Figure 5.1 *The temperature difference between the evaporator and condenser section of the heat pipe without working fluid at liquid nitrogen temperature.*

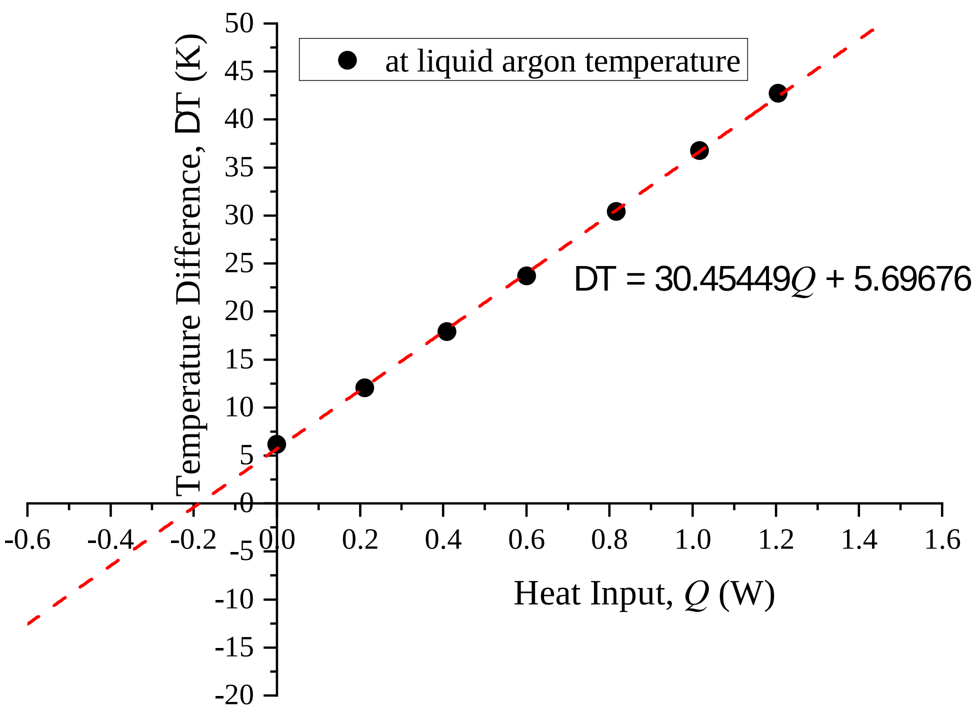

Figure 5.2 *The temperature difference between the evaporator and condenser section of the heat pipe without working fluid at liquid argon temperature.*

evaporator and condenser sections in the cryogenic temperature range without any heat addition from the heater during the experimental run. This result was converted into the heat leak, 0.10 W and 0.18 W for the nitrogen and the argon heat pipe experiments, respectively, as shown in Figures 5.1 and 5.2, which were taken into account in the calculation of the net heat transferred to the heat pipe.

The successful operation of heat pipes relies heavily on the purity of the working fluid and the absence of any foreign destructive material in the heat pipe wick structure. To ensure this, the heat pipe and all the connecting tubes were evacuated at room temperature and then flushed by working fluid (Ne, N_2, and Ar) in gas phase. This procedure was repeated for five times to remove any non-condensable foreign gas from the heat pipe. The vacuum chamber was continuously evacuated to prevent the parasitic heat leak due to gas conduction. The experiment was started after 24 hours from the start of the evacuation process, and the pressure of the vacuum chamber was kept at 1×10^{-4} Pa approximately throughout the experiments.

5.2 Filling Process of Working Fluid

After evacuating the heat pipe, working fluid in gas phase was charged from the high-pressure gas cylinder to the gas reservoir having a constant volume, as shown in Figure 5.3, while the valves V_1 and V_4 were closed. And then, by opening the valve V_1, working fluid gas flowed into the heat pipe through the stainless-steel capillary tube under room temperature condition. The amount of the working fluid gas that was charged into the heat pipe is indicated by the working fluid filling ratio. Heat pipe wick structure is in general designed so that the best heat pipe thermal performance should be achieved at 100% filling ratio. As the wick structure of the heat pipe tested in this study was originally designed to work best at room temperature by using water as a working fluid, the optimum thermal performance as cryogenic heat pipes would not be necessarily achieved at 100% filling ratio. The filling ratio in this

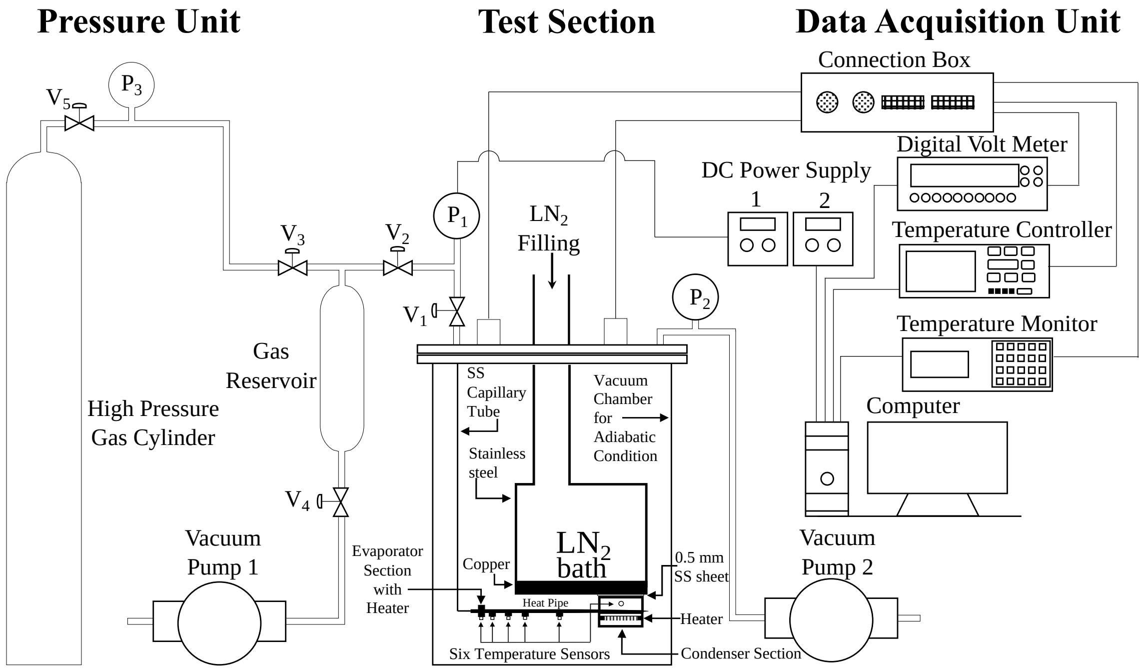

Figure 5.3 *The experimental setup by using liquid nitrogen bath as a cooling unit.*

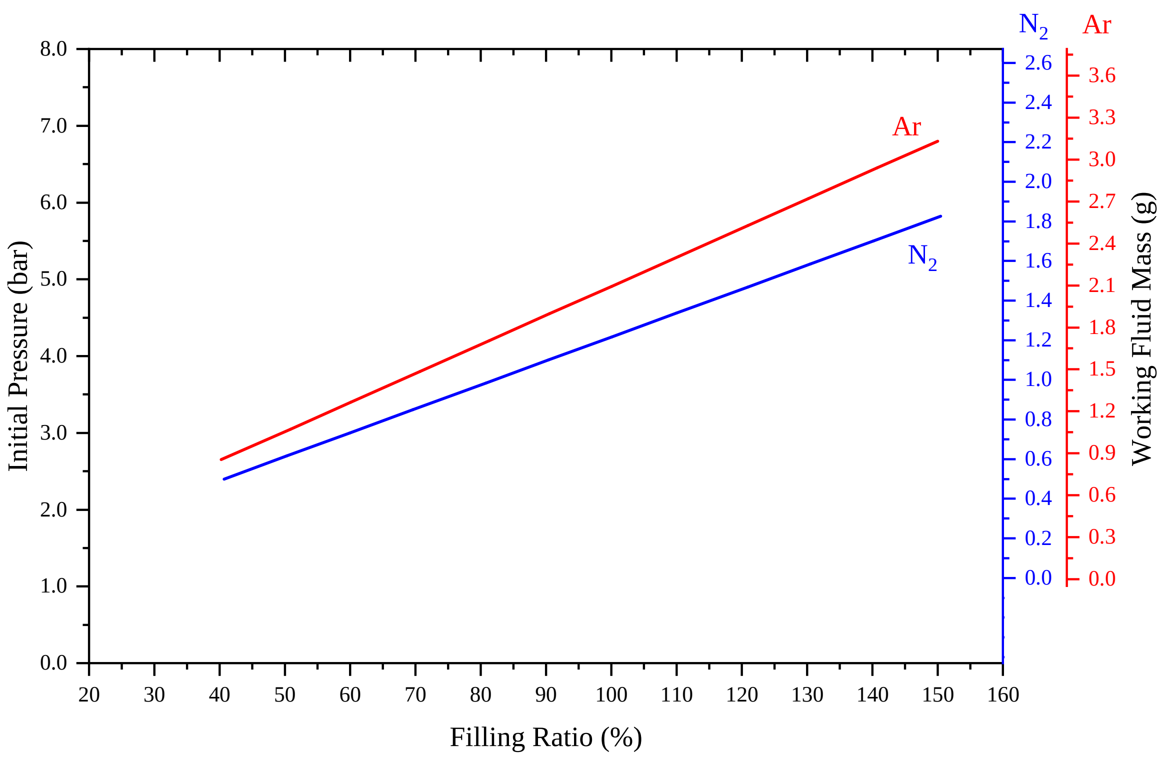

Figure 5.4 *The initial pressure and mass of working fluid as a function of filling ratio.*

experiment is defined by the volume of condensate liquid of working fluid in the wick structure divided by the total void volume of wick structure. For example, 100% fill is the amount of condensate liquid of working fluid fully saturating in the void volume of the wick structure. The amount of working fluid gas which was charged into a heat pipe can be indirectly measured by the pressure sensor (P_1) that was connected with the gas reservoir. The filling ratio f_r is defined as follows:

$$f_r = \frac{m - \rho_v A_v L}{\varepsilon \rho_l A_w L}, \tag{5.1}$$

where

$$m = \frac{(P_i - P_f) V_r}{R_v T}. \tag{5.2}$$

Here, P_i is the initial pressure of working fluid gas in the gas reservoir before the heat pipe was cooled down, and P_f is the final pressure of working gas, the order of 1 bar, in the gas reservoir after the working fluid gas flowed into the heat pipe and then was cooled to condense in the wick structure. And V_r is the volume of the gas reservoir, R_v is the gas constant of working fluid, T is the temperature of gas reservoir, f_r is the filling ratio, A_v is the vapor core cross-sectional area of the heat pipe, A_w is the wick cross-sectional area, ρ_l is the liquid density, ρ_v is the vapor density, ε is the wick porosity, and m is the working fluid mass. The estimated values of the void volumes of the filling tube, and the tube or valves between the gas reservoir and the vacuum chamber are 1×10^{-8} and 3×10^{-6} m^3, respectively. These are considerably small compared to the volumes of the gas reservoir and the heat pipe so they can be ignored in the calculation of the filling ratio. The calculation result of the amount of working fluid in term of filling ratio on the basis of Equations (5.1) and (5.2) is shown in Figure 5.4, where the initial pressure of working fluid gas in the gas reservoir, P_i, which was measured by pressure sensor

P_1, and the working fluid mass, *m*, in gram are given as a function of filling ratio. For example, at 100% filling ratio, the nitrogen gas was charged to the gas reservoir at 4.25 bar and the amount of nitrogen occupied in the heat pipe was 1.21 g. The effects of filling ratios were tested with various amount of working fluid in terms of the filling ratio according to Figure 5.4. The inclination angle of the heat pipe was set, in most cases 0˚. (horizontal), by adjusting the setting angle of the vacuum chamber.

5.3 Cooling Down Process

After filling the gas reservoir with working fluid when the valve V_3 was closed (Figure 5.3), the cooling down process started by filling the liquid nitrogen bath with LN_2 in case of cooling with the liquid nitrogen bath, or by switching on the cryocooler in case of cooling with the cryocooler. The vale V_1 was opened to allow working fluid flowing into the heat pipe.

For the case of cooling by using the cryocooler, the condenser temperature was set by the temperature controller at the temperature ranges of 24–110 K. Furthermore, the temperature of the filling tube was set at 180 K, which was considerably higher than the critical temperatures of nitrogen and argon, to avoid working fluid freezing in the tube. A number of examples of the time variations of the temperatures during the cooling processes from room temperature 290 to 77.4 K are shown in Figure 5.5, for three cases of (1) cooling by liquid nitrogen bath, (2) cooling by the cryocooler with connecting the condenser section to the 1st and 2nd stages of the cryocooler, and (3) cooling by the cryocooler with connecting the condenser section only to the 1st stage of the cryocooler. It takes about 20, 120 and 190 minutes in cases of (1), (2), and (3), respectively. This indicates that the wick functioned well and was saturated with liquid of working fluid. For the experiments of the cryogenic parallel heat pipe system that consist of single N_2- and Ar-heat pipes, two sets of the gas reservoirs and valves (V_1, V_2, V_3 and V_4) were used.

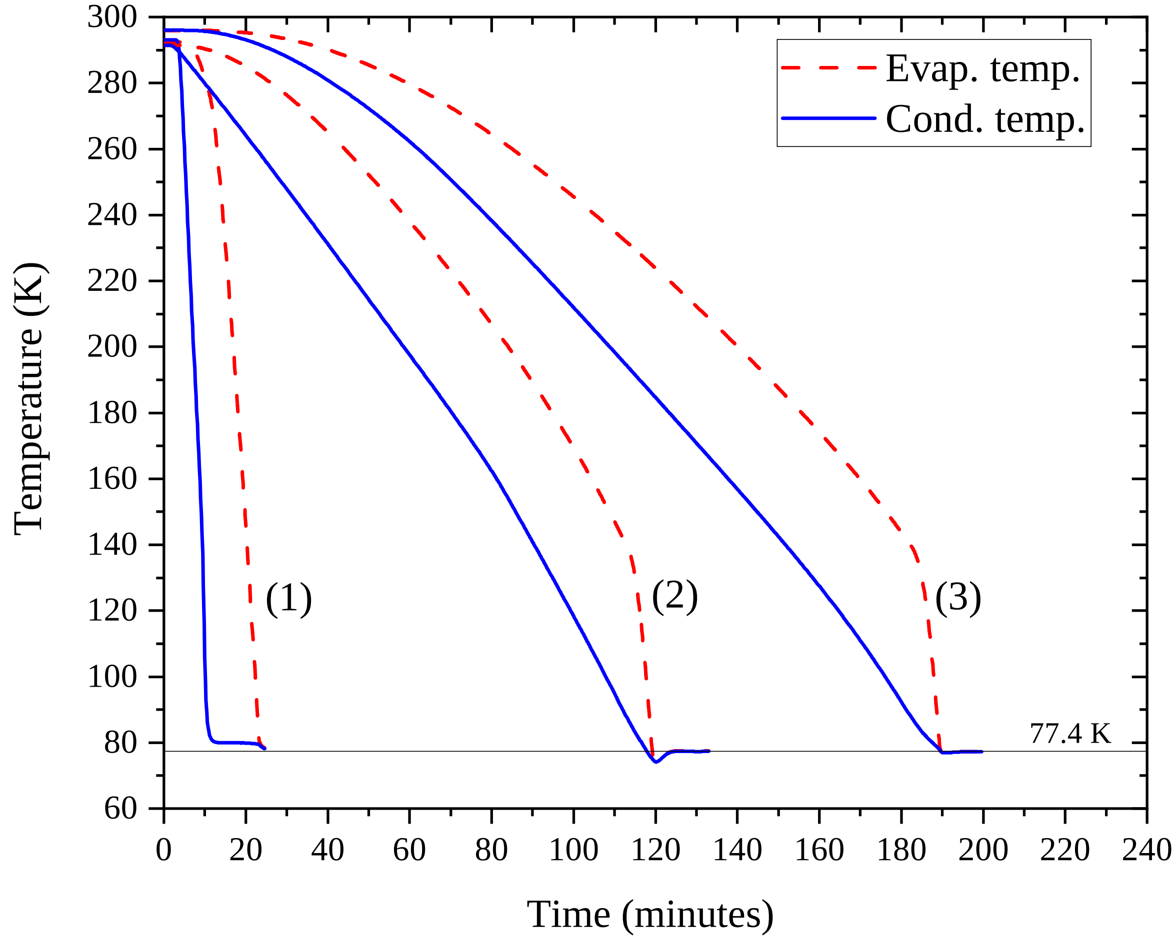

Figure 5.5 *Cooling process from 290 to 77.4 K.*

The typical variation of the thermophysical state during preliminary experiment of the cryogenic parallel heat pipe system is shown in Figure 5.6. This is the experimental data with the operating (condenser section) temperature at 82 K. The process starts after cooling the whole system without heat addition to the evaporator section from room temperature 290 K to a temperature below the critical temperatures of nitrogen and argon, in this particular case at 87.3 K. First, the temperature of the condenser section was set at 87.3 K for the Ar heat pipe to make condense gaseous Ar in the wick, then the valve V_2 (V_{2I}) of the Ar heat pipe was closed, when the temperature of the whole Ar heat pipe reached 87.3 K. In the next step, the temperature of the condenser section was changed to 77.4 K for making the N_2 heat pipe active, and then the valve V_2 (V_{2II}) of the N_2 heat pipe was closed, when confirming the temperature

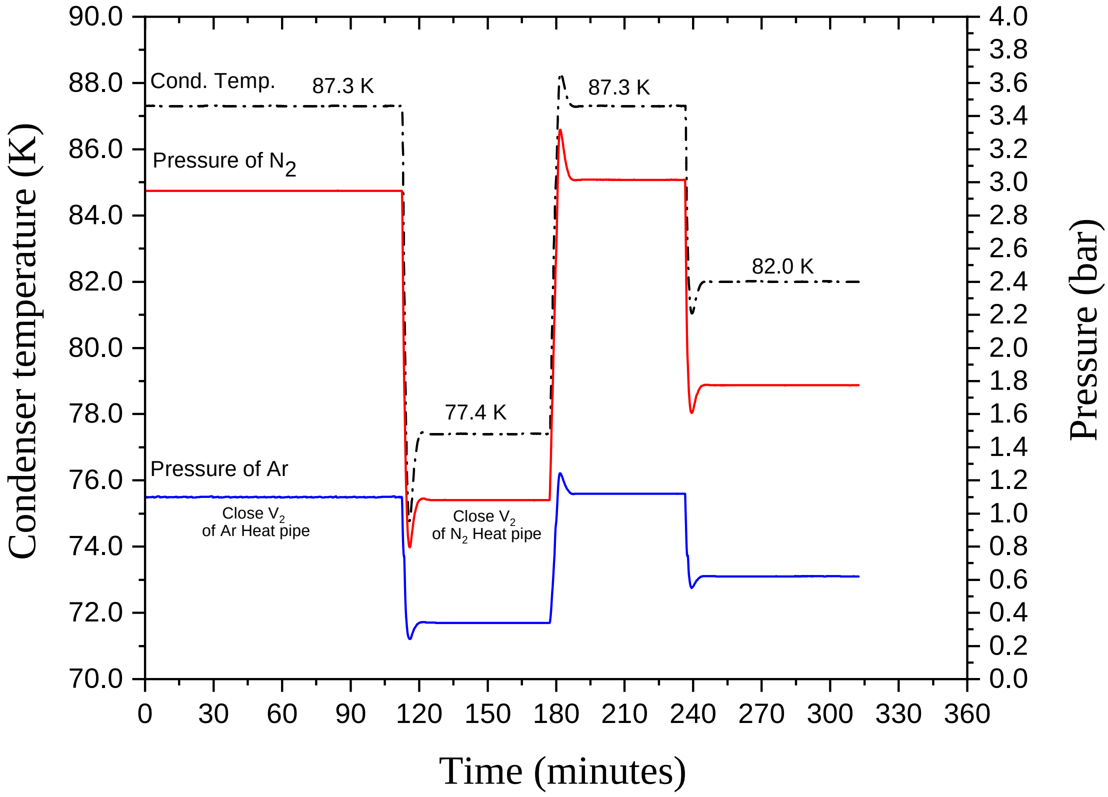

Figure 5.6 *The process of making the cryogenic parallel heat pipe system.*

reached 77.4 K. In the third step starting around 180 minutes, the temperature of the condenser section was again set at 87.3 K for confirmation of reproducibility and that there was no gas leak from the heat pipe. The result indicated that there was no gas leak. After this process, the predetermined operating temperature, 82 K, was set to start the experiment.

5.4 Experimental Procedure

The important information is obtained from the temperature difference between the evaporator and the condenser sections when the heat Q_e is applied from the electric heater in the evaporator section, where the heat input Q_e is calculated as follows;

$$Q_e = IV \ . \tag{5.3}$$

Here, V and I are the supply voltage and the current to the heater, respectively. The current I is measured from the voltage drop across the 0.1 Ω external shunt resistor connected with a D.C. power supply.

Experiments were carried out by increasing the heat input by an incremental step of 0.5 or 1.0 W every approximately 30 minutes. The pressure inside the heat pipe and the wall temperatures of the heat pipe were recorded in every steady state achieved by the heat input at each time. The heat transfer performance of a heat pipe is indicated by the thermal resistance. The overall thermal resistance (R_{th}) of a heat pipe is calculated by the temperature difference between the heat source (the evaporator section) and the heat sink (the condenser section) divided by the heat input Q_e as follows;

$$R_{th} = \frac{T_e - T_c}{Q_e} . \tag{5.4}$$

where T_e, T_a, T_c are the wall temperatures of the evaporator section, the adiabatic and the condenser sections, respectively.

The experiment was terminated when the temperature of the evaporator section reached 290 K for safety reasons. The typical three thermal resistances are recorded: the low thermal resistance region, the high thermal resistance region, and the transition region between the two.

5.5 Safety

The experiments of the cryogenic heat pipe were conducted at various temperatures of the condenser section cooled with the cryocooler. However, there is a limitation of operating temperature due to the pressure inside the heat pipe from the viewpoint of safety. Since heat

Table 5.1 *Constant values for Equation (5.5)*

Working fluid	**Temperature**	**A**	**B**	**C**
Argon [1, 2]	83.78 - 150.72	3.29555	215.24	-22.233
Nitrogen [3, 4]	63.14 - 126.0	3.7362	264.651	-6.788
Neon [5, 6]	24.0 - 44.0	3.75641	95.599	-1.503

pipes operate under the two-phase liquid–vapor working fluid state, the pressure inside a heat pipe can be predicted on the basis of the function of temperature by the Antoine equation;

$$\log_{10} P = A - \left(\frac{B}{T + C} \right), \tag{5.5}$$

where P is the vapor pressure in bar, T is the temperature in K, and A, B, C are constant values as given in Table 5.1

The relationships between the vapor pressure and the temperature for N_2 and Ar are shown in Figure 5.7. At the temperatures higher than 100 K, the vapor pressure is higher than approximately 8 bar and 3.5 bar for N_2 and Ar, respectively. The pressure of 8 bar for N_2 is

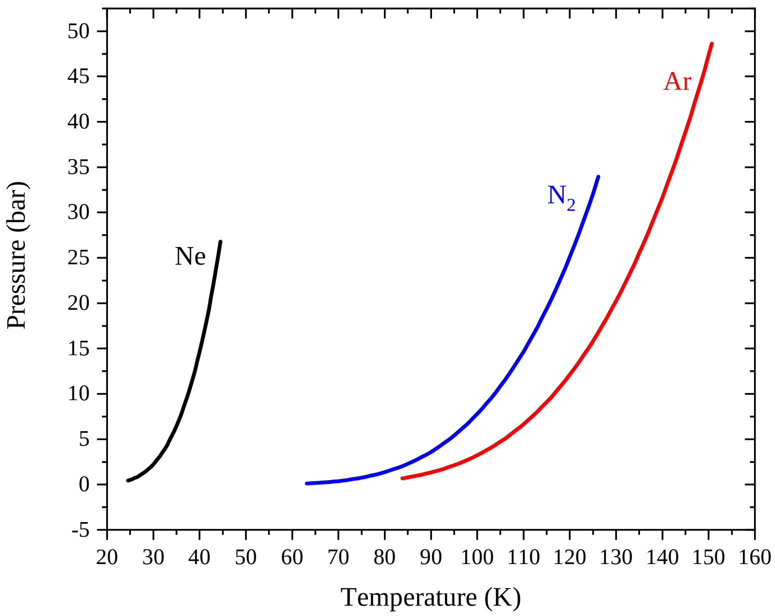

Figure 5.7 *The saturated vapor pressure as a function of temperature for neon, nitrogen, and argon.*

quite dangerous for experimental facility of this research. Therefore, the highest temperature of the condenser section to test N_2-heat pipe and Ar-heat pipe would be 87 K with pressure of 3 bar and 110 K with pressure of 6.9 bar, respectively.

When the cryogenic heat pipes were operated with the cooling unit by using liquid nitrogen bath, LN_2 should be handled in well-ventilated areas.

The cryogenic heat pipe experimental procedure shown step by step.

1. Evacuate the vacuum chamber to a pressure below 1×10^{-2} Pa at room temperature.
2. Evacuate the heat pipe with a vacuum pump to remove any non-condensable foreign gas from the heat pipe.
3. Fill the working fluid in gas phase to a predetermined filling ratio (normally 100% filling ratio).
4. Set up inclination angle of the vacuum chamber at a predetermined angle (normally 0˚ degree, i.e., horizontal).
5. Start cooling and maintaining the operating temperature at predetermined temperature with;
    5.1. Cooling unit by using liquid nitrogen bath: fill LN_2 into the liquid nitrogen bath.
    5.2. Cooling unit by using the cryocooler: turn on the chiller for the cooling of the compressor of the cryocooler and then start the cryocooler.
6. Set up the temperature and cool down until the temperature down to about 87 K for an Ar-heat pipe, 77 K for an N_2-heat pipe, and 27 K for an Ne-heat pipe.
7. Close the valve V_2 to seal the heat pipe.
8. Set up the temperature of the condenser section with the temperature controller at predetermined operating temperature.
9. Start the DC power supply for the heat input to the heat pipe in a step-by-step manner.
10. Stop the DC power supply to finish the experiment, when the temperature of the evaporator section reaches 290 K.
11. Open the valve V_2.
12. Stop the chiller and the cryocooler.
13. Introduce gas nitrogen into the vacuum chamber after the temperature is above 90 K, in order to uniformly warm up the whole experimental setup to room temperature.

5.6 References

[1] L. R. V. Drii, "Dependence of vapor pressure of argon," *Zhurnal Fizicheskoi Khimii,* vol. 40, p. 709–711, 1966.

[2] "Argon," National Institute of Standards and Technology, 2018. [Online]. Available: https://webbook.nist.gov/cgi/cbook.cgi?ID=C7440371&Mask=4#Thermo-Phase.

[3] G. T. Merardo P. Edejer, "Vapor pressures of liquid nitrogen between the triple and critical points," *J. Chem. Eng. Data,* vol. 12, no. 2, pp. 206-209, 19767.

[4] "Nitrogen," National Institute of Standards and Technology, 2018. [Online]. Available: https://webbook.nist.gov/cgi/cbook.cgi?ID=C7727379&Mask=4#ref-8.

[5] D. R. Stull, "Vapor Pressure of Pure Substances. Organic and Inorganic Compounds," *Ind. Eng. Chem.,* vol. 39, no. 4, pp. 517-540, 1947.

[6] "Neon," National Institute of Standards and Technology, 2018. [Online]. Available: https://webbook.nist.gov/cgi/inchi?ID=C7440019&Mask=4#ref-3.

Chapter 6
RESULTS AND DISCUSSION

This chapter describes the experimental results of the cryogenic heat pipes using commercially available heat pipes with nitrogen or argon or neon as a working fluid. The experimental heat pipes were mostly installed horizontally inside the vacuum chamber, of which condenser section was cooled by a liquid nitrogen bath or a cryocooler as a heat sink. The wall temperatures of the heat pipes were measured at the evaporator, adiabatic and condenser sections, and the absolute pressure of the vapor inside the heat pipe was also measured. The thermal performance of the heat pipes was derived from the experimental data in a wide range of operating temperature. The effects of the working fluid filling ratio, the inclination angle, and the working fluids on the performance were investigated. Thermal behavior in the dry-out state was specially investigated because of the potential application to high T_c superconducting coil cooling. In the transient cooling phase of such a large-scale cryogenic system, the heat pipes are supposed to be operated in the partial dry-out state with the condenser section temperature maintained at a low temperature of a cryocooler.

In the second part, the parallel heat pipe system using a nitrogen and an argon heat pipe, which are placed in parallel and used as a set, is proposed for the application to the cooling of high T_c superconducting coils in a wider temperature range. Additionally, the experimental results of the parallel heat pipe system consisting of a neon and a nitrogen heat pipe are presented together with the data of single heat pipe experiment.

6.1 Results and Discussion on Single Heat Pipe

This section is focused on the experimental results of the single heat pipe, N_2-heat pipe, Ar-heat pipe, and Ne-heat pipe. The thermal behavior and the effects of the working fluid filling ratio, the inclination angle, and the condenser temperature will be presented and discussed.

6.1.1 Time variations of the temperature and pressure of the heat pipe

The time variations of the temperatures of the N_2-heat pipe with 100% filling ratio were measured at the evaporator, adiabatic and condenser sections, together with the vapor pressure inside the heat pipe, P, for various values of the heat input. Examples of the results are shown in Figures 6.1 and 6.2 for the cases of cooling with a liquid nitrogen bath and a cryocooler, respectively.

In Figure 6.1 three quantities, the temperature T (K), the heat input Q_e (W), the pressure P (bar) are plotted on the Y-axes, and the time t (hours) on the X-axis. Six temperature sensors were distributed along the heat pipe, one at the evaporator section T_e, four at the adiabatic section in the order of T_{a1}–T_{a4} from the evaporator section side, and one at the condenser section T_c. The experiment was started after the pre-cooling down from room temperature to LN_2 temperature. The heat input, Q_e, to the evaporator section was increased step by step by 0.5 W after reaching a steady state, normally every 30 minutes in the the normal heat pipe operation phase and every more than 1 hour in the partial dry-out phase. All five temperatures except T_c did not vary significantly despite the heat being applied until Q_e reached 10 W (at 8.5 hours). Thus, it can be confirmed from this fact that the commercially available heat pipe can work at a cryogenic temperature by using nitrogen as a working fluid. It is true that this heat pipe literally functioned as a cryogenic heat pipe that could transfer certain amount of heat with an extremely small temperature drop at cryogenic temperatures. At 12 W of Q_e, T_e started to increase with the lapse of time, and, in addition, the pressure fluctuation is thought to be caused

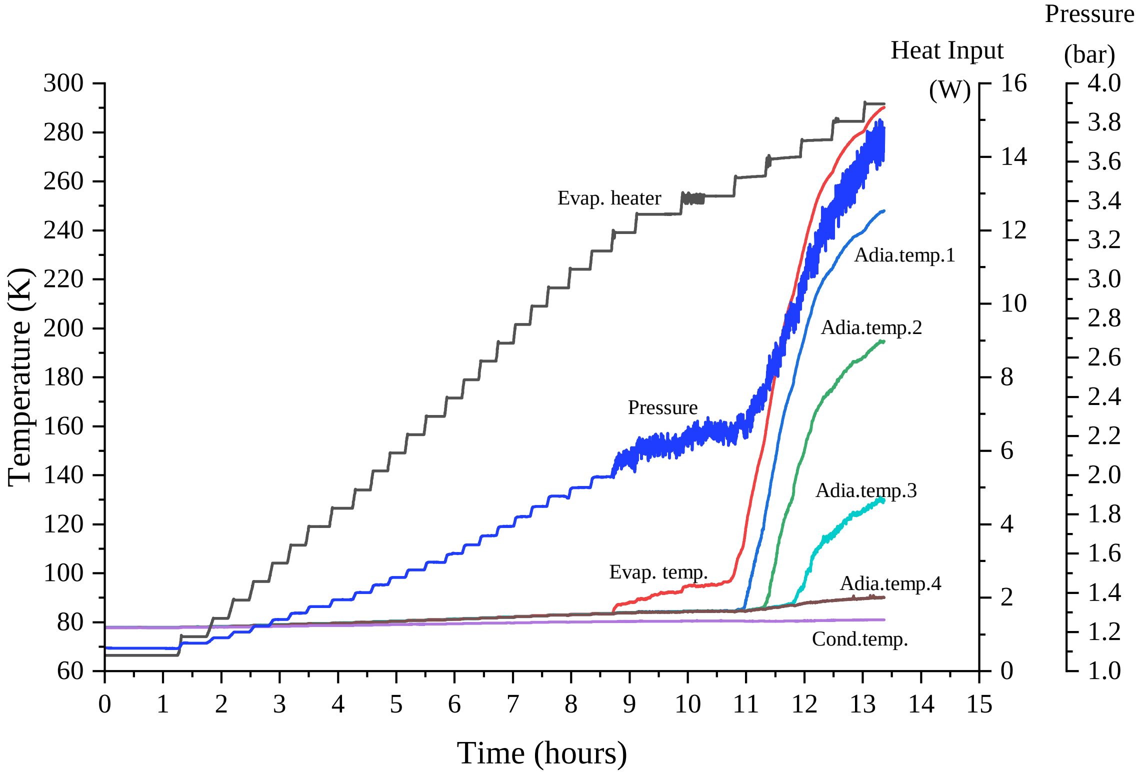

Figure 6.1 *Temperature and pressure variations of the N_2-heat pipe with 100% fill, tested by using liquid nitrogen bath setup as a heat sink.*

by the slow axial oscillating movement of the local dry-out region and the period of the pressure fluctuation, probably it is several to 10 min. Furthermore, probably somewhere between 12 and 13 W, the nucleate boiling in the evaporator section is considered to make transition to the film boiling. For the temperature in the adiabatic section, T_{a1}, T_{a2}, T_{a3}, and T_{a4} started to sharply increase at 13, 14, 14 and 15 W, respectively, while the condenser temperature, T_c, is still nearly constant at LN_2 heat sink temperature. It should be noted that this result of the temperature suggests that the heat pipe was not in the full dry-out state but in the local (or partial) dry-out state, where at least the condenser section was still in the two-phase liquid–vapor co-existing state. In the part of the co-existing state, the heat pipe operation still continued and thus the temperature was kept nearly constant equal to the heat sink temperature.

In Figure 6.2 the similar experimental result of the temperature and pressure variations of the N_2-heat pipe with 100% filling ratio are shown. In this case, the cryocooler was used for

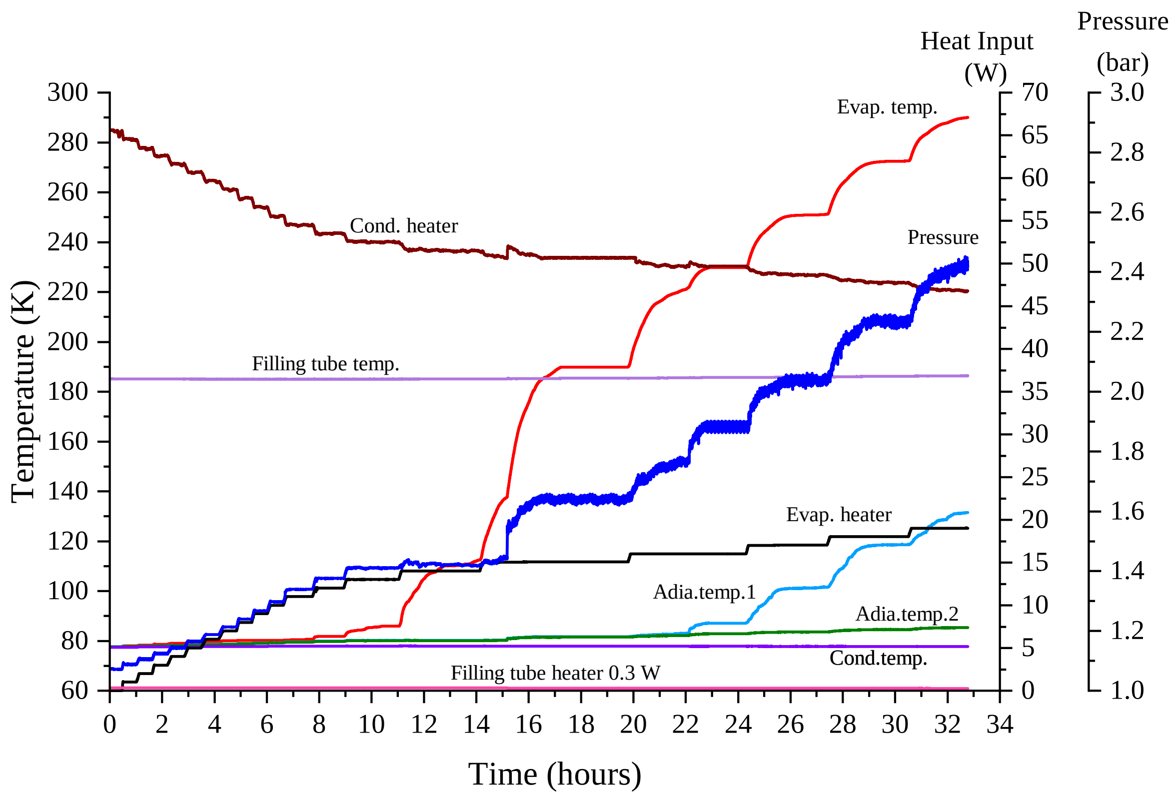

Figure 6.2 *Temperature and pressure variations of the N_2-heat pipe with 100% fill, tested by using the cryocooler as a heat sink.*

cooling the condenser section. An auxiliary heater (Q_c) was installed in the condenser block to control the temperature in the condenser section at a prespecified temperature that was higher than that of the second stage of the cryocooler. An additional heater (Q_f) was also installed over the filling tube to prevent from blocking the tube caused by freezing of working fluid inside the tube. The total heat transfer to the heat sink of the condenser section is always $Q_c + Q_e$ (65.5 W) during the experiments.

The heat input to the filling tube, Q_f, was constant at 0.3 W to keep the temperature at 180 K. In this experimental setup, the number of the temperature sensors in the adiabatic section were reduced to two, T_{a1} and T_{a2}. Although this experimental setup was different from the previous one, the results were almost identical to those shown in Figure 6.1; the rapid increase in T_e and the onset of the pressure fluctuation started at Q_e larger than 13 W. It may be concluded that there is almost no quantitative difference in the experimental data between the cases of using the nitrogen bath and of using the cryocooler as the heat pipe heat sink.

6.1.2 Steady state temperature and pressure plot against heat input

The experimental results of steady state temperatures at each step of the heat input, T_e, T_{a1}, T_{a2}, and T_c, the filling tube temperature, T_f , and the vapor pressure, P, plotted against heat input, Q_e, are shown in Figures 6.3 and 6.4 for the N_2- and Ar-heat pipes, respectively. Here the data are separately plotted for typical three condenser temperatures, including the normal boiling point temperatures of N_2 (77 K) and Ar (87 K). In all cases the cryocooler was used as the heat sink. The temperature in the evaporator, adiabatic and condenser sections, together with the temperature of the filling tube and the saturated vapor temperature, T_{sat}, which was calculated from measured pressure inside the heat pipe, are plotted in the figures.

6.1.2.1 Steady state temperature and pressure plots for nitrogen heat pipe

Figure 6.3-1 shows the result of the N_2-heat pipe operated at the condenser section temperature of 60 K that is lower than the triple point temperature of nitrogen (63.1 K), and thus the condenser section was in the frozen state. The result in the case of very low Q_e that T_e and T_{a1} once only slightly rose after the start of heating though T_c was maintained at the temperature (60 K) that was the temperature before the start of heating seems to suggest that the working fluid was in a frozen state throughout the heat pipe. Then when Q_e increased to 2 W, T_e and T_{a1} gradually decreased, when the working fluid in the evaporator and small part of the adiabatic sections melted and heat was transferred in a partial heat pipe operation state where heat pipe operation occurred not throughout the heat pipe but only locally in a limited area, in the evaporator section in this particular case. This was seen from the fact that T_e was significantly higher than T_c and furthermore was equal to the temperature of saturated vapor converted from the measurement data of the vapor pressure. The temperature T_e only gradually

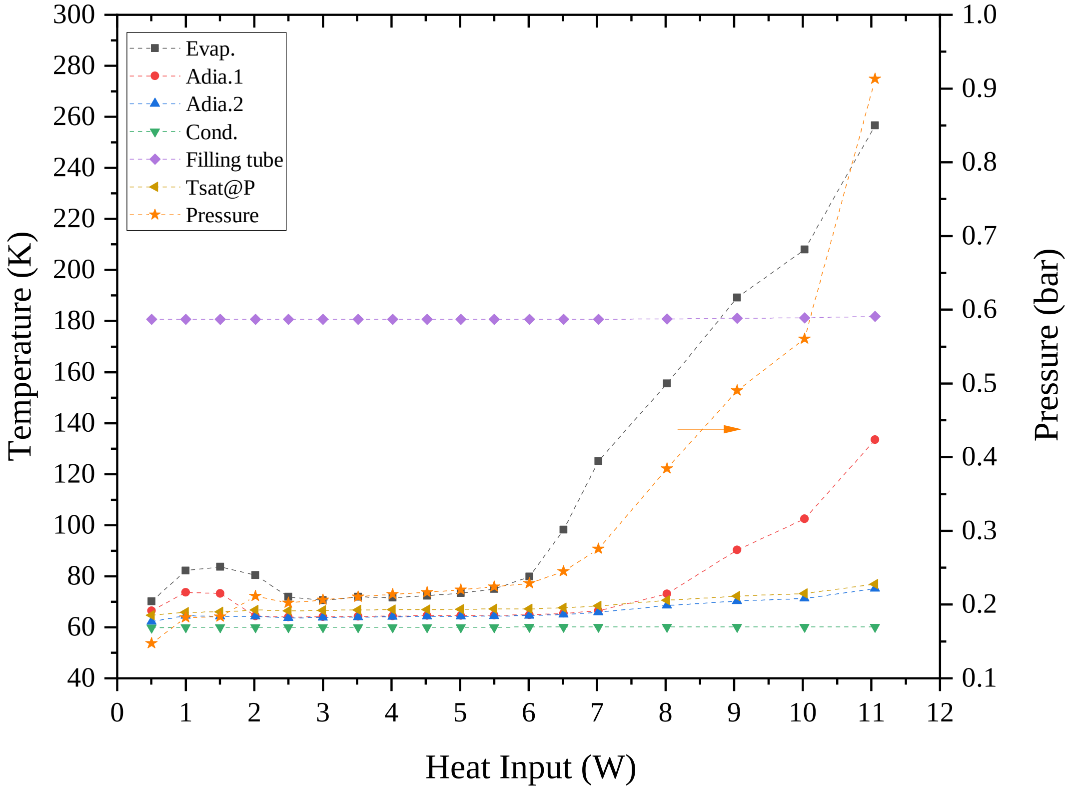

Figure 6.3-1 *Steady state temperature and pressure variation with heat input of N_2-heat pipe, 100% filling ratio, 60 K of condenser temperature.*

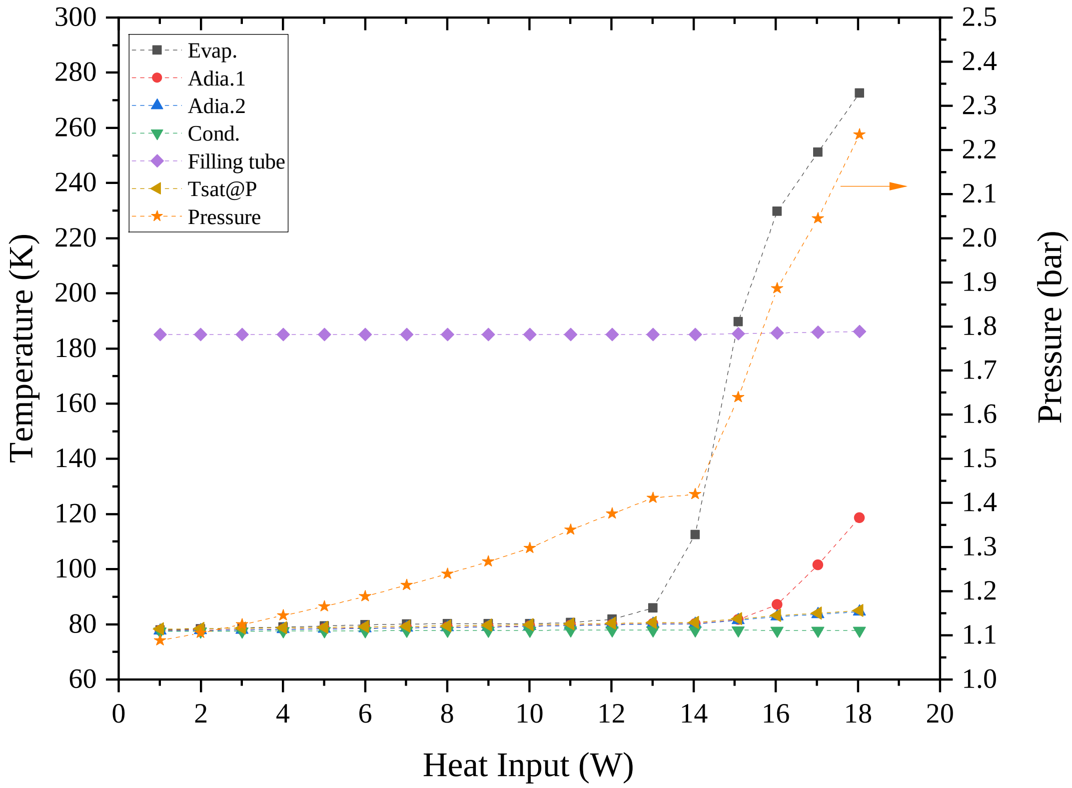

Figure 6.3-2 *Steady state temperature and pressure variation with heat input of N_2-heat pipe, 100% filling ratio, 77 K of condenser temperature.*

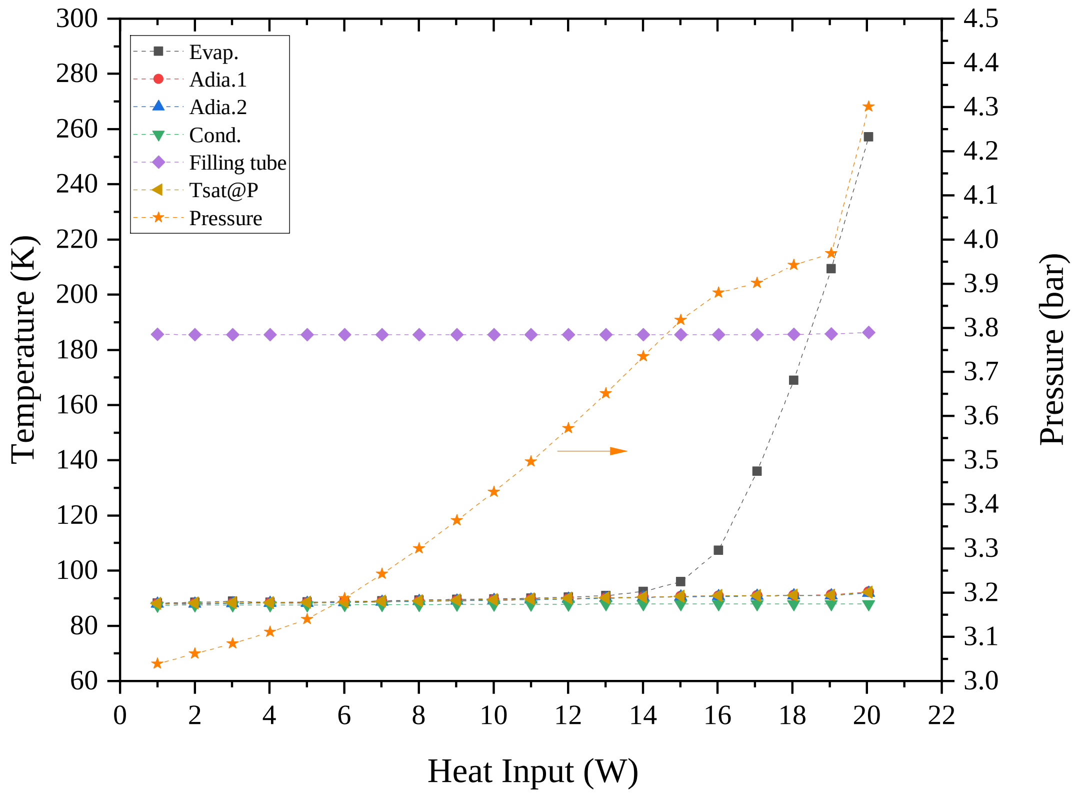

Figure 6.3-3 *Steady state temperature and pressure variation with heat input of N_2-heat pipe, 100% filling ratio, 87 K of condenser temperature.*

increased until Q_e increased to 6 W, due to the appearance of nucleate boiling. Above this value of Q_e, T_e rapidly rose because the dry-out occurred locally in the evaporator section initially, then above 7.5 W the dry-out region proceeded to expand to some area of the adiabatic section on the evaporator section side. It can be confirmed that some part of the adiabatic section and the full condenser section were still in the frozen state even very high Q_e. Throughout the experiment, T_f was controlled to be constant at 180 K to prevent the working fluid in the filling tube from freezing and blocking. The vapor pressure, P, was approximately 0.2 bar for small Q_e. For larger values of Q_e, P started to increase in response to an increase in T_e. The pressure P rose to 0.9 bar within the range of the experimental Q_e.

In Figures 6.3-2 and 6.3-3, the results of the N_2-heat pipe operated at 77 and 87 K of the condenser temperature are respectively shown. It is seen in both cases that as all the temperatures were slightly higher than T_c and since the operating temperature was higher than the tipple point temperature of nitrogen, the working fluid was in the two-phases liquid–vapor region and the heat pipe was in the normal heat pipe operation state. Above 13 and 15 W, which were defined as the maximum heat transport capability Q_{max} in cases of 77 and 87 K of the condenser temperatures respectively, T_e sharply increased. P began to rise from around 1.4 bar to 2.3 bar upon the occurrence of dry-out in the case of 77 K of the condenser temperature.

However, in the case of 87 K of the condenser temperature, the maximum P reached quite a high value of 4.3 bar. The following should be added here that experiments at still higher temperatures could not be performed due to safety reasons that this experimental setup could not withstand such high pressures though the critical temperature of nitrogen is 126.2 K.

6.1.2.2 Steady state temperature and pressure plot for argon heat pipe

In Figure 6.4-1 the experimental result of the Ar-heat pipe operated at 77 K of the condenser temperature that was lower than the triple point temperature of argon (83.8 K) is shown. Since the parallel heat pipe system (as discussed later) that consists of an N_2- and an Ar-heat pipes would be tested at the operating temperature at 77 K, the investigation of the Ar-heat pipe at 77 K is necessary. For small Q_e, the behavior of the Ar-heat pipe was quite similar to that of the N_2-heat pipe (Figure 6.3-1) except that not only T_e and T_{a1}, but also T_{a2} were different from T_c. However, above 3 W of Q_e, T_e was rather higher than the condenser section temperature, though it slightly decreased around 9 W. This may be the result of melting of the working fluid in the evaporator section. As the further increase in Q_e, the melting region expanded to the adiabatic section as seen from T_{a1} and T_{a2} that reduced to T_{sat} up to 20 W, above which value of Q_e the adiabatic section temperature T_{a1} started to rapidly increase. The evaporator temperature T_e steeply increased to a far higher value than T_c due to the occurrence of the local dry-out in the region. This indicates that there was no liquid in the evaporator section. In this state, T_{a2} was found to still agree with T_{sat}, and T_c was constant at 77 K, which

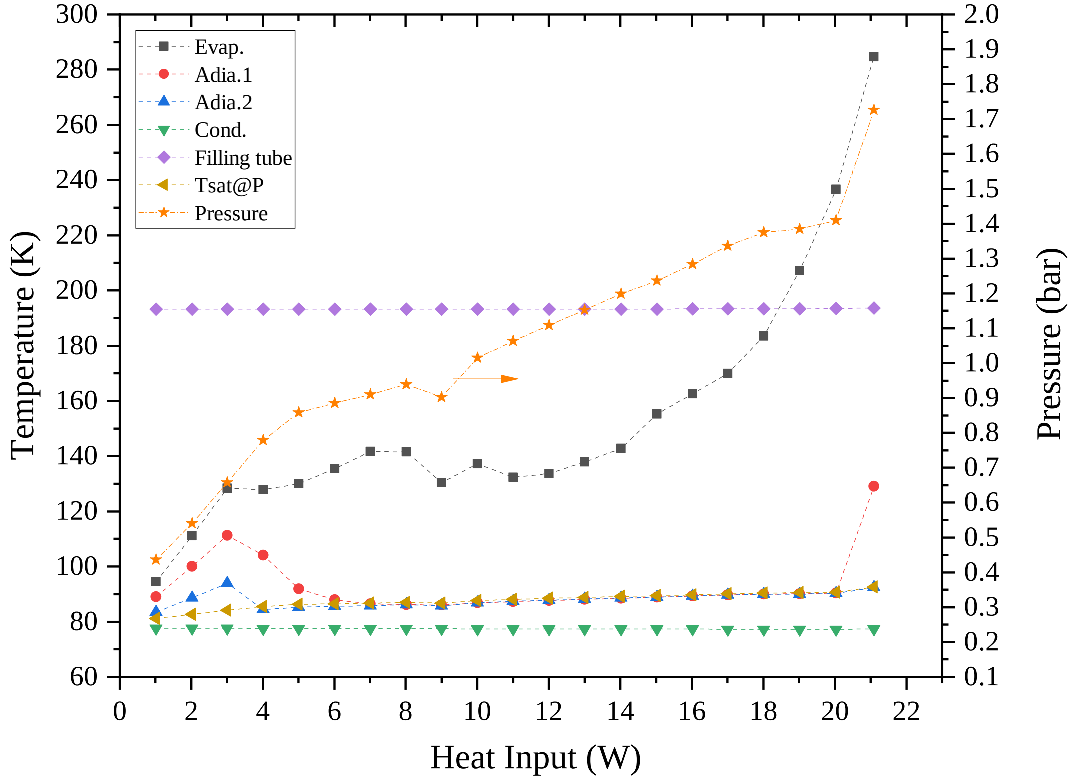

Figure 6.4-1 *Steady state temperature and pressure variation with heat input of Ar-heat pipe, 100% filling ratio, 77 K of condenser temperature.*

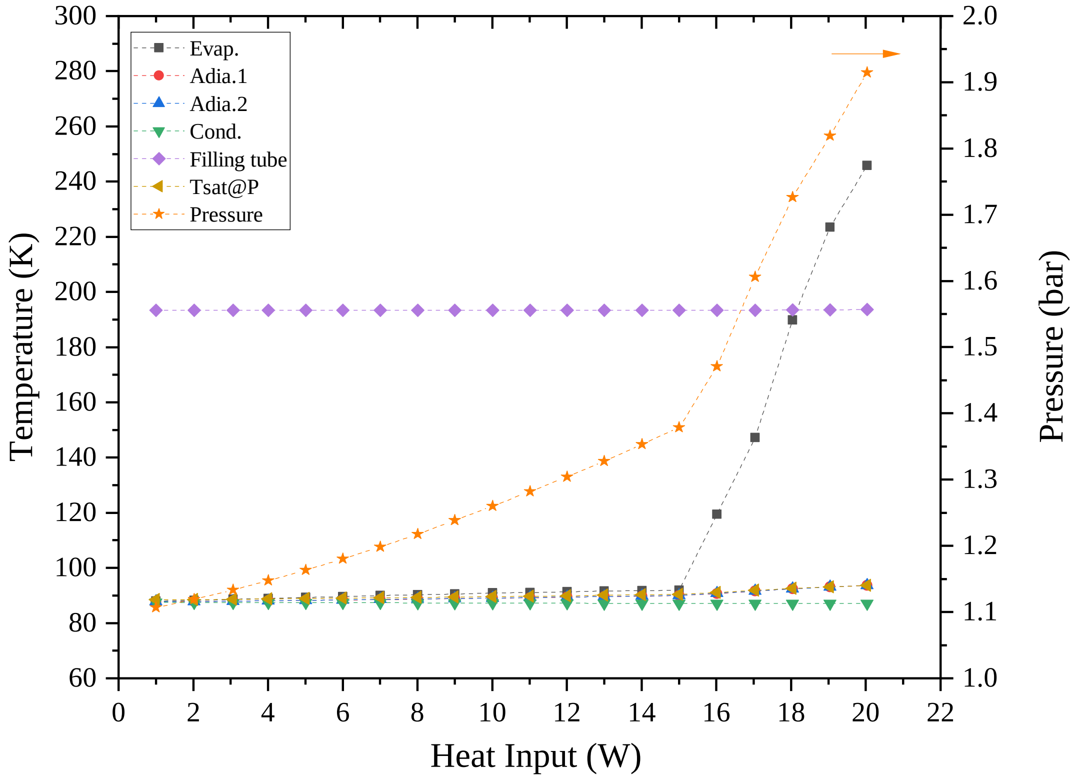

Figure 6.4-2 *Steady state temperature and pressure variation with heat input of Ar-heat pipe, 100% filling ratio, 87 K of condenser temperature.*

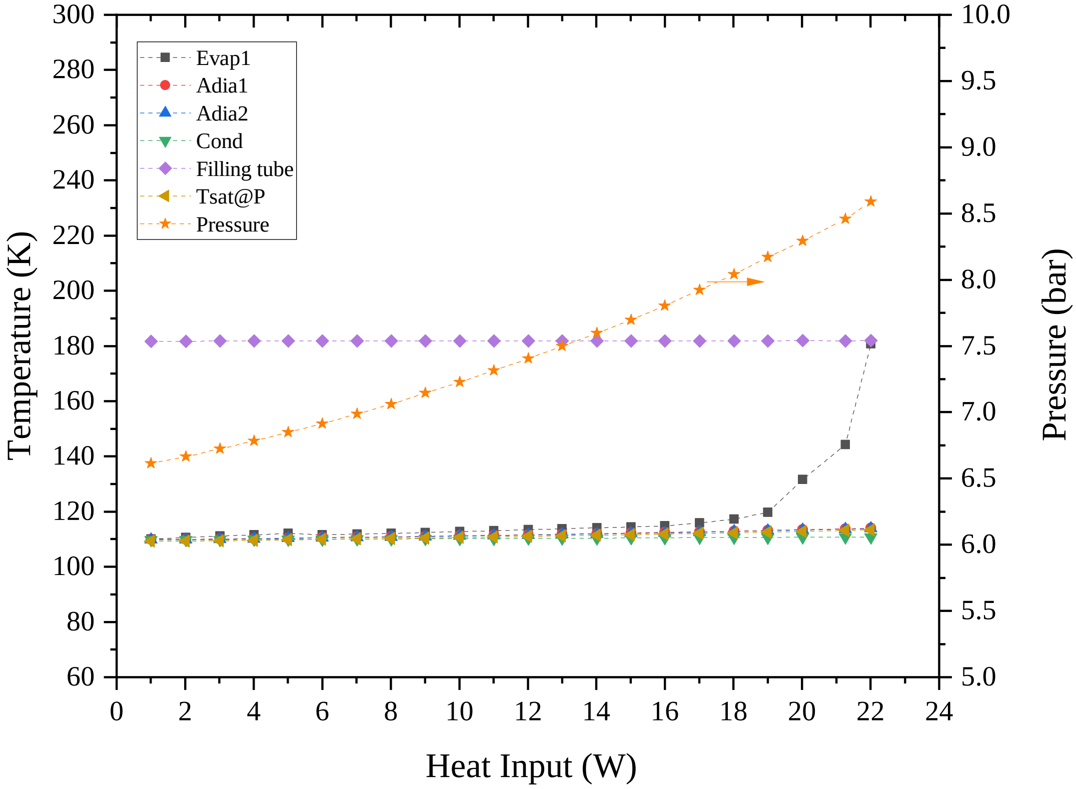

Figure 6.4-3 *Steady state temperature and pressure variation with heat input of Ar-heat pipe, 100% filling ratio, 110 K of condenser temperature.*

indicated that in the condenser side of the adiabatic section local heat pipe action occurred and, at the same time in the condenser section, the working fluid was still frozen.

In Figures 6.4-2 and 6.4-3 the results of the Ar-heat pipe operated at 87 and 110 K of the condenser temperatures, respectively are shown. It can be seen that there is an extremely small but significant temperature difference between T_e and T_c for both cases, which indicates that the heat pipe was in the normal heat pipe operation. T_e rapidly increased when Q_e reached 15 and 19 W for 87 and 110 K of condenser temperatures, respectively. Furthermore, T_{a1} and T_{a2} were in quite a good agreement with T_{sat} which were a little bit higher than T_c. Please note the value of P for the case of 110 K of the condenser temperature that it is extremely high though the critical temperature of argon is 150 K. Consequently, 110 K of the condenser temperature was the highest test temperature for this experimental setup.

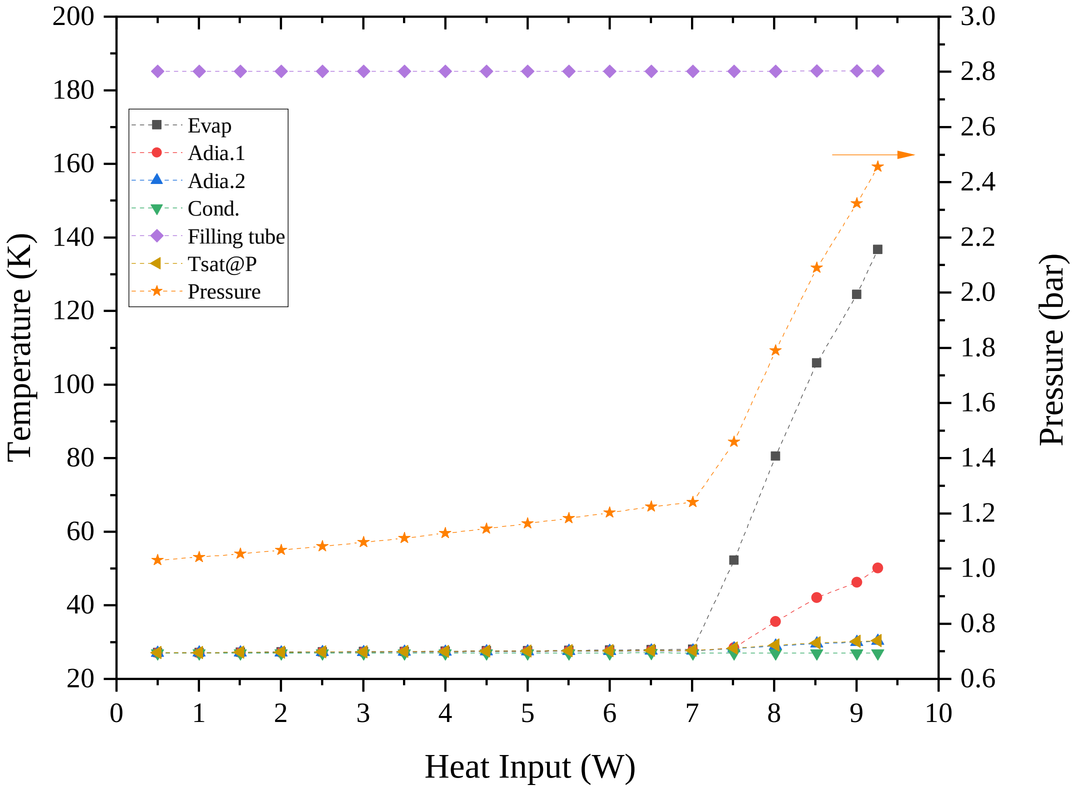

Figure 6.5 *Steady state temperature and pressure variation with heat input of Ne-heat pipe, 100% filling ratio, 27 K of condenser temperature.*

6.1.2.3 Steady state temperature and pressure plot for neon heat pipe

The experiments of commercially available conventional heat pipes with working fluid replaced with neon were conducted to examine the thermal behavior of the Ne-heat pipe and to explore the potential applicability to HTC magnet cooling. In Figure 6.5 the result of the Ne-heat pipe operated at 27 K of the condenser temperature, which is the normal boiling point of Neon, is shown. It is seen that the heat pipe was in the normal heat pipe operation state as the temperature was slightly higher than the triple point and thus the working fluid was in the two-phases liquid–vapor region just the same as in cases of the N_2-heat pipe and the Ar-heat pipe. It was indicated that it is possible for commercially available conventional heat pipes with working fluid replaced with neon to operate at 27 K. T_e and P rapidly increased when Q_e reached 7 W that was the Q_{max} of Ne-heat pipe with 100% filling ratio and 27 K of the condenser temperature in the horizontal arrangement. Furthermore, T_{a1} and T_{a2} were in quite a good agreement with T_{sat} which were a little bit higher than T_c. When Q_e reached 8 W, T_{a1} started increasing, which indicates that local dry-out region expended to some part of the adiabatic section while T_{a2} was still in fair agreement with T_{sat} .

6.1.3 Temperature distribution in the length direction of the heat pipe

In order to see the normal heat pipe action inside heat pipes in more detail, the temperature distributions along the heat pipes are examined, which were measured on the heat pipe outer surface.

Longitudinal temperature distributions are shown on the basis of four temperature measurement data in Figures 6.6 and 6.7 for the N_2- and Ar-heat pipes, respectively. In these figures, the triple point temperatures, 63.1 and 83.8 K, and the critical temperatures, 126.2 and 150.8 K are indicated by fine solid lines in cases of N_2 and Ar, respectively. Rough classification criterion for the physical states of working fluid, that is the frozen, two phases, film boiling or dry-out states are as follows:

- below 24.5 K, (Ne), 63.1 K (N_2), and 83.8 K (Ar); frozen state,
- above 44.5 K (Ne), 126.3 K (N_2), and 150.8 K (Ar); dry-out state,
- in between; two-phases liquid–vapor co-existing state including nucleate or film boiling.

6.1.3.1 Temperature distribution of nitrogen heat pipe

Figures 6.6-1–6.6-3 show the wall temperature distributions of the N_2-heat pipe operated at 60, 77 and 87 K of the condenser temperatures in cases of several values of the heat input Q_e. It can be seen in Figure 6.6-1 that the temperatures from the condenser section to some part of the adiabatic section, 120–200 mm, were below 63.1 K at low values of Q_e, which means the working fluid was frozen in this region. It is further plausible that the working fluid

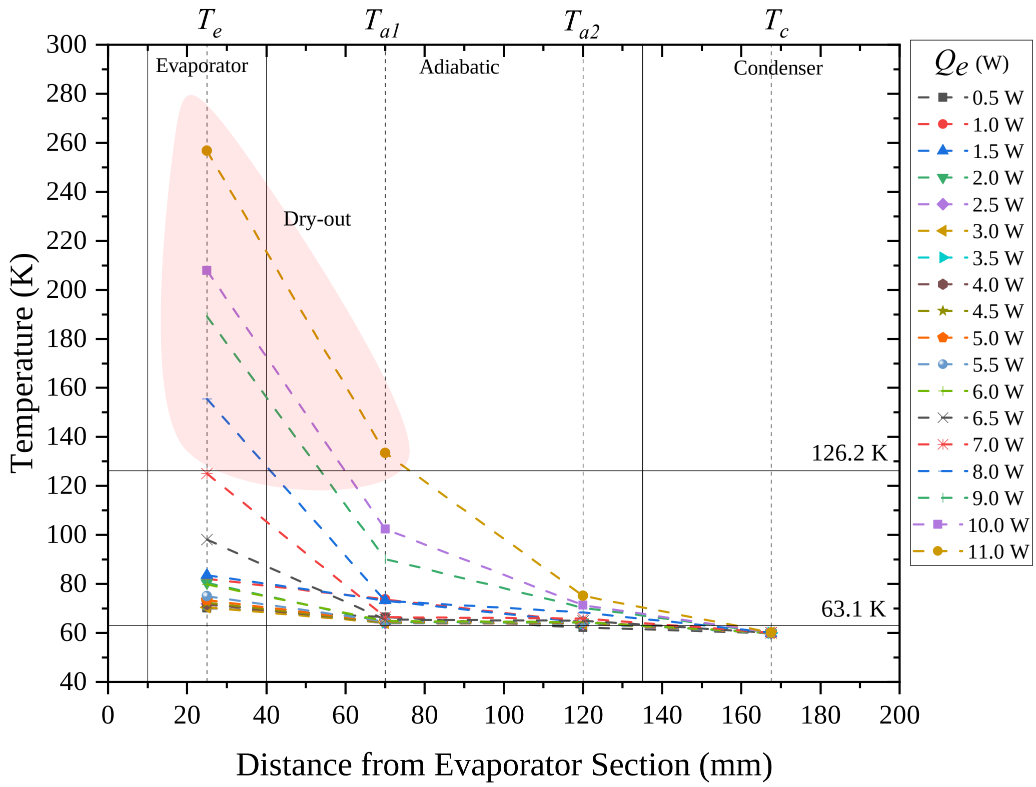

Figure 6.6-1 *Wall temperature distributions along the length of the heat pipes for various heat inputs to the N_2-heat pipe, 100% filling ratio, 60 K of condenser temperature.*

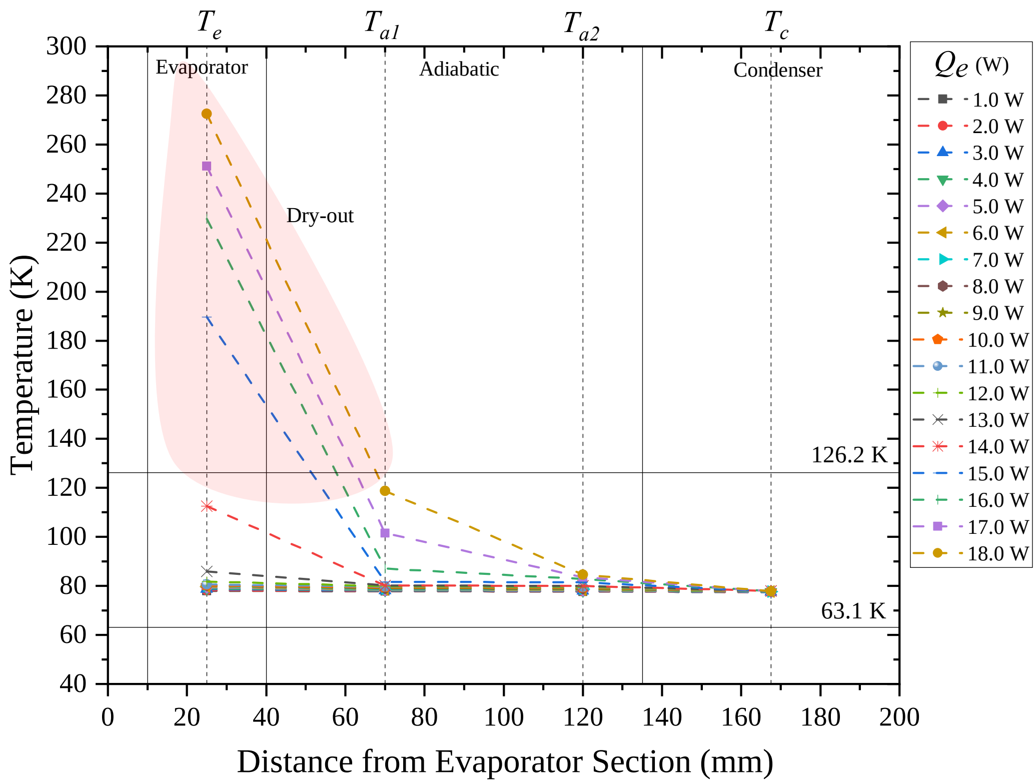

Figure 6.6-2 *Wall temperature distributions along the length of the heat pipes for various heat inputs to the N_2-heat pipe, 100% filling ratio,77 K of condenser temperature.*

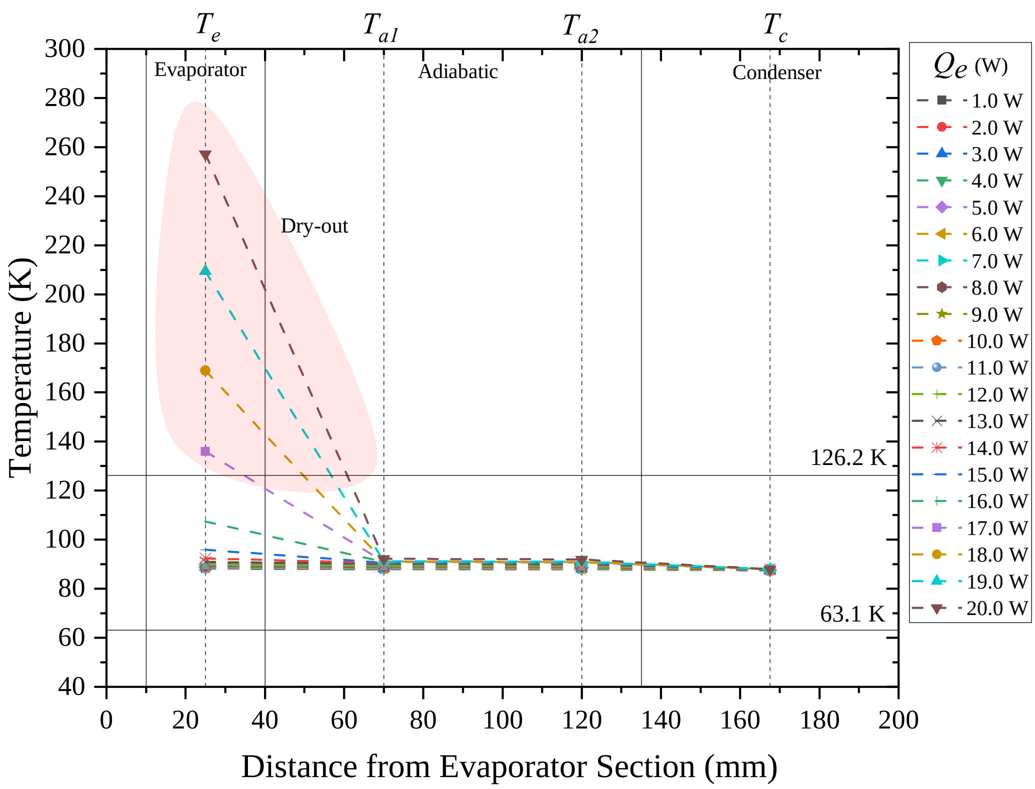

***Figure 6.6-3** Wall temperature distributions along the length of the heat pipes for various heat inputs to the N_2-heat pip, 100% filling ratio, 87 K of condenser temperature.*

was frozen from 160 to 200 mm for any values of Q_e. In contrast, there was no frozen working fluid throughout the heat pipe in cases of 77 and 87 K of the condenser temperature. It is seen in Figure 6.6-1 that the dry-out occurred in the evaporator section and some part of the adiabatic section for Q_e of 8–11 W (for 7 W, dry-out began only in the evaporator section). The dry-out state appeared in cases of Q_e of 15–18 W (14 W, film boiling occur) in the case of T_c at 77 K as shown in Figure 6.6-2, and 17–20 W in case of T_c at 87 K as shown in Figure 6.6-3.

6.1.3.2 Temperature distribution of argon heat pipe

Figures 6.7-1–6.7-3 show the wall temperature distribution of the Ar-heat pipe for several values of the heat input, Q_e, which was operated at 77, 87 and 110 K of the condenser temperatures, respectively. It is seen in Figure 6.7-1 for case of Q_e of 1 W that the temperatures

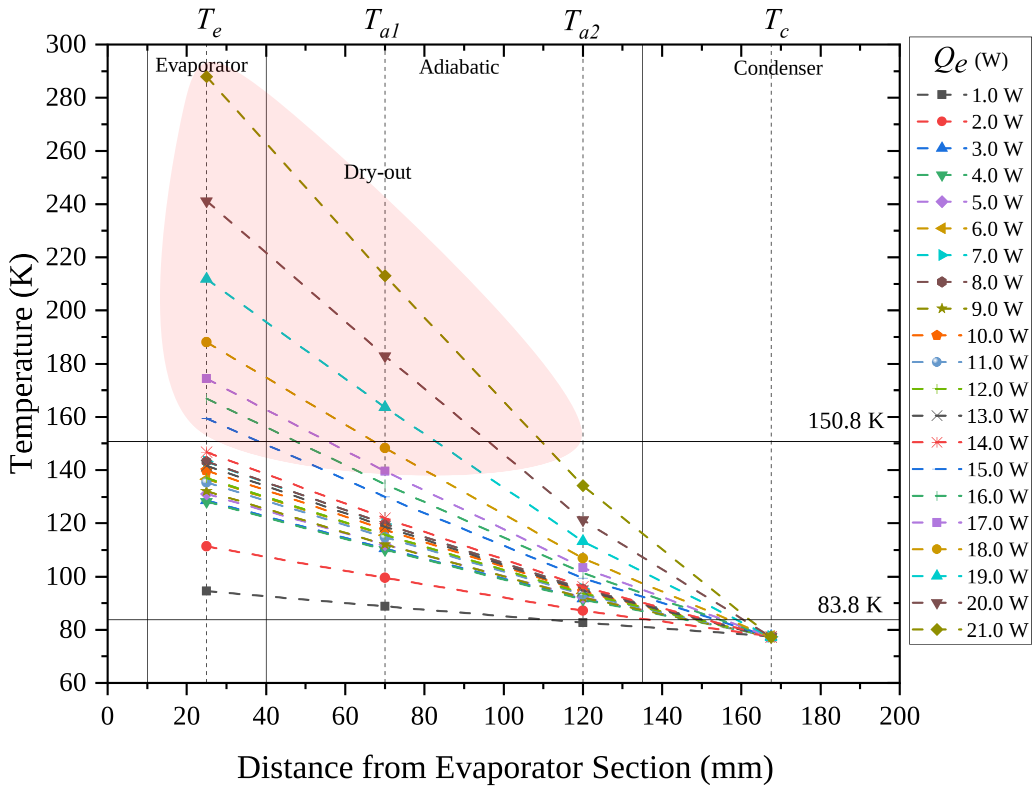

Figure 6.7-1 *Wall temperature distributions along the length of the heat pipes for various heat inputs to the Ar-heat pipe, 100% filling ratio, 77 K of condenser temperature.*

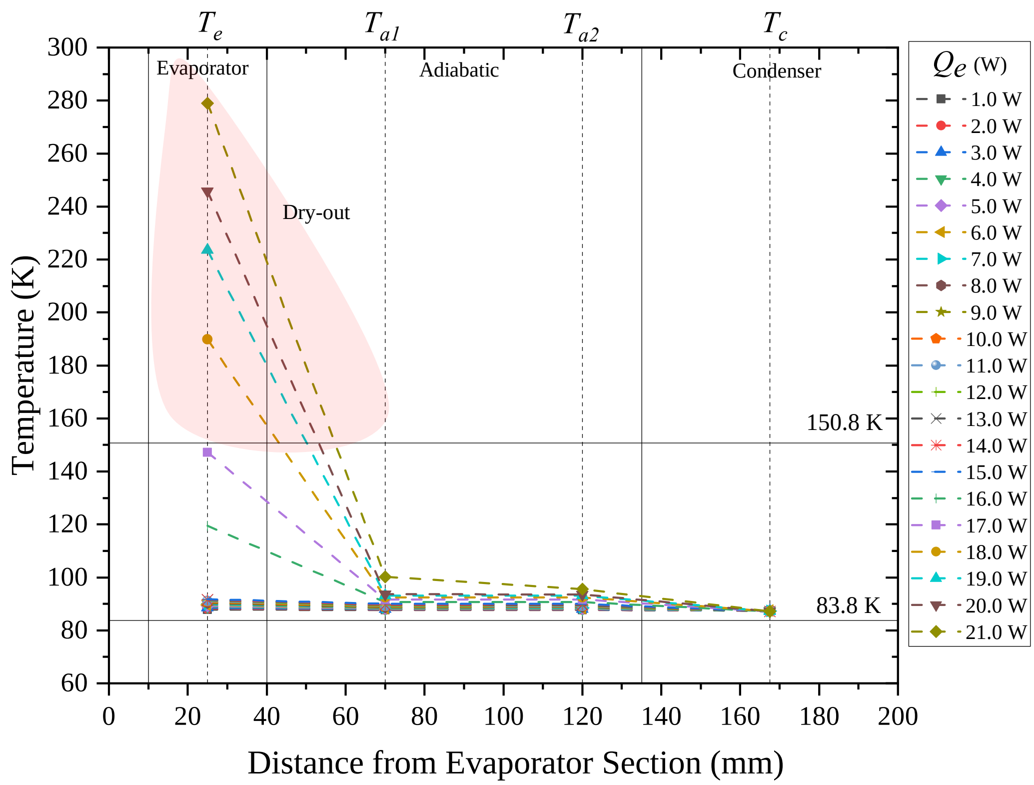

Figure 6.7-2 *Wall temperature distributions along the length of the heat pipes for various heat inputs to the Ar-heat pipe, 100% filling ratio, 87 K of condenser temperature.*

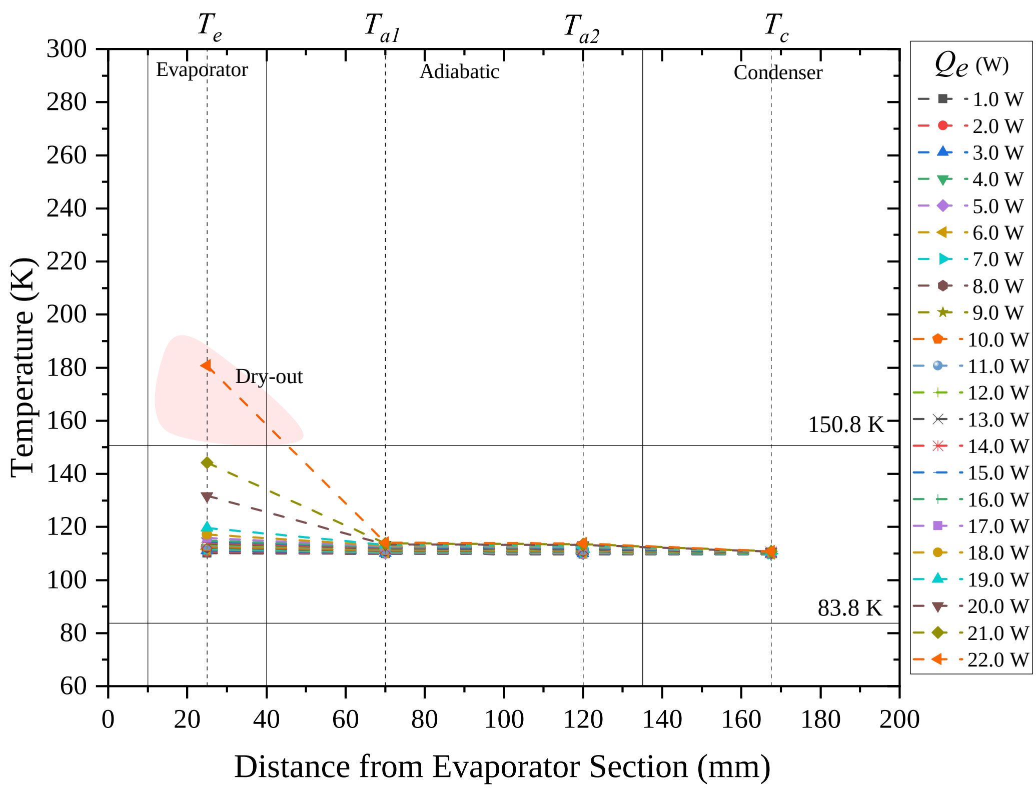

Figure 6.7-3 *Wall temperature distributions along the length of the heat pipes for various heat inputs to the Ar-heat pipe, 100% filling ratio, 110 K of condenser temperature.*

of the condenser section and some part of the adiabatic section between 120–200 mm was below 83.8 K. This result indicates that the working fluid was frozen in this region. This is also true from 160–200 mm irrespectively of Q_e. It is also indicated in Figure 6.7-1 that even for small values of Q_e there was a rather high temperature region in the evaporator and adiabatic sections, where the temperature distributions are nearly linear. These results seem to suggest that even for low values of Q_e the heat pipe was partially dry-out in the linear region, where there was no vapor flow to transfer heat and thus heat was transferred conductively through the pipe wall and frozen working fluid when the working fluid was frozen in the condenser section. With the increase of Q_e from 3 to 14 W, the temperatures changed almost linearly on a small scale, when the working fluid was in melted state in the evaporator section and some part of the adiabatic section, which resulted in the partial heat pipe action in the region. Above 14 W, there was not enough condensate liquid in the evaporator and the adiabatic sections, and dry-out occurred in the evaporator section and then the dry-out region expanded to the adiabatic section for very large Q_e. For operating temperature at 87 and 110 K the data are shown in Figures 6.7-2 and 6.7-3, respectively. It is seen that the normal heat pipe operation was occurring throughout the adiabatic section, when T_{a1} and T_{a2} rose slightly, and the condenser section temperature T_c rose relatively small. However, T_e increased beyond the critical temperature (150.8 K) due to complete dry-out in the evaporator section when Q_e exceeded 18 W as shown in Figure 6.7-2, and 22 W as shown in Figure 6.7-3.

6.1.3.3 Temperature distribution of neon heat pipe

Figure 6.8 show the wall temperature distribution of the Ne-heat pipe for several values of the heat input, Q_e, operated at 27 K of the condenser temperature, which was between the triple point (24.5 K) and the critical point (44.5 K). It is seen that the normal heat pipe operation was occurring with Q_e below 7.5 W. When Q_e was 7.5 W, T_e increased beyond the critical temperature and the evaporator section was completely in the dry-out state. At 8.5 W of Q_e, T_{a1} reached the critical temperature, which indicates that dry-out occurs also in some part of the adiabatic section.

6.1.4 Effect of filling ratio on the heat transfer performance

The thermal performance of a heat pipe can be characterized by the overall thermal resistance, which is defined as the ratio of the temperature difference between the evaporator T_e and the condenser T_c sections to the heat input Q_e ,

$$R_{th} = \frac{T_e - T_c}{Q_e} \tag{6.1}$$

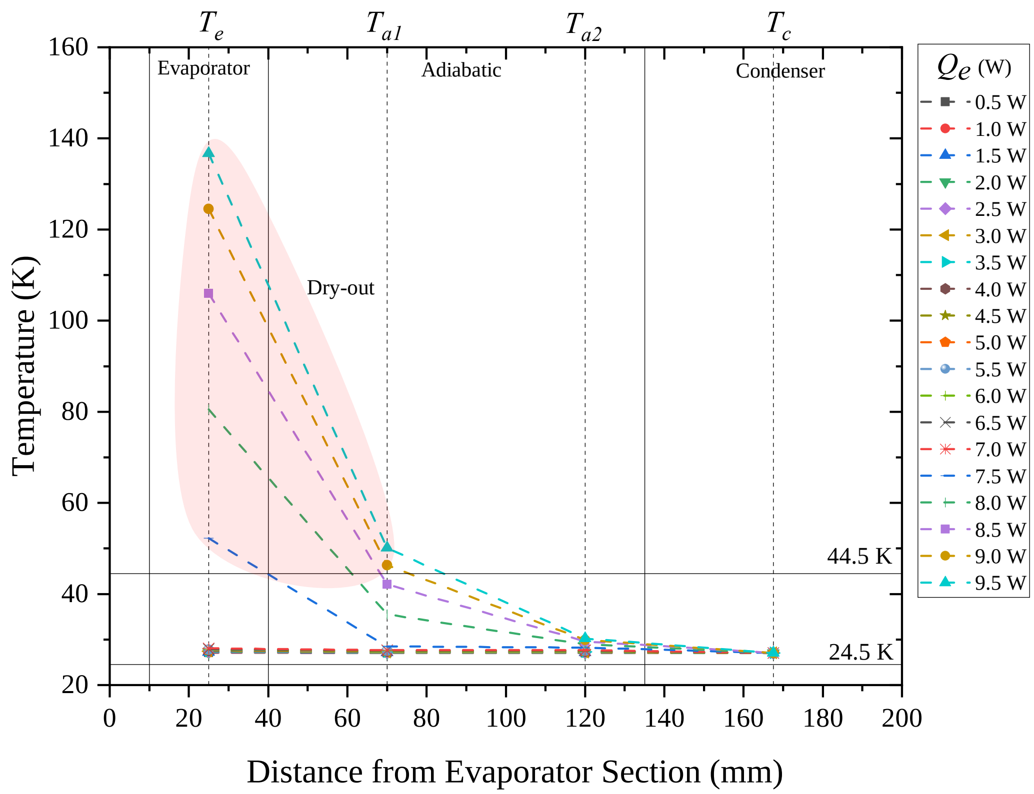

Figure 6.8 *Wall temperature distributions along the length of the heat pipes for various heat inputs to the Ne-heat pipe, 100% filling ratio, 27 K of condenser temperature.*

In Figures 6.9 and 6.10, the overall thermal resistance of the heat pipe is plotted as a function of heat input Q_e for several filling ratios for the N_2- and Ar-heat pipes, respectively. The overall thermal resistance result was obtained also for the case of the heat pipe without any working fluid (0% filling ratio), where heat was transferred solely by thermal conduction through copper heat pipe tube wall and the wick structure. In these two figures the calculation results of thermal resistance of a copper tube and a copper rod with the same diameter, length and material as the heat pipes are also presented as averaged values over the temperature from 77 K (N_2) and 87 K (Ar) to 300 K for comparison with the heat pipe results. It is seen in these figures that the experimental results of the thermal resistance of the heat pipe without working fluid inside for both cases of the N_2- and Ar-heat pipes well agree with the calculation results of the thermal resistance of empty copper tube with the same cross-sectional area as that of the present experimental heat pipe.

6.1.4.1 Effect of filling ratio of nitrogen heat pipe

It is seen in Figure 6.9 that the experimental result of 36% filling ratio is very close to the result of 0% filling ratio except the case of very small Q_e, where heat is transferred not only conductively through the heat pipe wall and the wick containing working fluid but also in a heat pipe mode only in the limited region near the condenser section. Thus, the temperature of the evaporator section is a little bit lower than that of 0% filling ratio. In cases of the filling ratios larger than 52%, the thermal resistance extremely decreases, which indicates that the N_2-heat pipe was in the normal heat pipe operation state, of which the overall thermal resistance is 0.2–0.3 K/W, approximately.

Three thermal regions can be distinguished with respect to the magnitude of the thermal resistance in Figure 6.9. First one is the lowest thermal resistance region in the normal heat pipe operation state. In this region the minimum thermal resistance is realized, and this is the basis for the excellent heat transfer performance of heat pipes. There is a transition region where Q_e is larger than that of the best performance, which leads to the local dry-out region. In the third region where the heat input is larger than the maximum heat transport capability, Q_{max}, the temperature begins to rise sharply in the evaporator section due to the dry-out. It should, however, be noted that the thermal resistance in the local dry-out state is still considerably smaller than that of pure thermal conduction through the pipe wall. This means that the local dry-out occurred in a limited local area in the evaporator and at most some part of the adiabatic sections but in the rest the heat pipe operation still continued. For still larger Q_e, the thermal resistance gets higher and higher toward the thermal resistance of the heat pipe without working fluid (0% filling ratio).

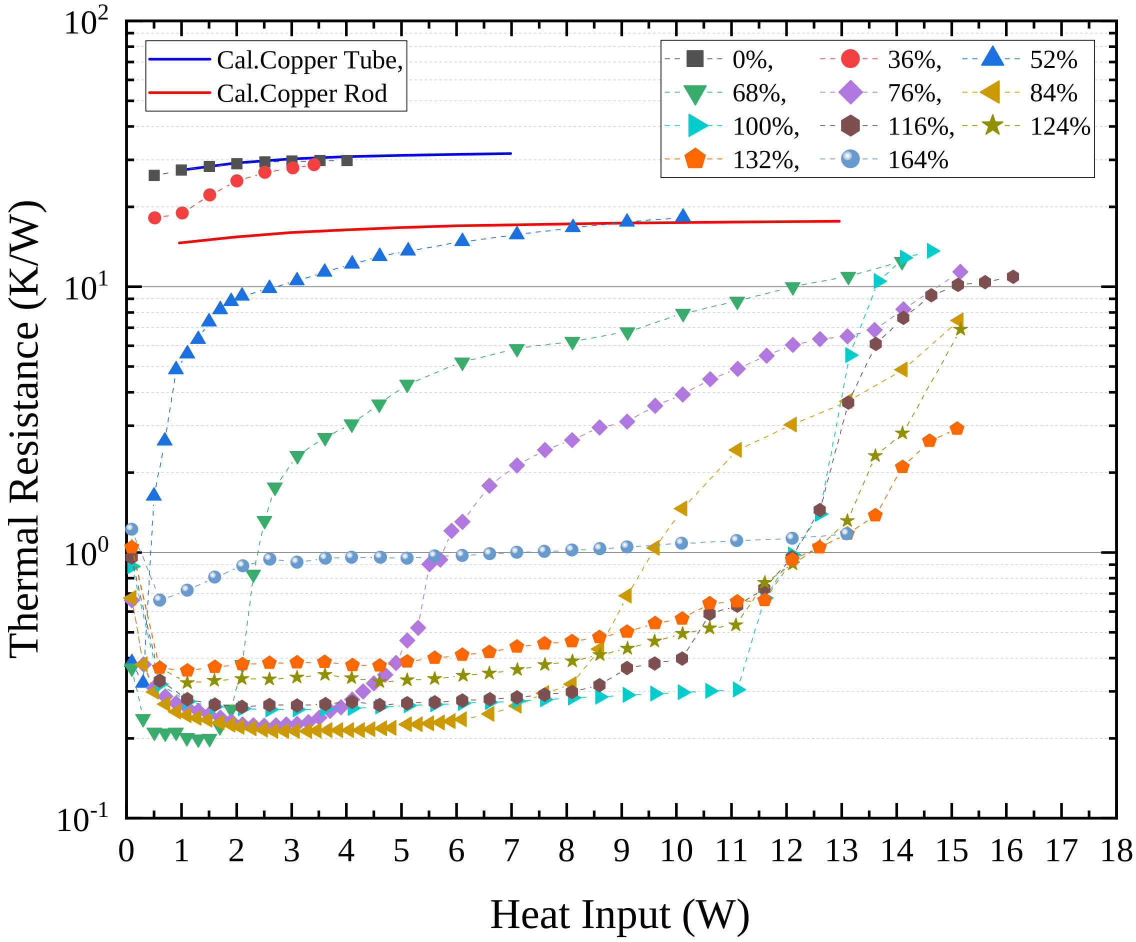

Figure 6.9 *Thermal resistances of N_2-heat pipe as a function of heat input for several filling ratios.*

In general, the thermal resistance, R_{th}, of a heat pipe was not so small for very small Q_e, because the heat pipe did not wholly work as a heat pipe. With a slight increase of Q_e, it decreased down to the minimum value, when the heat pipe exerted its maximum performance. The value of R_{th} slightly increased with a further increase in Q_e due to the onset of nucleate boiling in the wick of the evaporator section. This type of concave curve of R_{th} with the increase of Q_e has been confirmed in previous studies of heat pipes [1]. The Q_e value when the sharp temperature rise starts due to the appearance of the local dry-out in the evaporator section is defined as the maximum heat transport capability, Q_{max}, which is one of the important indicators of the heat transfer performance of a heat pipe as well as the thermal resistance.

The technical term of the local dry-out is used here to distinguish it from the complete dry-out. In the local dry-out state, only the evaporator section is in dry-out state characterized by a rapid temperature rise, but in the other sections the normal heat pipe operation still continues, which is suggested by much smaller value of R_{th} than that of a copper tube. As seen in Figure 6.9, the value of Q_{max} strongly depends upon the working fluid filling ratio. In general, the larger filling ratio results in the larger Q_{max}. For example, 0.5, 2, 4, 8, 12 W, are the Q_{max} values for 52, 68, 76, 84 and 100% filling ratios, respectively. For the filling ratios larger than 100%, Q_{max} does increase with the increase of the filling ratio if not noticeably. This will be discussed in more detail in the later section.

6.1.4.2 Effect of filling ratio of argon heat pipe

It is evident from the experimental result of the N_2-heat pipe that the filling ratio of less than 50% is not sufficient for heat pipes to satisfactorily operate. Therefore, in general, heat pipes with the filling ratio smaller than 50% should not be used in practical applications.

The Ar-heat pipe experiments start with 50% of filling ratio as shown in Figure 6.10. With increasing Q_e, from 0 W, the value R_{th} extremely decreases, and the Ar-heat pipe goes to the normal heat pipe operating state with the value of R_{th} 0.25–0.3 K/W, approximately. This result indicates that the Ar-heat pipe has the value of R_{th} slightly higher than of the N_2-heat pipe because the thermal conductivity of liquid Ar (LAr) is smaller than that of liquid N_2 and higher viscosity of LAr increases its flow resistance. It is found that there are also three operation regions in case of the Ar-heat pipe as with N_2-heat pipes. As seen in Figure 6.10, the values of Q_{max} for 50, 60, 70, 80, 90, 100 and 110% filling ratios are 0.5, 2, 4, 9, 13, 15 and 16 W, respectively.

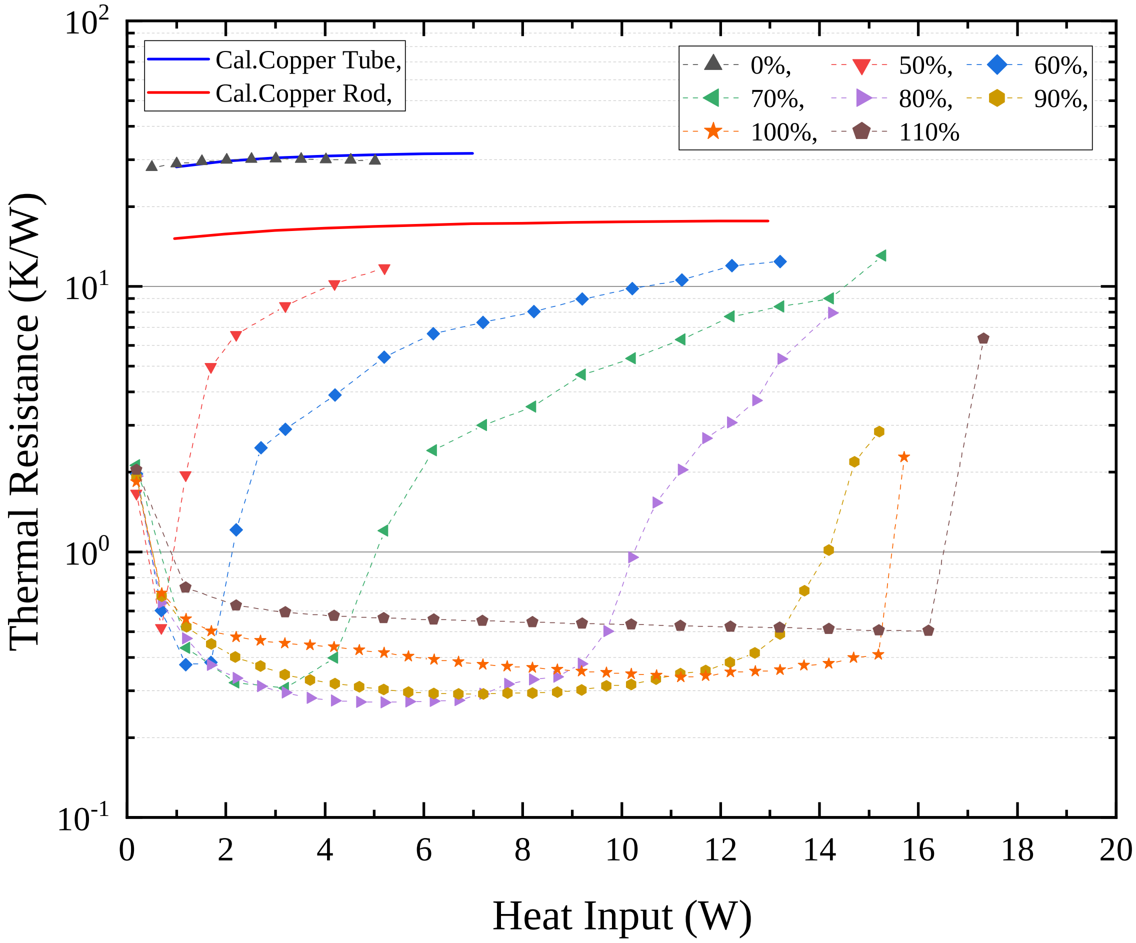

Figure 6.10 *Thermal resistances of Ar-heat pipe as a function of heat inputs for several filling ratios.*

6.1.4.3 Comparison of thermal resistance between nitrogen, argon and neon heat pipes

Nitrogen, argon, and neon have different thermophysical properties as shown in Table 6.1. That is why the thermal performance of the N_2-heat pipe, the Ar-heat pipe and the Ne-heat pipe are much different each other. Since the thermal conductivities of liquid and vapor neon are higher and liquid viscosity is lower than those of nitrogen and argon, R_{th} of the Ne-heat pipe is the lowest in normal heat pipe operation phase as seen in Figure 6.11. On the other hand, for the surface tension that is a decisive parameter for the capillary force, argon has a higher value than nitrogen and neon, and therefore, Q_{max} of the Ar-heat pipe is larger than those of the N_2-heat pipe and Ne-heat pipe with the same filling ratio as also seen in Figure 6.11.

Table 6.1 *Thermophysical properties of nitrogen, argon, and neon at their normal boiling points*

Working fluid	Temperature (K)	Pressure (bar)	Density (kg/m3) Liquid (Vapor)	Latent heat of vaporization (kJ/kg)	Liquid viscosity (μPa·s) Liquid (Vapor)	Therm. Cond. (W/(m·K)) Liquid (Vapor)	Surf. Tension (N/m)
Nitrogen [2]	77.4	1.01	805.9 (4.6)	199.1	160.4 (5.4)	0.146 (0.007)	0.008864
Argon [3]	87.3	1.01	1395.4 (5.8)	116.2	270.7 (7.1)	0.125 (0.005)	0.012531
Neon [4]	27.0	1.01	1207.1 (9.5)	85.8	116.2 (4.5)	0.155 (0.008)	0.0045265

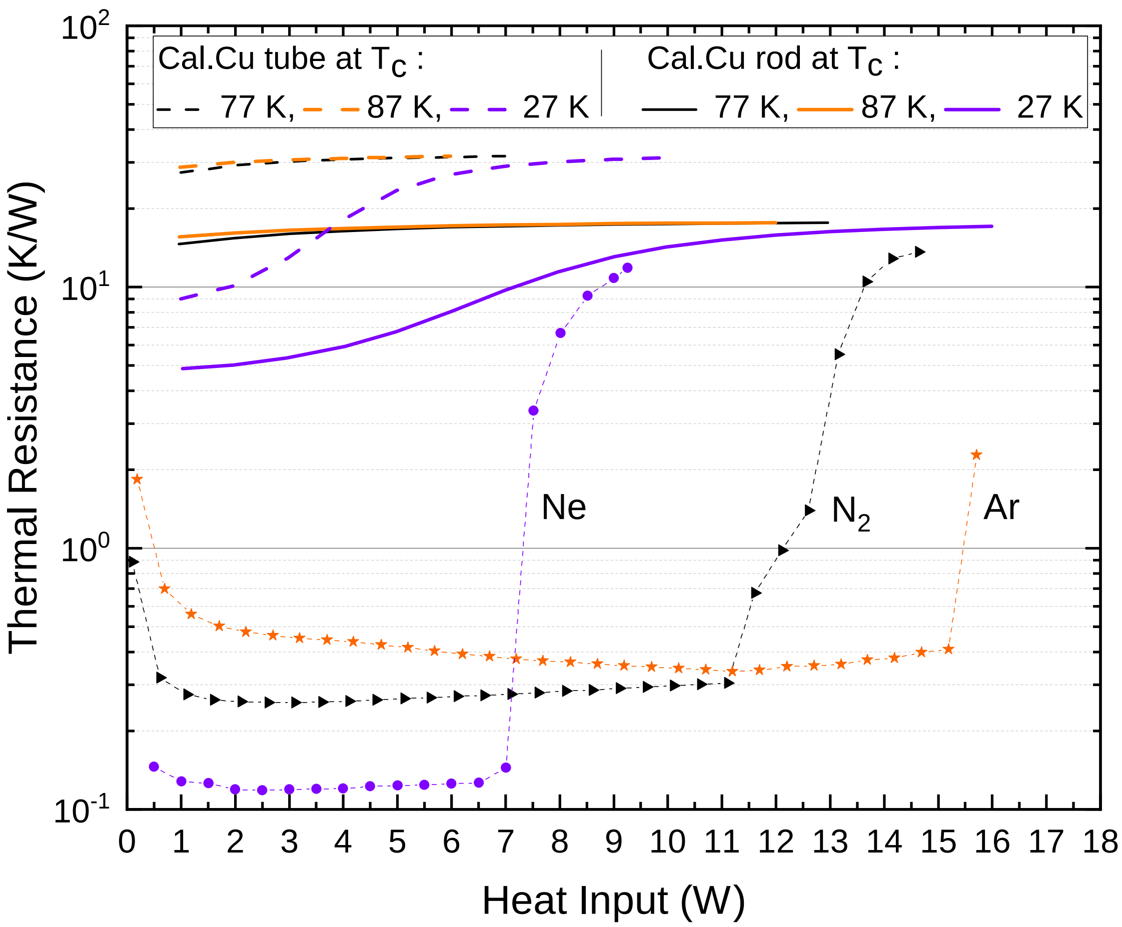

Figure 6.11 *Comparison of thermal resistances of N_2-heat pipe, Ar-heat pipe, and Ne-heat pipe for 100% filling ratio*

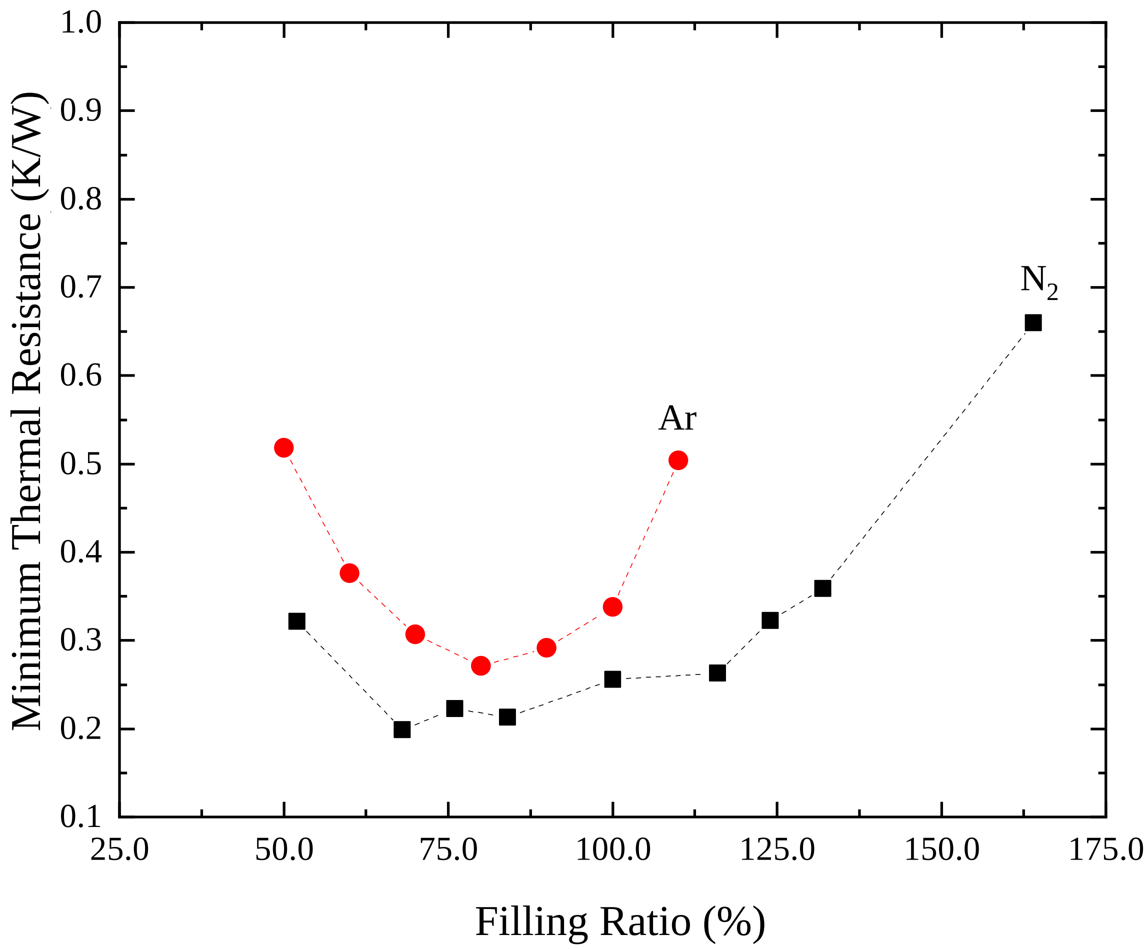

Figure 6.12 *Minimum thermal resistances of* N_2-heat pipe and *Ar-heat pipe as a function of filling ratio.*

In Figure 6.12 the minimum thermal resistance, $R_{th,min}$, in the normal heat pipe operation phase is plotted against the filling ratio for the N_2- and the Ar-heat pipes. It can be seen in Figure 6.12 that the N_2-heat pipe is superior to the Ar-heat pipe with respect to R_{th} for a wide range of the filling ratio. For the filling ratio less than 80%, $R_{th,min}$ decreases with the increase in the filling ratio. This result can be explained by the fact that the less working fluid, the more likely it is that the boiling in the wick of the evaporator section will occur. However, for filling ratio more than 80%, $R_{th,min}$ increases with the increase of the filling ratio. With the increase of the filling ratio, the thickness of the condensed liquid of working fluid increases resulting in larger thermal resistance in the heat transfer path across the wick. The reason why $R_{th,min}$ occurs not at 100 % but around 80 %, is that these heat pipes were originally designed to employ water as a working fluid in the room temperature range. Therefore, the best performance of water heat pipe would appear at 100 % filling ratio. The best performance of the N_2- or Ar-heat pipes appears not at 100 % but around 80 %.

6.1.4.4 Consideration on liquid distribution in the heat pipes

Heat pipes are typically filled with just enough working liquid to saturate the wick structure (100% filling ratio). However, excess liquid is often introduced intentionally to avoid an under-filling which may degrade the heat transport capability significantly as seen in Figures 6.9 and 6.10. Figure 6.13 is a schematic illustration of the liquid distribution in the normal heat pipe operation state. Figure 6.13(a) shows the liquid distribution in case of 100% liquid fill of the working fluid in the wick structure. As illustrated in Figures 6.13(b) and (c) if the filling ratio is higher than 100%, there would be an excess liquid puddle formed in the vapor-space end on the bottom of the condenser section, because the liquid that could not be absorbed in the wick was blown to the condenser section end by the vapor flow. The higher Q_{max} values results from the gravity force effect acting on the excess liquid on the magnitude of the hydrostatic height h that assists the liquid to return to the evaporator section as suggested in Figures 6.13(b) and (c). Although excess liquid increases the maximum heat transport capability, Q_{max}, it may somewhat degrade heat transfer performance, because the thick liquid layer increases the thermal resistance for the heat transfer through the wick and somehow blocks the condensation surface in the condenser section [5]. It can be concluded that high filling ratio can slightly increase Q_{max} but also increases R_{th} of the heat pipe. A trade-off between the two aspects is necessary to decide the working liquid filling ratio.

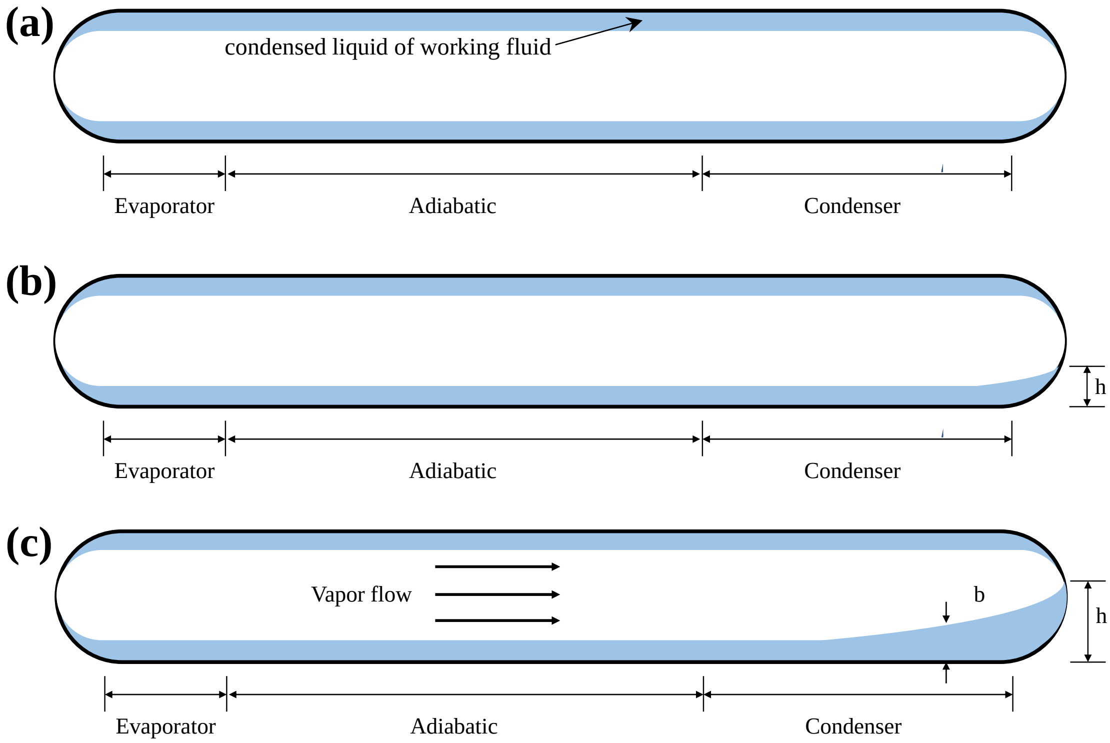

Figure 6.13 *Schematic illustration of working fluid distribution in the normal heat pipe operation state; (a) for 100% filling ratio, (b) and (c) for higher than 100% filling ratios.*

6.1.5 Effect of condenser temperature on the heat transfer performance of heat pipes

In Figures 6.14 and 6.15, the overall thermal resistance, R_{th}, of the heat pipe is plotted as a function of heat input, Q_e, for several condenser temperatures for the N_2- and Ar-heat pipes, respectively. In this study, the heat pipe was tested at specific constant condenser temperatures, whereas the temperatures at the evaporator and adiabatic section changed with the heat input. The condenser temperature was changed for each experiment, 60, 61, 62, 63, 67, 77, 82, 84 and 87 K for the N_2-heat pipe and 77, 82, 84, 87, 95, 100 and 110 K for the Ar-heat pipe.

6.1.5.1 Effect of condenser temperature for nitrogen heat pipe

It is found in Figure 6.14 showing the results of the N_2-heat pipe that when the condenser temperature is constant at 60, 61 and 62 K, which are all lower than the tipple point of nitrogen, the working fluid inside the heat pipe was frozen at least in the condenser section. Even under these conditions, when the condenser was in the frozen state, the partial heat pipe operation occurred locally in the evaporator, sometimes even in the adiabatic section. Under this situation, heat is transferred in the heat pipe operation in the active sections, and at the same time by thermal conduction through the pipe wall and frozen working fluid in the other sections. Thus, R_{th} gets worse by this thermal conduction contribution approximately by an order of magnitude as compared with the full normal heat pipe operation state. With the increase of Q_e, R_{th} deceases and the minimum values of the overall thermal resistance, $R_{th,min}$, are 2.7, 0.8, 0.6 K/W for cases of the condenser temperature of 60, 61 and 62 K, respectively. However, the value of $R_{th,min}$ in these imperfect heat pipe operation phase are still higher than $R_{th,min}$ for cases of full normal heat pipe operation. For the condenser temperature of 63 K or higher, the heat pipe works in a normal heat pipe operation state, where $R_{th,min}$ are in the range of 0.2–0.3 K/W.

It was found from the measured values of R_{th} that there are two physical states in normal heat pipe operation phase. As Q_e increases, the transition between the two occurs, from larger R_{th} to smaller R_{th}. For example, at the condenser section temperature of 77 K, this transition occurred around 8 W. It is, in fact, difficult to rigorously explain the cause of the transition phenomenon and to theoretically predict the critical value. It seems that the critical value of Q_e for this transition is more probabilistic than deterministic. The followings have been extracted from the present experiments: When repeating a series of experiments in which Q_e is increased, it seems that the critical value of Q_e for the transition tends to get smaller in the second or later experiment. Often, in the second and subsequent experiments, the smaller R_{th} value which appears normally after the transition in the first experiment appears from the beginning of the experiment with very small Q_e, and as Q_e further increases, the normal heat pipe operation state directly proceeds to the local dry-out state without going through the state with larger R_{th}.

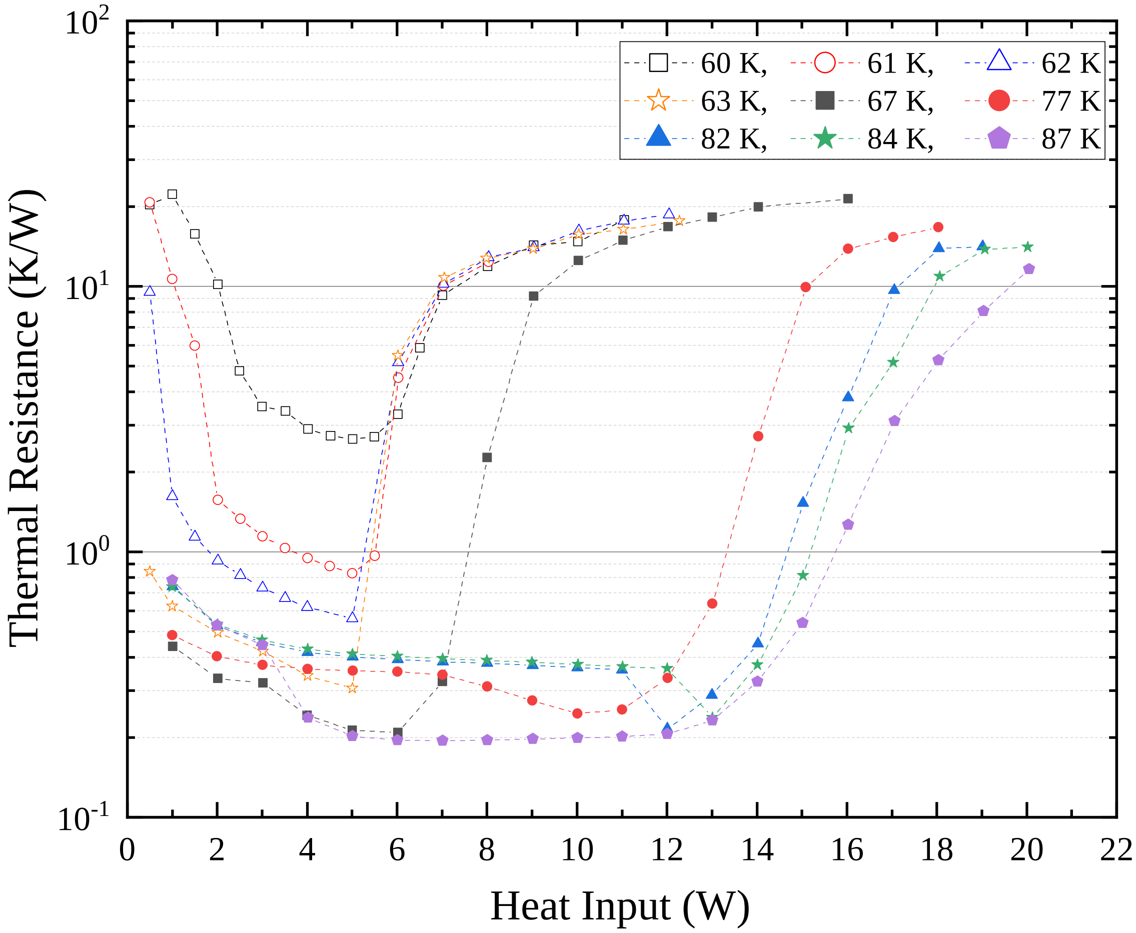

Figure 6.14 *Thermal resistances of N_2-heat pipe as a function of heat input for several condenser temperatures.*

Empirically derived hypothesis is as follows: In the state where residual bubbles or newly generated boiling bubbles are trapped in the porous structure of wick, the heat transfer property is deteriorated, and the heat transfer resistance R_{th} becomes slightly large. When this kind of trapped bubbles disappears, the heat transfer is improved and the thermal resistance R_{th} is reduced. It was evident that the temperature was reduced only in the evaporator section, while the temperature in the adiabatic section was nearly constant or increased when occurring the transition.

It can be explained on the basis of the magnitude of Q_{max} that there are three conditions of working fluid phase. First, in most sections of the heat pipe the working fluid is frozen and only in the limited area of the evaporator section liquid phase appears; for example, the case of the condenser section temperature of 63 K. In the second, there is small region with liquid phase; 67 K. In the third, complete two-phases liquid–vapor of working fluid coexists throughout the heat pipe; 77, 82, 84 and 87 K.

6.1.5.2 Effect of condenser temperature for argon heat pipe

Figure 6.15 shows the results of the Ar-heat pipe. Just like in the case of the N_2-heat pipe, when the condenser temperature was lower than the triple point of argon (83.8 K), the Ar-heat pipe also worked in a partial heat pipe operation state resulting in larger R_{th}. In case of 82 K of the condenser temperature that was close to the triple point but still slightly lower, there was small amount of frozen working fluid left at Q_e of 1 W, causing large R_{th}. However, when Q_e became 2 W or higher, R_{th} rapidly decreased down to R_{th} of the normal heat pipe operation, but it was still a little bit higher due to the existence of small frozen working fluid in the condenser section. In case of the condenser temperature at 84 K or higher, the results show that the heat pipe can work in the normal heat pipe operation state without frozen working fluid. It can also be seen in the figure that there are two physical states in the normal heat pipe operation when the thermal resistance is 0.25 or 0.4 K/W approximately, which was discussed above in case of the N_2-heat pipe. It is also seen that the value of Q_{max} slightly increases with the increase of the condenser temperature. Nevertheless, it can not be seen clearly that the values of Q_{max} widely varied with the condenser temperature just like the cases of the N_2-heat pipe. This may be because the temperature range between the triple point and the normal boiling point of argon is quite small (83.8–87.3 K) compare with nitrogen (63.1–77.4 K).

6.1.5.3 Comparison of the minimum thermal resistance as a function of condenser temperature between nitrogen and argon heat pipes

In Figure 6.16, the comparison of the minimum thermal resistance, $R_{th,min}$, between the N_2-heat pipe and the Ar-heat pipe is shown as a function of condenser temperature. In case of the

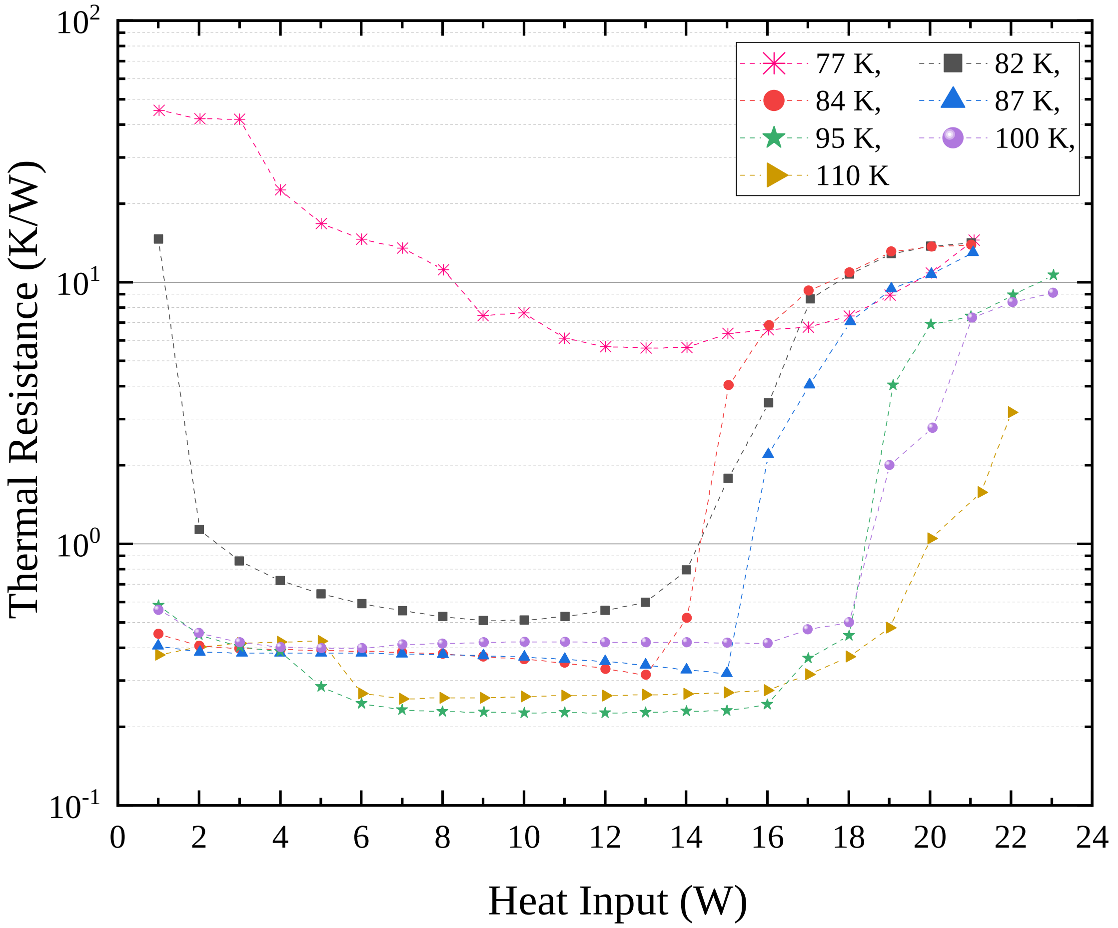

Figure 6.15 *Thermal resistances of Ar-heat pipe as a function of heat input for several condenser temperatures.*

condenser temperature lower than the triple point of nitrogen (63.1 K) and argon (83.8 K), $R_{th,min}$ is very large due to the existence of frozen working fluid in the condenser section. When the condenser temperature increased, higher than the triple point, $R_{th,min}$ decreased and became approximately constant around 0.25 K/W. It can be explained that both heat pipes have almost constant values of $R_{th,min}$, because the thermal conductivities of liquid and vapor nitrogen and those of argon do not vary much with the temperature. At the same temperatures around 82 to 87 K, $R_{th,min}$ of the N_2-heat pipe is slightly lower than that of the Ar-heat pipe because the thermal conductivity of liquid nitrogen is larger than that of argon.

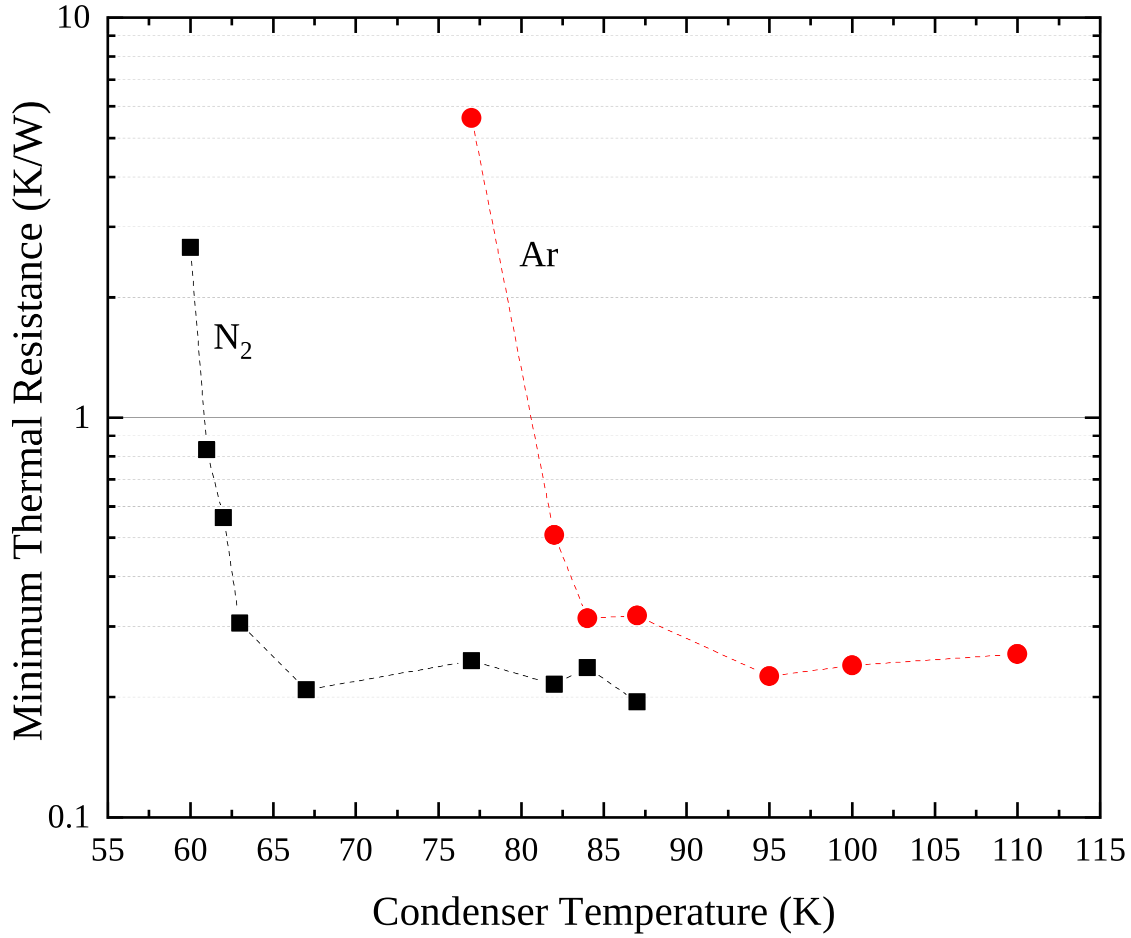

Figure 6.16 *Minimum thermal resistances of N_2-heat pipe and Ar-heat pipe plotted against condenser temperature.*

6.1.6 Heat pipe working mode map

The heat pipe working mode map of the N_2-heat pipe and the Ar-heat pipe is shown in Figure 6.17, where the heat transferred, Q_e, is plotted on the vertical axis and the condenser temperature on the horizontal axis. Solid and open symbols are separately used for the data of the N_2-heat pipe and the Ar-heat pipe, respectively. The data plots show the level of the values of R_{th} according to the color code shown in the inset of Figure 6.17. The operating states of cryogenic heat pipes are divided to such five states, as the frozen state of working fluid, the locally frozen state, the incomplete heat pipe operation state, the normal heat pipe operation state, and the local dry-out state, which are indicated by using different marks in the figure.

1) Frozen state of working fluid: R_{th} larger than 10 K/W. This state appears when heat pipes are heated while the condenser temperature is lower than the triple point, 63.1 K or 83.8 K for nitrogen and argon, respectively. The heat pipe as a whole will not normally operate as a heat pipe. When slightly heated, the heat pipe working fluid is still wholly frozen. As an increase of the heat input, the locally frozen state may start, and then as a result of large heating heat pipe may directly reaches the dry-out state in the evaporator section or sometimes expand to the adiabatic section without going through the normal heat pipe operation state. Occasionally, when heated with the condenser temperature much lower than the triple point, the working fluid is still totally frozen at low Q_e, and eventually reach the dry-out state without even occurring the locally frozen state.
2) Locally frozen state, 1 K/W < R_{th} < 10 K/W. As an increase of the heat input to frozen heat pipes, working fluid is melted locally in the evaporator section, or sometimes including the adiabatic section, where heat pipe operation may locally occur. In the still frozen sections, heat is transferred by thermal conduction through the wick saturated with the frozen working fluid and through the tube wall. Occasionally, the working fluid is melted including some part of the condenser section, and as a result, the operating length of the condenser section is simply shortened by the amount of the frozen part. In the locally frozen state, the overall thermal resistance is taken to be a larger value than during the normal heat pipe operation.
3) Incomplete heat pipe operation (partial heat pipe operation), 0.5 K/W < R_{th} < 1 K/W. This state occurs in cases of very small Q_e, when the vapor flow is too weak to reach the condenser section. Therefore, heat pipe operation locally occurs, and heat is transferred in a heat pipe mode within a limited range where vapor flow reaches. Vapor usually reaches the adiabatic section. In the rest sections heat is conductively

transferred through the heat pipe wall and working fluid in the wick structure. Therefore, the magnitude of R_{th} becomes larger than that in the normal heat pipe operation state. In cases where Q_e further increases, vapor velocity so increases to reach the condenser section end, and heat pipe operation proceeds to the normal heat pipe operation as a whole, resulting in very small R_{th}.

4) Normal heat pipe operation, R_{th} < 0.5 K/W. This state is achieved under the condition such as, working fluid filling ratio more than 50%, and the condenser section temperature higher than 61.3 and 83.8 K for the N_2-heat pipe and the Ar-heat pipe, respectively. In this state, the heat pipes give the best heat transfer performance where the temperature difference between the evaporator and condenser sections is very small even at a high Q_e.

5) Local dry-out of working fluid, R_{th} > 0.5 K/W. The local dry-out state normally appears in case of high Q_e. Occasionally, this state can occur even at low Q_e in case of low filling ratio of working fluid or at moderate Q_e in case of operating with the condenser temperature lower than the tipple point. It is important to note that the local dry-out state may have the value of R_{th} nearly the same as those in the locally frozen state of working fluid and in the incomplete heat pipe operation states. To identify the local dry-out state, attention should be paid to the vapor pressure inside heat pipe. Once the local dry-out occurs, the vapor pressure will start fluctuating and then rapidly rise together with the rapid temperature rise at the evaporator section. In contrast, in the frozen state and the locally frozen state, the value of R_{th} is high but the vapor pressure inside the heat pipe is low. The local dry-out state is characterized in this study by large scale temperature rise locally in the evaporator section or sometimes expanding to the adiabatic section for very large Q_e. In the rest sections, liquid and vapor phases still coexist where heat pipe operation is performed locally.

This is indicated by the fact that the vapor pressure inside heat pipe is just equal to the saturated vapor pressure.

In Figure 6.17, possible working areas where the N_2-heat pipe or the Ar-heat pipe works in the normal heat pipe operation mode are also drawn for both heat pipes, by the red line for the N_2-heat pipe and the blue line for the Ar-heat pipe, respectively, of which lines indicate the theoretical $Q_{c,max}$ given by Equation (2.1). It is plausible that the working areas of the heat pipes are in such ranges between the triple point and the critical temperatures, as 61.3–126.2 K and 83.8–150.8 K, respectively for the N_2-heat pipe and the Ar-heat pipe. The value of Q_{max} change with various condenser temperatures due to the temperature dependence of the thermo-physical properties of the working fluid. Specifically, the liquid viscosity is dominantly decrease at near triple point cause Q_{max} increases with increasing of temperature until maximum value of Q_{max}. For higher temperature to the critical temperature, the surface tension and the latent heat are dominantly decrease cause Q_{max} decreases with increasing of temperature. As the latent heat of vaporization is zero beyond the critical temperature, heat pipes cannot work in the supercritical state. However, in creating this working mode map, the experiment could not be carried out in the high temperature region exceeding the data symbol shown in Figure 6.17 for safety reasons. In such a temperature range, the vapor pressure of the working fluid in the heat pipes exceeds the proof pressure of the pipe. Therefore, in the temperature region between the maximum temperature at which the experiment was carried out and the critical temperature, the curve indicating the heat pipe working region is an assumed value without any experimental backing. It can be defined that the operating temperature range of a parallel heat pipe system consisting of the N_2-heat pipe and the Ar-heat pipe ranges from the triple point of nitrogen to the critical point of argon, where at least one of the two heat pipes is operating normally. The recommended operating region in which both heat pipes are operating normally is the overlapping region of the operating temperature ranges of each heat pipes.

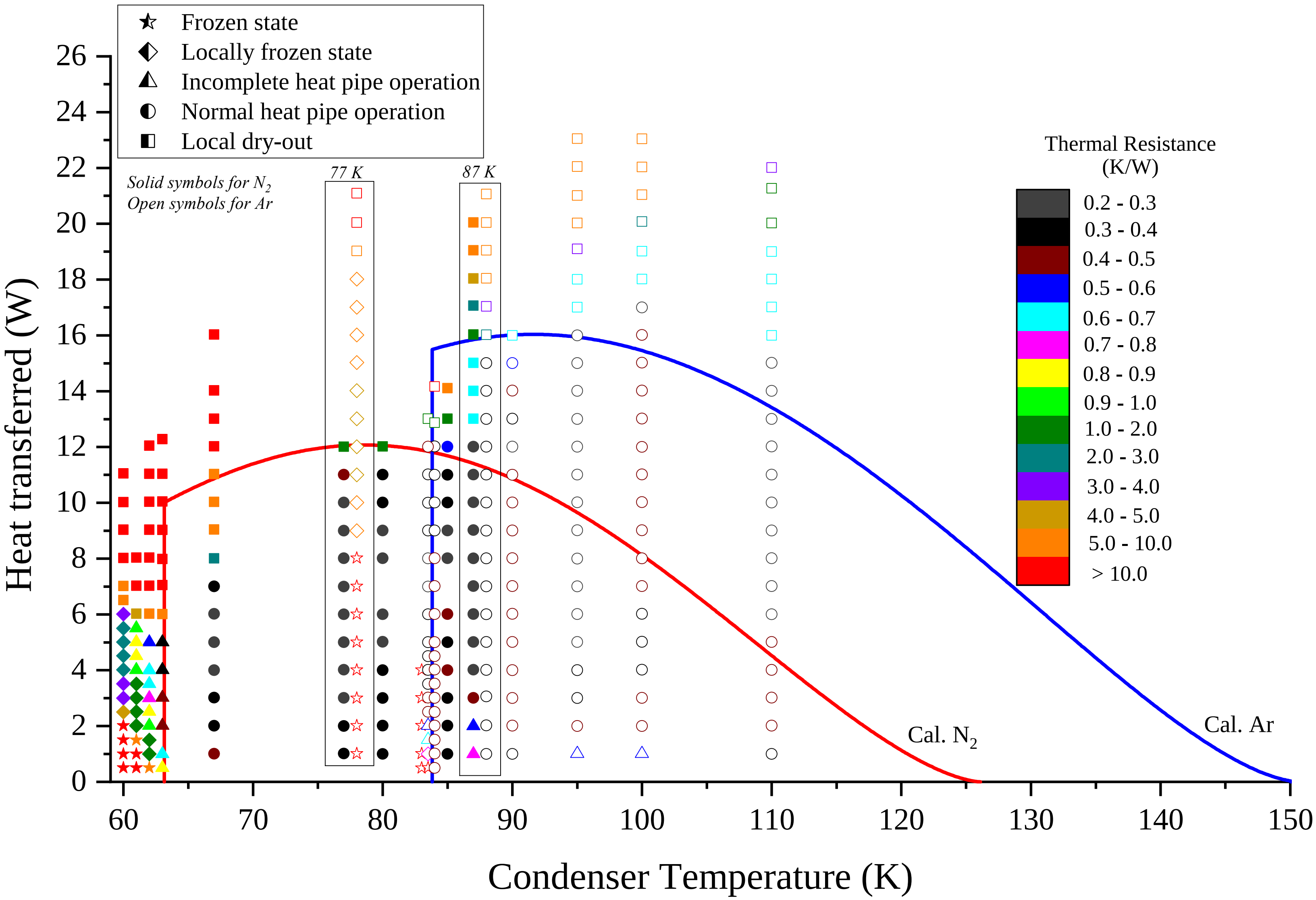

Figure 6.17 *Heat pipe working mode map for the N_2-heat pipe and the Ar-heat pipe.*

6.1.7 Effect of inclination angle on the heat transfer performance

In order to investigate the effect of the inclination on the heat transfer performance of the cryogenic heat pipe, the experiments were performed at several inclination angles in case where the evaporator section is set below (+) and above (-) the condenser section. Please note that the horizontal installation is set to the inclination angle 0˚.

6.1.7.1 Effect of inclination angle on the overall thermal resistance

In Figure 6.18 the thermal resistance, R_{th}, of the heat pipe is plotted as a function of heat input, Q_e, for several inclination angles. The experiments were performed for the heat pip under the condition of 100% filling ratio by using nitrogen as a working fluid operated at 77 K of the condenser temperature. In cases where the evaporator section was set above the condenser section (negative ψ), the performance of the heat pipe evaluated by Q_{max} was significantly degraded even if ψ is quite close to 0˚. The experimental results show the values of Q_{max} are only 5, 2 W and less than 1 W for the inclination angles of -0.5˚, -1˚, and -5˚, respectively, though corresponding R_{th} values are almost the same as that of 0˚. These values of Q_{max} are quite small as compared with the value of Q_{max}, approximately 10 W, in case of the horizontal installation. It is, however, interesting to compare the present results with those experimentally obtained by Loh et al. [6], who tested the heat pipe with dimension of 200 mm in length and 6 mm in diameter and using water as the working fluid. They found that the heat source position and gravity (the inclination angle) have less effect on the thermal performance of sintered powder metal wicked heat pipes due to the fact that this wick has the strongest capillary action. The difference between their results and those of the present cryogenic heat pipes shows how small the capillary pressure earned in the cryogenic heat pipes is compared with the hydrostatic head effect. It was also suggested in Reference 6 that heat pipes with grooved or mesh wick were, nevertheless, not desirable to use in the orientation of the evaporator above the condenser section. However, in Reference 6, the grooved heat pipe had better thermal performance than a mesh and a sintered powder metal wick heat pipes in the inclination angle range of +90˚ to 0˚ (horizontal). In most cases of the present experiments, the wick structure is a combination of axial groove and sintered metal powder. The groove wick may effect on reduction of Q_{max} when increasing the inclination angle in case where the evaporator section is above the condenser section. In order to operate with high performance even in such case, homogeneous sintered metal wick structure should be selected rather than axial groove wick. In case where the evaporator section is below (+) the condenser section, the thermal performance of the heat pipe for the inclination angle of +1˚ and +5˚ are not much different from that of 0˚. In fact, in case of room temperature operation the heat pipe length of 200 mm with the inclination of +5˚ generates only a small gravitational force as compared with the capillary force created by wick structure.

It is seen in Figure 6.18 that the values of Q_{max} significantly increase to 12, 13, 16, 19, and 26 W, when increasing the inclination angles of +10˚, +15˚, +30˚, +45˚, and +90˚, respectively. However, the values of R_{th} in the normal heat pipe operation phase are nearly the same except the case of the inclination angle of +90º (vertical position). It was reported in previous studies [6] on the effect of the inclination angle on heat pipe performance that the inclination angle of +90˚ did not provide the best performance of heat pipes though the inclination angle of +90˚ seems to make best use of the gravity effect. When operated at the inclination angle of +90˚, it should be taken account of many factors such as a huge amount of liquid with high speed from the condenser section flowing through a wick structure unlike the cases of wickless thermosyphons that have lower friction between the tube wall and the liquid. Another factor that should be considered is the entrainment limit at high relative velocities between the vapor flow and the liquid flow, where droplets of liquid can be torn from the wick surface and entrained into the vapor flowing toward the condenser section [7].

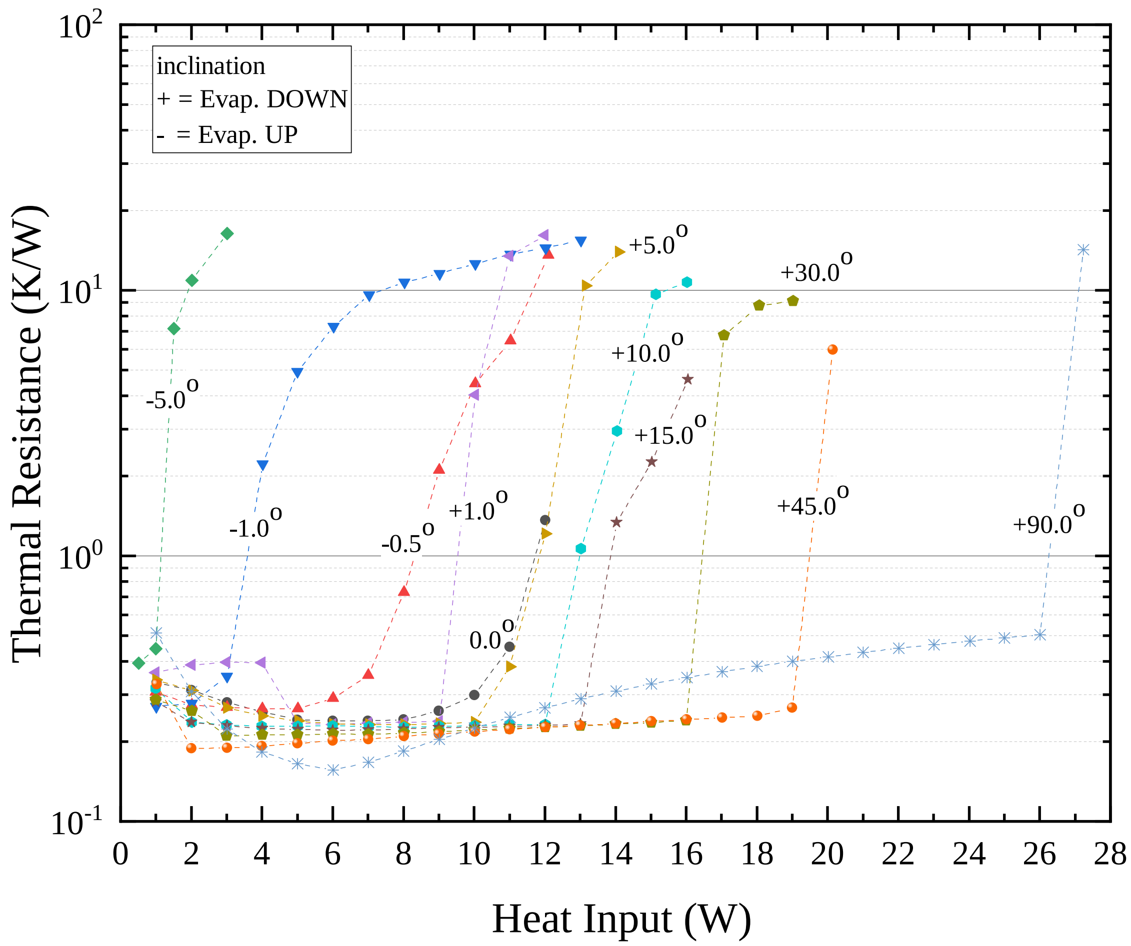

Figure 6.18 *Thermal resistance of the* N_2-heat pipe *as a function of inclination angle.*

If one looks at Figure 6.18 in more detail the inclination angle of +90˚, it can be seen that R_{th} gradually increases as Q_e increases over 6 W. Morteza Ghanbarpour [8] observed in his study that much more liquid supplied to the evaporator as a result of very high inclination angle may results in the performance degradation of the evaporator section due to the increase of the radial thermal resistance of the evaporator section because of the thicker liquid film. The optimum inclination angle would depend on the configuration even of working fluid in a heat pipe as well as the operating temperature. D.S. Naruka [9] tested the heat pipes which were fabricated using 200 mm long copper tube having 10 mm outer diameter and 2 mm thickness. Wire mesh of phosphorus bronze was used as the wick material (200 mesh). It was concluded that the best angle of inclination for the heat pipe was 45˚ as the thermal performances of the

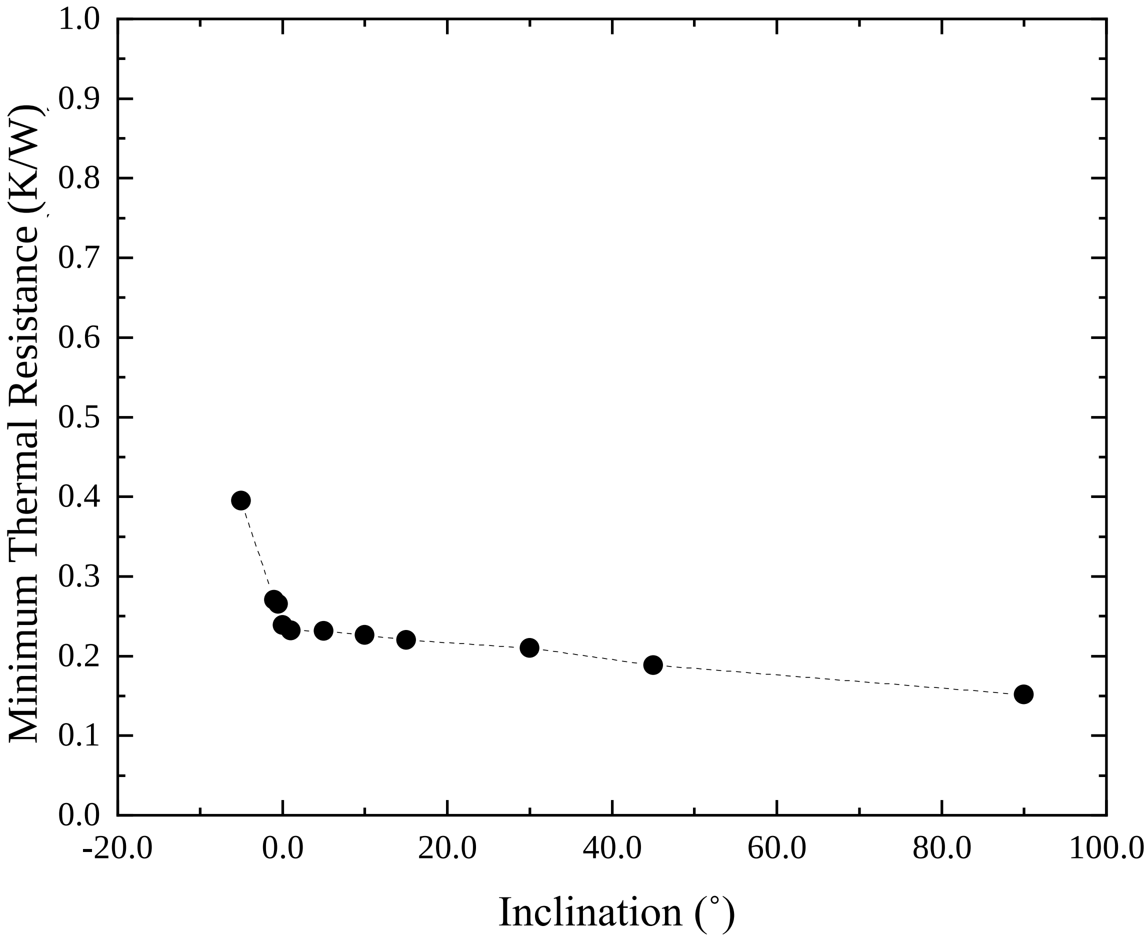

Figure 6.19 *The minimum thermal resistances of N_2*-heat pipe *as a function of inclination angle.*

heat pipes were optimal at this inclination angle. Morteza Ghanbarpour [8] tested the heat pipes using different types of nanofluids and concluded that the best performance with the lowest thermal resistance of the heat pipes was observed at the inclination angle of 60˚

6.1.7.2 Inclination angle that gives the minimum thermal resistance

Figure 6.19 shows the minimum thermal resistance, $R_{th,min}$, plotted against the inclination angle. It is seen that $R_{th,min}$ rapidly increases with negatively increasing the inclination angle. The reason for this is that the evaporator section is above the condenser section and thus liquid flows from the condenser section against gravity with insufficient amount of liquid to the evaporator section, which is apt to cause the local dry-out and resulting in large $R_{th,min}$. In case where the evaporator section is below the condenser section, $R_{th,min}$ gradually decrease with increasing inclination angle. This can be explained by the fact that with a high inclination angle working liquid cooled in the condenser section can flow rapidly to the evaporator section causing drop in the temperature, and resulting in reducing $R_{th,min}$.

6.1.8 Maximum heat transport capability

The maximum heat transport capability, Q_{max}, is experimentally determined as the upper limit of the heat input, Q_e, above which the temperature difference between the evaporator and condenser sections start to rise in a large scale as shown in Figure 6.20. In the experiment, Q_e, was stepwise increased until the local dry-out was detected, and this value of Q_e is defined as Q_{max}. Accordingly, some uncertainty is inevitable in determining Q_{max}. Moreover, sometimes the temperature difference increases only gradually with increasing Q_e, and it is difficult to determine the value of Q_{max} precisely, as seen, for example, in the variation around 12–14 W of 132% filling ratio data in Figure 6.20. In such cases, the determination of Q_{max} involves some error. For the theoretical estimation of the maximum heat transport capability as a function of filling ratios, the theory of the capillary limit is used, because in the present experiments it gives the lowest value among other limitations, namely, the boiling, the entrainment, the sonic and the viscous limits. The theoretical capillary limit was calculated by the following Reference 10.

For 100% filling ratio:

$$Q_{c,\,max} = \frac{P_c - \Delta P_{\perp}}{(F_l + F_v)\, L_{eff}} \quad . \tag{6.2}$$

For more than 100% filling ratio:

$$Q_{c,\,max} = \frac{P_c - \Delta P_{\perp} + P_e}{(F_l + F_v)\, L'_{eff}} \quad . \tag{6.3}$$

Here, the capillary pressure, P_c, is expressed by:

$$P_c = {}^{2\sigma \cos\alpha}\!/_{r_c} \;, \tag{6.4}$$

where σ is the liquid surface tension (N/m). It can be seen in this equation that the maximum capillary pressure exists when the cosine of the wetting angle is unity ($\alpha = 0$). r_c is the effective capillary radius of wick structure (m), which is given for the axial groove wick:

$$r_c = w \;, \tag{6.5}$$

For sintered metal powder wick, the effective capillary radius r_c (m) is conventionally given by:

$$r_c = 0.41\, r_s \;, \tag{6.6}$$

where r_s is the average radius of metal particle sphere.

Gravitational force in the direction perpendicular to the heat pipe axis is written as:

$$\Delta P_{\perp} = \rho_l\, g\, d_v \sin\psi \;, \tag{6.7}$$

The inclination angle of the heat pipe, ψ (+90˚ to -90˚) is measured from a horizontal line.

The gravity force caused by excess liquid puddle P_e is:

$$P_e = \rho_l\, g\, h \;, \tag{6.8}$$

Here ρ_l is the liquid density (kg/m^3), g is the gravitational acceleration (m/s^2), h is the height of the excess liquid puddle (maximum value would be equal to the diameter of vapor core) (m).

The frictional coefficient for liquid flow, F_l, is expressed as follows:

$$F_l = \frac{\mu_l}{K\, A_w\, \rho_l\, \lambda} \;, \tag{6.9}$$

Here μ_l is the liquid viscosity (N·s/m^2), A_w is the cross-sectional area of wick structure (m^2), λ is the latent heat of evaporation (J/kg), and K is the wick permeability (m^2).

The wick permeability for an axial groove wick is given by:

$$K = \frac{2\,\varepsilon\left(\frac{2w\delta}{w+2\delta}\right)^2}{(f_l\ Re_l)} \ , \tag{6.10}$$

Here ε is the wick porosity, δ is the groove depth (m), and $(f_l\ Re_l)$ is the frictional coefficient.

The wick permeability for a sintered metal powder wick is given by:

$$K = \frac{r_s^2 \varepsilon^3}{37.5\,(1-\varepsilon)^2} \ . \tag{6.11}$$

The frictional coefficient for vapor flow, F_v, is:

$$F_v = \frac{(f_v\ Re_v)\,\mu_v}{2\,r_{h,\,v}^2 A_v \rho_v\,\lambda} \ , \tag{6.12}$$

Here under the circumstances of this experiment, as the values of Re_v and M_v are less than 2300 and 0.2, respectively, which can be respectively calculated from Equations (2.8) and (2.9), the vapor flow can be considered laminar and incompressible. For laminar flow the values of $(f_v\ Re_v)$ and $(f_l\ Re_l)$ are a constant which can, therefore, be equal to 16 for a circular flow passage from the well know Hagen-Poiseuille's solution [10], μ_v is the vapor viscosity (N·s/m^2), $r_{h,\,v}$ is hydraulic radius for vapor flow (m), and ρ_v is the vapor density (kg/m^3). In the heat pipe used here, F_l is orders of magnitude larger than F_v under all conditions (for example, under the conditions of Q_e at $Q_{c,max}$ of N_2-heat pipe at 77 K, F_l = 660 s/m^4 and F_v = 0.95 s/m^4). The value of F_v is negligibly small. The effective length of the heat pipe, L_{eff}, is usually determined by:

$$L_{eff} = 0.5L_e + L_a + 0.5L_c \ , \tag{6.13}$$

Here L_e is the length of the evaporator section (m), L_a is the length of the adiabatic section (m), and L_c is the length of the condenser section (m).

The effective length of heat pipe, L'_{eff}, modified in case when an excess liquid puddle is formed:

$$L'_{eff} = L_{eff} - L_{el} \ , \tag{6.14}$$

where L_{el} is the length of excess liquid puddle occupying the vapor core in the condenser section (m).

The wick porosity ε in case of the filling ratio other than 100% is assumed to depend on the filling ratio f_r as $\varepsilon(f_r) = \varepsilon_{100\%} \cdot f_r$. The designed original values of the wick porosity $\varepsilon_{100\%}$ for the heat pipe in this study (designed employing water as a working fluid at room temperature) are 0.82 and 0.57 for the axial groove wick and the sintered metal powder wick, respectively. The values of the filling ratio f_r are between 0 and 1 that are required for the estimation of ε in Equations (6.10) and (6.11). For more than 100% filling ratio, the gravity effect on the excess liquid puddle and the change of the effective length of the heat pipe due to the excess liquid should be considered (for Equation (6.3)). More specifically, the action of gravity on excess liquid puddle formed in the end portion of the condenser section and shorter effective length of the heat pipe due to excess liquid occupation in the vapor core at the end portion of the condenser section are taken into consideration.

Figure 6.21 shows the plots of the comparison of Q_{max} between the calculation based on the capillary limit given by Equation (6.3) and the experimental results of the N_2-heat pipes with three kinds of wick structures, axial groove wick (G), sintered metal powder wick (S), and groove-sintered metal power composite wick (GS), of the Ar-heat pipe with S and GS wicks, and of the Ne-heat pipe with GS wick. In this figure the value of Q_{max} is plotted as a function

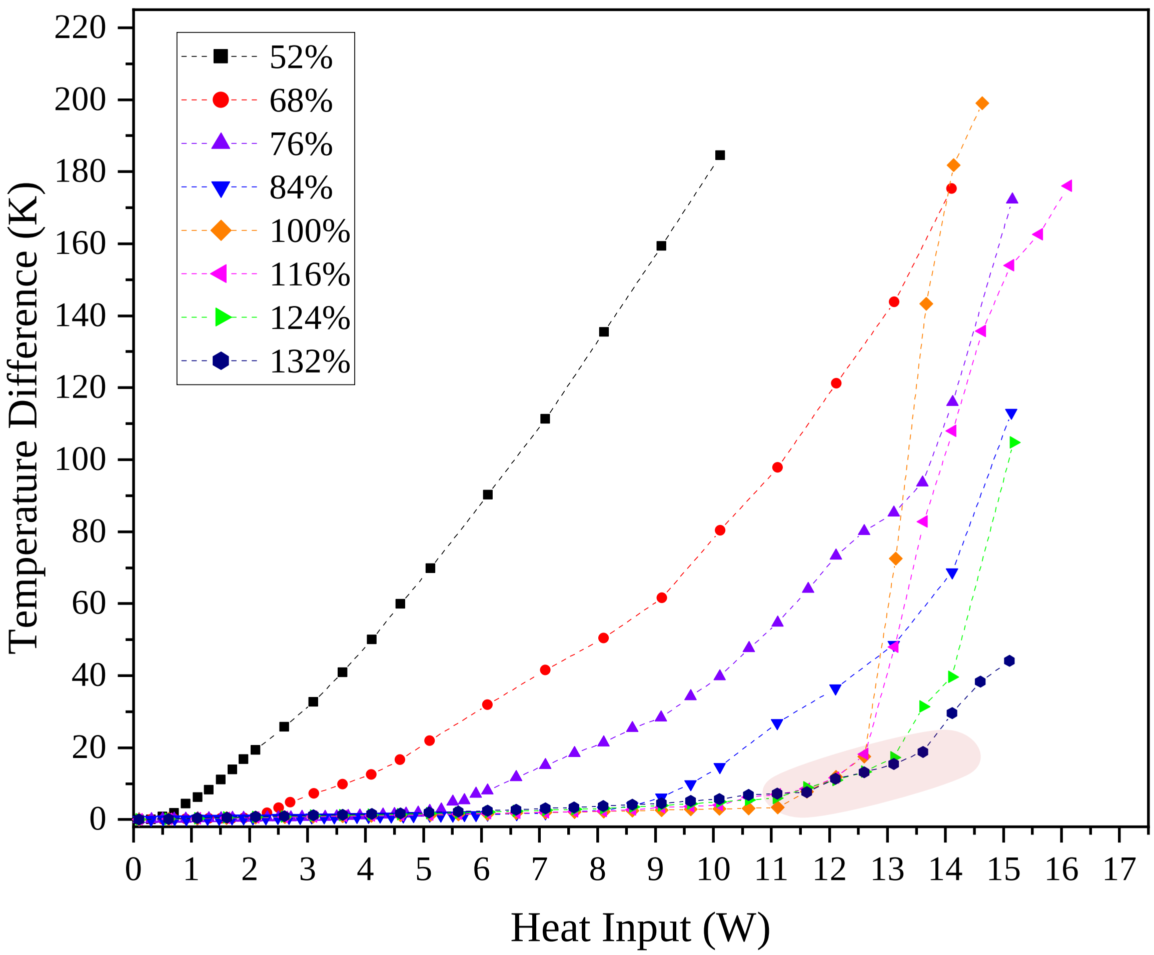

Figure 6.20 *The variations of temperature difference between the evaporator and condenser sections with heat input for several filling ratios of the N_2-heat pipe with grooved-sintered metal powder composite wick structure.*

of filling ratio in the cases where f_r is 50% or more, which is the minimum filling ratio to operate the heat pipes in a normal operation state. It was found that the experimental results of G wick and S wick with 85 μm of average sphere radius, r_s, satisfactorily agreed with the theoretical calculation data.

The following notes should be made here concerning how to find the value of r_s = 85 μm. The catalog value indicates that the radius of the micro-metal spheres that make up the sintered wick is widely distributed around an average value of 60 μm. However, when the theoretical values of Q_{max} were calculated with r_s = 60 μm in various cases, they did not agree well with the experimental values. Therefore, when this value was set to 85 μm, good agreement was

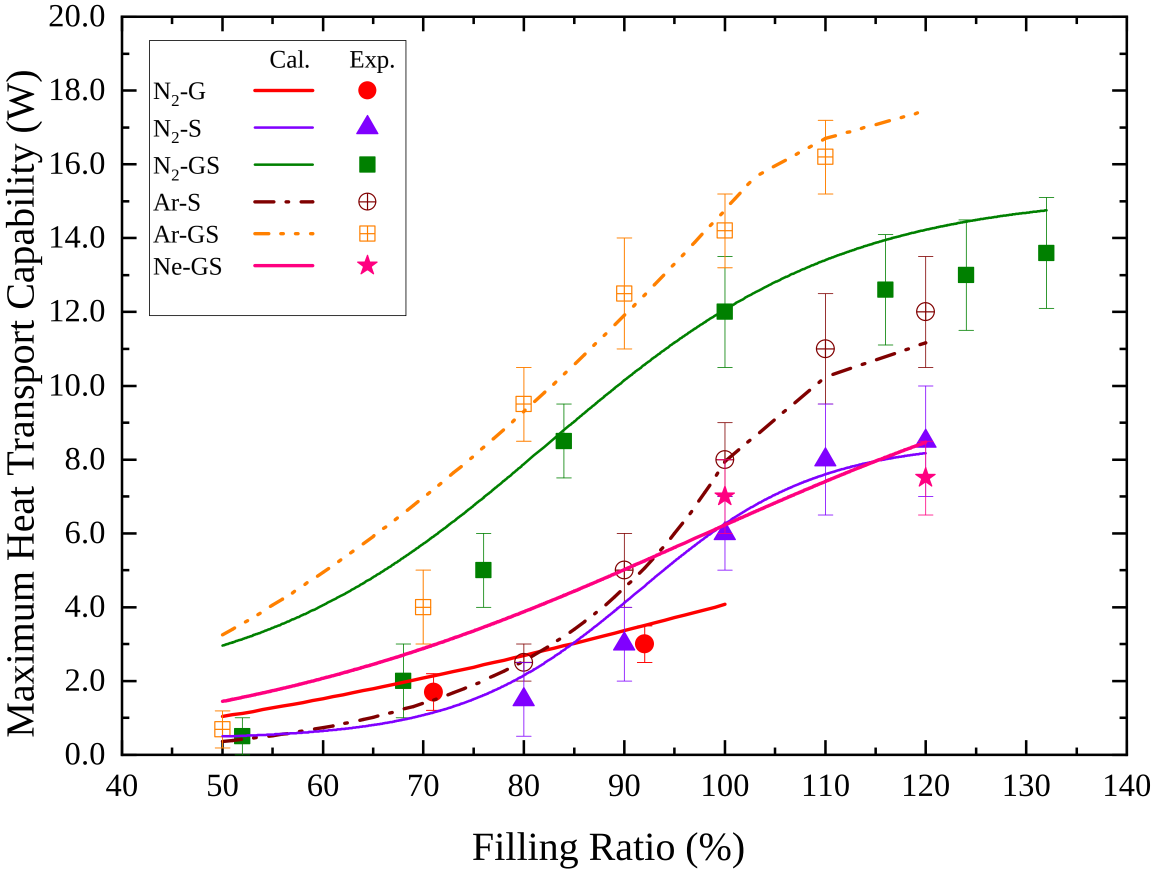

Figure 6.21 *The maximum heat transport capability as a function of filling ratio.*

found in many cases, and so it was decided to consider r_s = 85 μm thereafter. Presumably, as the result of insufficient compression process when packing the fine metal spheres before sintering, which resulted in many bulk void formations inside the sintered metal wick, it is considered that 85 μm is more appropriate than 60 μm for r_s. It should be noted that for the theoretical estimation of Q_{max} for GS wick, the maximum effective capillary pressure, P_c, was assumed to be produced exclusively by the sintered metal powder wick portion, and the frictional coefficient for the liquid flow, F_l, is done by the axial groove portion, respectively. It is also found in Figure 6.21 that the assumption for the capillary limit in the case of GS wick leads to considerable success in the theoretical prediction of Q_{max} for the N_2-heat pipe, the Ar-heat pipe, and the Ne-heat pipe with GS wick. On the other hand, below 75% filling ratios of both N_2-heat pipe and Ar-heat pipe with GS wick, the experimental results do not well agree with the theoretical calculation data. It is interesting to see that the experimental results of GS wick in case of the filling ratio below 75% are so small that they should rather well agree with the theoretical data of G wick and S wick. This can be explained that condensed liquid of working fluid imperfectly occupied only in portion of G wick or S wick due to small working fluid volume to fill the wick and thus the combined-wick structures do not work synergistically in this case.

The difference in Q_{max} between the N_2-heat pipe, the Ar-heat pipe, and the Ne-heat pipe with the identical GS wick may be explained by the differences in the working fluid thermophysical properties such as the surface tension, the liquid and vapor densities, the liquid and vapor viscosities and the latent heat of vaporization.

6.2 Results and Discussion on Parallel Heat Pipe System

This section is focused on the experimental results of the parallel heat pipe system, which is composed of a combination of an N_2-heat pipe and an Ar-heat pipe arranged in parallel. The experiments were performed at a number of condenser temperatures such as 77, 82, 84 and 87 K. The experiment of the parallel heat pipe system consisting of an N_2-heat pipe and an Ne-heat pipe was also conducted at the condenser temperatures of 27 and 35 K in order to investigate the thermal behavior and to test the possibility of the application to HTC magnet cooling. The two heat pipes have an outer diameter of 6 mm and a length of 200 mm with a combined wick structure consisting of axial grooves and sintered metal powder. Of the two heat pipes, one employs nitrogen, and the other does argon or neon as a working fluid both with a 100% filling ratio. The experimental setup is almost the same as the previous one as shown in the chapter of experimental apparatus (Figure 4.1). The evaporator section of each heat pipe set in parallel consists of a common top part and a bottom part (Figure 4.9) which are divided into two to attach the temperature sensors to each heat pipe as denoted by T_{e1} and T_{e2}. The condenser section has a common bottom part and separating top parts (Figure 4.13) for the temperature sensors of each heat pipe as denoted by T_{c1} and T_{c2}. Therefore, the measured temperatures are nearly the same for T_{e1} and T_{e2}, and also the same for T_{c1} and T_{c2}. In the adiabatic section, two sets of the temperature sensors were completely separately installed for each heat pipe, $T_{aI,1}$ and $T_{aII,1}$, $T_{aI,2}$ and $T_{aII,2}$. Here the subscript, 1refers to the N_2-heat pipe and 2 refers to the Ar-heat pipe (or the Neon-heat pipe). All four temperature sensors were attached on each heat pipe to measure the wall temperature along the length of heat pipe. And one pressure sensor was connected to each heat pipe to measure the vapor pressure of the working fluid inside each heat pipe.

6.2.1 Thermal performance with and without working fluid in parallel heat pipe arrangement

The experiments were carried out to test the thermal performance of the parallel heat pipe system. The preliminary experiments were performed with one heat pipe that was filled with working fluid (the fluid-filled heat pipe) and the other (vacuum heat pipe) without working fluid (an N_2-heat pipe & an empty-heat pipe, and an Ar-heat pipe & an empty-heat pipe) in order to acquire the basic data of individual heat pipes that make up the parallel heat pipe system. The results of these experiments show that the thermal performance of heat pipe in the parallel heat pipe arrangement quite well agreed with those of single fluid-filled heat pipe in the normal heat pipe operation. This means that the heat that was given from the heater in the common evaporator section was almost completely transferred to the condenser section through the fluid-filled heat pipe in the normal heat pipe operation state and little heat was transferred through the empty-heat pipe. However, at high Q_e, when the fluid-filled heat pipe was in the local dry-out state, the result is different. In this case the relative contribution of the heat transfer through the empty-heat pipe in the parallel heat pipe arrangement increased, because the thermal resistance of the fluid-filled heat pipe in the dry-out state was not so small. It may be concluded that the overall thermal resistances of a single heat pipe and the fluid-filled heat pipe in the parallel heat pipe arrangement are almost the same as long as they are in the normal operation state, but for high Q_e their relative contributions to heat transfer are different from each other.

The calculation of heat conduction through a simple copper tube was used to estimate the heat transfer through the empty-heat pipe. Therefore, the heat flow through the fluid-filled heat pipe in the parallel heat pipe arrangement would be given by subtracting the amount of conduction heat transmitted through the empty-heat pipe from the total heat input. The heat transfer rate through an empty-heat pipe can be calculated by the following given in Reference 11.

$$Q = \frac{A}{L} \int_{T_c}^{T_{e,\,i}} k\,(T)\,dT \;, \tag{6.15}$$

Here the temperature variation of the thermal conductivity is considered. A is the cross-sectional area (6 and 4 mm in the outer and the inner diameters, respectively), L is the total length (200 mm), T_c is the condenser temperature, $T_{e,i}$ is the evaporator temperature that changes with the total heat input.

The thermal conductivity, $k\,(T)$, can be calculated by:

$$k(T) \;=\; 10^{A(T)} \;, \tag{6.16}$$

where

$$A(T) \;=\; \frac{a + cT^{0.5} + eT + gT^{1.5} + iT^{2}}{1 + bT^{0.5} + dT + fT^{1.5} + hT^{2}} \;. \tag{6.17}$$

Here the coefficients in Equation (6.17) are given in Table 6.2.

Table 6.2 *Coefficients of Equation (6.17) for 4–300 K*

Coefficient	Value
a	1.8743
b	-0.41538
c	-0.6018
d	0.13294
e	0.26426
f	-0.0219
g	-0.051276
h	0.0014871
i	0.003723

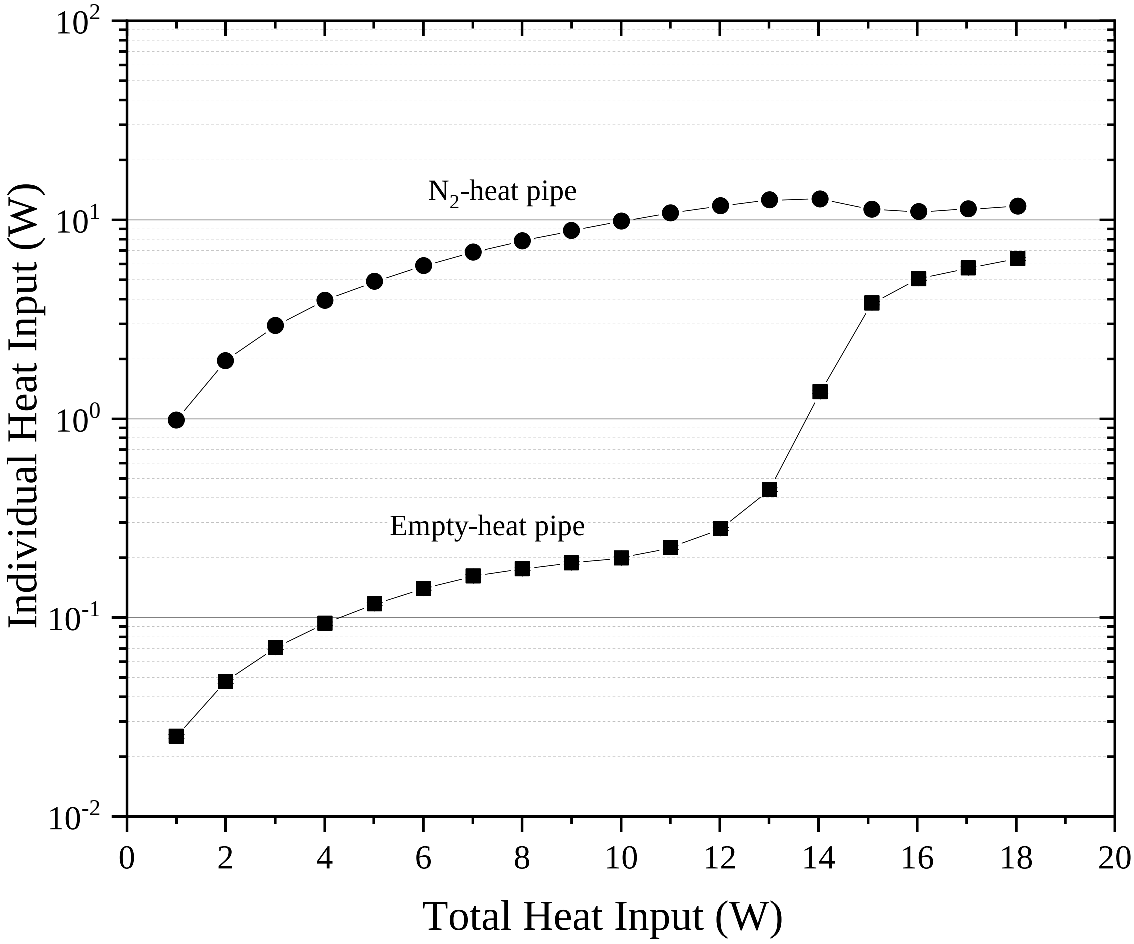

Figure 6.22 *Individual heat flow through N_2-heat pipe & Empty-heat pipe in parallel heat pipe arrangement at 77 K of the condenser temperature.*

To calculate the conductive heat transfer through the empty-heat pipe, OFHC copper tube and rod by Equation (6.15), the integration of *k(T)* was numerically performed together with Equation (6.16). The estimated error of this calculation is 2%.

In Figures 6.22 and 6.23, individual heat flows transferred through the N_2-heat pipe & the empty-heat pipe, and through the Ar-heat pipe & the empty-heat pipe are respectively plotted as a function of total heat input. The reason why the empty-heat pipe was included in the experiment in the parallel heat pipe arrangement is to confirm the two heat pipes are equivalent and whether mutual interference occurred between the two heat pipes during the normal heat pipe operation. The individual heat flow through the empty-heat pipe was easily calculated on

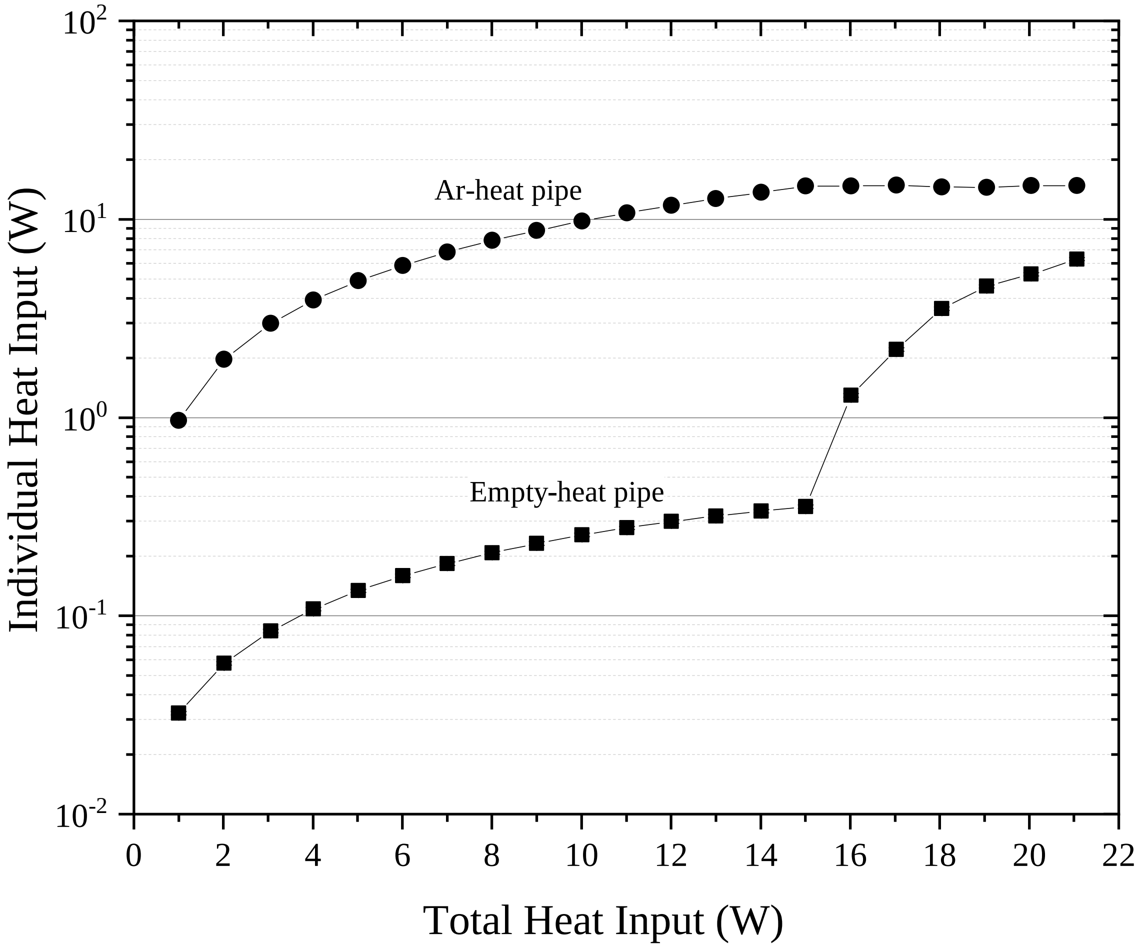

Figure 6.23 *Individual heat flow through Ar-heat pipe & Empty-heat pipe in parallel heat pipe arrangement at 87 K of the condenser temperature.*

the basis of Equation (6.15) in terms of the temperatures of the evaporator, T_{e2}, and the condenser, T_{c2}, sections, thermal conductivities of the materials of the heat pipe and the wick, and dimensions of the heat pipe. The remaining heat of the overall heat input was transferred through the fluid-filled heat pipe, i.e., the N_2-heat pipe or the Ar-heat pipe. It is seen in Figures 6.22 and 6.23 that the value of heat transferred through the fluid-filled heat pipe in the normal heat pipe operation state was nearly equal to the total heat input up to the Q_e value when the dry-out started at Q_{max} is 13 and 15 W for the N_2-heat pipe and the Ar-heat pipe, respectively. Above Q_{max} the heat transferred through the empty-heat pipe rapidly increased due to rapid increase in the temperature difference between the evaporator and the condenser sections, and it approached the heat transferred through the heat pipe in the local dry-out state. In fact, even when the heat pipe with working fluid was in the local dry-out state (dry-out occurred only in the evaporator section and in a part of the adiabatic section), the heat pipe surely transferred significant amount of heat, which was equal to that transferred through a heat pipe in the single heat pipe arrangement under the same temperature difference between the evaporator and the condenser sections.

6.2.2 Steady state temperature and pressure variation with heat input for parallel heat pipe system

The steady state temperatures at each step of the heating process, T_{e1} and T_{e2} in the evaporator section, $T_{aI,1}$, $T_{aII,1}$, $T_{aI,2}$ and $T_{aII,2}$ in the adiabatic section and T_{c1} and T_{c2} in the condenser section, and the vapor pressures P_1 and P_2 inside the heat pipe are plotted as a function of heat input Q_e to the parallel heat pipe system composed of the N_2- and the Ar-heat pipes both with 100% filling ratio. In addition, the temperature of filling tubes and the saturated vapor temperature of nitrogen and argon converted from the measured vapor pressure are also plotted. The results are shown in Figures 6.24–6.27 in cases of 77, 82, 84 and 87 K of the condenser temperatures, respectively, for the parallel heat pipe system. In these experiments, the cryocooler was used as a heat sink. These parallel heat pipe system experiments were conducted in three kinds of heat pipe combinations: ① N_2-heat pipe & Empty-heat pipe, ② Ar-heat pipe & Empty-heat pipe, and ③ N_2-heat pipe & Ar-heat pipe. The experiments of ① and ② were carried out to compare with the investigation and explanation of the results of ③.

The result of the parallel heat pipe system at 77 K of the condenser temperature (Figure 6.24-3) suggests that only the N_2-heat pipe operated in the normal heat pipe operation state. It is seen in Figure 6.24-1 that the N_2-heat pipe was in the normal heat pipe operation state at low values of Q_e up to 12 W, and in Figure 6.24-2 that the Ar-heat pipe was in the frozen state. Figure 6.24-3 shows that the temperatures T_{e1}, T_{e2}, $T_{aI,2}$ and $T_{aII,2}$ increased for Q_e larger than

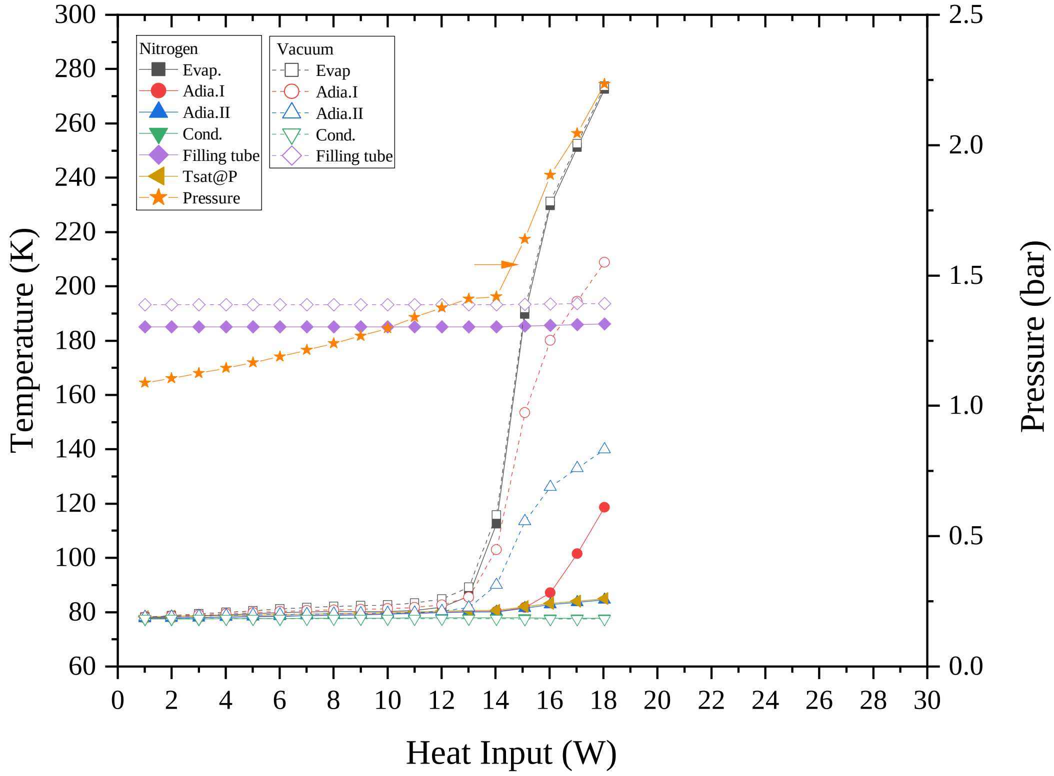

Figure 6.24-1 *Steady state temperature and pressure variation in parallel arrangement of N_2-heat pipe & Empty-heat pipe at 77 K of condenser temperature.*

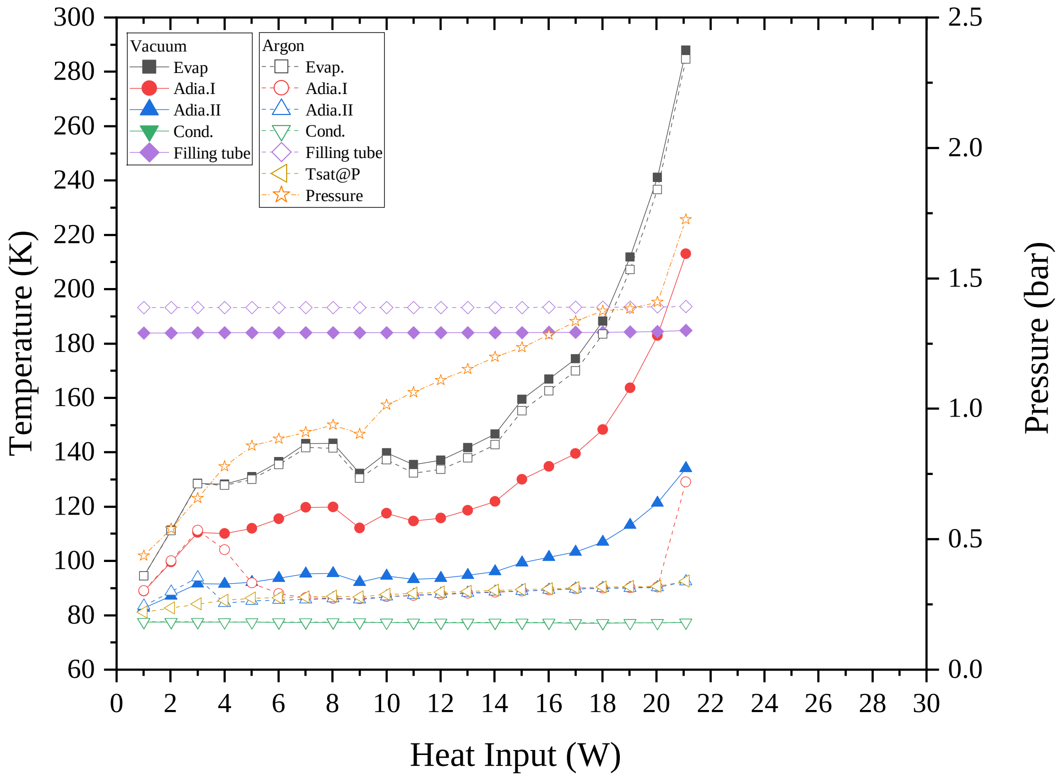

Figure 6.24-2 *Steady state temperature and pressure variation in parallel arrangement of Ar-heat pipe & Empty-heat pipe at 77 K of condenser temperature.*

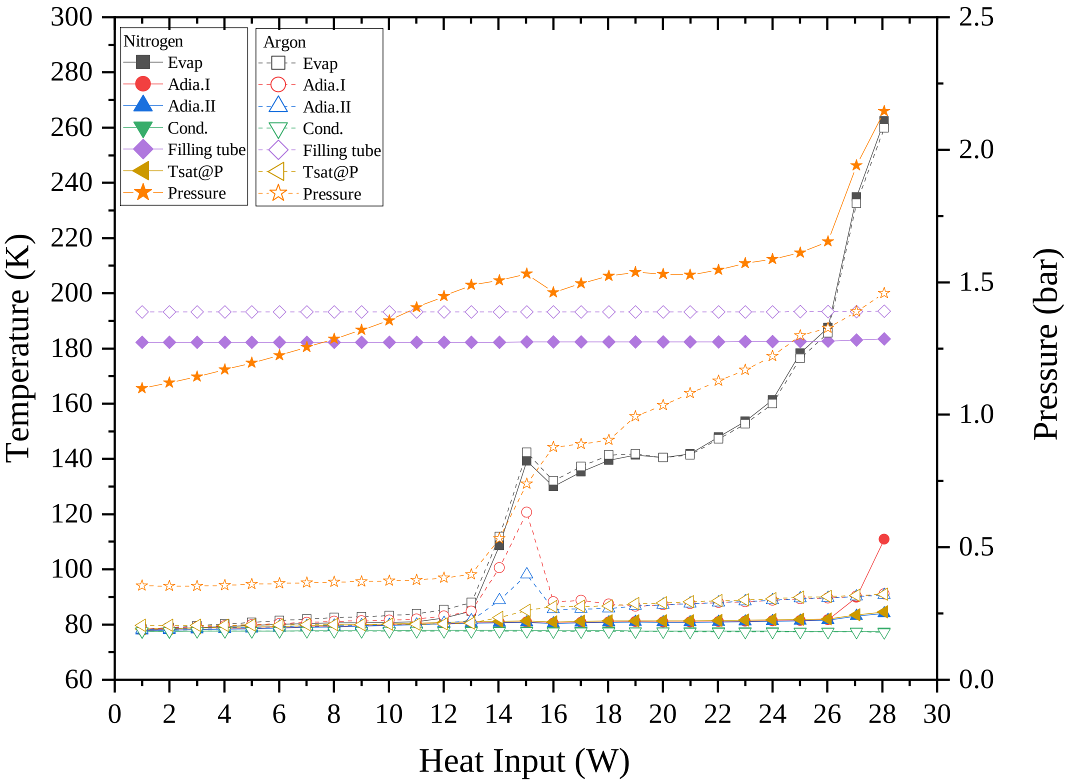

Figure 6.24-3 *Steady state temperature and pressure variation in parallel arrangement of N_2-heat pipe & Ar-heat pipe at 77 K of condenser temperature.*

12 W, and the pressure in the Ar-heat pipe (P_2) also steeply rose from a nearly constant value. When Q_e was 15 W, P_2 reached approximately 1 bar, T_{e1} and T_{e2} began to decrease, and $T_{aI,2}$ and $T_{aII,2}$ also decreased to nearly a constant value equal to the saturated vapor temperature of argon. The drop of temperatures in the evaporator and adiabatic sections indicated that the Ar-heat pipe entered the active working state. At still larger value of Q_e, as the Ar-heat pipe was in operation, the heat flow through the N_2-heat pipe slightly reduced, which caused slight increase in T_{e1} and T_{e2} with increasing the total heat input Q_e even the N_2-heat pipe was in the local dry-out state. It is observed in Figure 6.24-3 that T_{e1} and T_{e2} gradually increased again at Q_e more than 22 W. This was caused because the local dry-out occurred also in the Ar-heat pipe. A rapid increase of the temperature in the adiabatic section of the N_2-heat pipe ($T_{aI,1}$) was seen at Q_e more than 26 W. It can be seen in Figure 6.24-3 that the parallel heat pipe system did work in the normal heat pipe operation state (very small temperature difference

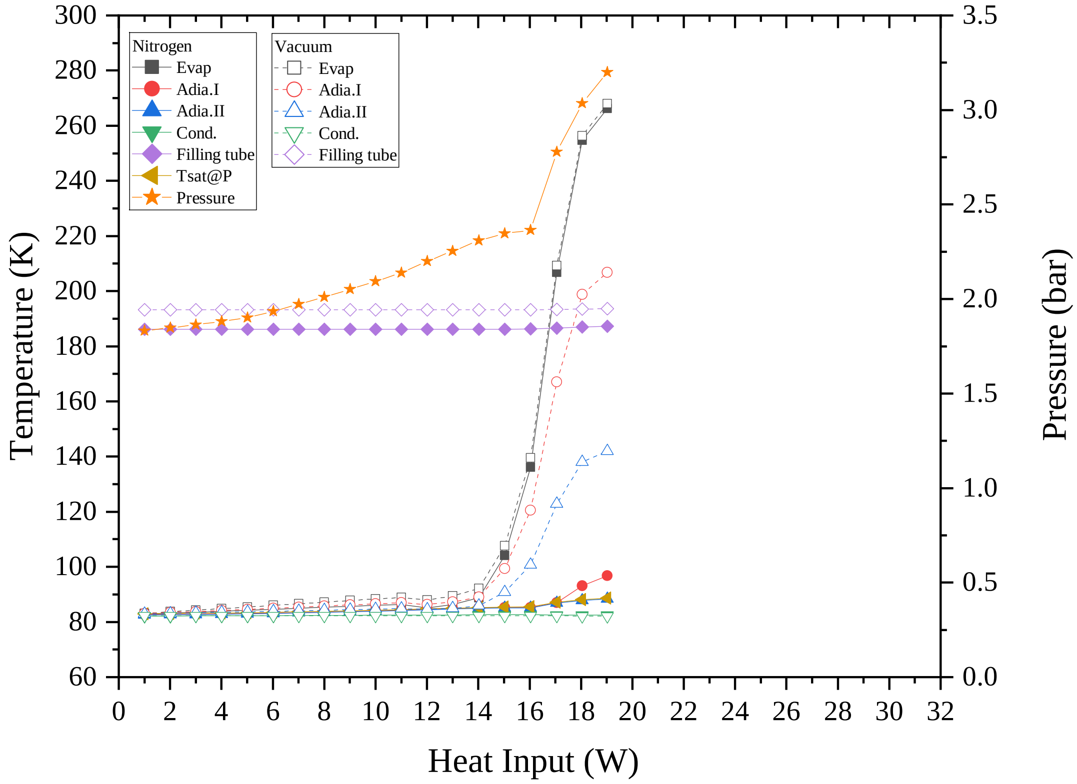

Figure 6.25-1 *Steady state temperature and pressure variation in parallel arrangement of N_2-heat pipe & Empty-heat pipe at 82 K of condenser temperature.*

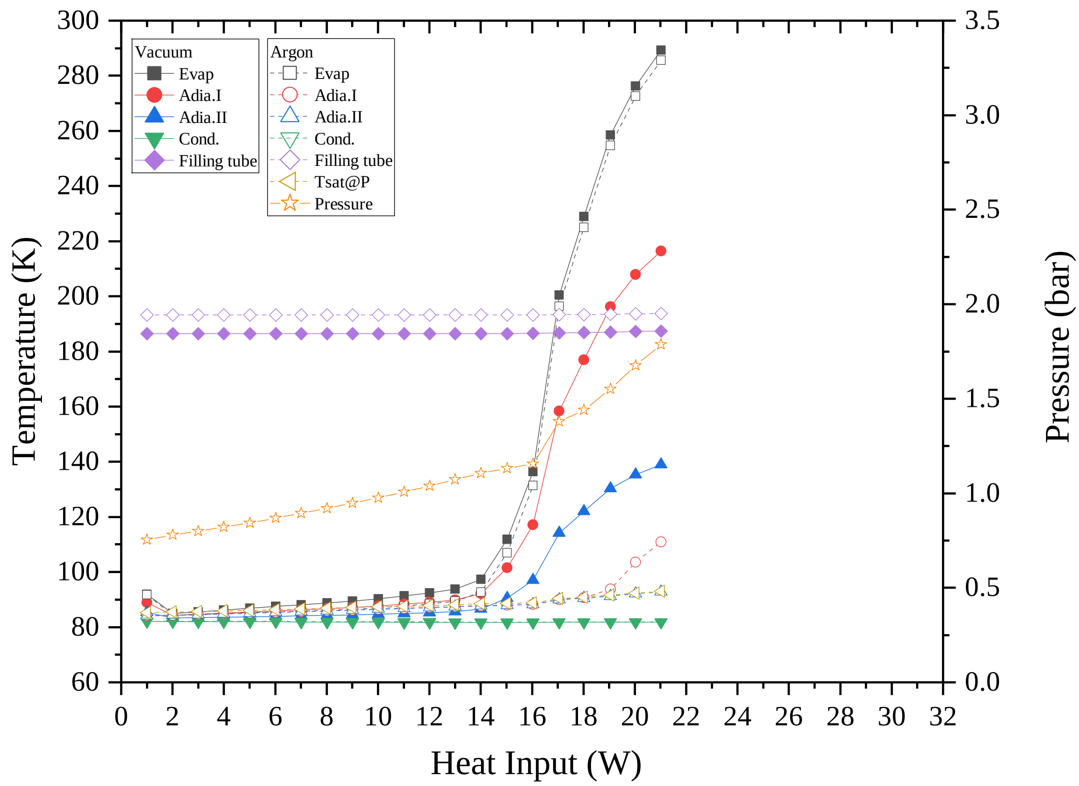

Figure 6.25-2 *Steady state temperature and pressure variation in parallel arrangement of Ar-heat pipe & Empty-heat pipe at 82 K of condenser temperature.*

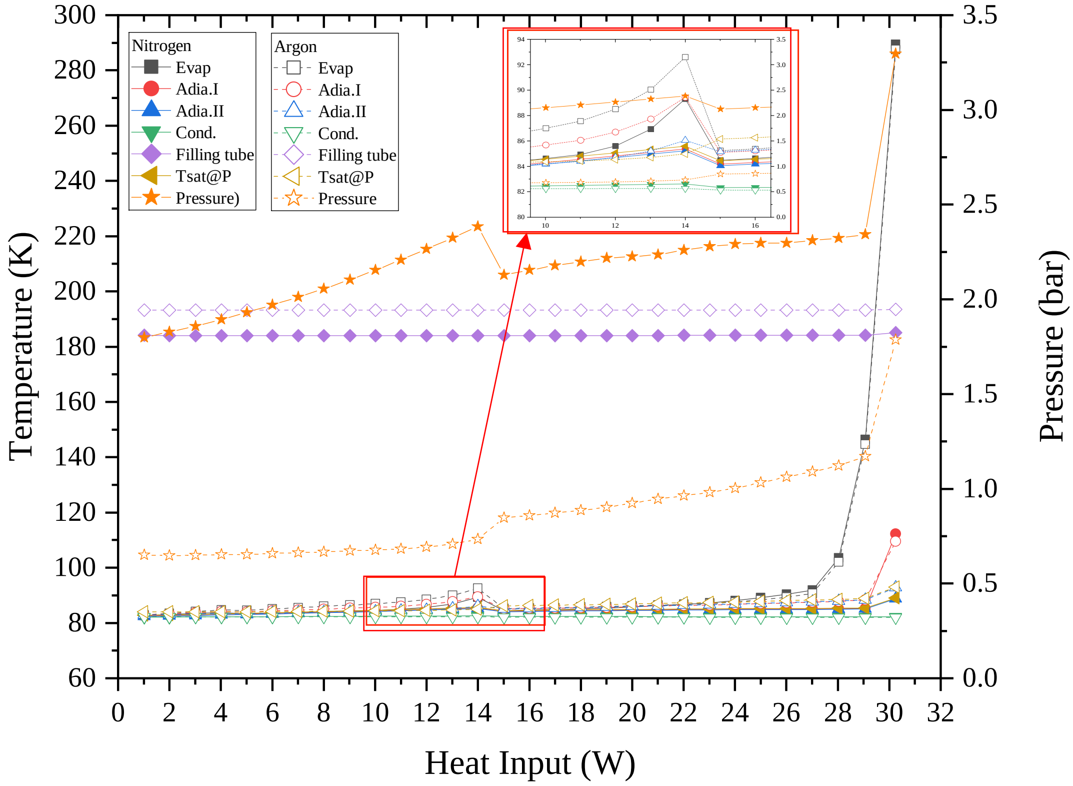

Figure 6.25-3 *Steady state temperature and pressure variation in parallel arrangement of N_2-heat pipe & Ar-heat pipe at 82 K of condenser temperature.*

between the evaporator and condenser sections) for Q_e up to 12 W, though, in fact, only the N_2-heat pipe operated.

Figure 6.25-3 indicates that the parallel heat pipe system worked in the special mode where the N_2-heat pipe was in the normal heat pipe operation state while the Ar-heat pipe was in the locally frozen state in case of Q_e up to 12 W. On the other hand, for the value of Q_e between 15 W and 28 W, both the N_2- and the Ar-heat pipes were supposed to be in the normal heat pipe operation state. In fact, individual N_2- and the Ar-heat pipes were in the normal heat pipe operation state both at Q_e up to 14 W as seen in Figures 6.25-1 and 6.25-2. It seems in Figures 6.24-3 and 6.25-3 that there are transition zones between the start of the local dry-out, or of inactivity of the N_2-heat pipe and the start of the operation, or of activity of the Ar-heat pipe in the range of Q_e, 12–16 W. However, no transition zone can be seen in the cases shown in Figures 6.26-3 and 6.27-3. This may be due to the fact that in cases when the condenser

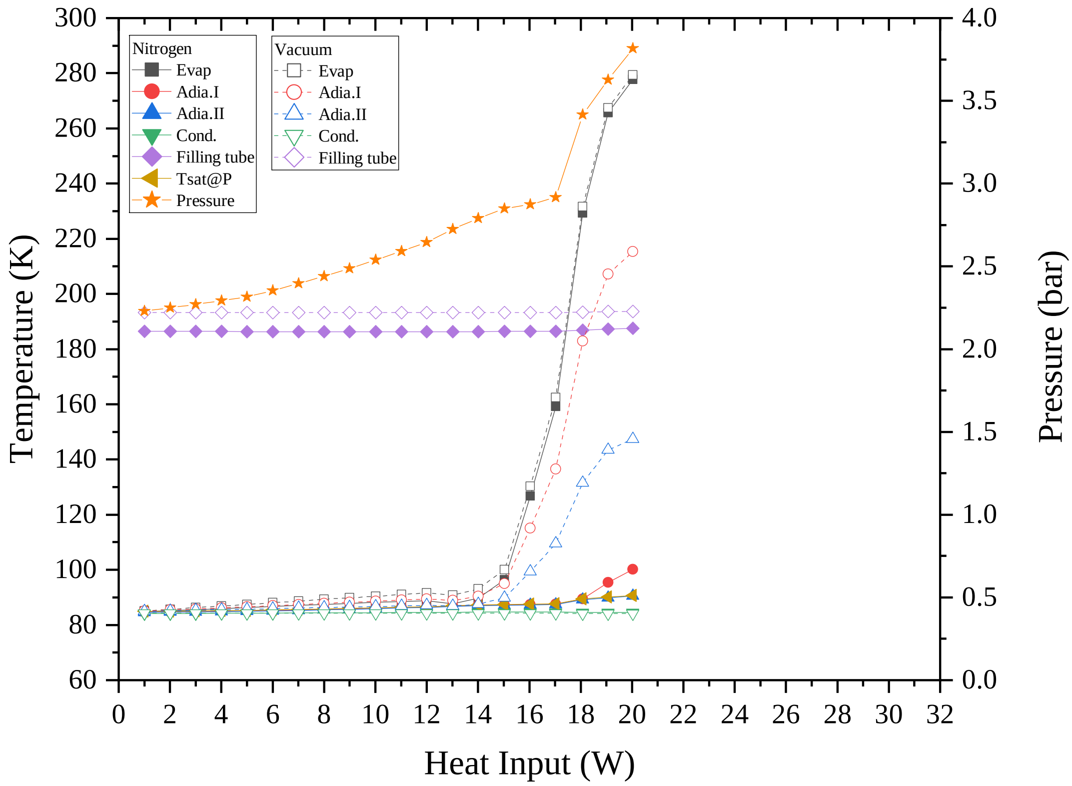

Figure 6.26-1 *Steady state temperature and pressure variation in parallel arrangement of N_2-heat pipe & Empty-heat pipe at 84 K of condenser temperature.*

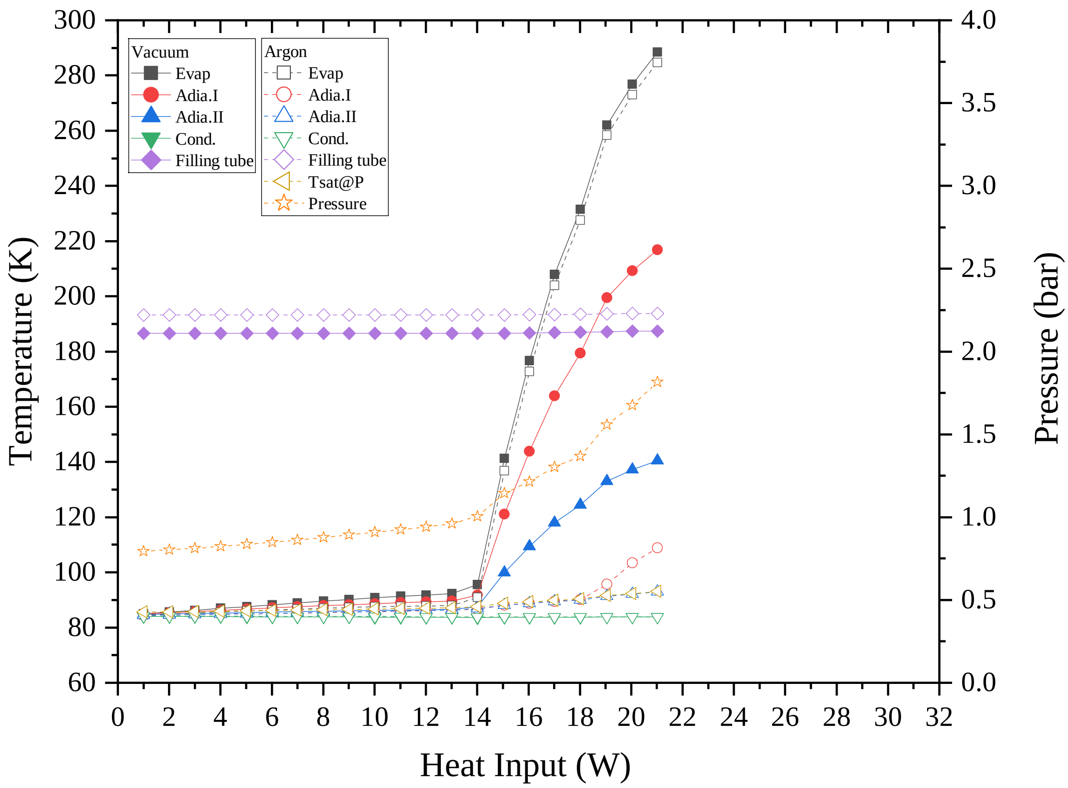

Figure 6.26-2 *Steady state temperature and pressure variation in parallel arrangement of Ar-heat pipe & Empty-heat pipe at 84 K of condenser temperature.*

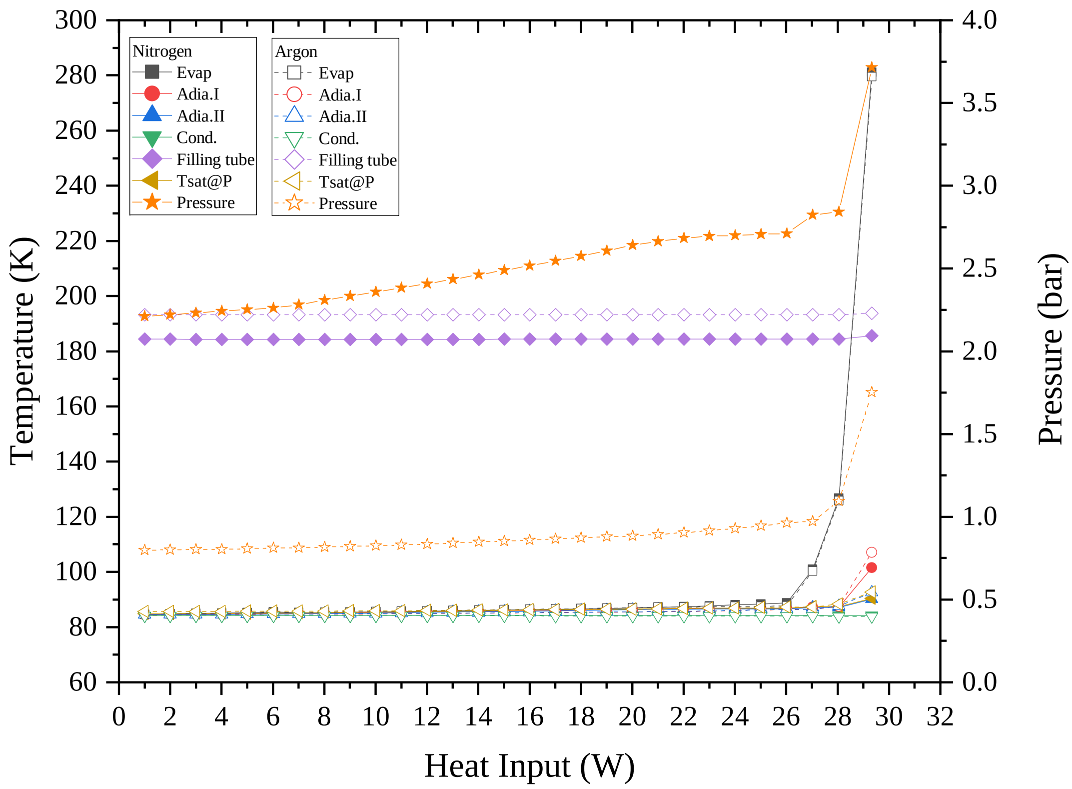

Figure 6.26-3 *Steady state temperature and pressure variation in parallel arrangement of N_2-heat pipe & Ar-heat pipe at 84 K of condenser temperature.*

temperatures were 84 and 87 K both the N_2- and the Ar-heat pipes operated simultaneously even at small Q_e. Owing to this overlap of the active regions of both heat pipes, the appearance of the transition zones seen in Figures 6.24-3 and 6.25-3 can be avoided.

It is shown in Figures 6.26-3 and 6.27-3 that the temperatures in all heat pipe sections were nearly the same and well agreed with the saturated vapor temperature converted from the measured vapor pressure. This is because both the heat pipes composing the parallel heat pipe system worked in the normal heat pipe operation state. It is suggested by the result shown in these figures that the parallel heat pipe system would proceed to the local dry-out state at a value of Q_e around 26 W, because it is known that both the heat pipes entered the local dry-out state after 13 W as seen in Figures 6.26-1 and 6.26-2, if both the heat pipes were separately operated. It is, in fact, found in the result shown in Figure 6.26-3 that the dry-out of the parallel heat pipe system certainly started at 26 W. Figures 6.27-1 and 6.27-2 that are the result of the

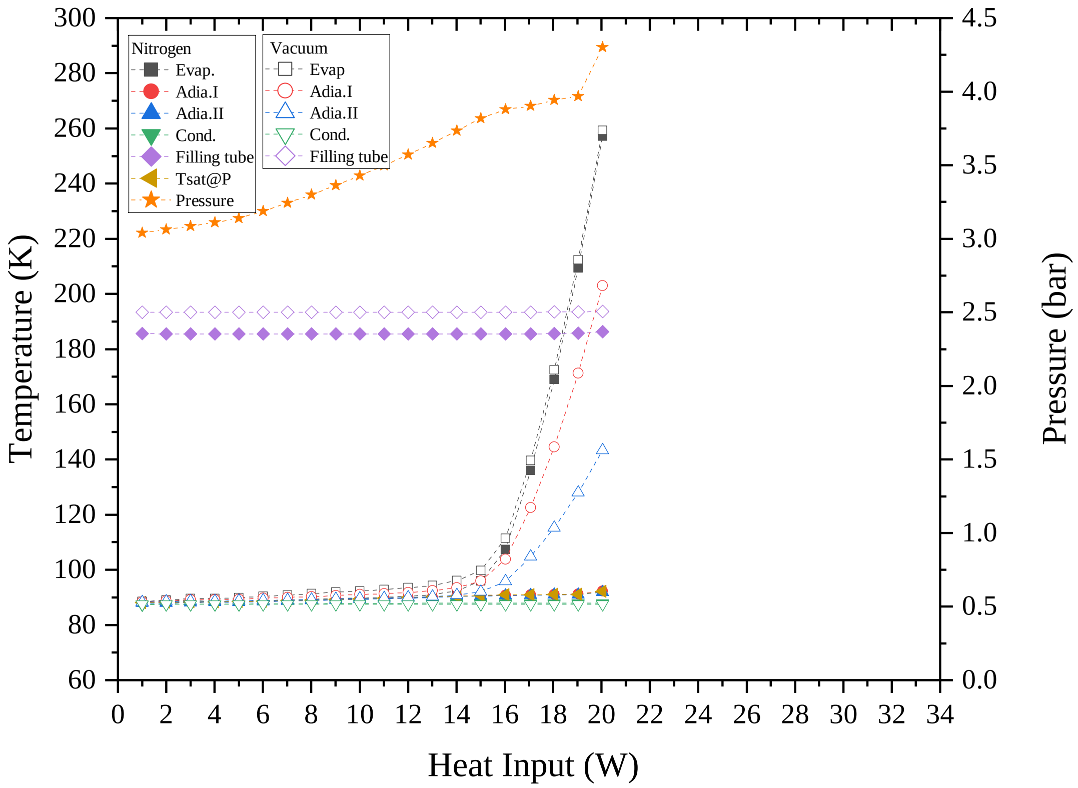

Figure 6.27-1 *Steady state temperature and pressure variation in parallel arrangement of N_2-heat pipe & Empty-heat pipe at 87 K of condenser temperature.*

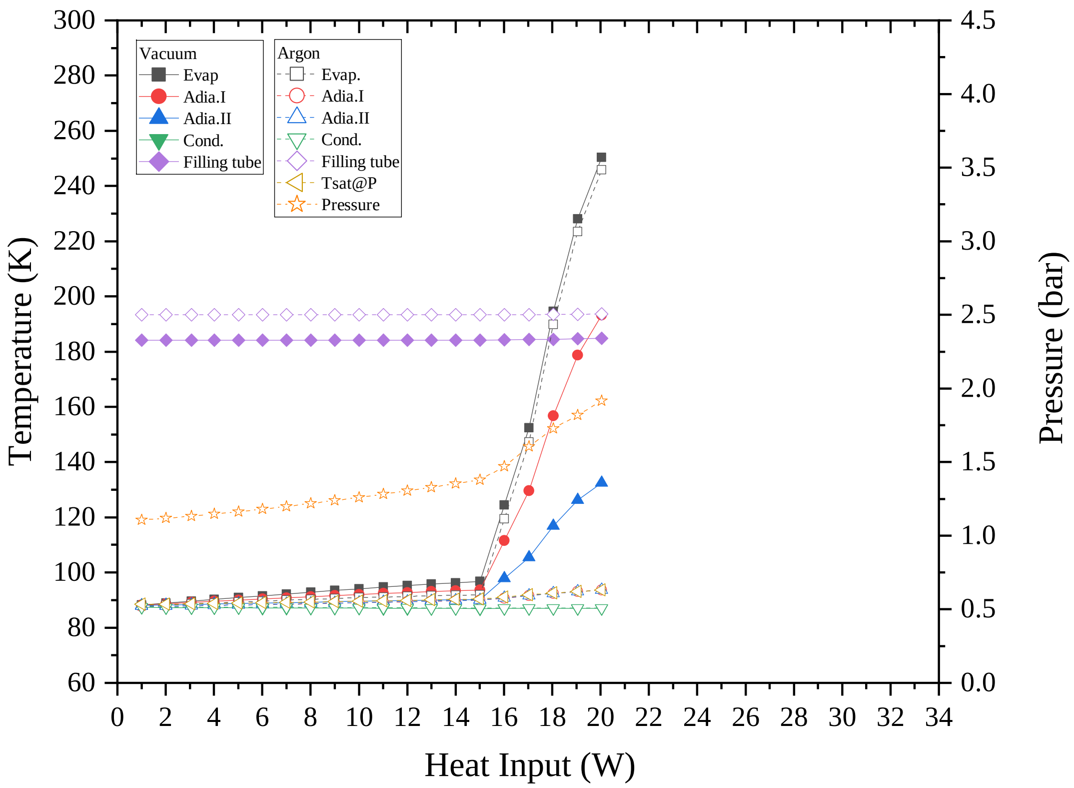

Figure 6.27-2 *Steady state temperature and pressure variation in parallel arrangement of Ar-heat pipe & Empty-heat pipe at 87 K of condenser temperature.*

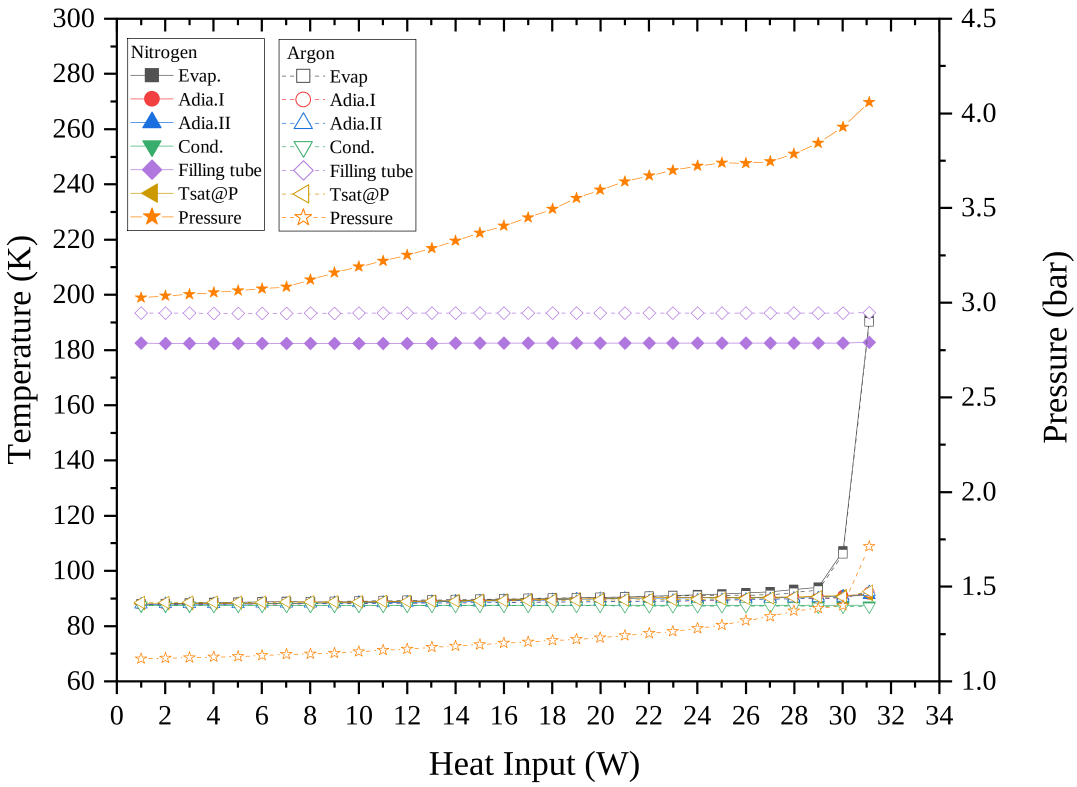

Figure 6.27-3 *Steady state temperature and pressure variation in parallel arrangement of N_2-heat pipe & Ar-heat pipe at 87 K of condenser temperature.*

case when the condenser temperature was 87 K show that the evaporator temperatures started to rise at 14 W and 15 W for the N_2- and Ar-heat pipes, respectively. For the experiments of the parallel heat pipe system, the local dry-out started at 29 W as seen in Figure 6.27-3. It is suggested that the operation of the parallel heat pipe system consisting of the N_2- and the Ar-heat pipes can possibly enhance the maximum heat transport capability at still higher condenser temperatures. However, the experiment at such high temperatures could not be carried out from the viewpoint of safety because the pressure of the N_2-heat pipe may become too high.

Figure 6.28 shows the results of the parallel heat pipe system which consists of the N_2- and the Ne-heat pipe at 27 K of the condenser temperature. It is clear that only the Ne-heat pipe operated in the normal heat pipe operation state, as the condenser temperature is considerably lower than the triple point temperature of nitrogen. The thermal behavior of this parallel heat pipe system is similar to that of the single Ne-heat pipe. It is seen in Figure 6.5 that the Ne-heat

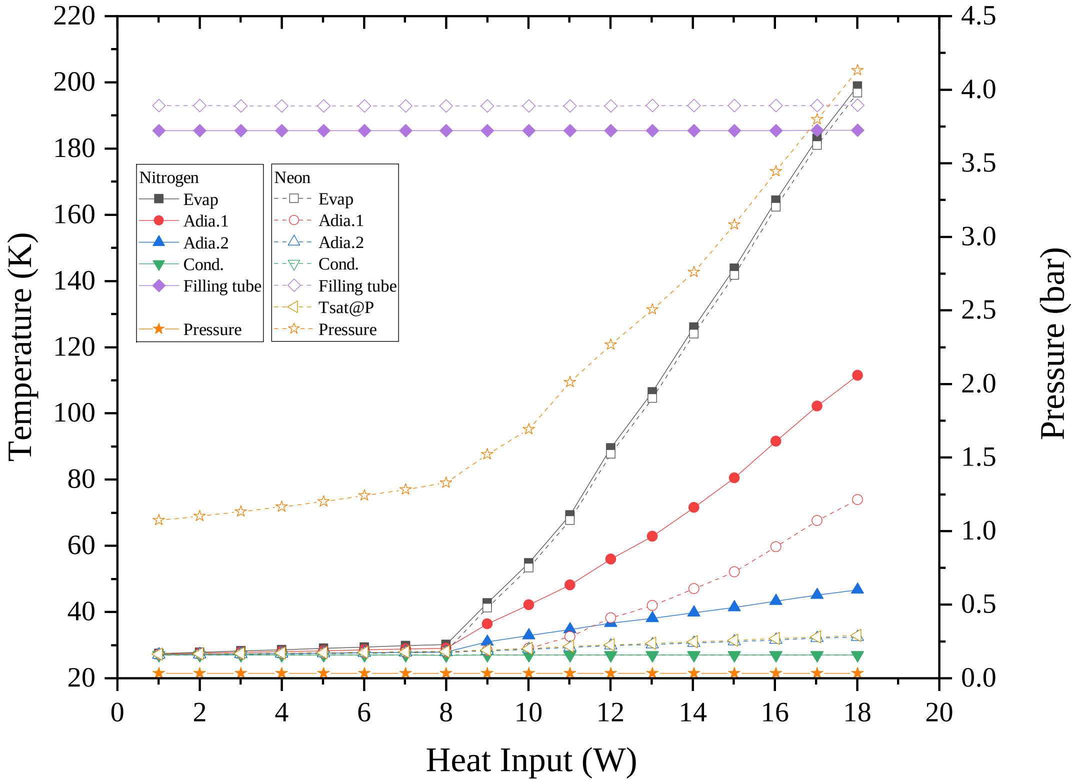

Figure 6.28 *Steady state temperature and pressure variation in parallel arrangement of N_2-heat pipe & Ne-heat pipe at 27 K of condenser temperature.*

pipe was in the normal heat pipe operation state at low values of Q_e up to 7 W. It is also seen from the fact that the pressure of the N_2-heat pipe was very low, almost 0 bar, that nitrogen was in frozen state. However, the value of Q_{max} in Figure 6.28 is 8 W which is slightly higher than the value of Q_{max} in the single Ne-heat pipe experiment, because heat was also conducted through the heat pipe wall and the frozen working fluid in the N_2-heat pipe.

6.2.3 Overall thermal resistance of parallel heat pipe system

In Figures 6.29-1–6.29-4 the overall thermal resistance, R_{th}, of the parallel heat pipe system is plotted as a function of Q_e in cases of the condenser temperatures of 77, 82, 84 and 87 K, respectively. In case of 77 K of the condenser temperature (Figure 6.29-1), R_{th} of the parallel heat pipe system (case 3) is nearly the same as that of single N_2-heat pipe (case 1) up to 14 W as there is no normal heat pipe action in Ar-heat pipe (very large R_{th}), and

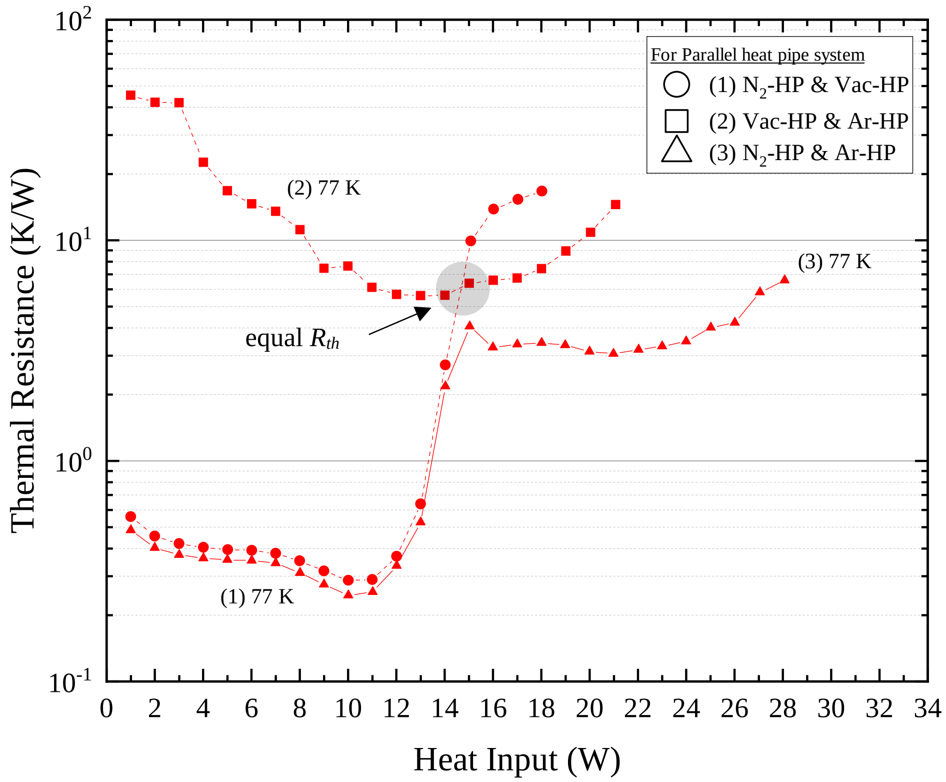

Figure 6.29-1 *The overall thermal resistance of the parallel heat pipe system at 77 K of the condenser temperature.*

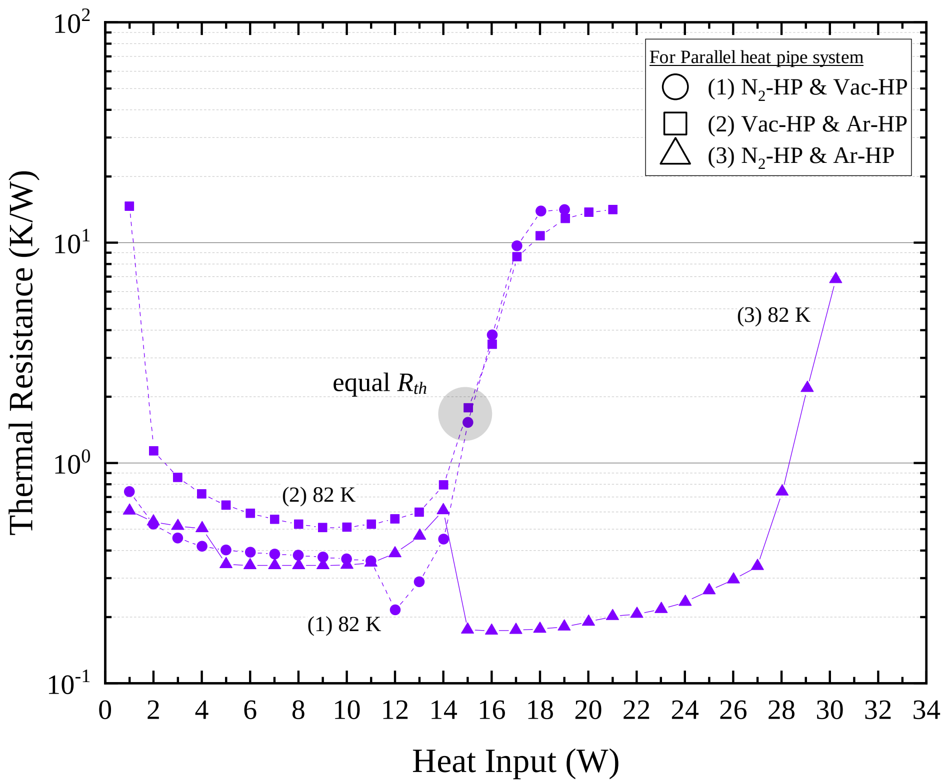

Figure 6.29-2 *The overall thermal resistance of the parallel heat pipe system at 82 K of the condenser temperature.*

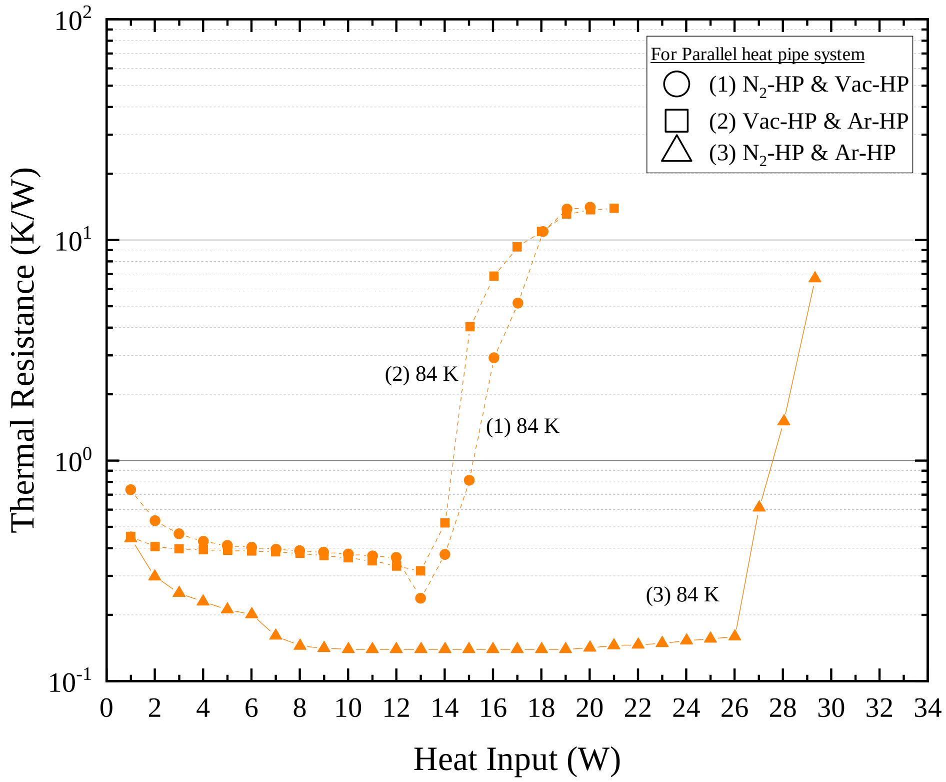

Figure 6.29-3 *The overall thermal resistance of the parallel heat pipe system at 84 K of the condenser temperature.*

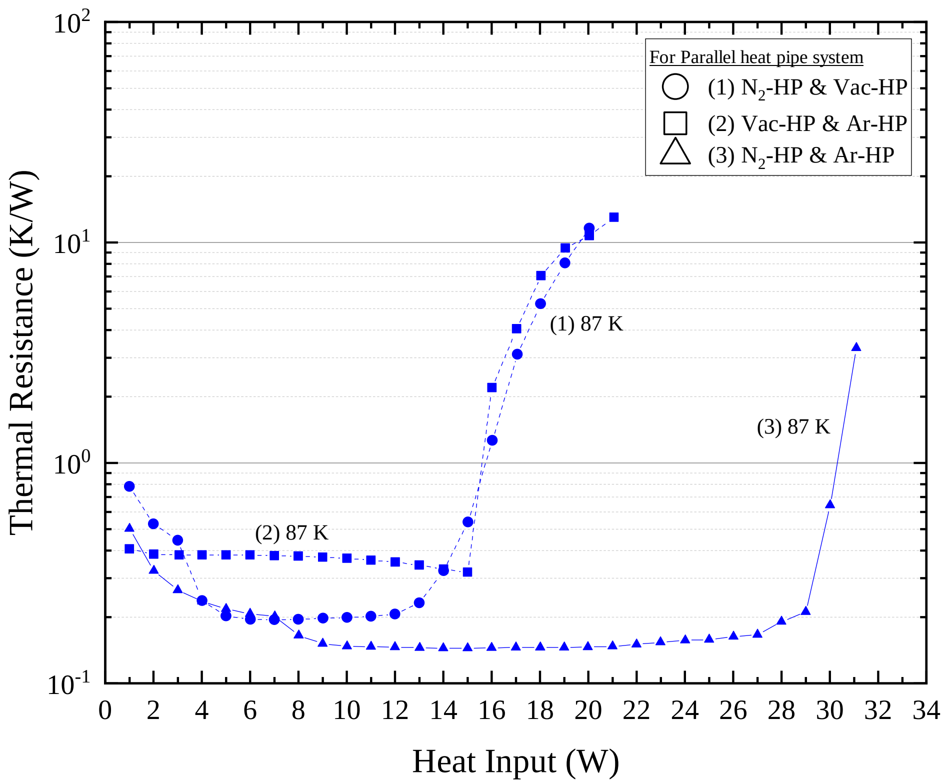

Figure 6.29-4 *The overall thermal resistance of the parallel heat pipe system at 87 K of the condenser temperature.*

thus, heat was transferred only through the N_2-heat pipe. It is shown in Figure 6.29-1 that R_{th} of the single N_2-heat pipe (case ①) became the same as that of the single Ar-heat pipe (case ②) at 14 W. As a result of this, some of the total heat input got transferred through the Ar-heat pipe and the heat through the N_2-heat pipe reduced. It is roughly estimated that some 7 W of the total heat input of 14 W was transferred through the N_2-heat pipe and 7 W through the Ar-heat pipe. In case of the condenser temperature of 82 K (Figure 6.29-2) the value of R_{th} of the single N_2-heat pipe (case ①) became the same as that of the single Ar-heat pipe (case ②) at 15 W, resulting in the value of R_{th} in the parallel heat pipe system (case ③) reduced. As shown in Figures 6.29-3 and 6.29-4, no sudden decrease in the overall thermal resistance, R_{th}, occurred in cases of the condenser temperatures of 84 and 87 K, respectively, because in the heat range up to 13 W both the N_2- and Ar-heat pipes worked in the normal heat pipe operation state, and thus the parallel heat pipe system kept a small value of R_{th} up to the total heat flux of about 26 W. In this range of the total heat input, heat was shared and transferred by both the N_2- and Ar-heat pipes. In case of the parallel heat pipe system, the maximum heat transport capability, Q_{max}, was defined also by the value of Q_e, where the evaporator section temperature suddenly increased, for example, 26 and 29 W as seen in Figures 6.29-3 and 6.29-4, respectively.

It is presumed that the overall thermal resistance of the parallel heat pipe system, $R_{th,3}$, can be estimated in terms of the thermal resistances of the single N_2-heat pipe, $R_{th,1}$, and the Ar-heat pipe, $R_{th,2}$, considering that a parallel heat conduction path is formed, as follows;

$$\frac{1}{R_{th,3}} = \frac{1}{R_{th,1}} + \frac{1}{R_{th,2}} . \tag{6.18}$$

Here, the temperatures for both the N_2- and the Ar-heat pipes are assumed to be equal respectively in the evaporator and condenser sections, as the actual experimental setup was like that. The comparison result is shown in Table 6.3, where the overall thermal resistances are compared between the experimental data of the parallel heat pipe system ③ and the prediction in terms of the thermal resistances of the individual N_2- ① and the Ar-heat pipe ② at approximately the same evaporator section temperatures in case of the condenser temperature of 87 K (Figure 6.29-4). It is found in this table that the prediction result quite well agrees with the experimental result of the overall thermal resistance of the parallel heat pipe system. These results are shown in Figure 6.30 in the form of the plot against the total heat input ($Q_3 = Q_1 + Q_2$).

Figure 6.31 shows the variation of the overall thermal resistance of the parallel heat pipe system composed of the N_2- and Ar-heat pipes ③ as a function of total heat input for several condenser temperatures. It is seen that the overall thermal resistances at 77 and 82 K are nearly the same at low Q_e, but they are quite different at Q_e above15 W. This difference arises depending on whether the Ar-heat pipe was activated or not at 15 W and higher. In case of the condenser temperature of 82 K it was in the normal heat pipe operation state at 15 W and higher, but in case of the condenser temperature of 77 K it was not. However, in cases of 84 and 87 K, as no dry-out state appeared in the Ar-heat pipe even at 15 W or higher, and, of course, the N_2-heat pipe was always in the normal heat pipe operation state in this Q_e range, the variation of the overall thermal resistance was smooth without any switching phenomenon of the operating states. The overall thermal resistances in two cases of the condenser section temperature at 84 and 87 K are identical for all the values of Q_e except when it is larger than respectively, 26 and 29 W, which are Q_{max}. Here the variations of the overall thermal resistance of the parallel heat pipe system composed of the N_2- and the Ne-heat pipes at 27 and 35 K are included. Please note that 35 K was the highest limit temperature with respect to the inside pressure in the heat pipe derived from the safety point of view of the experimental setup. Both results of 27 and 35 K are similar to that of the single Ne-heat pipe because the N_2-heat pipe in the parallel heat pipe system was still in the frozen state.

Table 6.3 *The experimental data of the parallel heat pipe system at 87 K of the condenser temperature.*

N_2-heat pipe ①			Ar-heat pipe ②			Cal. R_{th} from ① and ②	Parallel heat pipe system ③		
$T_{e,1}$	Q_1	$R_{th,1}$	$T_{e,2}$	Q_2	$R_{th,2}$		$T_{e,3}$	Q_3	$R_{th,3}$
88.2	1.0	0.8	88.2	2.0	0.4	**0.25**	88.2	3.0	**0.27**
88.5	2.0	0.5	88.6	3.0	0.4	**0.22**	88.5	5.0	**0.22**
88.8	3.0	0.4	88.9	4.0	0.4	**0.20**	88.8	7.0	**0.20**
89.0	7.0	0.2	89.3	5.0	0.4	**0.13**	89.2	12.0	**0.15**
89.3	8.0	0.2	89.3	5.0	0.4	**0.13**	89.3	13.0	**0.14**
89.5	9.0	0.2	89.6	6.0	0.4	**0.13**	89.6	15.0	**0.14**
90.0	11.0	0.2	89.9	7.0	0.4	**0.13**	90.1	18.0	**0.15**
90.9	13.0	0.2	90.9	10.0	0.4	**0.14**	91.0	23.0	**0.15**

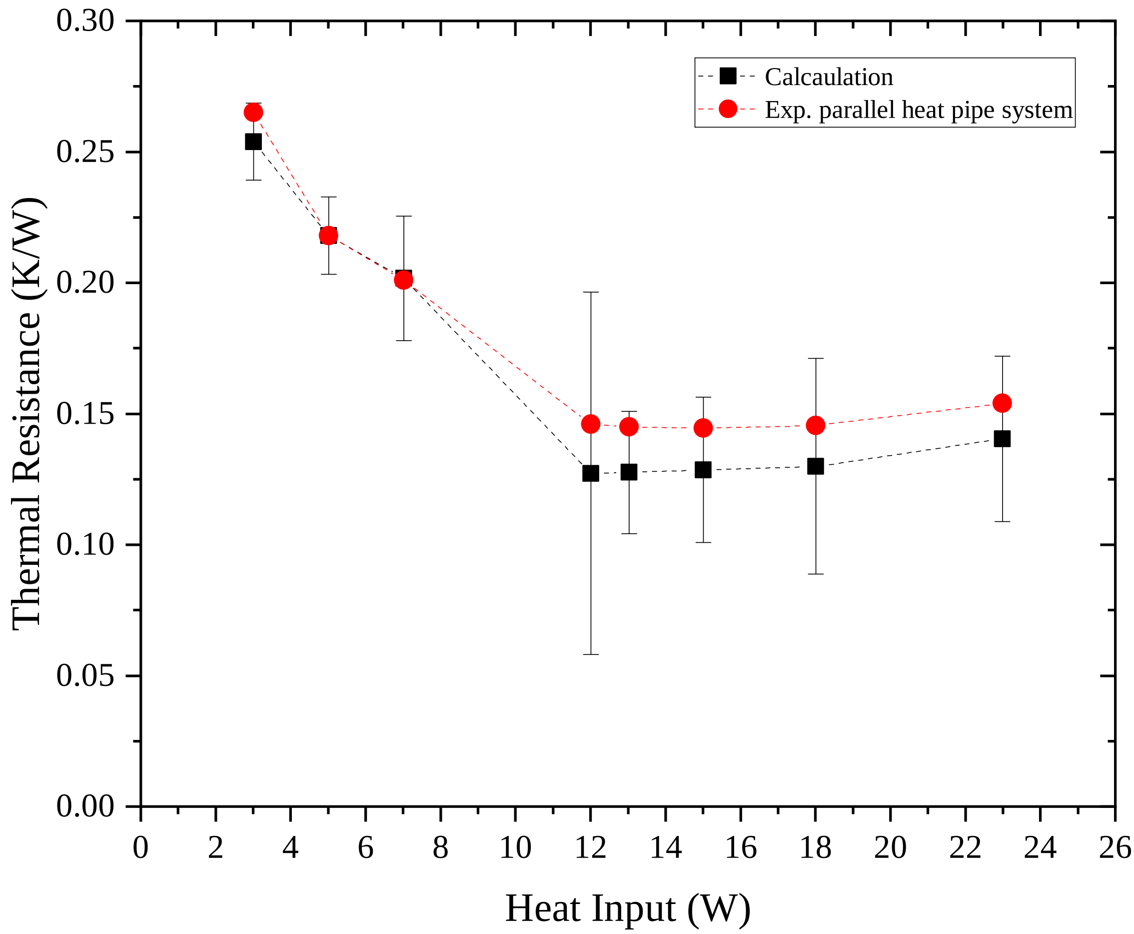

Figure 6.30 *Comparison of overall thermal resistance between experimental data of the parallel heat pipe system and the prediction plotted against heat input at 87 K of the condenser temperature.*

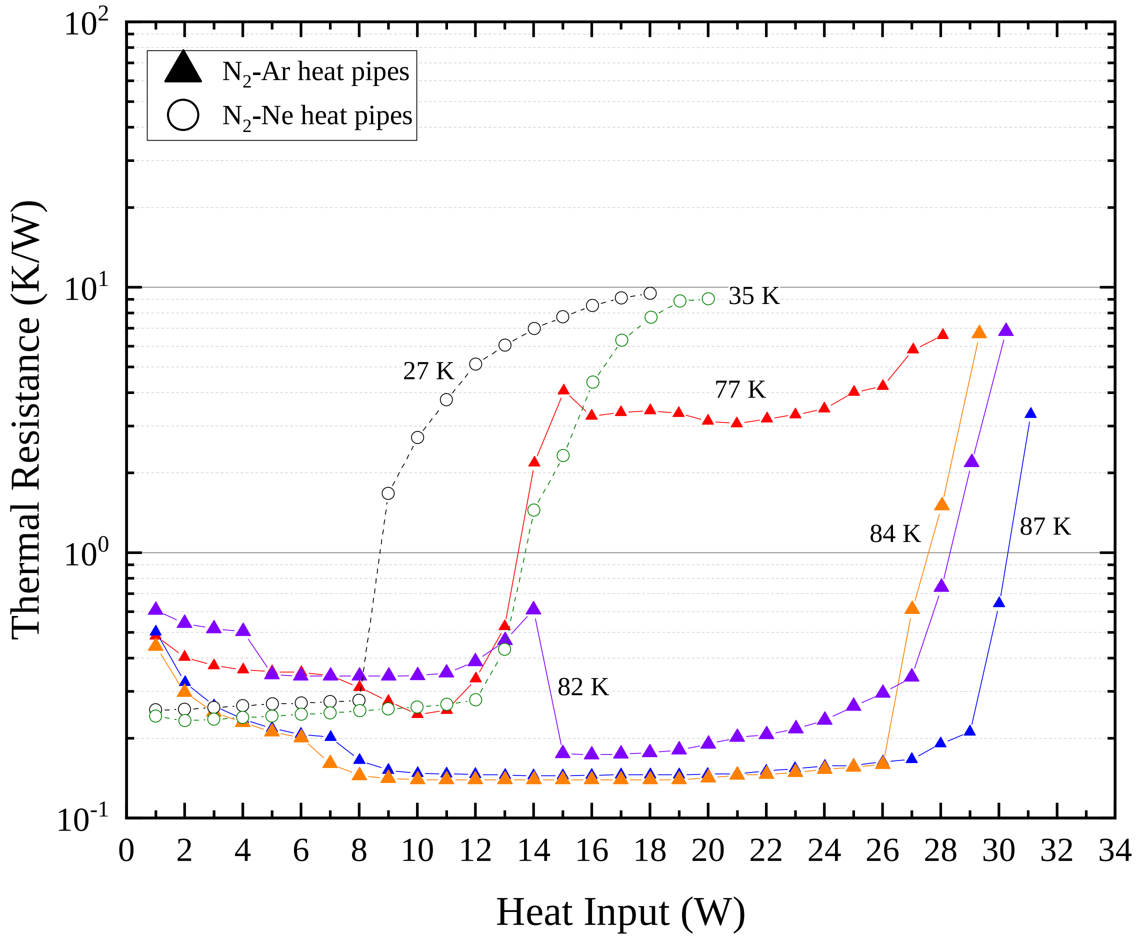

Figure 6.31 *The comparison of the overall thermal resistance of N_2-heat pipe & Ar-heat pipe, and N_2-heat pipe & Ne-heat pipe in parallel for various condenser temperatures.*

It is seen in Figure 6.31 that the value of Q_{max} in case of 35 K of the condenser temperature is larger than that in case of 27 K. The reason is the fluid property depends on the temperature. In particular, the vapor density significantly increases, and the liquid viscosity decreases while other properties change only slightly with the temperature variation from 27 to 35 K. This causes reducing in the friction force of the vapor and the liquid flows. It can be considered that the operating temperature range of the present parallel heat pipe system (the N_2- & the Ar-heat pipe, and the N_2- & the Ne-heat pipe) would be 24.5–150.8 K, which can be derived from the merged range of the operable temperatures for the Ne-heat pipe, 24.5–44.5 K, for the N_2-heat pipe, 63.1–126.2 K and for Ar-heat pipe, 83.8–150.8 K. A rise in the condenser temperature, except for the region near the critical temperature, may result in a slight increase in the maximum heat transport capability, Q_{max}, of the parallel heat pipe system.

6.2.4 Estimation of individual heat flow for N_2- and Ar-heat pipes in parallel heat pipe system

The individual heat flow through the N_2-heat pipe in the N_2-heat pipe & empty-heat pipe system ① or through the Ar-heat pipe in the Ar-heat pipe & empty-heat pipe system ② can be simply estimated by subtracting the heat transferred by conduction through the empty-heat pipe from the total heat input. This simple approach would be justified because in the present experiment of the parallel heat pipe system ③ the evaporator section temperatures for both component heat pipes are the same and the condenser section temperatures are also the same due to the common blocks for the two heat pipes in both the evaporator and the condenser sections. It is confirmed that the sum of the individual heat flows transferred through the N_2-heat pipe and the Ar-heat pipe that were derived from the data of the parallel heat pipe system experiments with an empty-heat pipe agreed reasonably well with the total heat input to the parallel heat pipe system.

Figures 6.32-1–6.32-4 show the estimation of the individual heat flows transferred through each N_2-heat pipe & Ar-heat pipe in the parallel heat pipe arrangement at 77, 82, 84 and 87 K of the condenser temperatures, respectively. The heat flow sharing situation between both the heat pipes can be better understood by referring to Figures 6.32 and 6.29. It is understood that for the case of 77 K shown in Figures 6.32-1 and 6.29-1 the total heat input was transferred mostly through the N_2-heat pipe as only this heat pipe worked in the normal heat pipe operation state up to 14 W, but the Ar-heat pipe was in the frozen state. The Ar-heat pipe started to work and the heat flow increased at the total heat input larger than 14 W, while the heat flow through

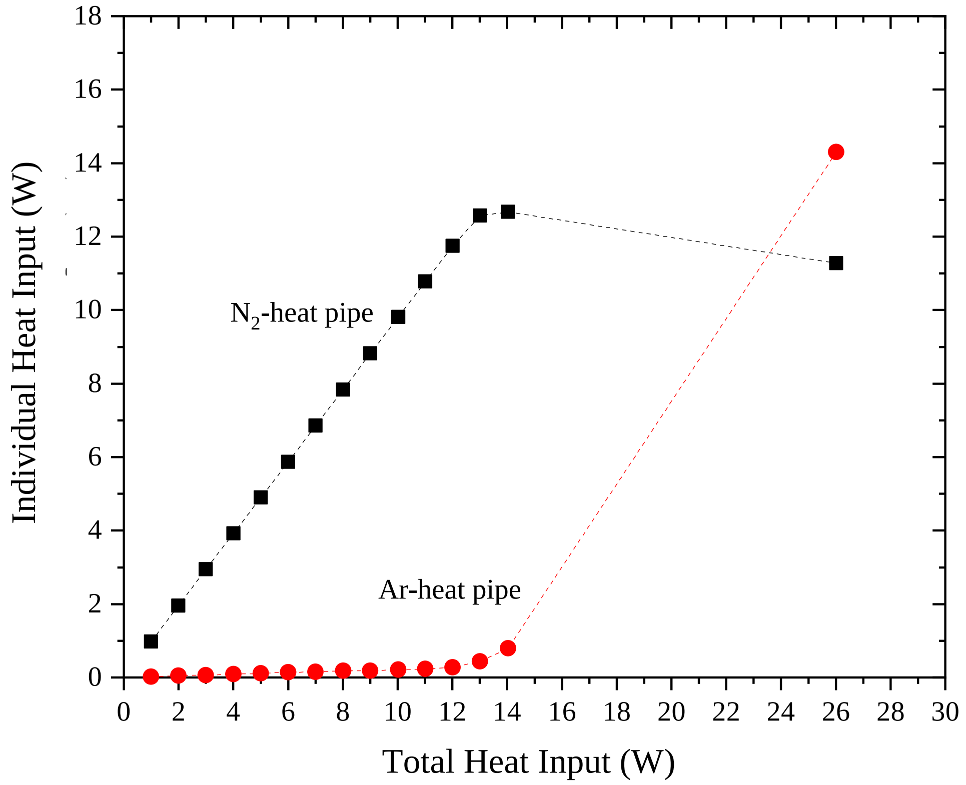

Figure 6.32-1 *The estimation of individual heat transfer for each N_2-heat pipe and Ar-heat pipe in the parallel heat pipe system (experiment ③) at 77 K of the condenser temperature.*

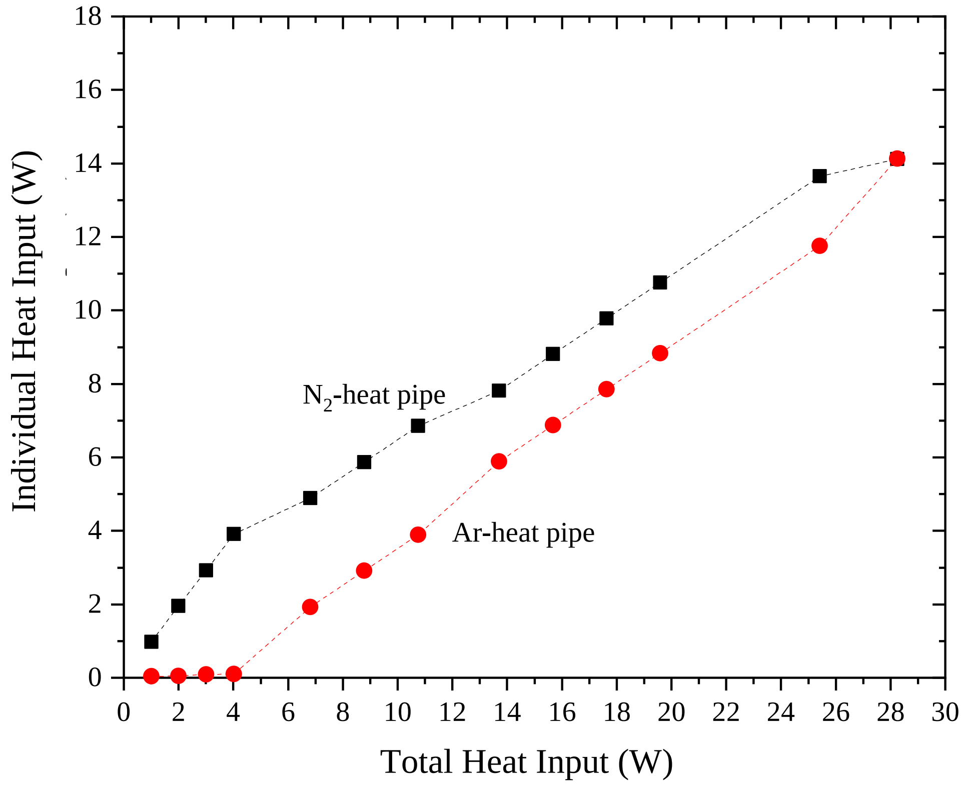

Figure 6.32-2 *The estimation of individual heat transfer for each N_2-heat pipe and Ar-heat pipe in the parallel heat pipe system (experiment ③) at 82 K of the condenser temperature.*

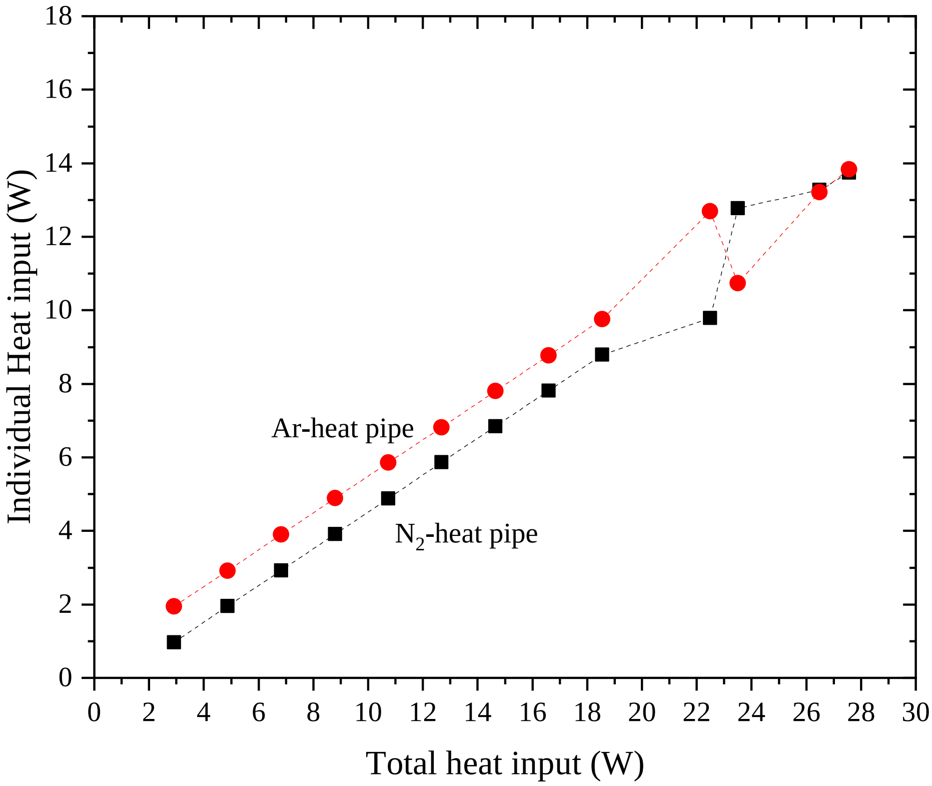

Figure 6.32-3 *The estimation of individual heat transfer for each N_2-heat pipe and Ar-heat pipe in the parallel heat pipe system (experiment ③) at 84 K of the condenser temperature.*

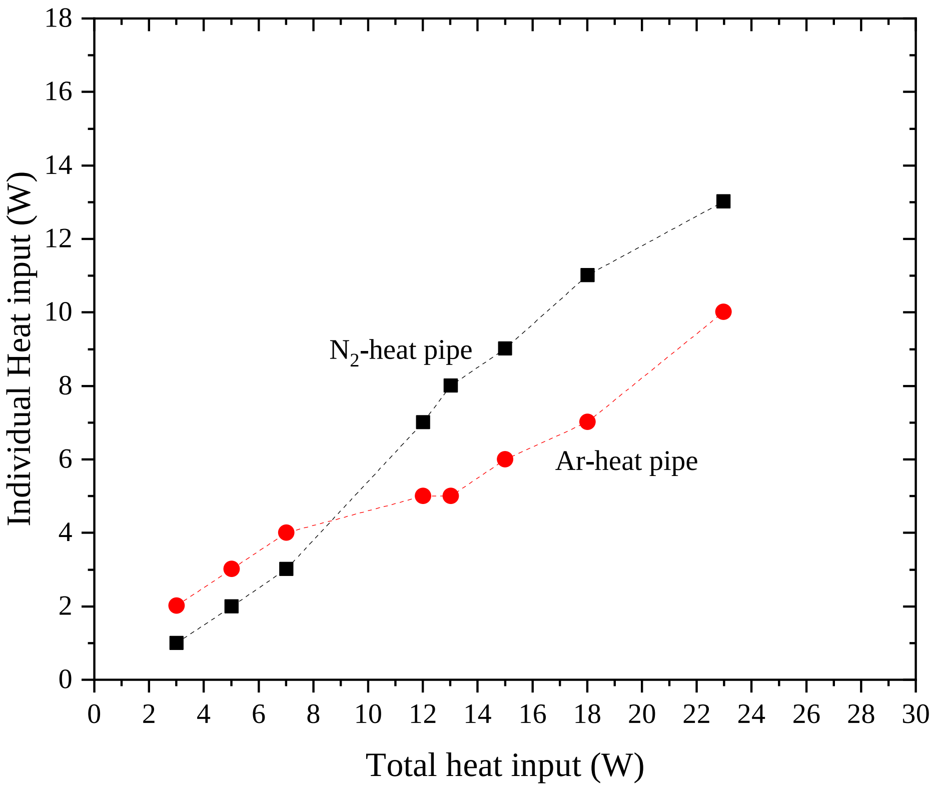

Figure 6.32-4 *The estimation of individual heat transfer for each N_2-heat pipe and Ar-heat pipe in the parallel heat pipe system (experiment ③) at 87 K of the condenser temperature.*

the N_2-heat pipe started to slightly decrease due to the occurrence of the local dry-out resulting in large R_{th}. The heat flow through the Ar-heat pipe increased with Q_e value over 14 W, and R_{th} of the Ar-heat pipe become slightly smaller as shown in Figure 6.29-1.

In case of the operation at 82 K (Figure 6.32-2), the Ar-heat pipe was already in operation with the total heat input Q_e over 4 W, and as a result of the activation of the Ar-heat pipe the increasing rate of the individual heat flow through the N_2-heat pipe slightly went down. The heat was transferred by sharing through both the N_2- and the Ar-heat pipes, though a little bit larger amount of heat was transported through the N_2-heat pipe. The individual heat flows through the N_2- and Ar-heat pipes became almost the same at the total heat input of 28 W (14 W each). It is, in fact, clear in Figure 6.29-2 that R_{th} of the N_2- and the Ar-heat pipes were nearly equal at the total heat input of 14 W. In case of the operation at 84 K (Figure 6.32-3), the Ar-heat pipe worked even at small total heat input and the amount of the heat transferred through this heat pipe was a little bit larger than that through the N_2-heat pipe, which is evident from the result in Figure 6.29-3 where R_{th} of the Ar-heat pipe is slightly lower than that of the N_2-heat pipe for the heat input lower than 12 W. In case of the operation at 87 K (Figure 6.32-4), the result was qualitatively similar to that of 84 K.

6.2.5 Effective utilization of the dry-out state of heat pipe

When the heat input, Q_e, to a heat pipe is larger than of the maximum heat transport capability, Q_{max}, the local dry-out would occur in the evaporator section or sometimes would expand to the adiabatic section, while in the other sections (the adiabatic or condenser sections) two-phases liquid–vapor coexist and the normal heat pipe operation is performed. Figure 6.33 shows the plots of wall temperature distributions along the length of the heat pipe.

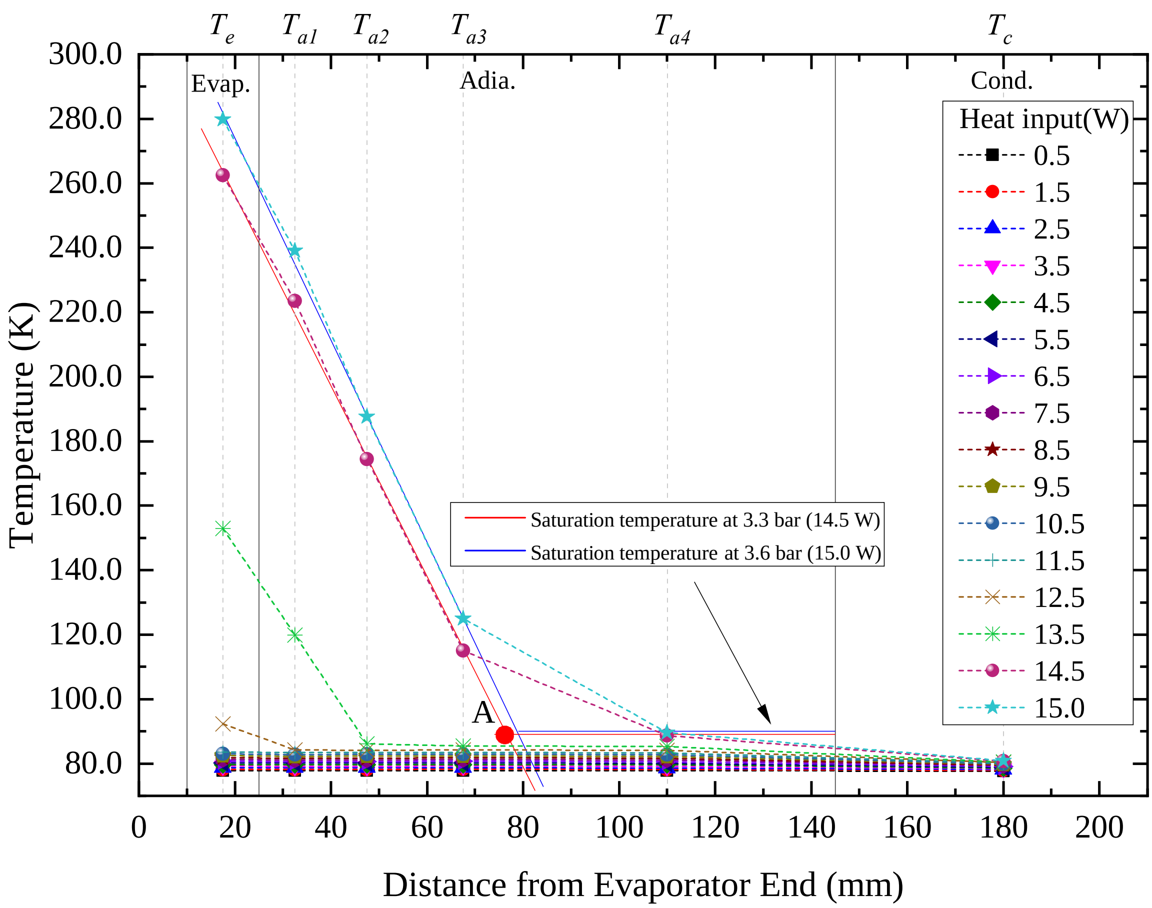

Figure 6.33 *Wall temperature distributions along the length of the heat pipes with six temperature sensors for various heat inputs to the* N_2*-heat pipe, 100% filling ratio, 77 K of condenser temperature.*

In this experiment, the number of temperature sensors was increased to six in order to observe the development of the local dry-out region in the adiabatic section in detail. It is evident in this figure that although the local dry-out occurs (for example in case of 14.5 W) the temperature in some part of the adiabatic section near the condenser section, T_{a4}, is still the same as the saturated vapor temperature. In Figure 6.33 in case of the heat input of 14.5 W a plausible temperature distribution is shown by the two solid red lines, one is the temperature distribution in the local dry-out state where heat is conductively transferred through heat pipe wall (from the point T_e to the extrapolated point A), another is the horizontal line at the saturated vapor temperature corresponding to 3.3 bar of the nitrogen vapor pressure. The former linear temperature distribution is a result of heat transfer due to thermal conduction. From this temperature distribution, it can be inferred that in this heat pipe, a normal heat pipe operation does occur locally from around the point A to the end of the adiabatic section. This is the reason why the overall thermal resistance of this heat pipe is relatively small even when it is in the local dry-out state. Its thermal resistance value is considerably smaller than the thermal resistance due to natural convection that may occur in the vapor core or that of thermal conduction heat transfer through the tube wall and the wick containing working fluid.

The experimental results that the heat pipe may be utilized even in the local dry-out state as long as the pressure is not extremely high, or the evaporator temperature does not reach room temperature. Of course, for such applications of heat pipes in the local dry-out state, attention should be paid to instantaneous increase in the vapor pressure and the condenser temperature. Through the experiments of the cryogenic heat pipes, the following facts have been found regarding the operation of the cryogenic heat pipes. As long as the condenser section is thermally connected to such a large-capacity heat sink as a cryocooler reliably and keeps cryogenic temperatures, even if the evaporator section comes to a local dry-out state, in other sections (adiabatic and condenser sections), the heat pipe operation continues and furthermore, the vapor pressure increase inside the heat pipe is not abrupt.

In Figure 6.34 the variations of the heat flow through the parallel heat pipe system are plotted as a function of evaporator temperature at several condenser temperatures, 77, 82, 84 and 87 K together with the calculated data of the conduction heat flow through oxygen-free high thermal conductivity copper (OFHC Cu) rods and tubes with the same dimensions, 200, 6, and 4 mm in length, outer and inner diameter as the heat pipe tested. As the conduction heat flow through OFHC Cu is calculated as a function of temperature difference, the calculations were made on the basis of the measured temperature difference between the evaporator and the

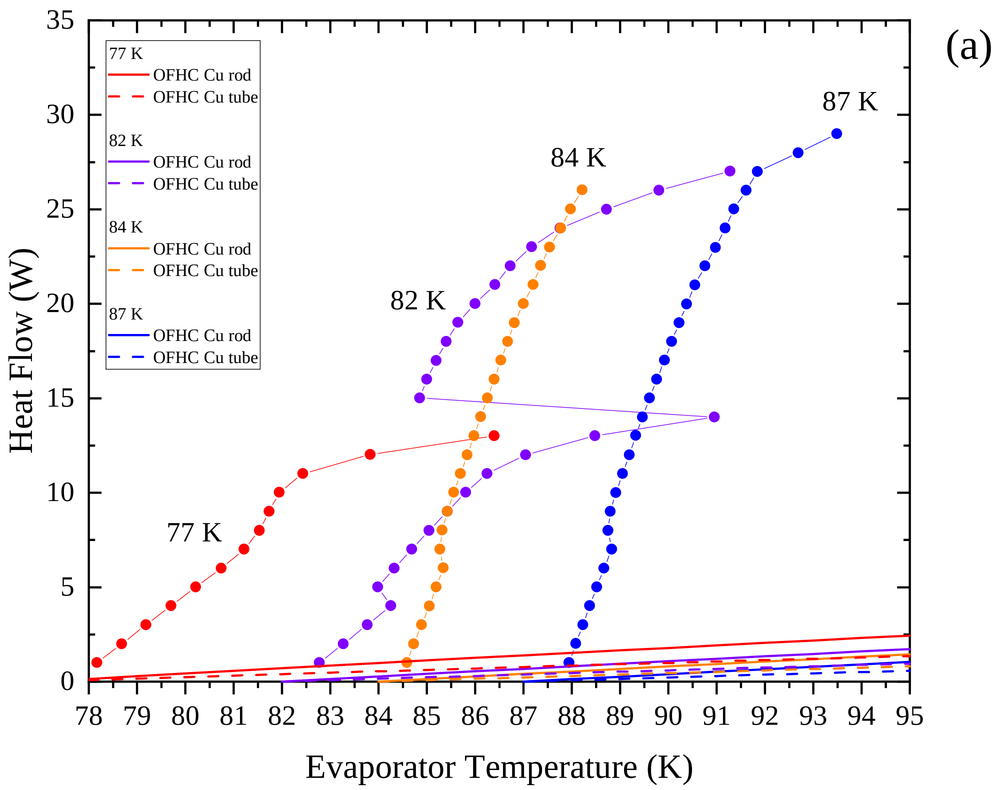
(a)
77 K
OFHC Cu rod
OFHC Cu tube
82 K
OFHC Cu rod
OFHC Cu tube
84 K
OFHC Cu rod
OFHC Cu tube
87 K
OFHC Cu rod
OFHC Cu tube
87 K
84 K
82 K
77 K
Heat Flow (W)
Evaporator Temperature (K)

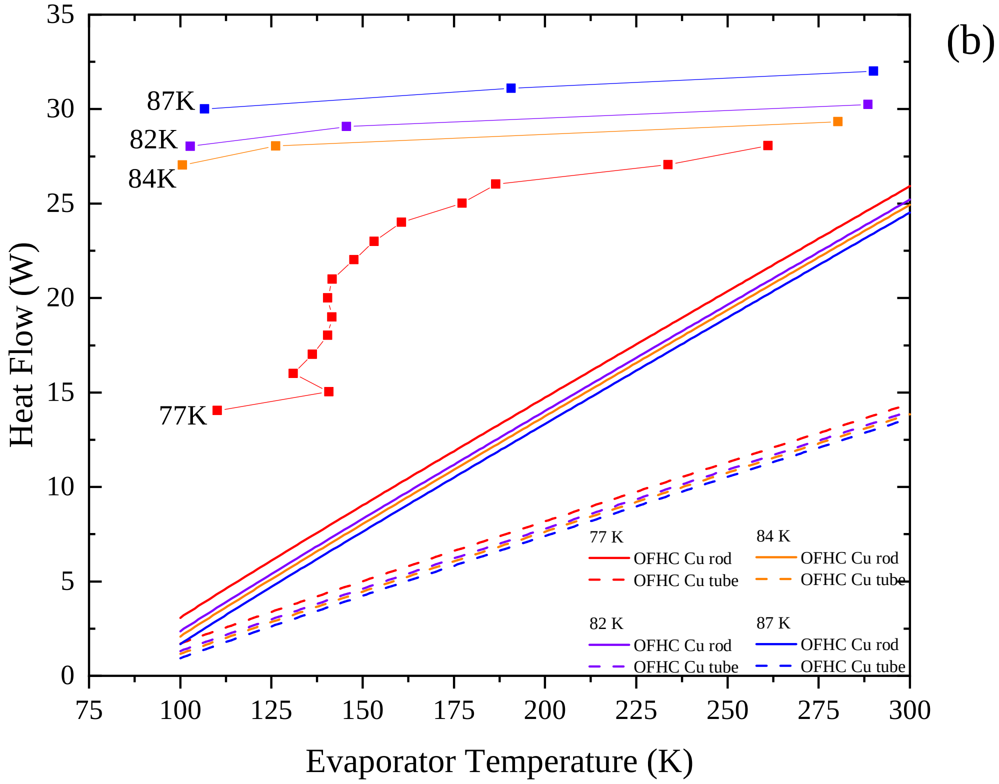
(b)
87K
82K
84K
77K
77 K
OFHC Cu rod
OFHC Cu tube
84 K
OFHC Cu rod
OFHC Cu tube
82 K
OFHC Cu rod
OFHC Cu tube
87 K
OFHC Cu rod
OFHC Cu tube
Heat Flow (W)
Evaporator Temperature (K)

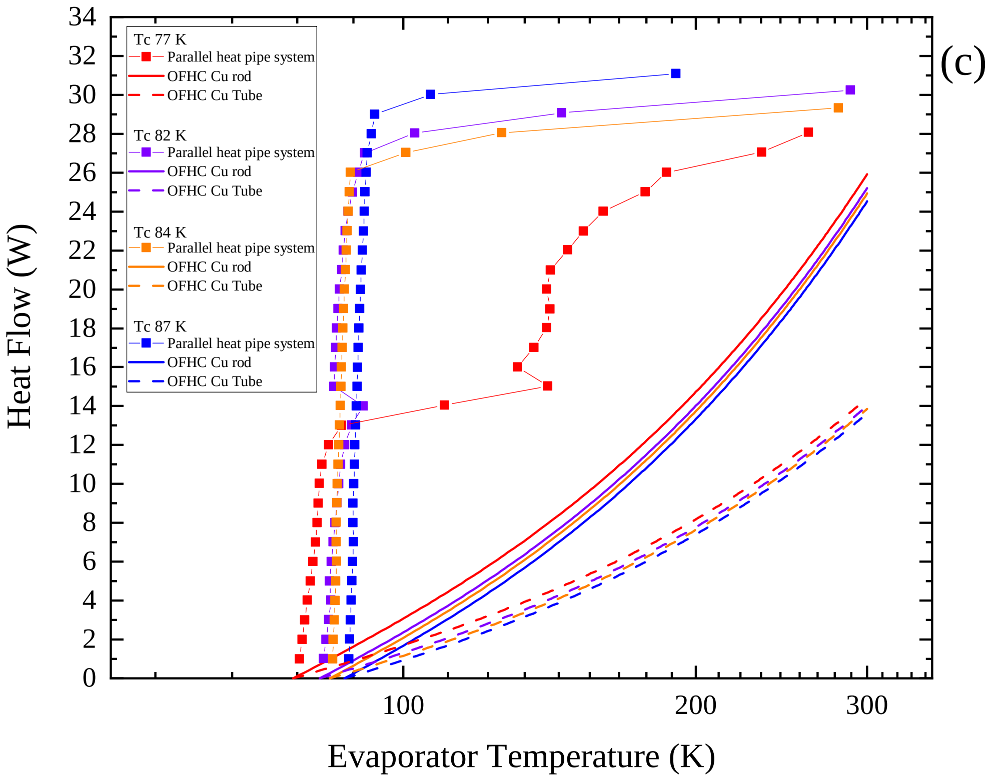

Figure 6.34 *Comparison of heat flow through the parallel heat pipe and OFHC rod and tube as a function of evaporator temperature at several condenser temperature; (a) normal heat pipe action state and (b) dry-out state, (c) figures (a) and (b) were merged and plotted for the entire evaporator temperature range.*

condenser sections. Figure 6.34(a) is the data plots of the heat flow through the parallel heat pipe system in the normal heat pipe operation state and through OFHC Cu rods and tubes. As the evaporator temperature rose while the condenser section temperature was kept constant, the heat flow increased and reached about 30 W with a temperature difference between the evaporator and the condenser sections of 5–10 K approximately. In an exceptional case where the condenser temperature was kept constant at 77 K, the maximum heat flow was at most 14 W because only the N_2-heat pipe was working in the normal heat pipe operation state. In case of the condenser temperature of 82 K, the transition of the heat pipe working state is confirmed in Figure 6.34(a), which is symbolized by the sudden temperature drop in the evaporator section. The N_2-heat pipe resumed to the normal heat pipe operation from the local dry-out state as a result of the transition of the Ar-heat pipe from an inactive locally frozen state to the normal heat pipe operation state at the total heat flow of 14 W. The heat flow through OFHC Cu linearly increased with the evaporator temperature and reached the maximum only 2.5 W for OFHC Cu rods at the temperature difference between 95 and 77 K. Figure 6.34(b) is a data plot of the heat flow in the heat pipe dry-out state when the evaporator temperature became rather high. The heat flow through the parallel heat pipe system was approximately constant at 30 W over a wide range of the evaporator temperature from 100 to 300 K. It, however, seems for the experiment at 77 K of the condenser temperature that the heat flow once reached a stationary value of 14 W, but it further increased and eventually reached approximately 30 W, when the evaporator temperature reached 140 K and the Ar-heat pipe started locally working. For the OFHC Cu rods and tubes, the heat flows were estimated to be 25 W and 14 W at room temperature, respectively (Figures 6.34(b) and (c)).

6.2.6 Model calculation of conduction cooling with parallel heat pipe system

In order to obtain a concrete concept of conduction cooling using the parallel heat pipe system, a model calculation was performed. In the calculation, cooling of a 100 kg mass from 300 K to 77 K with the parallel heat pipe system and two OFHC Cu rods that have the same dimensions as the parallel heat pipe system, which were supposed to be connected to a heat sink kept at a constant temperature of 77 K. The model calculation result is shown in Figure 6.35, where the time variation of the temperature is plotted during the cooling from 300 K down to 77 K. The calculation was performed on the basis of the equation of transient cooling by conduction as follows;

$$\frac{dT_e}{dt} = \frac{A}{L\, m\, c_p(T)} \int_{T_c}^{T_{e,\,i}} k(T)\, dT\ , \tag{6.19}$$

Here A is the cross-sectional area (6 and 4 mm in the outer and inner diameters, respectively), L is the total length (200 mm), T_c is the constant condenser temperature of 77 K, $T_{e,i}$ is the evaporator temperature that changes with time, $k(T)$ is the thermal conductivity which can be calculated by Equations (6.16) and (6.17), and $c_p(T)$ is the specific heat capacity as a function of evaporator temperature that can be calculated by:

$$c_p(T) = 10^{B(T)}, \tag{6.20}$$

and

$$B(T) = a + b(\log_{10}T) + c(\log_{10}T)^2 + d(\log_{10}T)^3 + e(\log_{10}T)^4 + f(\log_{10}T)^5 + g(\log_{10}T)^6 + h(\log_{10}T)^7 + i(\log_{10}T)^8. \tag{6.21}$$

Here the coefficients in Equation (6.21) are given in Table 6.4

Table 6.4 *Coefficients of Equation (6.21) for 60–300 K*

Coefficient	Value
a	15503.11
b	-37280.38
c	26788.42
d	7010.09
e	-22731.65
f	15386.53
g	-5175.80
h	896.97
i	-64.06

Figure 6.35 shows that the cooling time to reach 77 K with the parallel heat pipe system is approximately one-third of that with OFHC Cu rods. It is quite natural to consider that increasing the number of the heat pipes involved in the system would increase the heat flow,

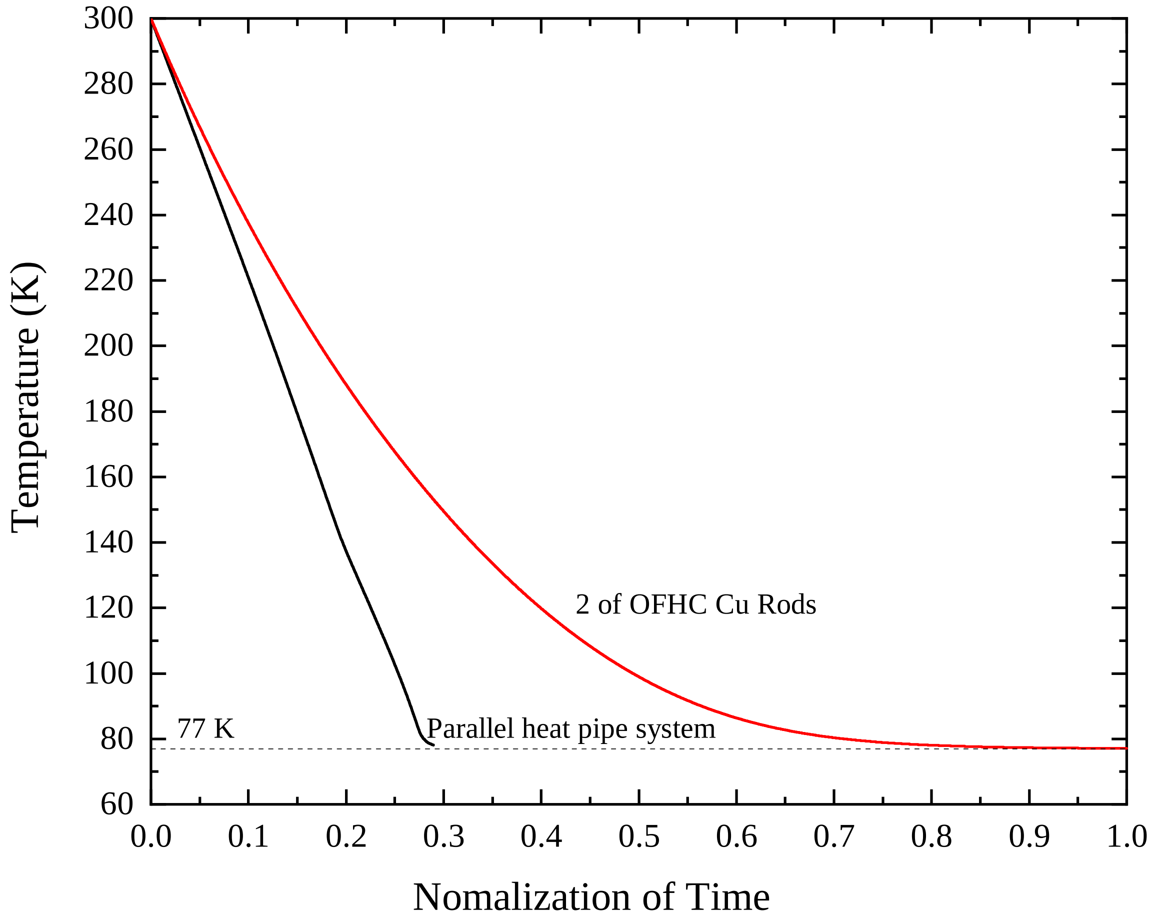

Figure 6.35 *The estimation of cooling time from 300 to 77 K of mass 100 kg by the parallel heat pipe system and two of OFHC Cu rods.*

which results in the reduction of the cooling-down time. It may be concluded that the present study of the parallel heat pipe system demonstrated that it could be used for high performance conduction cooling. The parallel heat pipe system can be used for wide range of operating temperature with the selection of the appropriate multi-working fluids through the operation not only in the normal heat pipe operation state but also in the local dry-out state in order to achieve high cooling rate.

6.3 References

[1] G. Kumaresana, S. Venkatachalapathy and L. G. Asirvathamb, "Experimental investigation on enhancement in thermal characteristics of sintered wick heat pipe using CuO nanofluids," *International Journal of Heat and Mass Transfer*, vol. 72, pp. 507-516, 2014.

[2] "Thermophysical Properties of Nitrogen," National Institute of Standards and Technology, 2018. [Online]. Available: https://webbook.nist.gov/cgi/fluid.cgi?ID=C7727379&Action=Page.

[3] "Thermophysical Properties of Argon," National Institute of Standards and Technology, 2018. [Online]. Available: https://webbook.nist.gov/cgi/fluid.cgi?ID=C7440371&Action=Page.

[4] "Thermophysical Properties of Argon," National Institute of Standards and Technology, 2018. [Online]. Available: https://webbook.nist.gov/cgi/fluid.cgi?ID=C7440019&Action=Page

[5] J. E. Eninger, "Excess liquid in heat-pipe vapor space," in *The AIAA 12th Thermophysics Conference*, Albuquerque, 1977.

[6] C. K. Loh, E. Harris and D. J. Chou, "Comparative study of heat pipes performances in different orientations," in *Semiconductor Thermal Measurement and Management IEEE Twenty First Annual IEEE Symposium*, San Jose, CA, USA, 2005.

[7] A. Fahgiri, "Heat Pipes, Review, Opportunities and Challenges," *Frontiers in Heat Pipes (FHP)*, vol. 5, no. 1, pp. 1-48, 2014.

[8] M. Ghanbarpour, "Investigation of Thermal Performance of Cylindrical Heat pipes Operated with Nanofluids," Doctoral Thesis in Energy Technology, Stockholm, Sweden, 2017.

[9] D. S. Naruka, R. Dwivedi and P. K. Singh, "Experimental inquisition of heat pipe: performance evaluation for different fluids," *A Journal of Thermal Energy Generation, Transport, Storage, and Conversion*, vol. 33, no. 7, pp. 668-682, 2020.

[10] S. W. Chi, Heat pipe theory and practice, United States: Hemisphere, 1976.

[11] "Material Properties: OFHC Copper," NIST: National Institute of Standards and Technology, [Online]. Available: https://trc.nist.gov/cryogenics/materials/OFHC%20Copper/OFHC_Copper_rev1.htm.

Chapter 7
CONCLUSION

The commercially available conventional heat pipe by using nitrogen, argon or neon as a working fluid was tested as the cryogenic heat pipe that may be potentially used to cool high temperature superconducting magnets. For the detail of the thermal behavior and performance of the cryogenic heat pipes, the experiments were performed by testing the single N_2-heat pipe (60–87 K), Ar-heat pipe (77–110 K), Ne-heat pipe (27–35 K), and also the parallel heat pipe system (a combination of an N_2-heat pipe & an Ar-heat pipe at 77 – 87 K, and a combination of an N_2-heat pipe & an Ne-heat pipe at 27–35 K) with respect to the effects of the filling ratio, the condenser temperature, the inclination angle as well as of the wick structures. The following conclusions were drawn through the experiment.

1. It is possible for commercially available conventional heat pipes with working fluid replaced with nitrogen, argon, or neon to achieve relatively high effective thermal conductivity in the cryogenic temperature range, though the heat pipe tested was not designed to work optimally in the cryogenic temperature range.
2. The commercially available conventional heat pipes with three kinds of wick structures, axial groove (G), sintered metal powder (S), and combination of them (GS), can work in the cryogenic temperature range. The performance rank by the wick structures on the basis of Q_{max} is as follows in descending order; GS, S and G.

3. The minimum value of R_{th}, which appears during the normal heat pipe operation, is 0.12, 0.20 and 0.25 K/W for the Ne-heat pipe, N_2-heat pipe, and Ar-heat pipe, respectively. These R_{th} values are approximately 150 and 75 times lower than a simple copper tube and a copper rod with an equivalent geometry to the heat pipe.
4. As the heat input, Q_e, increases, nucleate boiling begins in the evaporator section, and the effective thermal resistance turns to slightly increase still in the normal heat pipe operation state. When Q_e further increases and exceeds Q_{max}, the boiling state changes to the film boiling, and as a result, the temperature of the evaporator section rises sharply, and the transition to the local dry-out state occurs.
5. The filling ratio of a working fluid should be higher than 50% to activate the cryogenic heat pipe. It is found that in this particular heat pipe, when the working fluid filling ratio exceeds 100%, Q_{max} becomes large due to the gravitational effect on the rise of the excess working liquid puddle blown to the end portion of the condenser section by the vapor flow. However, increased liquid thickness in the wick at the condenser section results in increasing R_{th}.
6. At the temperatures below the triple point temperature of the working fluid, the condenser section is in the frozen state, but the heat pipe operation may occur locally in the evaporator, and sometimes even in the adiabatic section, where heat is efficiently transferred in a heat pipe operation state. However, in the frozen region, heat is only thermally conducted through the tube wall, the wick and the frozen working fluid, which results in a slightly higher thermal resistance R_{th}.
7. The operation of the heat pipe placed with the evaporator section above the condenser section gives small Q_{max}. The value of Q_{max} can be significantly improved when the evaporator section is set below the condenser section.

8. The Ar-heat pipe has the best performance value of Q_{max} (14 W at 87 K) that is larger than those of the N_2-heat pipe (12 W at 77 K) and the Ne-heat pipe (7 W at 27 K) with 100% filling ratio.
9. The experimental results for homogeneous wick structure, G and S wicks, are in good agreement with the theoretical calculation data for the variation in Q_{max} with the change in the wick structure and the filling ratio. Furthermore, the satisfactory agreement of the experimental results with the theoretical calculation for the case of composite wick structure, GS wick, seems to confirm our hypothesis for the wick function.
10. The parallel heat pipe system can enhance the performance of a single heat pipe with respect to Q_{max} and expand the operating temperature range. The maximum Q_{max} of 29 W was obtained at the operating temperature of 87 K (the N_2- & the Ar-heat pipes).
11. It is found that the parallel heat pipe system can be utilized even in the local dry-out state as long as the temperature of the condenser section is kept in the cryogenic temperature range with a cryocooler. In such a state, as the parallel heat pipe system works in a partially activated state, the thermal resistance is moderately small compared with that of metal rod or tube, and the vapor pressure inside the heat pipe is not extremely high.
12. The commercially available conventional heat pipe can be used as a cryogenic heat pipe for the application to conduction-cooled superconducting magnets. The thermal behavior of the cryogenic parallel heat pipe system demonstrates that both the normal heat pipe operation and the local dry-out state can be respectively utilized for thermal management (very small temperature gradient) and cooling from high temperature (high heat transfer rate).